



**UNIVERSITÀ DEGLI STUDI DI TRIESTE**

**XXIX CICLO DEL DOTTORATO DI RICERCA IN**

**BIOMEDICINA MOLECOLARE**

Tesi redatta con il contributo finanziario di  
GSK Vaccines Institute for Global Health S.r.l.

**Characterization of polysaccharide-based  
vaccines against invasive nontyphoidal  
*Salmonella* disease (iNTS)**

Settore scientifico-disciplinare: **BIO/10**

DOTTORANDO  
**Gianluigi De Benedetto**

COORDINATORE  
**Prof. Germana Meroni**

SUPERVISORE DI TESI  
**Dr. Paola Cescutti**

CO-SUPERVISORE DI TESI  
**Dr. Francesca Micoli**  
GSK Vaccines Institute for Global Health S.r.l.

**ANNO ACCADEMICO 2015/2016**





**UNIVERSITÀ DEGLI STUDI DI TRIESTE**

**XXIX CICLO DEL DOTTORATO DI RICERCA IN  
BIOMEDICINA MOLECOLARE**

Tesi redatta con il contributo finanziario di  
GSK Vaccines Institute for Global Health S.r.l.

**Characterization of polysaccharide-based vaccines  
against invasive nontyphoidal *Salmonella* disease (iNTS)**

Settore scientifico-disciplinare: **BIO/10**

**DOTTORANDO**  
**Gianluigi De Benedetto**

**COORDINATORE**  
**Prof. Germana Meroni**

**SUPERVISORE DI TESI**  
**Dr. Paola Cescutti**

**CO-SUPERVISORE DI TESI**  
**Dr. Francesca Micoli**

GSK Vaccines Institute for Global Health S.r.l.

**ANNO ACCADEMICO 2015/2016**



*Ai miei genitori*





## Abstract

Invasive nontyphoidal *Salmonella* disease (iNTS) is a leading cause of death and morbidity in developing countries and no vaccines are currently available. The most common pathogens are *Salmonella enterica* serovars Typhimurium and Enteritidis. The O-antigen (OAg) portion of their lipopolysaccharide (LPS) is a target of protective immunity and two OAg-based vaccine strategies have been evaluated at GSK Vaccines Institute for Global Health (GVGH): bivalent formulation of *S. Typhimurium* and *S. Enteritidis* Generalized Modules for Membrane Antigens (GMMA) and conjugation of *S. Typhimurium* and *S. Enteritidis* OAg to CRM<sub>197</sub> carrier protein.

The first part of my Ph.D. project focused on the characterization of GMMA produced by *S. Typhimurium* and *S. Enteritidis* mutated strains, with particular attention to the OAg component, in a process of screening to identify the most suitable GMMA candidate vaccines. GMMA are outer membrane vesicles naturally released by Gram-negative bacteria. *S. Typhimurium* and *S. Enteritidis* strains were engineered to increase GMMA production and detoxify the lipid A moiety of LPS. We found that genetic mutations can impact expression of OAg chains and their structural characteristics, such as chain length and level and position of *O*-acetylation. However, when tested in mice, all GMMA induced high levels of anti-OAg-specific IgG functional antibodies, despite variation in density and OAg structural modifications.

Methods to check quality, consistency of production, stability of GMMA vaccines are of fundamental importance. Not only it is important to characterize the key antigens displayed on GMMA surface and presented to the immune system, but also to characterize GMMA as particles. In this context, we compared Dynamic Light Scattering (DLS), Multi-Angle Light Scattering (MALS) and Nanoparticle Tracking Analysis (NTA) for size distribution determination and for verifying integrity and eventual aggregation of GMMA particles. Each methodology resulted to have strengths and weaknesses, but all the three techniques provided complementary information allowing a more complete evaluation of GMMA size.



Unlike the MALS diameter, the DLS diameter correlated with the number of OAg chains per GMMA particle. NTA allows real time visualization and simultaneously tracking and counting of individual particles, but it is deeply operator dependent, making more difficult to obtain consistent results.

Second part of my Ph.D. project focused on the in depth characterization of OAg-CRM<sub>197</sub> glycoconjugates. OAg was extracted by direct acid hydrolysis of bacteria and conjugated to CRM<sub>197</sub> through reductive amination of the terminal reducing sugar, which is expected to be 3-Deoxy-D-manno-oct-2-ulosonic acid (KDO) of the LPS core region. KDO structural rearrangements after acid hydrolysis have been reported in literature and its high reactivity in reaction of reductive amination has been attributed to these chemical modifications. Here, analysis by MS and NMR of the core oligosaccharide (OS) extracted from *S. Typhimurium* bacteria showed the presence of KDO in its native form with no structural changes. Core OS was fully characterized and conjugated to CRM<sub>197</sub>, through insertion of adipic acid dihydrazide (ADH) and adipic acid bis-(N-hydroxysuccinimide) ester (SIDEA) as linkers. KDO was the sugar involved in the first step, with kinetic of reductive amination with ADH faster than KDO monosaccharide, due to the linkage in position 5 to the sugar chain. The step of SIDEA introduction was not selective as the linker reacted also with the pyrophosphorylethanolamine (PPEtN) group present in the core region, even in the presence of ADH and by performing the reaction at low pH. Glycosylation sites investigation confirmed that the conjugation process used is highly random involving many lysine residues of CRM<sub>197</sub>, with preference for those surface exposed. The method also allowed investigation of the regioselectivity of the reaction confirming that OAg chains linkage to the protein happened through both SIDEA on PPEtN group and on ADH.

These studies contributed to better characterize the *Salmonella* antigens and help to define and improve manufacturing processes and analytical methods for OAg-based vaccines in general.





## Riassunto

La malattia invasiva provocata da *Salmonelle* non tifoidee (iNTS) è una delle principali cause di morte e morbilità nei paesi in via di sviluppo e nessun vaccino è attualmente disponibile. Gli agenti patogeni più comuni sono *Salmonella enterica* sierotipi Typhimurium ed Enteritidis. L'antigene O (OAg) del loro lipopolisaccaride (LPS) è un bersaglio per la protezione immunitaria e due strategie per lo sviluppo di vaccini basate sull'OAg sono state prese in considerazione in GSK Vaccines Institute for Global Health (GVGH): una formulazione bivalente di Generalized Modules for Membrane Antigens (GMMA) prodotte da *S. Typhimurium* e *S. Enteritidis* e la coniugazione delle catene di OAg di *S. Typhimurium* e *S. Enteritidis* alla proteina carrier CRM<sub>197</sub>.

La prima parte del mio progetto di dottorato è focalizzata sulla caratterizzazione delle GMMA prodotte da ceppi mutati di *S. Typhimurium* e *S. Enteritidis*, con particolare attenzione all'OAg, in un processo di screening per individuare i candidati più idonei per lo sviluppo di un vaccino basato sulle GMMA. Le GMMA sono vescicole di membrana esterna spontaneamente rilasciate da batteri Gram-negativi. Ceppi di *S. Typhimurium* e di *S. Enteritidis* sono stati geneticamente modificati per aumentare la produzione stessa di GMMA e per detossificare la componente di lipide A dell'LPS. Abbiamo riscontrato che le mutazioni genetiche introdotte possono influenzare l'espressione stessa delle catene di OAg e le loro caratteristiche strutturali, quali la lunghezza di catena e il livello e la posizione dei gruppi *O*-acetile. Tuttavia, quando testate nei topi a parità di dose di OAg iniettata, tutte le GMMA hanno indotto simili alti livelli di anticorpi funzionali specifici per l'OAg, indipendentemente dalla densità delle catene di OAg sulle GMMA e dalle loro differenze strutturali.

Metodi per verificare qualità, consistenza della produzione, stabilità dei vaccini basati sulle GMMA sono di fondamentale importanza. Non solo è importante caratterizzare gli antigeni chiave esposti sulla superficie delle GMMA e presentati al sistema immunitario, ma anche caratterizzare le GMMA come particelle. In questo contesto, abbiamo confrontato varie tecniche fra cui Dynamic Light Scattering (DLS), Multi-Angle Light Scattering (MALS) e Nanoparticle Tracking Analysis (NTA) per la



determinazione della distribuzione delle dimensioni e per la verifica dell'integrità e dell'eventuale aggregazione delle GMMA. Ogni tecnica ha mostrato punti di forza e punti deboli, ma tutte e tre hanno fornito informazioni complementari consentendo una valutazione più completa delle dimensioni delle GMMA. Diversamente dal diametro ottenuto dopo analisi MALS, il diametro ottenuto dopo analisi DLS aveva una correlazione con il numero delle catene di OAg per particella di GMMA. L'NTA permette la visualizzazione in tempo reale e il monitoraggio e il conteggio simultaneo di singole particelle, ma è profondamente dipendente dall'operatore, rendendo più difficile ottenere risultati coerenti.

La seconda parte del mio progetto di dottorato è incentrata sulla caratterizzazione approfondita dei coniugati OAg-CRM<sub>197</sub>. L'OAg è stato estratto per idrolisi acida diretta sui batteri e coniugato con il CRM<sub>197</sub> attraverso l'amminazione riduttiva dello zucchero all'estremità riducente, che dovrebbe essere l'acido 3-Deossi-D-manno-ott-2-ulosonico (KDO) della regione core dell'LPS. Riarrangiamenti strutturali del KDO dopo idrolisi acida sono stati riportati in letteratura e la sua elevata reattività nelle reazioni di amminazione riduttiva è stata attribuita a queste modifiche chimiche. In questo lavoro, analisi di spettrometria di massa (MS) e di spettroscopia di risonanza magnetica nucleare (NMR) del core oligosaccaridico (OS) estratto da batteri di *S. Typhimurium* hanno mostrato la presenza del KDO nella sua forma nativa senza modifiche strutturali. Il core OS è stato completamente caratterizzato e coniugato con il CRM<sub>197</sub>, attraverso l'inserimento della diidrazide dell'acido adipico (ADH) e dell'estere disuccinimidil adipato (SIDEA) come molecole linker. Il KDO è stato lo zucchero coinvolto nella prima fase, con una cinetica di reazione di amminazione riduttiva con ADH più rapida rispetto al KDO monosaccaride, a causa del legame in posizione 5 alla catena saccaridica. Il passaggio di introduzione della SIDEA non è risultato essere selettivo poiché il linker reagisce non solo con l'ADH, ma anche con la fosfoetanolamina presente nella regione del core oligosaccaridico, anche effettuando la reazione a un basso valore di pH. L'analisi dei siti di glicosilazione del CRM<sub>197</sub> ha confermato che il processo di coniugazione usato è molto casuale coinvolgendo molti residui di lisina, con preferenza per quelli esposti in superficie. Il metodo ha permesso anche un'indagine della regioselettività della reazione, che



conferma che la coniugazione delle catene di OAg alla proteina è avvenuta sia attraverso la SIDEA legata alla fosfoetanolamina che all'ADH.

Questi studi hanno contribuito a caratterizzare meglio gli antigeni di *Salmonella* e ad aiutare a definire e migliorare i processi di produzione e i metodi analitici applicabili a vaccini basati sull'OAg in generale.



## Table of contents

<b>1. Introduction</b>	<b>1</b>
<b>1.1 <i>Salmonella</i> classification and host range infections</b>	<b>2</b>
<b>1.2 Nontyphoidal <i>Salmonella</i> burden of disease</b>	<b>5</b>
<b>1.3 iNTS risk factors</b>	<b>7</b>
<b>1.4 iNTS as neglected disease</b>	<b>8</b>
<b>1.5 Targets for <i>Salmonella</i> vaccines development</b>	<b>9</b>
<b>1.6 Vaccines against iNTS</b>	<b>12</b>
<b>1.7 Development of a vaccine against iNTS in GVGH</b>	<b>15</b>
<b>1.7.1 OAg-CRM<sub>197</sub> conjugate vaccines</b>	<b>15</b>
<b>1.7.2 GMMA vaccines</b>	<b>16</b>
<b>1.8 Description of research aims</b>	<b>17</b>
<b>2. Characterization of OAg delivered by Generalized Modules for Membrane Antigens (GMMA) vaccine candidates against iNTS</b>	<b>18</b>
<b>2.1 Introduction</b>	<b>19</b>
<b>2.2 Materials and Methods</b>	<b>22</b>
<b>2.2.1 NTS parent strains for GMMA production</b>	<b>22</b>
<b>2.2.2 GMMA production and characterization</b>	<b>24</b>
<b>2.2.3 OAg purification and characterization</b>	<b>27</b>
<b>2.2.4. Immunogenicity of candidate <i>Salmonella</i> GMMA vaccines in mice and serological analysis</b>	<b>29</b>
<b>2.3 Results</b>	<b>30</b>
<b>2.3.1 OAg characterization of SEn 618 wild type bacteria</b>	<b>31</b>
<b>2.3.2 OAg characterization of SEn 618 GMMA</b>	<b>34</b>
<b>2.3.3 OAg characterization of STm 1418 GMMA</b>	<b>39</b>
<b>2.3.4 Immunogenicity in mice</b>	<b>44</b>
<b>2.4 Discussion</b>	<b>46</b>
<b>3. Determination of nontyphoidal <i>Salmonella</i> GMMA particle size distribution</b>	<b>49</b>
<b>3.1 Introduction</b>	<b>50</b>



<b>3.2 Materials and methods</b>	<b>58</b>
3.2.1 NTS parent strains for GMMA production	58
3.2.2 GMMA protein quantification	58
3.2.3 Dynamic Light Scattering (DLS)	59
3.2.4 Size Exclusion Chromatography coupled to Multi-Angle Light Scattering (SEC-MALS)	59
3.2.5 Nanoparticle Tracking Analysis (NTA)	60
3.2.6 HPLC-SEC	61
<b>3.3 Results</b>	<b>61</b>
3.3.1 Size distribution analysis by DLS	61
3.3.2 Size distribution analysis by SEC-MALS	64
3.3.3 Size distribution analysis by NTA	68
3.3.4 Comparison of DLS, MALS and NTA results	75
<b>3.5 Discussion</b>	<b>80</b>
<b>4. KDO reactivity and selectivity in the synthesis of OAg-CRM<sub>197</sub> glycoconjugate vaccines</b>	<b>82</b>
4.1 Introduction	83
4.2 Materials and Methods	86
4.2.1 <i>B. cepacia</i> strain BTS13 for exopolysaccharide (EPS) production	86
4.2.2 <i>B. cepacia</i> BTS13 EPS hydrolysis and oligosaccharides purification	86
4.2.3 STm 1418 $\Delta tolR \Delta wbaP$ GMMA production and characterization	86
4.2.4 LPS core OS purification	86
4.2.5 De-phosphorylation of core OS	87
4.2.6 Reduction of native and de-phosphorylated core OS	87
4.2.7 LPS core OS characterization	87
4.2.8 ESI-MS analysis	88
4.2.9 MALDI-TOF-MS analysis	88
4.2.10 Reaction of core OS with adipic acid dihydrazide (ADH)	89



4.2.11 Characterization of core OS-ADH intermediate	89
4.2.12 Reaction of core OS-ADH and core OS with adipic acid bis-(N-hydroxysuccinimide) ester (SIDEA)	90
4.2.13 Characterization of SIDEA-derivatized core OS intermediates	91
4.2.14 Synthesis of core OS-CRM <sub>197</sub> conjugates	92
4.2.15 Characterization of purified OS-CRM <sub>197</sub> conjugates	92
4.2.16 Synthesis and characterization of OAg-ADH-SIDEA- CRM <sub>197</sub> conjugate	93
4.2.17 Glycoconjugates de-glycosylation by trifluoromethanesulphonic acid (TFMS)	93
4.2.18 Trypsin digestion of de-glycosylated conjugates	93
4.2.19 MALDI-MS analysis for peptide mapping	94
4.2.20 LC-ESI-MS analysis for peptide mapping	94
4.3 Results	95
4.3.1 Characterization of core OS from STm 1418 $\Delta tolR \Delta wbaP$ GMMA	95
4.3.2 Characterization of the oligosaccharides from <i>B. cepacia</i> BTS 13 EPS	101
4.3.3 Investigation on KDO reactivity	102
4.3.4 Core OS conjugation to CRM <sub>197</sub>	103
4.3.5 Glycosylation sites of core OS- and OAg-CRM <sub>197</sub> conjugates	112
4.4 Discussion	121
5. Conclusions	124
6. References	127
Acknowledgements	143
Annexes	145



## **1. Introduction**



## 1.1 *Salmonella* classification and host range infections

*Salmonellae* are Gram-negative, facultative anaerobic and nonspore-forming bacilli, with cell diameters between 0.7 and 1.5  $\mu\text{m}$ , lengths from 2 to 5  $\mu\text{m}$  and peritrichous flagella [1, 2]. *Salmonella* species are facultative intracellular pathogens, capable to infect a wide range of species, from reptiles and birds to mammals, including humans, causing a wide spectrum of diseases [3]. Host infection (also known as salmonellosis) is generally due to oral ingestion of contaminated food or water, direct faecal-oral spread, contact with infected animals and nosocomial exposure [4, 5]. Contact with pet reptiles and amphibians, also represents a risk for salmonellosis [6]. *Salmonellae* have been isolated from rivers, sewage, and soil, demonstrating a wide colonization of the environment. Moreover, they have been detected in fruits, vegetables and animal feeds.

The genus *Salmonella* belongs to the family of *Enterobacteriaceae* [7]. The genus comprises a large and closely related population of medically relevant pathogens. They take name from the veterinary pathologist Daniel Elmer Salmon, administrator of the Veterinary Division of the United States Department of Agriculture in 1885, where the medical research scientist Theobald Smith discovered this new type of bacteria in porcine intestine.

Despite *Salmonella* has been recognized as an important pathogen, its complex nomenclature system is quite confusing and remains unfamiliar to clinicians. Although uniformity in nomenclature is considered necessary for communication among scientists, health officers and the public, different systems have been used to refer to this genus. Since its isolation, several taxonomy classification systems have been proposed, inconsistently dividing the genus into species, subspecies, subgenera, groups, subgroups, and serotypes or serovars. The terms serotype and serovar (short for serological variant) have been both frequently used, but the latter has been preferred, according to the rules proposed by the Judicial Commission of the International Committee on the Systematics of Prokaryotes in 1990. Initially many *Salmonellae* were differentiated [8] on the basis of the serologic identification of bacterial surface moieties such as the O-antigen (OAg) of lipopolysaccharide (LPS)





(O somatic antigen), the Vi capsular polysaccharide (CPS) antigen and the flagellar antigen (H antigen). In agreement with this classification system introduced in 1966, known as Kauffmann-White classification [9], each serotype was considered a separate species, resulting in more than 2,500 *Salmonella* species. Agglutination reactions based on O and H antigens have been used by clinical laboratories to divide *Salmonella* into serogroups which include A, B, C1, C2, D, E [10]. Other taxonomic proposals have been based on the animal species from which the organism was isolated, on the clinical role of a strain, on the biochemical characteristics, on genomic relatedness, or on the geographical area where the strain was first isolated. Many of these names, after being commonly used for years, were accepted with no revision of the antigenic formulae system [7].

The current antigenic classification system of the genus *Salmonella*, accepted and used by World Health Organization (WHO), Centers for Disease Control and Prevention (CDC) and the American Society for Microbiology (ASM), is the result of many changes made overtime and it is still evolving [11]. The genus contains two species: *S. enterica*, and *S. bongori*. These two species are further divided into subspecies, which are referred to by a Roman number and a name. Subspecies within *S. bongori* are more associated with cold-blooded animals, such as reptiles and birds, and have only rarely been known to infect humans [12]. *S. enterica* consists of six subspecies (subsp.): I, *S. enterica* subsp. *enterica*; II, *S. enterica* subsp. *salamae*; IIIa, *S. enterica* subsp. *arizonae*; IIIb, *S. enterica* subsp. *diarizonae*; IV, *S. enterica* subsp. *houtenae*; VI, *S. enterica* subsp. *indica*. *S. bongori* has only one subspecies, subsp. V. Subspecies are differentiated biochemically and by genomic relatedness. In subspecies I, serovars are designated by a name, indicative of associated diseases, geographic origins, or usual hosts, for example serotypes Enteritidis, Typhimurium, Typhi, and Choleraesuis [10] (Fig. 1).

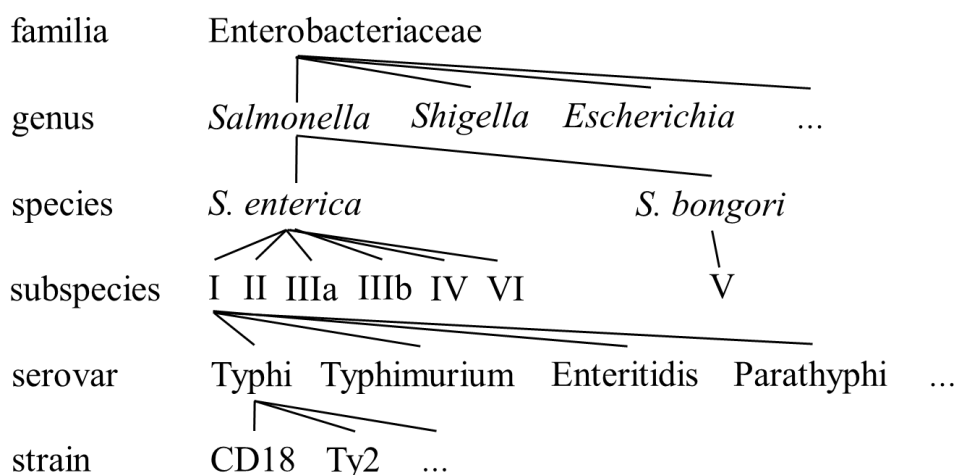


**Fig. 1.** Currently accepted taxonomic classification of *Salmonella* genus.

From a clinical point of view, *Salmonella enterica* serotypes, which contains over 60% of the total number of serovars of the genus and 99% of which are capable of infection in humans [2], have been categorized as typhoidal *Salmonellae* and nontyphoidal *Salmonellae* (NTS) serovars, based on host preference and disease manifestations in humans [4, 13]. Typhoidal serovars, which include *Salmonella enterica* subsp. *enterica* Typhi and *S. Paratyphi* A, B, and C, are specific for humans and do not occur in animals. They are usually contracted through direct contact with the faecal matter of an infected person. NTS serovars instead are zoonotic in origin, meaning that they can be transferred between animals and humans [14]. Poultry and eggs represent the most common source of NTS, together with reptiles, rodents, cats and dogs [15, 16]. NTS strains may be host generalists, infecting or colonizing a broad range of vertebrate animals, or may be adapted or restricted to particular nonhuman animal species.

Despite their genetic similarity, serovars of typhoidal and nontyphoidal *Salmonella* can elicit very different diseases, in relation to their targets in the infected organisms and symptoms they can cause, as well as distinct immune responses, reflecting also host factors [17, 18]. The spectrum of diseases can range from gastroenteritis, enteric systemic fever (typhoid and paratyphoid fever), bacteraemia, focal infections, to a convalescent lifetime carrier state. Though primarily enteric pathogen, provoking



common diarrheal illness symptoms, *Salmonella enterica* (both typhoidal and NTS) is responsible for a considerable yet under-appreciated global burden of invasive disease, especially in developing countries of both Asia and Africa [19-22]. Since the early use of blood cultures, invasive *S. enterica* infections appeared to be common in Africa [23, 24].

## 1.2 Nontyphoidal *Salmonella* burden of disease

NTS serovars are responsible of a huge burden of morbidity and mortality worldwide [21, 25-28]. The global incidence of NTS gastroenteritis was estimated to be 93 million episodes in 2010, and 80 million contracted the infection via food-borne transmission [29]. 2010 estimates reported that NTS infections were associated with 4,847,000 disability-adjusted life years (DALY) lost and 81,300 diarrheal deaths [30, 31]. Of the more than 2,500 NTS serovars, *Salmonella* Typhimurium and *Salmonella* Enteritidis account for approximately 50% of all human isolates of NTS reported globally [32].

In developed countries, NTS serovars are predominantly responsible of self-limiting food-borne diarrheal illness in healthy individuals, with rare cases of bloodstream and focal infections and rarely life-threatening [33], except for specific risk factors [34]. NTS infection, instead, has emerged as a leading cause of community-acquired extra-intestinal, invasive bacteraemia, referred to as invasive nontyphoidal *Salmonella* disease (iNTS), in developing countries [14, 35] (Fig 2).

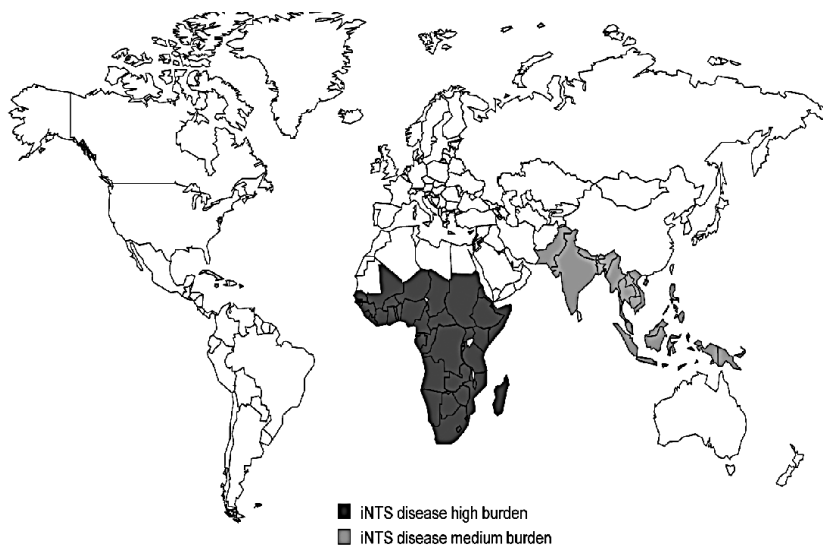


**Fig. 2.** Geographical distribution invasive nontyphoidal *Salmonella* disease (iNTS) indicating countries with high (> 100 cases/100,000 population/year) and medium (10-100 cases/100,000 population/year) disease burden [25].

Recent published data suggest that, globally, there are 49 cases (range of 30-94) of iNTS per 100,000 population which means that 3.4 (range 2.1-6.5) million cases occur globally each year (681,316 deaths annually, range of 415,164 to 1,301,520) [36]. In Africa, the iNTS incidence is high (227 cases per 100,000, range of 142-341), associated with case fatality rates of 20%. Metanalyses data which were extrapolated from 22 studies conducted in 34 African sites showed that 29% of community-acquired bloodstream infections were caused by *Salmonella enterica* [37], and a high proportion of these infections (87-97%) were attributable to NTS [14]. iNTS had comparable incidence rates as invasive pneumococcal infection, for which a vaccine is available [37]. *S. Typhimurium* and *S. Enteritidis* were the most common serovars causing iNTS, accounting for 65.2% and 33.1% of all NTS serotyped isolates respectively, as also indicated by the WHO Global Food-borne Infections Network (GFN) [38]. Other serotypes implicated in provoking iNTS are *S. Isangi*, *S. Concord*, *S. Stanleyville*, and *S. Dublin* [39].

There are not clear ideas of why invasive *Salmonella* disease is a problem in middle- and low-income countries and not in developed world [26]. However, there



are several established factors that include increased invasiveness of distinct clades specific to Africa, increased opportunities for transmission and differences in routes of transmission and compromised host immunity in those individuals with HIV infection, malaria, malnutrition [25, 32]. The routes of transmission of iNTS are poorly understood. Studies of *Salmonella* carriage among livestock of families with iNTS cases have found that animal isolates are distinct from those associated with iNTS in man [25]. This suggests that iNTS in Africa, unlike in industrialized countries, does not have an animal reservoir. Recently, a strain of *S. Typhimurium*, known as ST313, has been identified as responsible for a notable proportion of iNTS in multiple sites in sub-Saharan Africa (SSA). The pathogen appears to be restricted to Africa [35], with strong genomic associations with *S. Typhi*. In particular, aside from showing multiple drug resistance, this strain has adapted itself to immunosuppressed persons, above all those living with HIV.

### 1.3 iNTS risk factors

Predisposing host factors appear to be important for iNTS infection and genetic immunodeficiency that affect innate and acquired immunity pathways and comorbidities are associated with iNTS [40-43]. In Africa, high incidence and increased severity of iNTS have been observed in young children below 72 months of age, in patients with acute or recent malaria, malarial anaemia and severe anaemia, in individuals with malnutrition, HIV, sickle cell disease, and haemolysis [44-50] resulting in high case-fatality rates.

A study conducted in Mozambique reported an incidence of 388/100,000 in infants less than one year of age, and 262/100,000 in those under the age of five [51]. Significant discordance in the burden of iNTS between continents exists [52], and surveillance data from the United States showed, for example, that the incidence of iNTS was 7.8 cases per 100,000 in infants (aged less than one year) compared to less than 0.8 cases per 100,000 in older children [53].

In adults with HIV infection, recurrent iNTS cases have been well documented. NTS bacteraemia is particularly virulent in HIV-infected African adults who have a



mortality rate of 47% and recurrence rate of 43% [54]. However, severe iNTS accompanied by high case-fatality rates is also a common cause of bacteraemia in countries such as Mali, where HIV prevalence is low, and continues to be a problem in children not infected with HIV [39]. In contrast, HIV infection does not appear to predispose to infection with *S. Typhi* in those parts of Africa where typhoid fever is reported [55].

The high prevalence of malaria, and its association with iNTS, has been postulated as one reason for the different incidence between Africa and other continents [56]. Association between malaria and invasive *Salmonella* infections was suggested in 1929 [57] and confirmed in 1987 [58]. Interestingly, recent studies in Gambia, Kenya and Tanzania have shown that the marked decline in malaria prevalence has been paralleled by a similar reduction in iNTS [59]. Nevertheless, iNTS remains a problem in locations where malaria is absent [59].

#### **1.4 iNTS as neglected disease**

iNTS has been overshadowed in the past by other diseases for which better data were available, such as malaria and AIDS [32]. A key problem, common for the whole invasive *Salmonella* disease and not only iNTS, is the lack of appropriate diagnostic facilities, especially in Africa rural settings [25]. At the moment, microbiological blood cultures are the only way for the detection of *Salmonella* infections and for a proper clinical diagnosis of invasive *Salmonella* and iNTS, and facilities for blood cultures and other culture-based methods are extremely rare in low-resource settings of African countries [60]. This lack of wide available *Salmonella* diagnostic facilities does not produce results in time to inform the initial management of individual patients [61]. Moreover, efforts should be made also to develop non-culture-based diagnostic tests that are useful especially in more remote environments. Such efforts are needed not only to improve individual patient diagnosis and treatment, but also to better assess burden of disease and to support prevention measures, including vaccines [62, 63].



Another problem is that a proper and specific diagnosis of iNTS is troublesome, due to the lack of distinctive clinical features associated with this disease, being confused with malaria [58] or severe pneumonia [26, 56]. In fact, signs and symptoms that distinguish iNTS from other common febrile infections do not exist [22, 55]. iNTS usually presents as febrile illness, frequently without diarrhoea and other gastrointestinal symptoms, in both adults and children. Because of these diagnostic problems, invasive *Salmonella* infections, and in particular iNTS, have been neglected and not considered as a significant global disease burden. By definition, neglected diseases fail to receive the level of support of better-known infectious diseases in Africa, such as HIV, malaria and tuberculosis. As a result, progress towards non-vaccine and vaccine strategies against iNTS has also been slow [64]. Antibiotics have been widely used, although not always available in rural African settings, but increasing levels of multidrug-resistance to several antimicrobial classes [22], including extended spectrum cephalosporins and fluoroquinolones, are limiting their effectiveness [34, 52, 65-68]. A recent study conducted in Malawi emphasized that 90% of invasive NTS serovars isolates were multidrug resistant [34].

Until good sanitary and hygienic conditions, provision of clean drinking water, food safety and appropriate diagnostic facilities are not available, alternative ways for the control of iNTS in developing countries are strongly needed [69, 70]. Vaccines against typhoid fever are widely available, but unfortunately there are no licensed vaccines against iNTS, in particular against *S. Typhimurium* and *S. Enteritidis*. Efforts should be intensified to identify protective antigens and best strategies for vaccine development [25, 32, 71, 72].

### **1.5 Targets for *Salmonella* vaccines development**

For the development of vaccines mediating protection against *Salmonella*, components of the outer surface of bacteria can be targeted, representing both essential virulence factors and important target antigens for protective antibodies induction [32].



The cell wall of Gram-negative bacteria is composed of a lipid outer and inner membrane with a layer of peptidoglycan in between. The outer membrane is an asymmetric lipid bilayer with phospholipids in the inner leaflet and glycolipids, predominantly LPS, in the outer leaflet [73]. The LPS layer surrounding Gram-negative bacteria constitutes a strong barrier against toxic compounds, such as antibiotics and allowing survival in harsh environments. LPS is also a potent activator of the innate immune response and acts as a conserved pathogen associated molecular pattern (PAMP) recognized by innate immune receptors [74]. LPS is a powerful immunomodulatory and may cause endotoxic shock in infected people. Architecture of LPS is shared by Gram-negative bacteria, but structural motifs vary considerably from one serovar to another (Fig. 3) [75].

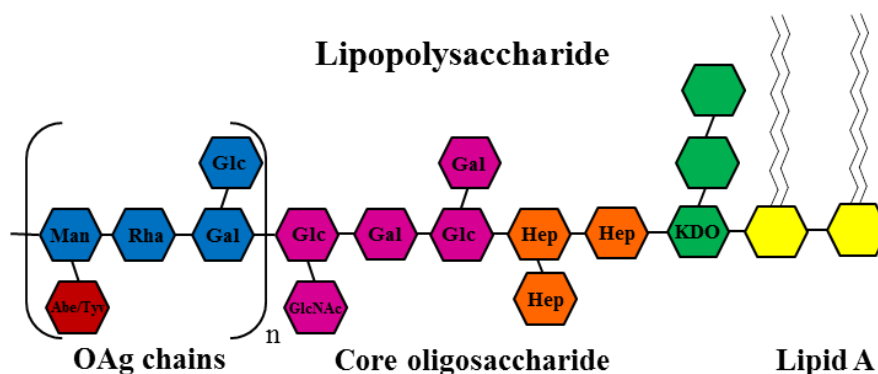


**Fig. 3.** Structure of the LPS molecule found in the outer membrane of *S. Typhimurium* and *S. Enteritidis*.

LPS molecules generally consist of three components [75]:

- the lipid A;
- the core oligosaccharide;
- the O-antigen (OAg) chain.

The lipid A is anchored in the outermost membrane leaflet and represents the hydrophobic part of LPS. Lipid A is composed by a backbone consisting of a  $\beta$ -1,6-linked D-glucosamine (D-GlcN) disaccharide, *O*- and *N*-acylated with fatty acids of variable length, and phosphate groups at positions C-1 and C-4'. The lipid A domain





is responsible for much of the toxicity of Gram-negative bacteria and is a much conserved component of the LPS.

The core oligosaccharide is covalently bound at the position C-6' of the non-reducing glucosamine residue of lipid A through the acidic sugar 3-Deoxy-D-manno-oct-2-ulopyranosonic acid (KDO). The proximal “inner core” region contains heptose residues (Hep), often substituted by phosphate (P), phosphorylethanolamine (PEtN) or pyrophosphorylethanolamine (PPEtN) groups. The “outer core” region of NTS serovars usually consists of neutral or amino hexoses such as D-glucose, D-galactose, D-glucosamine or *N*-acetyl derivatives.

The OAg is a repetitive glycan polymer attached to the core oligosaccharide, and comprises the outermost domain of the LPS molecule. The composition of the OAg chains varies from strain to strain. OAg has been reported to help the bacteria to escape the host defence system, and in particular the attack of serum complement. Antibodies directed against OAg have been shown to be able to mediate bacterial killing [64, 76] and to confer protection against infection in animal models [77-80]. Passive transfer of targeting-OAg antibodies has been reported to protect against challenge [81, 82]. In addition, immunization with heat-killed *S. Typhimurium* ST313 bacteria evoked bactericidal antibodies directed against OAg [76].

In addition to the OAg chains of the LPS, *Salmonella* surface proteins have been proposed as target antigens. *Salmonella* flagella are virulence factors that extend from the outer membrane and act in response to chemical information from the environment, allowing regulated movements of the bacteria [83]. Flagellin is a globular protein that arranges itself in a hollow cylinder to form the filament in a bacterial flagellum. Flagella consist of three elements, a basal body, a transmembrane motor and a filament consisting of multiple repeats of flagellin protein. Amino acid sequences for flagellin differ among serovars [84]. Mice have shown protection after immunization both with flagellin alone [79, 85, 86] or flagellin as carrier protein in OAg-based glycoconjugates [79, 87]. Flagellin is also crucial for Toll-like receptor 5 (TLR5) stimulation and consequently involved in innate immune signalling [88, 89].

*Salmonella* porins are particularly abundant in the outer membrane and are channel proteins allowing passive diffusion of small molecules. Typically they consist of



around 16 tilted  $\beta$ -strands connected by periplasmic and extraplasmic loops [90], and are exclusively found as homo- or heterotrimers in the membrane [91]. Porins differ in their loop topology and surface charge, and the most common porins found in *Salmonella* are outer membrane porin (Omp) C, OmpF and OmpD [92]. Porins are useful widely-conserved *Salmonella* surface proteins and have shown potential for use in broadly protective vaccines [82].

## 1.6 Vaccines against iNTS

The development of vaccines against iNTS has been slower with respect to vaccines against typhoid fever [20]. This is likely to be attributable to a general lack of appreciation and awareness of the problem of iNTS in the global health community [69]. The development of iNTS vaccines was also complicated by the immunocompromised nature of susceptible patients [48, 49], which should be addressed early in clinical development. However, the enhanced activity in the field of vaccine development against *Salmonella* in the recent years has increased the attention on iNTS and strategies for vaccine design are being evaluated and several preparations are in preclinical studies phase [32]. Although several groups are working towards vaccines against iNTS, no licensed vaccines against iNTS are currently available [25]. Vaccine strategies against iNTS consist of live attenuated whole bacterial cells or nonliving preparations [28] (Fig. 4).

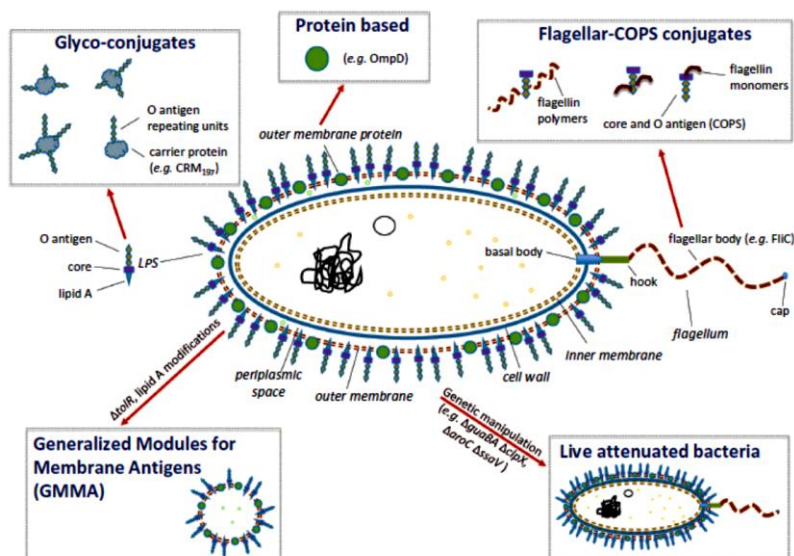


**Fig. 4.** Schematic representation of NTS, highlighting the main approaches currently under evaluation to develop vaccines against iNTS [28].

Live attenuated vaccines show a number of potential advantages, having the possibility of inducing broad protection against several *Salmonella* serovars, since multiple *Salmonella* antigens are delivered to the immune system [93]. Many attenuating mutations have been considered and tested in preclinical studies, conferring protection against challenge with the homologous serovars [25, 94]. Potential candidates for iNTS vaccination are *S. Typhimurium* and *S. Enteritidis*  $\Delta$ *guaBA*  $\Delta$ *clpX*, which showed encouraging safety, high immunogenicity, and protection against lethal challenge with the homologous serovars in mice [95, 96]. The only live attenuated iNTS vaccine to be tested to date in man is WT05, a *S. Typhimurium*  $\Delta$ *aroC*  $\Delta$ *ssaV* mutant [97]. When tested in Phase 1 study, it induced variable serum antibody responses and prolonged stool shedding was found in volunteers for up to 23 days, so that the vaccine has not been tested further. The achievement of the right balance between immunogenicity and safety remains a major challenge of live attenuated iNTS vaccines.

Nonliving iNTS vaccines consist either of defined antigens or preparations that contain multiple antigens together. Glycoconjugation technology [98] represents one of the most advanced strategies for the development of a vaccine against iNTS [72].



Glycoconjugates against iNTS are based on the covalent conjugation of surface OAg to suitable carrier proteins [72, 99-101]. Tetanus toxoid (TT) [80, 102, 103], diphtheria toxoid (DT) [104] and nontoxic recombinant form of diphtheria toxin (CRM<sub>197</sub>) [77, 105-107], have been used as heterologous carrier proteins. These non-*Salmonella* proteins are known to be safe and effective at inducing strong immune response against the polysaccharide antigen [78]. In addition to these carrier proteins, the use of *Salmonella* proteins has been considered. This could result in more effective vaccines than those with exogenous carriers, as they would target the immune response to two different *Salmonella* antigens. Svenson *et al* showed that *S. Typhimurium* OAg conjugated to *S. Typhimurium* porins gave better protection in mice than vaccination with porin vaccines alone or an analogous DT conjugate [86, 108-110]. Simon *et al* showed enhanced immunogenicity with *S. Typhimurium* and *S. Enteritidis* conjugates of *Salmonella* flagellin compared with flagellin alone [79, 87].

Outer membrane proteins (OMPs) constitute the main alternative subunit approach for *Salmonella* vaccine development. The NTS surface proteins that have received most attention have been flagellin and porins OmpC, F and D. In preclinical studies, these antigens showed to successfully protect mice against *Salmonella* challenge [79, 87, 88]. OmpC and OmpF induce long-lasting antibody responses in mice [111] and have been found to be safe and immunogenic when tested in a Phase 1 study in man [110, 112]. However, manufacturing processes in purifying and producing outer membrane proteins are quite complicated. It may be crucial to preserve the correct conformation of these antigens and failure of recombinant *Salmonella* porins to protect mice has been reported [113]. Flagellin and porins, with high level of homology between serovars, have been linked to OAg and conjugates have shown high immune response.

An innovative strategy for the development of a vaccine against iNTS is represented by Generalized Modules for Membrane Antigens (GMMA) technology [114]. GMMA are small outer membrane vesicles-like blebs (40-200 nm diameter) spontaneously released by Gram-negative bacteria mutated to increase blebbing. Multiple surface antigens are presented to the immune system in the context of a membrane, in their native conformation. GMMA are also self-adjuvants, delivering

innate signals through TLR ligands and other pathogen-associated molecular patterns (PAMPs). Unlike the case with live attenuated vaccines, there is no possibility of infection. *Salmonella* GMMA remain to be evaluated in humans, but *Shigella sonnei* GMMA have shown to be safe and immunogenic in Phase 1 trials in adults [115, 116]. GMMA are produced through a simple and low cost process, that make this technology particularly suited for the development of vaccines for low- and middle-income countries, where the cost of production is a key consideration [69, 70].

### **1.7 Development of a vaccine against iNTS in GVGH**

GSK Vaccines Institute for Global Health (GVGH) [117] is working at the development of a vaccine against iNTS [25, 32]. Two approaches, both OAg-based, have been evaluated. The first approach is based on glycoconjugation, where *S. Typhimurium* and *S. Enteritidis* OAg are independently linked to CRM<sub>197</sub> as carrier protein. The second approach is represented by the development of a bivalent formulation of *S. Typhimurium* and *S. Enteritidis* GMMA.

#### **1.7.1 OAg-CRM<sub>197</sub> conjugate vaccines**

GVGH has developed a simplified method for OAg extraction and purification [118]. In the adopted strategy, the labile linkage between the KDO of the core region and the lipid A is cleaved directly in the bacterial growth medium by acetic acid hydrolysis. The OAg, still linked to the core oligosaccharide, is then easily purified from the cells and used for the production of conjugate vaccines. In this way, LPS purification from bacterial membranes, a very time consuming process that makes use of hazardous chemicals, is avoided. The conjugation approach used involves the terminal KDO sugar, without affecting the OAg sugar chain [106] (Fig. 5).

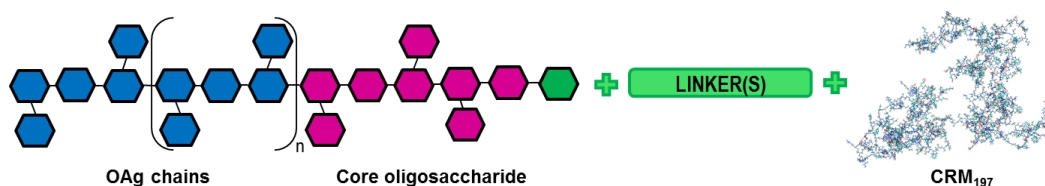


**Fig. 5.** Glycoconjugation technology for the synthesis of OAg-CRM<sub>197</sub> conjugates developed in GVGH.

Different *S. Typhimurium* and *S. Enteritidis* strains, as source of OAg, were screened to identify the most suitable and appropriate strains for large scale OAg production and generation of conjugates [119]. It was found that OAg structural characteristics, such as chain length, *O*-acetylation and glucosylation level and position can affect the immunogenicity of corresponding glycoconjugate vaccines [77] as well as OAg/carrier protein ratios, conjugation chemistry involved [107, 120] and glycosylation sites in which the carrier protein is attached to the OAg [121].

### 1.7.2 GMMA vaccines

GMMA are naturally released from the surface of NTS bacteria, but the natural shedding is too low to be useful for vaccine production (Fig. 6).

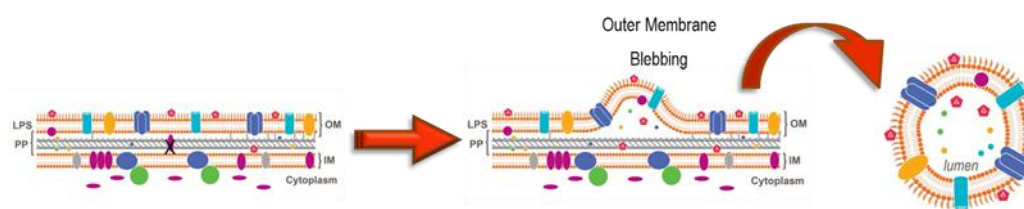


**Fig. 6.** Schematic representation of GMMA blebbing from the outer membrane of Gram-negative bacteria.

NTS parent strains have been genetically modified to increase shedding [114, 122]. Additional genetic modifications have been introduced into *S. Typhimurium* and *S.*



Enteritidis parent strains to reduce lipid A toxicity [123, 124]. Several mutated NTS strains have been tested to identify the most suitable GMMA producers.

### **1.8 Description of research aims**

In the context of the development of a bivalent vaccine against iNTS, this project had three main objectives:

- 1) full characterization of the OAg component of GMMA produced by mutated strains of *S. Typhimurium* and *S. Enteritidis* to verify the impact that mutations introduced to increase GMMA production and reduce reactogenicity can have on the key target antigen for inducing an immune response against iNTS;
- 2) determination of the particle size distribution of NTS GMMA, by use of different techniques suitable for size measurements;
- 3) investigation on the presence and the structure of the terminal KDO unit at the reducing end of the OAg chain after direct extraction on bacteria and study of its reactivity and selectivity in the synthesis of OAg-CRM<sub>197</sub> glycoconjugate vaccines.

All these objectives have as main targets the improvement of technologies for the production and the development of analytical methods for the characterization of vaccines against iNTS.



**2. Characterization of OAg delivered by Generalized Modules  
for Membrane Antigens (GMMA) vaccine candidates against  
iNTS**



## 2.1 Introduction

*Salmonella enterica* Typhimurium and Enteritidis are the most common serovars responsible for invasive nontyphoidal *Salmonella* disease (iNTS) in Africa [21, 22, 26, 31, 32], resulting in case-fatality rates of around 20% [36]. iNTS is closely associated with malaria and malnutrition among African infants and children and with HIV infection in all age groups [14]. Antibiotics are not always available in rural African settings, and increasing levels of multidrug-resistance are limiting their effectiveness [34, 67, 68], making this disease a high priority for vaccine development. Currently, there are no licensed vaccines against iNTS and efforts are ongoing to identify protective antigens and best strategies for vaccine development [25, 28, 32].

Antibodies directed against the OAg portion of *Salmonella* LPS have been shown to be able to mediate killing [76-78, 125, 126] and protect against infection in animal models [77, 78, 80]. *S. Typhimurium* and *S. Enteritidis* OAg share a common backbone consisting of mannose (Man), rhamnose (Rha) and galactose (Gal), which serologically constitutes epitope O:12 [127]. A different 3,6-dideoxy-hexose residue is linked to Man in these two serovars: abequeose (Abe), conferring O:4 specificity to *S. Typhimurium* or tyvelose (Tyv), conferring O:9 specificity to *S. Enteritidis* [128, 129] (Fig. 7).

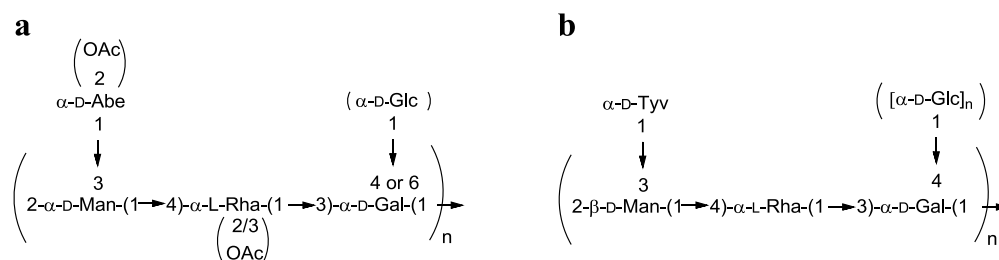


**Fig. 7.** OAg repeating unit structure of (a) *S. Typhimurium* (O:4,5) and (b) *S. Enteritidis* (O:9) [128, 129].



*Salmonella* OAg can demonstrate high levels of heterogeneity in terms of chain length and variation in *O*-acetylation and glucosylation of the repeating units [77, 119, 130-132]. For *S. Typhimurium*, Abe may be *O*-acetylated at position C-2, which adds O:5 specificity [133]. The additional presence of *O*-acetyl groups at C-2 and C-3 of Rha has also been reported [130, 131, 134]. OAg chains can also be variably glucosylated, with glucose (Glc) linked at C-4 (O:12<sub>2</sub> specificity) or C-6 (O:1 specificity) to Gal [130, 135]. Studies in mice indicated that all these structural modifications can impact the immunogenicity of the corresponding glycoconjugate vaccines [77, 119].

GVGH is investigating the Generalized Modules for Membrane Antigens (GMMA) [114] approach for the development of a bivalent vaccine against *S. Typhimurium* and *S. Enteritidis* [124]. In *Salmonella*, deletion of the *tolR* gene has been used to increase blebbing. Such mutation affects the stability of the linkage between the inner and the outer membrane, and results in an enhanced shedding process [114, 115, 122-124]. GMMA derived from the surface of Gram-negative bacteria contain potent immunostimulatory components, such as lipoproteins and LPS, which can contribute to their immunogenicity, but also to reactogenicity [136, 137]. In GMMA vaccine development, removal or modification of such components may alter the balance between reactogenicity and immunogenicity. One way of detoxifying LPS, the most abundant immunostimulatory component on GMMA, is to modify its acylation pathway, for example by deletion of *msbB*, *pagP* and *htrB* genes [115, 123, 124]. A lipid A with a decreased number of fatty acid chains bound through ester and amide linkages at the sugar component of LPS resulted in a substantially reduced ability of NTS GMMA to stimulate cytokine release from human peripheral blood monocytes (PBMC) [123, 124]. Deletions of genes encoding the late acyltransferase enzymes *msbB*, *pagP*, and *htrB* result in the removal of acyl groups from the wild type mixture of hexa- and hepta-acylated lipid A, obtaining a pure penta-acylated lipid A. A strongly reduced stimulation of human Toll-like receptor 2 (TLR2) and 4 (TLR4) was showed by GMMA of  $\Delta msbB$  and  $\Delta pagP$  mutants *S. Enteritidis* and *S. Typhimurium* [124]. The steps of removal of acyl chains and consequent reduced reactogenicity applied to *Salmonella* were different with



respect to other *Enterobacteriaceae* genus members like *Shigella* [138]. *Salmonella* wild type lipid A is constituted by a mixture of hepta- and hexa-acylated lipid A molecules (Fig. 8-a). The enzyme involved in the production of hepta-acylated lipid A is the acyltransferase *pagP*, which transfers a palmitoyl (C16:0) chain in the secondary position of the hydroxymyristate chain at position 2 in the classical wild type hexa-acylated lipid A [139]. Acyl transferase *msbB* [140, 141] transfers a secondary myristoyl (C14:0) chain in position 2' and deletion of its encoding gene in both *S. Enteritidis* and *S. Typhimurium* resulted in a mixture of penta-acylated and hexa-acylated lipid A molecules (Fig. 8-b). After the deletion of the *pagP* gene in the *msbB* mutant, a pure penta-acylated lipid A in line with lack of palmitoylation due to the absence of *pagP* was obtained (Fig. 8-c). Acyl transferase *htrB* [142], which transfers a secondary lauroyl (C12:0) chain in position 3', was deleted either in *S. Enteritidis* and *S. Typhimurium* and resulted in a variety of lipid A forms (Fig. 8-d). A mixture of penta-acylated lipid A species lacking the lauroyl chain from the wild type lipid A were observed, together with a pleiotropic effect, resulting in the replacement of the lauroyl chain with a palmitoleoyl chain. Thus  $\Delta htrB$  mutants, in addition to the presence of penta-acylation, were also characterized by a mixture of hexa- and hepta-acylated species with the compensatory presence of palmitoleoyl chains respect to the hexa- and hepta-acylated wild type lipid A.

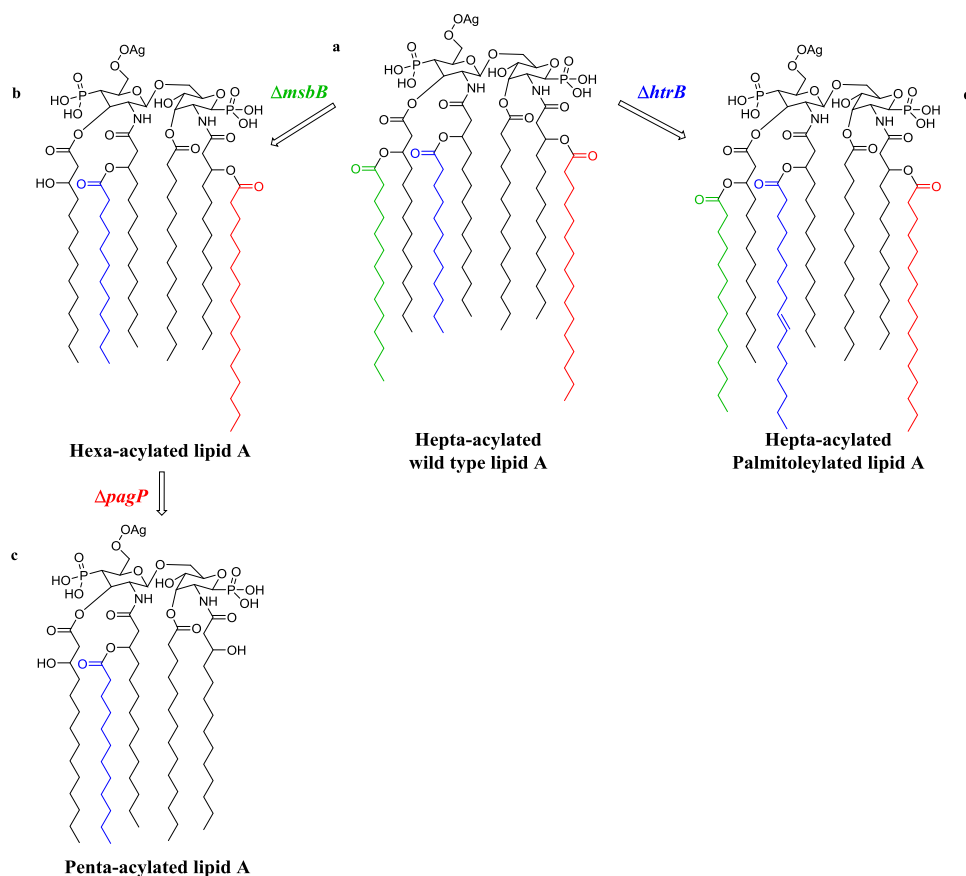


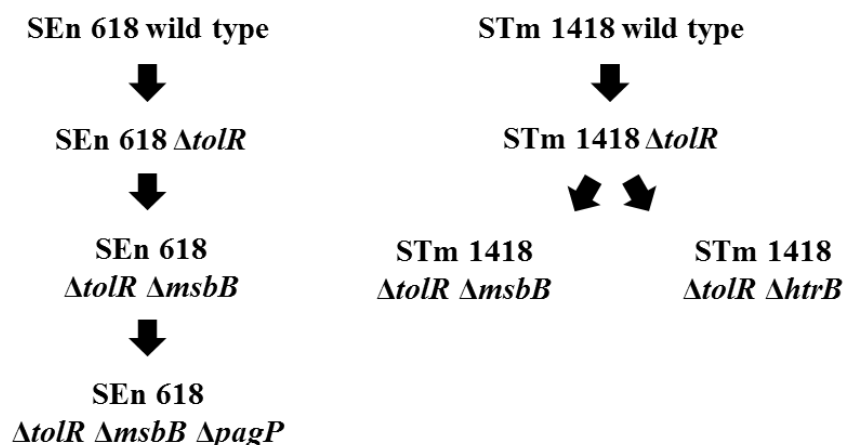
**Fig. 8.** *Salmonella* lipid A structures obtained after deletion of *msbB* (b), *pagP* (c), and *htrB* (d) gene deletions to the wild type lipid A (a).

Genetic mutations introduced in *S. Typhimurium* and *S. Enteritidis* strains to increase GMMA release and decrease reactogenicity could impact the expression of OAg chains, as well as result in changes of OAg structure. In this chapter, a panel of analytical methods was put in place for GMMA characterization, with particular attention to the OAg component. GMMA produced from different mutated strains were fully characterized and were tested in mice, with the aim to evaluate how mutations introduced can impact on OAg structure and GMMA immune response.

## 2.2 Materials and Methods

### 2.2.1 NTS parent strains for GMMA production

*Salmonella enterica* serovar Enteritidis SA618 (SEn 618) (CEESA EASSA II collection [143] of Quotient Bioresearch Limited) and Typhimurium isolate SGSC1418 (STm 1418) (LT-2 collection [144], University of Calgary), both isolated from animals, were chosen as parent strains [119]. Mutants (Scheme 1) were generated by GVGH staff as described by Rossi *et al.* [124].



**Scheme 1.** GMMA of *S. Enteritidis* and *S. Typhimurium* mutated strains chosen for characterization [124].

To generate mutants, the kanamycin resistance gene *aph* was used to replace the *tolR* gene, the chloramphenicol resistance gene *cat* was used to replace the *htrB* and *pagP* coding sequences, and the tetracycline resistance cassette *tetRA* was used to replace the *msbB* gene. The desired resistance cassette replacement constructs were amplified using forward and reverse primers composed of approximately 50 bp homologous to the flanking regions of the gene to be deleted and approximately 20 bp at the 3' end matching the flanking region of the respective resistance gene. Approximately 2  $\mu$ g of linear PCR product (purified using PCR purification Qiagen kit following manufacturer recommendations) were used for integration onto the chromosome of recombination-prone *Salmonella* recipient cells by following methods described previously [114, 145]. A modification of the lambda red method was used (pBAD $\lambda$ red induced with 0.2% arabinose, for preparation of electro competent cells).

### 2.2.2 GMMA production and characterization

GMMA were produced and purified as described [124]. Bacterial strains were routinely grown at 30 °C in liquid or on solid Luria-Bertani medium without salt (LBON). For GMMA production, overnight cultures were grown in the presence of the selective antibiotics, e.g., kanamycin (30 µg/mL), chloramphenicol (20 µg/mL), or tetracycline (20 µg/mL), and were used to inoculate the production medium (without antibiotics) to an optical density (OD) at 600 nm of 0.03 to 0.05. Production cultures were incubated at 30 °C and 200 rpm overnight. Culture supernatants were collected by centrifugation for 10 min at 5,000 x g, followed by 0.22 µm filtration. GMMA were concentrated using an Amicon stirrer cell with a regenerated cellulose filter with a nominal molecular size limit of 100 kDa (Amicon Ultracell) under a nitrogen flow, or a TFF (cut off 100 kDa) was performed. The retentate was collected in 70-mL propylene ultracentrifuge tubes (Beckman Coulter) and was ultracentrifuged at 186,000 x g for 2 h at 4 °C using a Ti rotor (Beckman Coulter). Additionally, S110-AT 2121 (100000 rpm, 30 min, 4 °C) or S50-A 2109 (50000 rpm, 1 h, 4 °C) rotors on a Sorvall MX Plus Micro-Ultracentrifuge (Thermo Fisher) were used. Pellets were suspended in phosphate-buffered saline (PBS), followed by 0.22 µm filtration. GMMA were stored at 4 °C.

GMMA samples were analysed by HPLC-SEC with Sepax SRT-C 2000-1000 columns in series equilibrated in PBS and with in-line UV, fluorescence emission, dRI and MALS detectors. A volume of 80 µL of samples with a concentration of 100 µg/mL protein content was injected and eluted with a flow rate of 0.5 mL/min. MALS data were collected and analysed using ASTRA 6 software (Wyatt Technology).

GMMA quantities were expressed as the total protein content present in GMMA quantified using the Detergent Compatible (DC) protein assay (Bio-Rad), which is based on the Lowry assay [146, 147]. A 2 mg/mL solution of serum bovine albumin (BSA) was used to create a calibration curve in the 9.0 to 60.0 µg/mL range. Samples were diluted with phosphate buffered saline (PBS, 140 mM NaCl, 2.7 mM KCl, 20 mM (PO<sub>4</sub>)<sup>3-</sup>) in order to obtain sample protein concentration in the range of the calibration curve. Samples and calibration curves were created in duplicates and to a



final volume of 400  $\mu$ L. CTC solution was prepared mixing 3 mL of 0.4% potassium tartrate/0.2% cupric sulphate solution and 3 mL of 20% sodium carbonate solution. Folin reactive was prepared mixing 1 mL of Folin Ciocalteus solution and 5 mL of MilliQ water. Reagent A was prepared just before use. A volume of 400  $\mu$ L of Reagent A (6 mL CTC solution + 6 mL SDS 10% + 6 mL 0.8 N NaOH + 6 mL MilliQ water) were added to each samples. Samples were vortexed and added of 200  $\mu$ L of Folin Reactive. Samples were incubated for 75 minute at room temperature (RT). Samples were analysed using a spectrophotometer and absorbance was measured at 750 nm.

OAg sugar content was quantified by High-Performance Anion-Exchange Chromatography coupled to Pulsed Amperometric Detector (HPAEC-PAD) [106, 130], after performing acid hydrolysis directly on GMMA. GMMA components did not interfere in the quantification of the OAg sugar monomers. Rha, Gal, Glc, and Man, each occurring once in the OAg chain repeating unit, and *N*-acetyl glucosamine (GlcNAc), a sugar uniquely present in the core oligosaccharide region, were estimated by HPAEC-PAD after acid hydrolysis of the OAg to release the monosaccharides. Commercial monomer sugars were used for building the calibration curves. For Rha, Gal, Glc, Man and GlcNAc quantification, OAg samples, diluted to have each sugar monomer in the range 0.5-10  $\mu$ g/mL, were hydrolysed at 100 °C for 4 h in 2 M trifluoroacetic acid (TFA). This hydrolysis condition was optimal for release of all monomers without their degradation. For GlcNAc quantification, OAg samples, diluted to have a GlcNAc concentration in the range 0.5-10  $\mu$ g/mL, were hydrolysed at 100 °C for 6 h in 1 M TFA. After the hydrolysis, samples were chilled at 2-8 °C for about 30 min, dried by SpeedVac overnight, reconstituted in MilliQ water, and filtered using 0.45- $\mu$ m Acrodisc (PALL) filters before chromatographic analysis. HPAEC-PAD was performed with a Dionex ICS3000 equipped with a CarboPac PA10 column (4 x 250 mm) coupled with a PA10 guard column (4 x 50 mm). Separation of the sugars was performed with a flow rate of 1 mL/min, eluting in a gradient from 10 to 18 mM NaOH over 20 min. After being washed for 20 min with 100 mM AcONa in 28 mM NaOH, the column was re-equilibrated with 10 mM NaOH for 20 min. The effluent was monitored using an electrochemical detector in





the pulsed amperometric mode with a gold working electrode and an Ag/AgCl reference electrode. The Dionex standard quadruple-potential waveform for carbohydrates was used. The resulting chromatographic data were processed using Chromeleon software 6.8. Calibration curves were built for each sugar monomer (0.5-10 µg/mL). The standards were hydrolysed and analysed in the same way as samples. For GlcNAc, glucosamine was the species detected by HPAEC-PAD after hydrolysis.

The amount of core oligosaccharide reducing end unit, KDO (2-keto-3-deoxy-octonate) was assumed equal to the amount of lipid A and quantified by semicarbazide/High Performance Liquid Chromatography - Size Exclusion Chromatography (HPLC-SEC) method after sugar extraction [130]. OAg samples were analysed by HPLC-SEC after derivatization with semicarbazide to quantify  $\alpha$ -ketoacid present at the reducing end. This reaction was performed as a slight modification of the semicarbazide assay for  $\alpha$ -ketoacid determination [148]. OAg samples and KDO standards (100 µL of total volume in water), with a C=O concentration between 15.7 and 156.7 nmol/mL, were added to 100 µL of semicarbazide solution (100 mg semicarbazide hydrochloride + 90.5 mg of sodium acetate anhydrous in 10 mL of MilliQ water). Sample blanks were prepared by adding 100 µL of sodium acetate (90.5 mg of sodium acetate anhydrous in 10 mL of MilliQ water) to 100 µL of the OAg samples at the same concentration used for the analysis. All samples and standards were heated at 50 °C for 50 min and then analysed by HPLC-SEC (80 µL injected), on a TSK gel G3000 PWXL column with guard column in 0.1 M NaCl, 0.1 M NaH<sub>2</sub>PO<sub>4</sub>, 5% CH<sub>3</sub>CN, pH 7.2, mobile phase at the flow rate of 0.5 mL/min (isocratic method for 30 min). Detection was done at 252 nm. The peak area corresponding to OAg after derivatization with semicarbazide was corrected by subtracting the area of the corresponding blank. The amount of KDO was calculated using the calibration curve built with the peak areas of derivatized KDO standard at 252 nm. The percentage of OAg chains was calculated as the molar ratio of their KDO divided by total KDO, including low molecular mass LPS molecules, including those containing only the core oligosaccharide without OAg repeating units.

NMR analysis on the liquid state was performed to confirm the identity of the OAg samples by detecting typical signals of the OAg chain, confirming the presence of the





characteristic sugars, as well as for calculating the molar ratio of Tyv or Abe to Rha, by comparing the integrals of the two peaks corresponding to Tyv or Abe H-6 and Rha H-6 [130]. Dried OAg samples (2.5 mg total sugar) were solubilized in 650  $\mu$ L deuterated water ( $D_2O$ , Sigma-Aldrich) and transferred to 5-mm NMR tubes. Proton NMR experiments were recorded at 25 °C on a Varian VNMR5-500 spectrometer, equipped with a Pentaprobe. Acquisition time of 5 s, relaxation delay of 15 s, and number of scans of 64 were set for recording the spectra. For data acquisition and processing VNMRJ version 2.2 revision C and Mestrenova 6.1 (Mestrelab Research) were used, respectively. One-dimensional proton NMR spectra were collected using a standard one-pulse experiment. Chemical shifts were referenced to hydrogen deuterium oxide (HDO) at 4.768 ppm ( $^1H$ ). De-*O*-acetylation was performed by addition of sodium deuterioxide (NaOD, Sigma-Aldrich) to the tube containing the sample in  $D_2O$ .

Lipid A structures were investigated by Matrix-Assisted Laser Desorption/Ionization-Mass Spectrometry (MALDI-MS) [124].

Protein pattern profile was analysed by Sodium dodecyl sulphate-polyacrylamide gel electrophoresis (SDS-PAGE) analysis. GMMA samples were analysed using 10% Bis-Tris gel (NuPAGE, Invitrogen). Samples (5 and 10  $\mu$ g GMMA protein) were mixed with 0.5 M dithiothreitol (1/5 v/v), NuPAGE LDS sample buffer (1/5 v/v) and heated at 100 °C for 10 min. The gel, containing loaded samples, was electrophoresed at 80 mA in NuPAGE MOPS SDS running buffer (20x, Invitrogen) and stained with Brilliant Blue G - Colloidal Concentrate, Electrophoresis Reagent (Sigma).

### 2.2.3 OAg purification and characterization

OAg extraction and purification from wild type bacteria was performed as previously described [118]. For extraction of the OAg from GMMA, a similar procedure was used: mild acid hydrolysis (v/v 2% acetic acid at 100 °C for 1 h) was performed directly on the GMMA suspension (protein concentration of 1 mg/mL) to cleave the acid-labile KDO-lipid A linkage. The OAg chains released into the supernatant were recovered after centrifugation (14000 rpm, 1 h, 4 °C). The acidic



supernatant was evaporated under reduced pressure and washed 3 times with water, in order to remove the residual acetic acid, and then freeze-dried. Gel filtration chromatography with differential refractive index (dRI, WGE Dr. Bures  $\Delta n$ -1000, Labservice Analytica) detection was used to fractionate the OAg chains obtained after extraction from GMMA. Samples were separated on Sephacryl S-300 column (90 cm x 1.6 cm i.d., GE Healthcare Life Sciences). The mobile phase was  $\text{NaNO}_3$  0.05 M at the flow rate of 8 mL/h. Fractions from Sephacryl S-300 were collected at 15 min intervals and were desalted by gel filtration chromatography on Biogel P-2 column (90 cm x 1.6 cm i.d., flow rate 8 mL/h, Bio-Rad) or on a Bioline preparative chromatographic system equipped with Superdex 30 Prep Grade column (90 cm x 1.0 cm i.d., flow rate 1.5 mL/min, GE Healthcare Life Sciences) and dRI (Smartline 2300, Knauer). OAg structural analysis on OAg populations purified following gel filtration chromatography was performed as reported in the previous paragraph by HPAEC-PAD, HPLC-SEC after derivatization with semicarbazide,  $^1\text{H}$  NMR and phenol sulphuric acid assay.

Sugar composition analysis of OAg either from SEn 618 and STm wild type strains and GMMA produced by SEn 618 and STm 1418 mutants was also performed by gas liquid chromatography (GLC), after hydrolysis of the polysaccharides with 2 M TFA at 125 °C for 1 h, and derivatization to alditol acetates [149]. The sugar linkage positions were determined by GLC coupled to mass spectrometry (GLC-MS) after per-methylation of the samples, hydrolysis with 2 M TFA at 125 °C for 1 h, followed by reduction and per-acetylation to obtain the partially methylated alditol acetates (PMAA) derivatives [150]. Peak areas were corrected by using the effective carbon response factors [151]; for Tyv and the response factor of 6-deoxy hexose were applied. Determination of the absolute configuration of the sugar residues of OAg samples was performed as described by Gerwig *et al* [152]. Trimethylsilylated (+)-2-butyl methyl glycosides were obtained by derivatization with the reagent Sylon<sup>TM</sup> HTP (Sigma) after methanolysis of the polysaccharide with 2 M HCl in methanol at 85 °C for 16 h and after butanolysis in 1 M HCl in S-(+)-2-butanol for 16 hr at 80 °C. In order to determine the position of the *O*-acetyl groups, the *O*-polysaccharides were per-methylated following the method of Prehm [153], which



leaves the *O*-acetyl groups in their native positions. Samples were then treated as above to obtain the PMAA derivatives, which were then analysed by GLC and GLC-MS. Analytical GLC was performed on a Perkin Elmer Autosystem XL gas chromatograph equipped with a flame ionization detector (FID) and a SP2330 capillary column (Supelco, 30 m), using He as carrier gas. The following temperature programs were used: for alditol acetates, 200 °C 1 min, 200-245 °C at 4 °C/min; for PMAA on SP2330 column, 150-245 °C at 2 °C/min and on HP-1 column (Agilent J&W, 30 m), 150-245 °C at 2 °C/min. Separation of the Trimethylsilylated (+)-2-butyl glycosides, for determining the absolute configuration of the sugars, was obtained on a HP-1 column, using the following temperature program: 50 °C 1 min, 50-130 °C at 45 °C/min, hold 1 min, 130-200 °C at 1 °C/min, hold 10 min. GLC-MS analyses were carried out on an Agilent Technologies 7890A gas chromatograph coupled to an Agilent Technologies 5975C VL MSD. The following temperature programs were used: for PMAA on SP2330 column, 150 °C for 2', 150-250 °C at 2 °C/min, at 245 °C for 20' and on HP-1 column, 140 °C for 1', 140-280 °C at 5°C/min, at 280 °C for 30'.

OAg peak molecular weight (MW) was calculated after HPLC-SEC analysis and using a calibration curve obtained with standard dextrans (12-150 kDa) having different peak MW on TSK gel G3000 PWXL column (30 cm x 7.8 mm; particle size 7 µm, Tosoh Bioscience) and with in-line dRI detector. A volume of 80 µL of samples with a concentration of 100 µg/mL polysaccharide content was injected and eluted at the flow rate of 0.5 mL/min with 0.1 NaCl, 0.1 NaH<sub>2</sub>PO<sub>4</sub>, 5% CH<sub>3</sub>CN, pH 7.2 as mobile phase.

#### **2.2.4. Immunogenicity of candidate *Salmonella* GMMA vaccines in mice and serological analysis**

Five groups of eight 5-weeks old female CD1 mice were purchased from Charles River Laboratory and maintained at GSK Vaccines Animal Care Facility. Mice received two subcutaneous immunizations at 28 days interval with 200 µL/dose of 1 µg of OAg formulated with Alhydrogel (final concentration 0.7 mg/mL Al<sup>3+</sup>). Mice



were bled before the first immunization (sera pooled for each group at day 0) and at days 14, 28 and 42 after the first immunization (collected as single sera). All animal protocols were approved by the local animal ethical committee (approval N. AEC201309) and by the Italian Minister of Health in accordance with Italian law and immunizations and bleeds were done by GSK Animal Care Facility. Individual mouse sera, collected at each time point, were tested for anti-OAg IgG antibody titers by ELISA by the GVGH Immunoassay Unit, as described by Lanzilao *et al* [119]. For each group, equal volumes of sera collected at day 42 from each mouse were pooled and tested for serum bactericidal activity (SBA) against *S. Typhimurium* D23580, an endemic clinical isolate from Malawi [67, 125], obtained from the Malawi-Liverpool-Wellcome Trust Clinical Research Programme, Blantyre, Malawi, or against the laboratory strain *S. Enteritidis* CMCC4314, (corresponding to ATCC4931) obtained from the Novartis Master Culture Collection (NMCC), as previously described [119].

Bactericidal activity was determined by the GVGH Immunoassay Unit as serum dilutions necessary to obtain 50% colony forming units (CFU) reduction after 3 hours incubation at 37 °C, compared with CFU counted at time 0. To evaluate possible nonspecific inhibitory effects of baby rabbit complement (BRC) or mouse serum, bacteria were also incubated with SBA buffer and active BRC as negative control, and with pooled sera from a control placebo group diluted at the same dilutions of test sera (starting from 1:100) with active BRC. For all negative controls killing effect was not observed up to the highest serum concentration tested of 1:100 (assay's baseline).

Statistical and graphical analysis was performed using GraphPad Prism 6 software. The non-parametric Mann-Whitney test (two-tailed) and Kruskal-Wallis analysis with Dunn's test for post hoc analysis were used to compare two or multiple groups, respectively. Response at day 14 and 42 for each group was compared by Wilcoxon matched-pairs signed rank test (two-tailed).

### 2.3 Results

As part of a previous work carried out at GVGH, several different *S. Typhimurium* and *S. Enteritidis* isolates were screened as sources of OAg for use in a bivalent

glycoconjugate vaccine against iNTS [119]. Based on the results obtained, SEn 618 and STm 1418 strains were selected for use as GMMA-producing strains. They were genetically modified through deletion of *tolR* gene for GMMA overproduction and of further genes ( $\Delta msbB$ ,  $\Delta htrB$  and  $\Delta pagP$ ) to reduce reactogenicity [124]. Some of the resulting GMMA (Scheme 1) were fully characterized and tested in mice. Interleukine-6 (IL-6) release was used as an indicator for proinflammatory responses to Toll-like receptors (TLR) stimulation. The combination of  $\Delta msbB$  and  $\Delta pagP$  mutations provoked the least stimulation of cytokine release from human PBMC compared to GMMA with wild type lipid A. The residual activity was largely due to TLR2 activation, although GMMA significantly signalled through TLR4 [124].

### 2.3.1 OAg characterization of SEn 618 wild type bacteria

OAg from SEn 618 wild type bacteria was fully characterized and used as reference structure for comparison with OAg present on GMMA obtained from genetically modified GMMA-producing strains, in order to examine how mutations impacted on structural features. SEn 618 OAg exhibited high levels of purity, with protein and nucleic acid content <1% (w/w respect to sugar content) and endotoxin level <0.1 EU/ $\mu$ g of sugar, indicating complete removal of the lipid A. The OAg was characterized by one main population with average MW of 29.6 kDa. Based on the average number of repeating units (RU) and the mass contribution from *O*-acetylation, the average MW was 18.9 kDa. The average number of RU was determined from the molar ratio of Rha (OAg chains sugar) and GlcNAc (core region sugar) from sugar composition analysis by HPAEC-PAD, the level of *O*-acetylation was determined by  $^1\text{H}$  NMR analysis.

Composition analysis by HPAEC-PAD revealed the presence of Rha, Gal, and Man, the sugars constituting the backbone of the OAg chain, in a ratio 1:1:1, while a glucosylation level of 0.19 was found. This composition was confirmed by GLC analysis of the alditol acetates derivatives [149] (Table 1). In the absence of a monomer standard, Tyv was identified by GLC-MS and quantified by  $^1\text{H}$  NMR which yielded the expected molar ratio of 1:1 with respect to Rha.

**Table 1.** Sugar composition of SEn 618 wild type OAg by GLC and by HPAEC-PAD.

Residues	Molar ratios	
	by GLC	by HPAEC-PAD
<b>Rha</b>	1.00	1.00
<b>Man</b>	1.05	1.00
<b>Gal</b>	1.04	1.08
<b>Glc</b>	0.21	0.19

The linkage positions for the constituent sugars of the OAg sample were determined by GLC and GLC-MS of the partially-methylated alditol acetate (PMAA) derivatives [150] (Table 2). As expected [129], the OAg chain contained terminal non-reducing 3,6-dideoxyhexose (t-Tyv), 4-linked Rha (4-Rha), 3-linked galactose (3-Gal), 2,3-linked mannose (2,3-Man). As it was seen in other *Salmonella* strains analysed [130], the most intense signal of 4-Rha overlapped with the signal arising from terminal non-reducing glucose (t-Glc). The analysis of the PMAA derivatives on a non-polar column (HP-1, Agilent J&W, 30 m) allowed identification of a small amount of t-Glc. In addition, a similar small amount of 4-linked glucose (4-Glc) was found, indicating that short Glc chains can be linked to Gal, as reported for *S. Enteritidis* OAg [129].

**Table 2.** Glycosidic linkages in SEn 618 wild type OAg obtained by GLC-MS of PMAA derivatives on HP-1 column.

OAg monosaccharides	t-Tyv	4-Rha	t-Glc	4-Glc	3-Gal	3,4-Gal*	2,3-Man
<b>Molar ratios</b>	0.26	1.00	0.08	0.05	0.93	0.12	1.04

\*GLC on SP2330 column (Not integrable in HP-1 chromatogram).

In order to determine the position of *O*-acetyl groups detected in the  $^1\text{H}$  NMR spectrum, the OAg was permethylated following the procedure reported by Prehm [153], which allows the retention of the *O*-acetyl groups in their native positions. Analysis of the corresponding PMAA derivatives was performed by GLC and GLC-

MS. Comparing the chromatograms of the PMAA obtained with (Fig. 9-A) and without (Fig. 9-B) retention of the *O*-acetyl groups, a small amount of 2,4-Rha was present, in addition to the expected 4-Rha, indicating partial esterification with acetyl substituents of the 4-linked Rha on C-2 (data from GLC on SP2330 column, Supelco, 30 m).

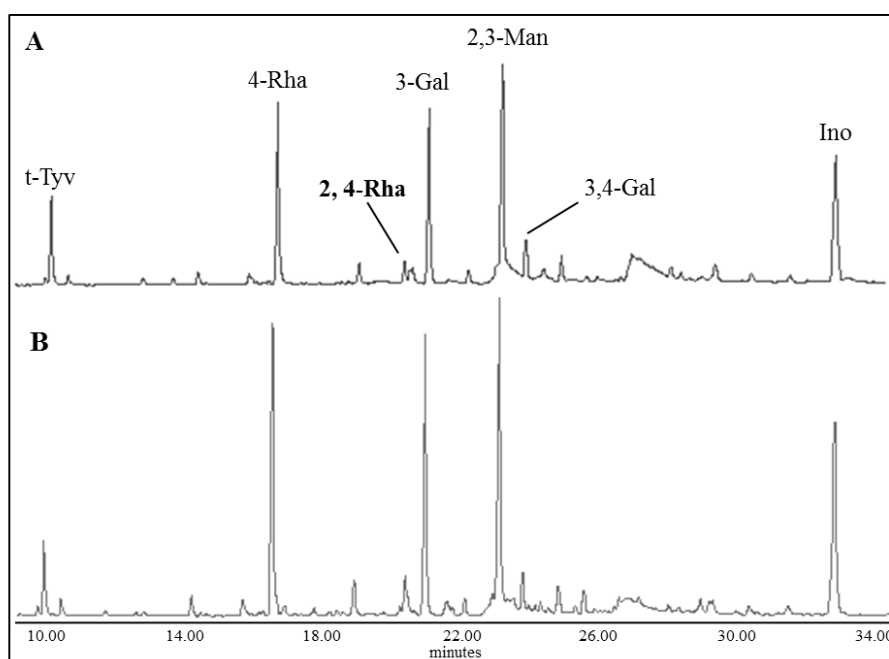


**Fig. 9.** Comparison of GLC chromatograms of the PMAA derivatives obtained with (A) and without (B) retention of the native *O*-acetylation positions. The numbers indicate the position of glycosidic linkages. Major peak assignments are reported and the acetylated residue is reported in bold.

Analysis of the OAg by  $^1\text{H}$  NMR (Fig. 10) showed two singlets at 2.16 and 2.20 ppm designed as *O*-acetyl groups after treatment with NaOD 200 mM, with an *O*-acetylation level close to 16%. By comparison with OAg from *S. Typhimurium* D23580 [130], it is possible to assign the two methyl signals of *O*-acetyl groups on C-2 and C-3 of Rha. Anomeric protons were assigned after inspection of the COSY and TOCSY plots (data not shown).



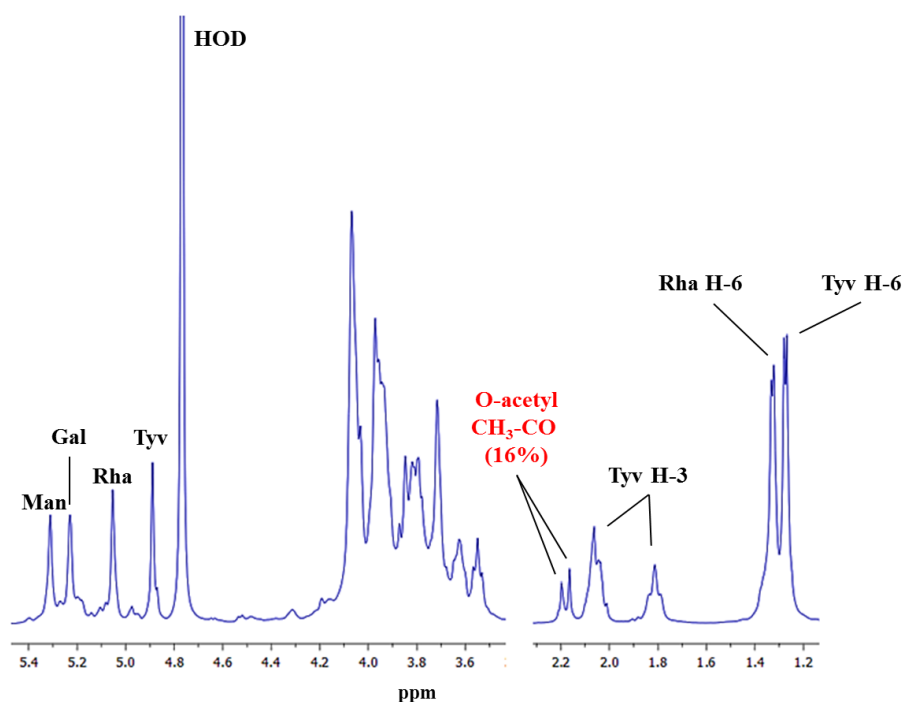


**Fig. 10.**  $^1\text{H}$  NMR spectrum of the OAg purified from *S. Enteritidis* 618 wild type, with emphasis on the *O*-acetyl groups identified.

GLC analysis of the chiral glycosides of the OAg sample showed that the hexoses were in the D absolute configuration and Rha in the L absolute configuration. This analysis could not be performed for Tyv due to the lack of a standard.

All results obtained are consistent with the structure previously reported for *S. Enteritidis* OAg [129] (Fig. 1).

### 2.3.2 OAg characterization of SEn 618 GMMA

After the complete characterization of the OAg extracted from SEn 618 wild type, the structure of OAg chains present on the surface of GMMA produced by the mutated strains of SEn 618 were investigated. HPLC-SEC fluorescence emission profile of GMMA samples from all mutated strains revealed very low residual soluble proteins (< 5%), indicating good sample purity (Fig. 11).



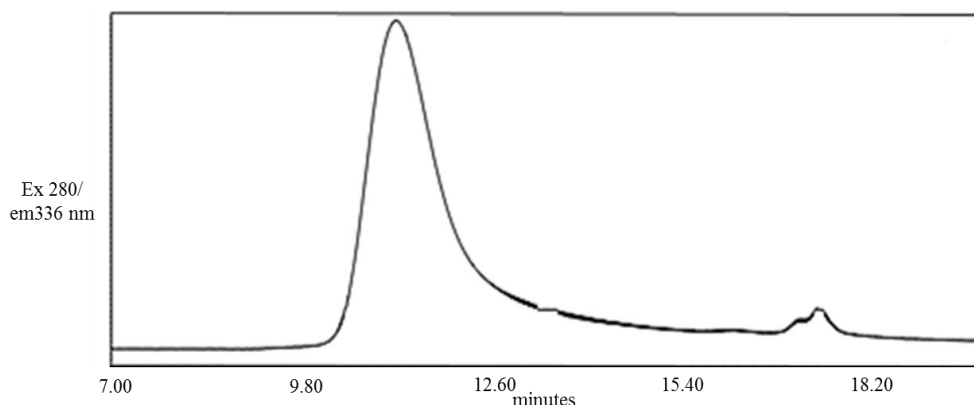


**Fig. 11.** HPLC-SEC chromatogram of GMMA from SEn 618  $\Delta tolR$  strain (fluorescence emission profile; Sepax SRT-C 2000-1000 columns; PBS; 0.5 mL/min; 80  $\mu$ L injected of GMMA 100  $\mu$ g/mL protein content;  $V_0$  8.992 min;  $V_{tot}$  17.033 min).

The particle size of GMMA from SEn 618 mutated strains was similar, as estimated by HPLC-SEC analysis coupled with MALS detector (Table 3). The w/w ratio of OAg chains per mg of total protein was high for all SEn 618 GMMA. OAg chains constituted a low percentage of total LPS molecules containing core oligosaccharide, indicating that a large proportion of LPS molecules contain very few or no OAg repeating units (Table 3).

**Table 3.** Characterization of GMMA from SEn 618 mutated strains.

GMMA	w/w OAg/GMMA protein ratio	molar % OAg chains/total LPS	nmol lipid A/mg GMMA protein	nm radius (MALS)
<b>SEn 618 <math>\Delta tolR</math></b>	0.6	14	156.6	22
<b>SEn 618 <math>\Delta tolR \Delta msbB</math></b>	1.7	22	240.1	23
<b>SEn618 <math>\Delta tolR \Delta msbB \Delta pagP</math></b>	1.5	12	528.0	20

Analysis by SDS-PAGE performed by on SEn 618  $\Delta tolR \Delta msbB \Delta pagP$  GMMA (Fig. 12) showed no major changes in the protein pattern compared to GMMA with no lipid A modification ( $\Delta tolR$ ).

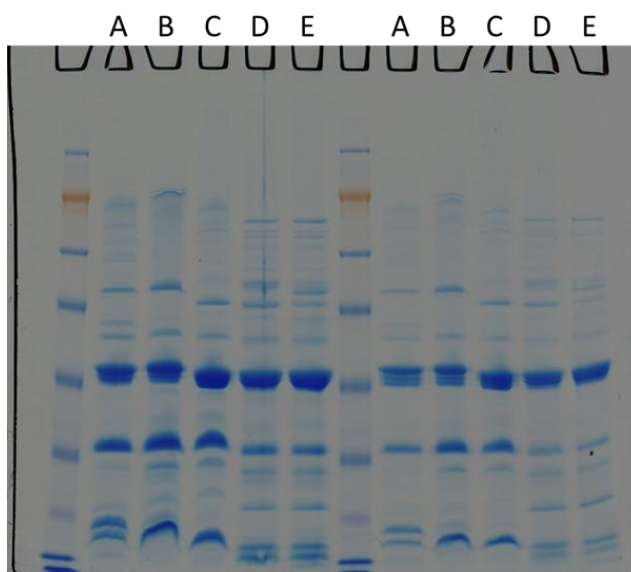


**Fig. 12.** SDS-PAGE protein profile of GMMA from SEn 618  $\Delta tolR$  (A), SEn 618  $\Delta tolR \Delta msbB \Delta pagP$  (B), 1418  $\Delta tolR$  (C), 1418  $\Delta tolR \Delta htrB$  (D) and 1418  $\Delta tolR \Delta msbB$  (E) strains. 10  $\mu$ g (left side) and 5  $\mu$ g (right side) GMMA protein were loaded on a 10% SDS-PAGE gel.

Following sugar extraction by acetic acid hydrolysis of GMMA suspensions, OAg populations were isolated by size exclusion chromatography and compared to the OAg populations purified from the wild type strain (Fig. 13). OAg populations from all GMMA and wild type strain showed a similar average number of repeating units close to 25. GMMA produced by  $\Delta tolR$  single-mutant SEn 618 expressed a distinct additional OAg population of relatively higher molecular weight (MW), with an average of 70 repeating units. This population appeared to be present also as a shoulder in the HPLC-SEC profile of the OAg from the wild type strain (Fig. 13). The two OAg populations at different MW from  $\Delta tolR$  GMMA were quantified by the phenol-sulphuric acid assay. The higher MW (HMW) and lower MW (LMW) fractions represented 22% and 44% respectively of the total amount of sugar extracted. For GMMA derived from the other two 618 mutant strains, OAg chains accounted for 75% ( $\Delta tolR \Delta msbB$ ) and 68% ( $\Delta tolR \Delta msbB \Delta pagP$ ) of total sugar extracted. These percentages are in agreement with the molar ratios of OAg chains to total LPS molecules found (Table 3).

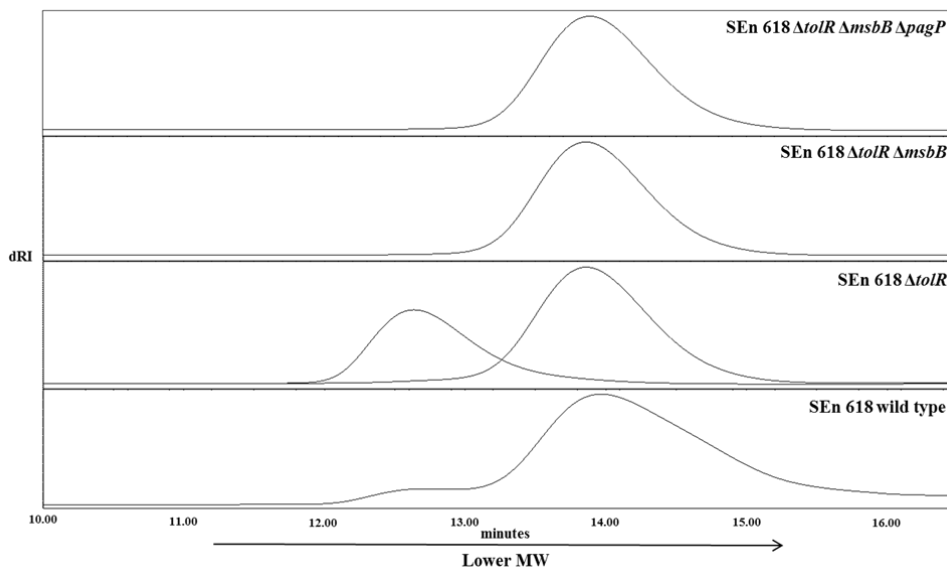


**Fig. 13.** HPLC-SEC chromatograms of OAg populations extracted from GMMA produced by mutated strains of SEN 618 and compared to OAg purified from the wild type SEN 618 isolate (dRI profiles; TSK gel 3000 PWXL column; NaPi 100 mM NaCl 100 mM 5% CH<sub>3</sub>CN pH 7.2; 0.5 mL/min; V<sub>0</sub> 11.20 min; V<sub>tot</sub> 23.29 min).

All OAg populations derived from all mutated as well as wild type SEN 618 strains revealed similar sugar composition by HPAEC-PAD and NMR (Table 4), in agreement with that expected for *S. Enteritidis* OAg [129]. All samples were characterized by low glucosylation levels of 8-11%, compared to 19% for the wild type OAg (Table 4).

**Table 4.** Characterization of OAg populations extracted from GMMA produced by SEn 618 mutated strains and comparison with the OAg from the corresponding wild type strain. Sugar composition (molar ratio relative to Rha) and average number of repeating units (RU) were calculated by HPAEC-PAD and HPLC-SEC/semicarbazide (assay for KDO quantification). *O*-acetylation (*O*-Ac) level was obtained from integration of the peak area of methyl signals of *O*-acetyl groups of <sup>1</sup>H NMR spectra.

OAg	Tyv*	Rha	Man	Gal	Glc	Number RU (peak MW**)	<i>O</i> -Ac %
<b>SEn 618 wild type</b>	1.00	1.00	1.00	1.08	0.19	28 (HMW 88.3; LMW 27.3)	16
<b>SEn 618 <math>\Delta tolR</math> (HMW OAg)</b>	0.99	1.00	1.04	1.05	0.12	70 (90.3)	8
<b>SEn 618 <math>\Delta tolR</math> (LMW OAg)</b>	0.93	1.00	0.99	1.07	0.11	23 (30.3)	4
<b>SEn 618 <math>\Delta tolR \Delta msbB</math></b>	0.97	1.00	1.00	1.05	0.09	26 (30.4)	3
<b>SEn 618 <math>\Delta tolR \Delta msbB</math> <math>\Delta pagP</math></b>	0.97	1.00	0.99	1.06	0.08	27 (29.5)	2

\*calculated by <sup>1</sup>H NMR; \*\*peak MW: molecular weight in kDa calculated by HPLC-SEC analysis by using dextrans as standards.

*O*-acetylation levels were low for all GMMA OAg samples and decreased with the addition of mutations into the GMMA-producing strain, from 16% found in the wild type (non-GMMA) OAg to 2% for the OAg purified from the ‘triple-mutant’ GMMA (Fig. 14). HMW OAg from SEn 618  $\Delta tolR$  GMMA had an *O*-acetylation level of 4% (Table 4).

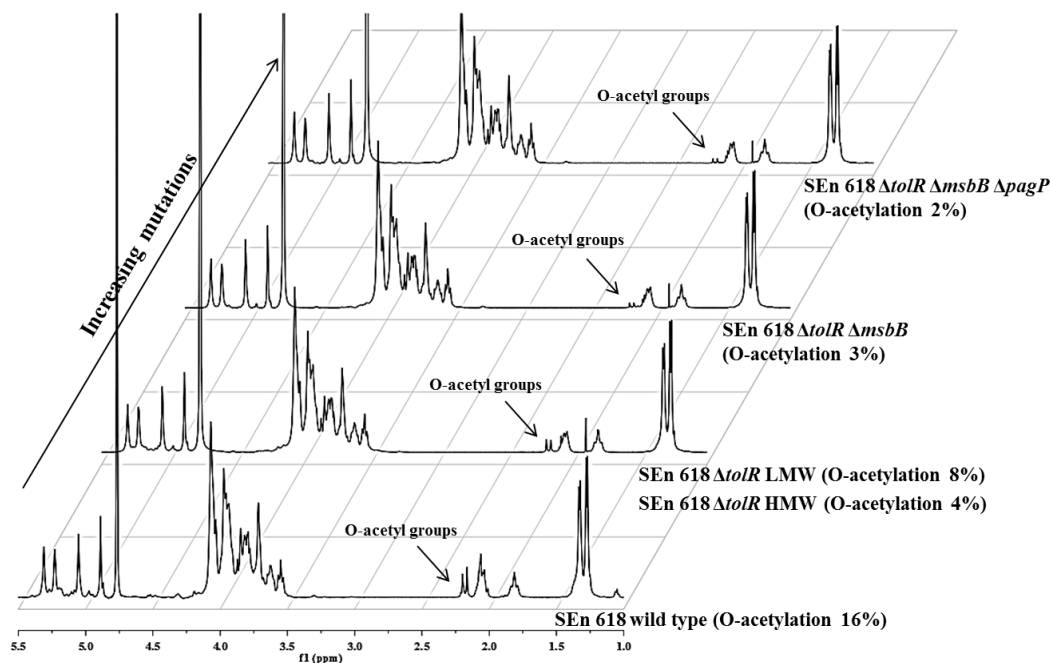


**Fig. 14.**  $^1\text{H}$  NMR spectra of the OAg populations from GMMA of the SEN 618 mutant strains (LMW OAg for SEN 618  $\Delta\text{tolR}$  mutant) and comparison with the mixed OAg purified from the corresponding wild type strain.

### 2.3.3 OAg characterization of STm 1418 GMMA

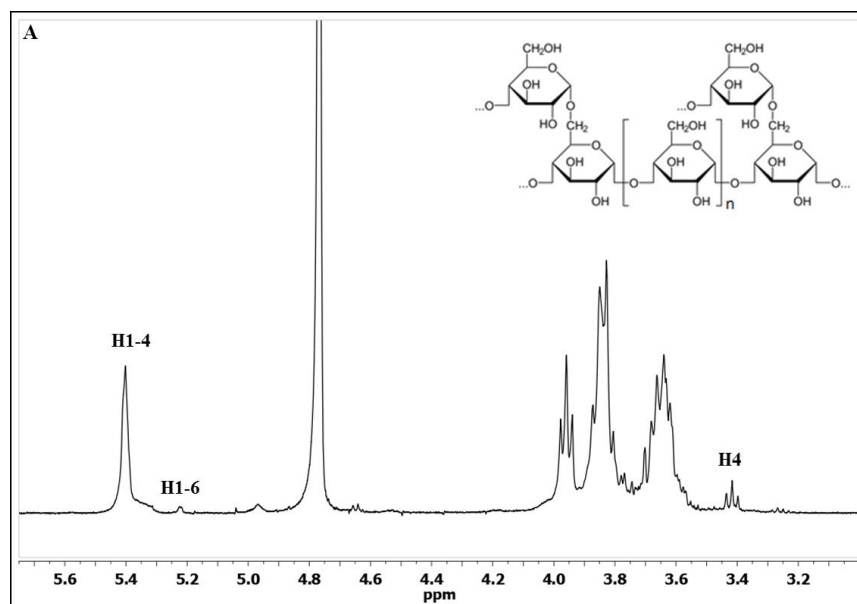
OAg from STm 1418 wild type strain has been fully characterized previously [128, 130]. Table 5 details the main characteristics of GMMA from the corresponding mutant GMMA-producing strains.

**Table 5.** Characterization of GMMA from STm 1418 mutated strains.

GMMA	w/w OAg/GMMA protein ratio	molar % OAg chains/total LPS	nmol lipid A/mg GMMA protein	nm radius (MALS)
STm 1418 $\Delta\text{tolR}$	0.7	10	172.8	22
STm 1418 $\Delta\text{tolR}$ $\Delta\text{msbB}$	0.03	<1	108.2	15
STm 1418 $\Delta\text{tolR}$ $\Delta\text{htrB}$	0.02	0.45	154.8	11

As for SEn 618 GMMA, all preparations were free from soluble proteins, as indicated by HPLC-SEC analysis (data not shown). After the introduction of the  $\Delta tolR$  mutation, the w/w ratio of OAg chains per total protein amount was high (0.66), indicating maintenance of good levels of OAg expression. However, after the introduction of  $\Delta htrB$  or  $\Delta msbB$  mutations in the  $\Delta tolR$  strain, OAg to GMMA protein ratio was greatly reduced, consistent with inhibition of OAg production (Table 5). At the same time, MALS analysis showed that GMMA-producing lower amount of OAg chains were characterized by reduced size with respect to  $\Delta tolR$  GMMA (Table 5). No major changes in the SDS-PAGE protein pattern after introduction of  $\Delta htrB$  and  $\Delta msbB$  mutations to reduce reactivity compared to GMMA with no lipid A modification ( $\Delta tolR$ ) were observed (Fig. 12).

For  $\Delta tolR \Delta htrB$  GMMA, the presence of an extra polysaccharide was revealed and identified as glycogen by  $^1H$  NMR [154] (Fig. 15-A). In  $\Delta tolR \Delta msbB$  GMMA, very high levels of Glc were quantified by HPAEC-PAD analysis and HPLC-SEC (dRI) chromatography revealed the presence of an additional peak, thus strongly suggesting glycogen production by this mutant as well (Fig. 15-B).



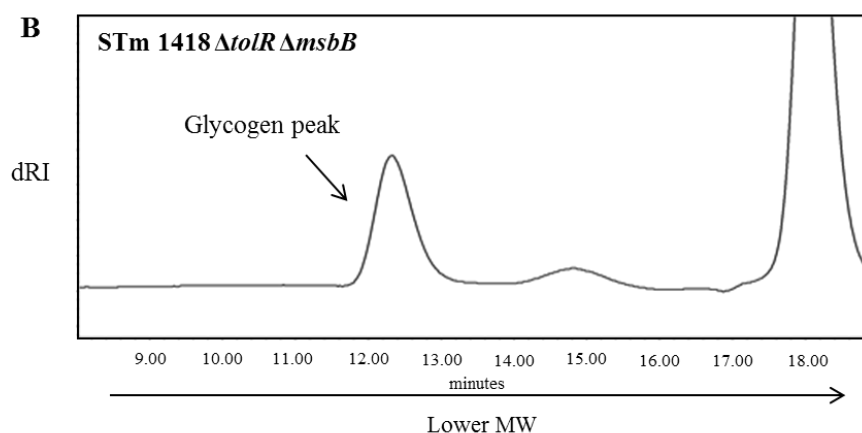


**Fig. 15.**  $^1\text{H}$  NMR spectrum (A) and HPLC-SEC chromatogram (B) of the extra polysaccharide extracted from GMMA produced by STm 1418  $\Delta\text{tolR}$   $\Delta\text{htrB}$  and  $\Delta\text{tolR}$   $\Delta\text{msbB}$  mutated strains.

OAg from  $\Delta\text{tolR}$  GMMA showed two main populations with different average MW, consisting of 75 and 25 repeating units respectively, similar to those OAg populations from the corresponding wild type strain, but with different relative proportions (Table 6, Fig. 16).

**Table 6.** Characterization of OAg populations extracted from GMMA produced by STm 1418  $\Delta\text{tolR}$  mutant and comparison with the OAg from the corresponding wild type strain. Sugar composition (molar ratio relative to Rha) and average number of repeating units (RU) were calculated by HPAEC-PAD and HPLC-SEC/semicarbazide (assay for KDO quantification). *O*-acetylation (*O*-Ac) level was obtained from integration of the peak area of methyl signals of *O*-acetyl groups of  $^1\text{H}$  NMR spectra.

OAg	Abe*	Rha	Man	Gal	Glc	Number RU (peak MW**)	<i>O</i> -Ac %
STm 1418 wild type	1.00*	1.00	1.00	1.00	0.80	na	73
STm 1418 $\Delta\text{tolR}$ (HMW OAg)	0.91*	1.00	0.97	0.98	1.00	75 (104.7)	54
STm 1418 $\Delta\text{tolR}$ (LMW OAg)	0.93*	1.00	0.98	1.04	0.96	25 (32.9)	79

\*calculated by  $^1\text{H}$  NMR; na: not applicable. \*\*peak MW: molecular weight in kDa calculated by HPLC-SEC analysis by using dextrans as standards.

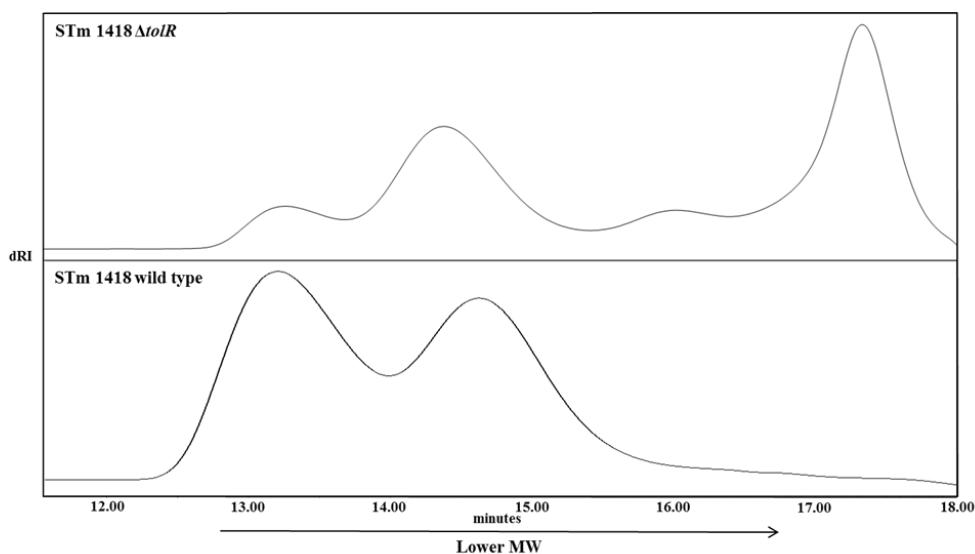


**Fig. 16.** HPLC-SEC chromatograms of the OAg populations extracted from STm GMMA of the  $\Delta tolR$  mutant and compared with the OAg purified from the wild type strain (TSK gel 3000 PWXL column; NaPi 100 mM NaCl 100 mM 5% CH<sub>3</sub>CN pH 7.2; 0.5 mL/min;  $V_0$  11.20 min;  $V_{tot}$  23.29 min). The component eluting at 17.30 min in the  $\Delta tolR$  OAg refers to the core oligosaccharide of the LPS. Core oligosaccharide fractions for wild type OAg were lost in the purification process.

The two populations had the same sugar composition, in agreement with OAg from 1418 wild type strain, with glycosylation levels >80% (Table 6). Glycosidic linkages analysis confirmed that the main linkage for Glc was in position C-6 on the Gal residue (Table 7).

**Table 7.** Glycosidic linkages analysis of STm 1418 wild type OAg and HMW, LMW OAg populations from  $\Delta tolR$  GMMA (molar ratio relative to 2,3-Man).

OAg from STm 1418	t-Abe	4-Rha	t-Glc	3-Gal	3,6-Gal	2,3-Man
wild type*	0.16	0.87	0.63	0.26	0.59	1.00
$\Delta tolR$ (HMW OAg) <sup>§</sup>	0.43	0.77	0.70	0.04	0.72	1.00
$\Delta tolR$ (LMW OAg) <sup>§</sup>	0.64	0.77	0.67	0.14	0.64	1.00

\*GLC on SP2330 column; <sup>§</sup>GLC on HP1 column; t-Abe with low molar ratios due to its chemical lability in the analysis conditions.





*O*-acetyl groups quantification by Gas Liquid Chromatography (GLC) and Gas Liquid Chromatography Coupled to Mass Spectrometry (GLC-MS) [130] performed on these populations detected the presence of *O*-acetyl groups only on C-2 of Abe, with *O*-acetylation levels of 39% for the OAg population at HMW and 32% for that at LMW, compared to 52% for the wild type OAg (Table 8).

**Table 8.** *O*-acetylation levels of STm 1418 wild type OAg and HMW, LMW OAg populations from  $\Delta tolR$  GMMA calculated by GLC and  $^1H$  NMR.

OAg from STm 1418	% <i>O</i> -Ac on C-2 Abe by GLC	% <i>O</i> -Ac on C-2 Rha by GLC	% <i>O</i> -Ac on C-2 Abe by $^1H$ NMR	% <i>O</i> -Ac on C-2 Rha by $^1H$ NMR
wild type	52	nd	73	nd
$\Delta tolR$ (HMW OAg)	39	nd	42	12
$\Delta tolR$ (LMW OAg)	32	nd	69	10

nd: not detected.

$^1H$  NMR spectroscopy analysis confirmed the presence of *O*-acetyl groups on C-2 of Abe (*O*-acetyl signal at 2.10 ppm, H-2 of Abe2OAc at 5.10 ppm) in both samples (43% for HMW, 69% for LMW OAg populations), as well as in the OAg produced by the wild type strain (73%) [130]. An additional peak at 2.17 ppm (12% for HMW, 10% for LMW OAg populations) (Fig. 17) was tentatively attributed to the *O*-acetyl group on C-2 of Rha, by comparison with the *O*-acetylation pattern assigned to the OAg from *S. Typhimurium* D23580 strain [130].

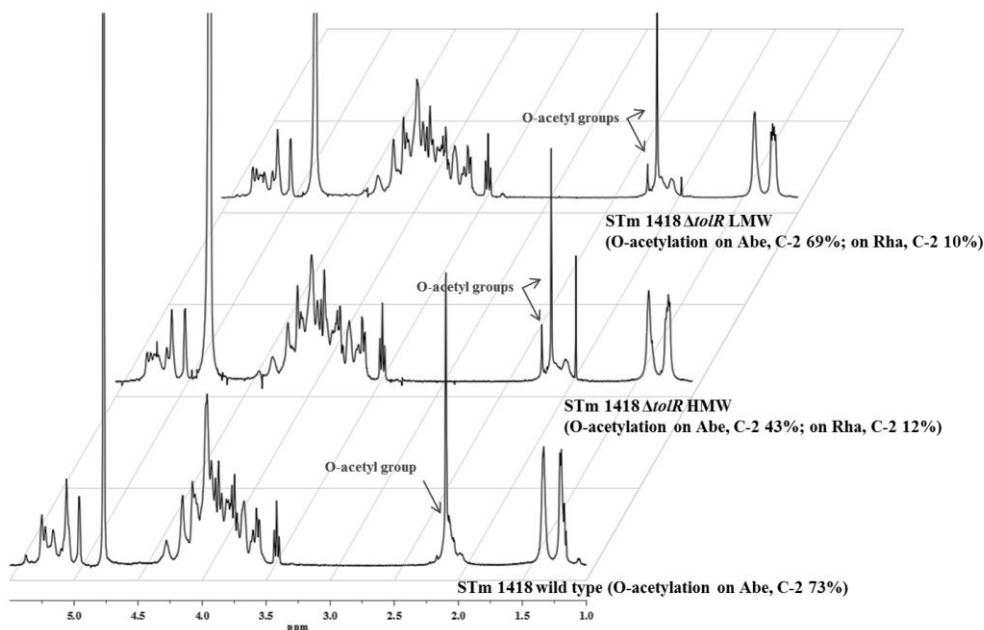


**Fig. 17.**  $^1\text{H}$  NMR spectra of the OAg populations from STm 1418  $\Delta\text{tolR}$  GMMA and comparison with the mixed OAg purified from the corresponding wild type strain.

The low amount of OAg chains on the double mutant GMMA impeded their detailed structural characterization.

### 2.3.4 Immunogenicity in mice

Groups of mice were immunized with SEn 618  $\Delta\text{tolR}$  and  $\Delta\text{tolR}$   $\Delta\text{msbB}$   $\Delta\text{pagP}$  GMMA, and STm 1418  $\Delta\text{tolR}$ ,  $\Delta\text{tolR}$   $\Delta\text{msbB}$  and  $\Delta\text{tolR}$   $\Delta\text{htrB}$  GMMA. All the GMMA candidate vaccines were compared at the same OAg dose of 1  $\mu\text{g}$ . The main objective was to verify the ability of GMMA to induce an immune response and whether the observed OAg modifications, following the genetic manipulations required to generate GMMA-producing strains, affected immunogenicity in terms of anti-OAg responses. Fourteen days after the second injection, all GMMA were able to induce a serovar-specific anti-OAg IgG response, with no significant differences among GMMA of the same serovar (Mann-Whitney test for SEn 618 GMMA and Kruskal-Wallis for STm 1418 GMMA). However, more variability was observed in the anti-OAg IgG response induced in mice injected with SEn 618  $\Delta\text{tolR}$   $\Delta\text{msbB}$

$\Delta pagP$  GMMA (3 non-responders) compared to 618  $\Delta tolR$  GMMA, and with STm 1418  $\Delta tolR \Delta htrB$  GMMA compared to 1418  $\Delta tolR$  GMMA. All GMMA were able to boost the anti-OAg IgG response (same p value of 0.0078 comparing day 14 and day 42 response for each group) (Fig. 18). Immune sera were also bactericidal against *S. Typhimurium* D23580 or *S. Enteritidis* CMCC4314 (Fig. 18).

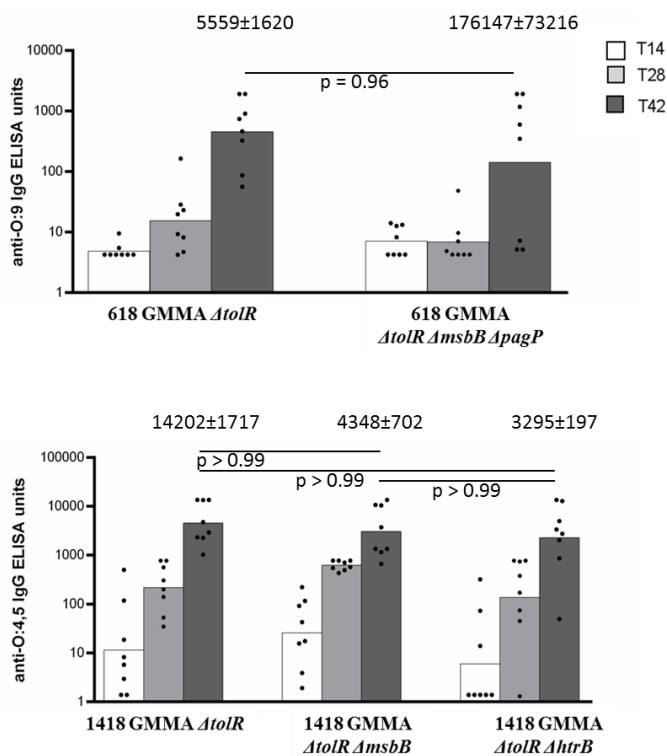


**Fig. 18.** Summary graphs of anti-OAg IgG geometric means (bars) and individual antibody levels (dots) induced in CD1 mice by GMMA vaccines injected at days 0 and 28 at 1 $\mu$ g OAg dose. Mice were bled before the first immunization (pooled sera from each group at day 0) and at days 14, 28 and 42 after the first immunization. ELISA limit of detection was calculated as 2.9 and as 2.2 ELISA units/mL for anti-O:9 and anti-O:4,5 IgG, respectively. Numbers above day 42 bars represent SBA results of pooled sera collected at day 42 from each group against *S. Enteritidis* CMCC4314 or *S. Typhimurium* D23580. SBA titers were calculated as the serum dilution necessary to obtain 50% bacterial killing after 3 hours incubation at 37 °C compared with bacteria counted at time 0. Each serum pool was tested in triplicate in three independent experiments, except for SEn 618  $\Delta tolR$  serum, which was tested in duplicate. Initial serum dilution was 1:100.

## 2.4 Discussion

GMMA are nano-sized particles, displaying high-densities of repeated antigens and containing bacterial pathogen associated molecular patterns (PAMPs), with the potential to trigger strong immune responses [136, 137]. Furthermore, GMMA can be produced efficiently, economically and rapidly [114, 115, 122], making them an attractive vaccine candidate, particularly for low and middle income countries.

A comprehensive panel of analytical methods has been assembled for GMMA characterization with particular attention to their surface OAg, which is a key target of protective antibody responses. Such methods allowed verification of whether mutations introduced into GMMA-producing strains impact on OAg expression and structure, enabling the identification of optimal potential GMMA candidate vaccines against iNTS. Furthermore, such methods are of fundamental importance in the process of vaccine development, to ensure consistency of production, vaccine efficacy and to monitor stability of GMMA vaccines.

The  $\Delta tolR$  mutation introduced to increase GMMA production (approximately 300 mg GMMA OAg content obtained per liter of fermentation broth) was accompanied by changes in the OAg chain length distribution in both SEn 618 and STm 1418 strains. In contrast to what was observed for SEn 618  $\Delta tolR$  GMMA, the  $\Delta tolR$  mutation in the STm 1418 strain caused a reduction of the OAg population at HMW compared to the wild type strain. In addition, mutations to modify lipid A and reduce toxicity need to be carefully monitored as they may inhibit OAg production, as observed in this study with one of the STm 1418 clones.

With STm 1418, a reduction in the amount of OAg was associated with the production of glycogen as additional polysaccharide on GMMA. Production of such polysaccharide was not observed in a panel of nontyphoidal *Salmonella* wild type strains previously characterized [119, 131]. This phenomenon has also been observed in other mutants, derived both from *S. Enteritidis* and *S. Typhimurium* GMMA-producing strains, when genetic mutations have resulted in low OAg expression (data not shown). The reasons for this are not clear and it would be interesting to verify whether there is a correlation between lack of OAg production and glycogen



formation and what functional implications this may have. Glycogen has been described to be a major energy storage compound in many *Enterobacteriaceae*, including *S. Typhimurium* and *S. Enteritidis* and to accumulate in cytoplasmic granules [155]. It is a polysaccharide containing glucose units in a branched structure comprising predominantly  $\alpha$ -1,4 linkages (90%) and a smaller number of  $\alpha$ -1,6 branching glucosyl linkages. It is usually produced in the presence of rich medium containing glucose, or when growth is limited by a lack of a required nutrient (ammonia, amino acids, sulphur or phosphate), or when the bacteria enter stationary phase of growth, or under stresses associated with infection and environmental survival [222]. Glycogen production in *S. Enteritidis* has previously been reported and shown to be related to virulence, colonization and resistance mechanisms, including the production of biofilm, obtained from glycogen cell stores [156]. The strongly decreased production of OAg chains and the associated overproduction of glycogen could be attributed to compensatory effects related to *tolR* and *msbB/htrB* gene deletions in the STm 1418 genotype. The introduction of mutations in the Tol pathway and the knock-out of *msbB/htrB* genes are reported to induce loss of regulation in genes encoding for the synthesis of the OAg repeating units, or for the synthesis and the accumulation of glycogen, in response to extra-cytoplasmic stress [223].

OAg chain length and *O*-acetylation level are parameters that are known to affect the immunogenicity of OAg-based vaccines [77, 80, 102, 119, 133]. Mutations introduced into the wild type strains affected also the OAg *O*-acetylation pattern. When tested in mice at the same OAg dose, all GMMA were able to induce anti-OAg IgG specific antibodies, with functional activity, independent of the OAg to total protein GMMA ratio and with no major impact of any OAg structural modification. The effective amount of OAg injected, rather than its density on GMMA, appears to determine the anti-OAg antibody response. In fact, when GMMA were injected at the same protein dose, anti-OAg IgG response induced by *S. Typhimurium* 1418  $\Delta$ *tolR*  $\Delta$ *msbB*/ $\Delta$ *htrB* GMMA was significantly lower than that induced by *S. Typhimurium* 1418  $\Delta$ *tolR* (data not shown). The implication of this observation is that a higher OAg to GMMA ratio should permit the use of a lower amount of GMMA per vaccine dose



for the same anti-OAg antibody response. This will have potential benefits in relation to cost and safety of the vaccine.

In a parallel work, same GMMA characterized here were also assessed for their reactogenicity. The combination of  $\Delta msbB$  and  $\Delta pagP$  mutations resulted to be the optimal approach to minimize reactogenicity of *S. Enteritidis* and *S. Typhimurium* GMMA, resulting in uniformly penta-acylated lipid A [124]. GMMA from this triple mutant strain provoked the least stimulation of cytokine release from human PBMC, compared to GMMA with wild type lipid A, and stimulatory potential similar to that of a *Shigella sonnei* GMMA vaccine tested in Phase I clinical trials [115, 123]. *S. Enteritidis* and *S. Typhimurium* GMMA with reduced toxicity, without a major impact on OAg expression level, seem to be good components for a vaccine against iNTS. Mutations introduced to reduce GMMA reactogenicity have been verified not to have major impact on the protein pattern profile. A more accurate analysis will be done on the final selected strains in order to identify the nature and the amount of the most abundant proteins, considering that they may be additional key mediators of functional antibody. It will be important to verify batch to batch consistency, and to investigate the contribution that anti-protein antibodies can have on the overall immune response induced by GMMA vaccines.

Simplicity of manufacturing process and low costs of production, coupled with encouraging immunogenicity data, make the GMMA vaccine approach particularly attractive. The comparison of OAg-GMMA with other candidate vaccines under development against iNTS, such as live attenuated and glycoconjugate vaccines, will be of great interest for the development of a successful and efficacious intervention against iNTS.



### **3. Determination of nontyphoidal *Salmonella* GMMA particle size distribution**



### 3.1 Introduction

Particle size and particle size distribution (PSD) are among the characteristics of GMMA to be investigated for their full characterization [157-159].

A number of techniques for particle size, shape and size distribution measurements are available and can be commonly employed in quality control as well as in research and development fields [160, 161]. However, as it will be described later, each methodology leads to different “observables” which have to be clearly defined. Depending on the nature of the product, the methodologies include Dynamic Light Scattering (DLS), Tunable Resistive Pulse Sensor (TRPS), Electron Microscopy (EM), Flow Cytometry (FC), Differential Centrifugation Sedimentation (DSC), and others. No gold standard exists for the detection of vesicles and each of these techniques has strengths and weaknesses. Some of them are labour intensive and time demanding, whereas others are cost effective and user friendly. For example, Transmission Electron Microscope (TEM) has well known drawbacks such as cost, lengthy sample preparation and analysis time and, above all, uncertainty on the real size of sample, with a multitude of possible measurement artifacts due to sample pre-treatments. In the context of the characterization of NTS GMMA vaccines, TEM analysis has been previously employed to evaluate shape and size distribution of GMMA released by different STm and SEn mutants [124]. In that study, the results (size distribution and mean diameters), obtained after negative staining and manual measurements, were not different among all the samples analysed. Diameters ranged between 20 and 110 nm, with mean values between 40 and 50 nm (Fig. 19).



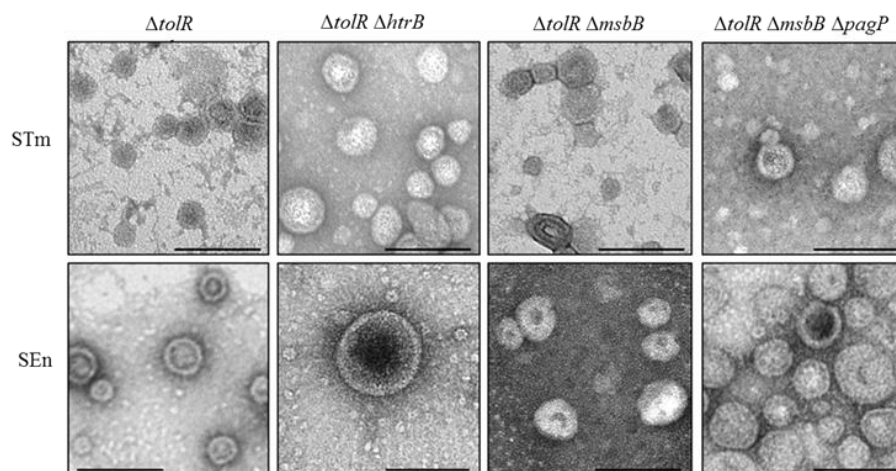


**Fig. 19.** TEM of GMMA purified from STm and SEn mutants (bar length = 100 nm) [124].

Here, PSD of GMMA produced by different *S. Typhimurium* and *S. Enteritidis* mutated strains have been investigated by means of three different size-analysing techniques:

- Dynamic Light Scattering (DLS);
- Multi-Angle Light Scattering (MALS);
- Nanoparticle Tracking Analysis (NTA).

Advantages, limitations and shortcomings of each type of instruments and methods are discussed, as well.

A wide range of definitions for particle size exists [162]. Particles are three-dimensional objects for which length, breadth and height should be considered in order to provide a complete description. All particle-sizing techniques have a unique target that is to provide a single figure indicative of the particle size. Most techniques used for size measurement assume that the particles being analysed are spherical and estimate the particle size as the diameter of the “equivalent sphere” that would give the value as the particle analysed. Unfortunately, nice spherical particles rarely exist, forming instead other shapes, with the complication that particles in a mixture could have different sizes. For irregular-shaped particles, the assigned equivalent sphere

approximation depends upon the method of measurement and the physical property underlying one specific technique. Description of particle size is not unique, but a combination of methods can provide a reliable description of the sample [162]. Of the many sphere-equivalent diameters that describe the size of a particle, the two most commonly used are hydrodynamic radius ( $R_h$ ) and radius of gyration ( $R_g$ ).

$R_h$  is defined as the radius of an equivalent hard sphere diffusing at the same rate as the particle under observation. Practically, the hydrodynamic size is indicative of the apparent size of the dynamic hydrated particle, considering the layer of solvent associated with the particle surface, taking into accounts its shape and behaviour in solution. In reality, the determined  $R_h$  closely reflects the apparent size adopted by the solvated particle. On the other hand,  $R_g$  is defined as the mass weighted average distance of each element of the particle from its center of mass. Both  $R_h$  and  $R_g$  can be used to gain a more complete description of particles and the ratio  $R_g/R_h$  ( $\rho$ ) provides information about their structure and density [163]. The characteristic  $R_g/R_h$  value for a globular structure is  $\sim 0.775$ , which means that  $R_g$  is smaller than  $R_h$ . When particles deviate from globular to non-spherical or elongated structures,  $R_g/R_h$  ratio tends to values greater than 0.775.

At last, measurement of particles concentration represents a ubiquitous requirement in the study of particulate samples. In many cases, the only knowledge of particle size and distribution is not enough, as particles concentration may also affect the pharmaceutical performance or the immune response of a particulate drug substance. There is a wide variety of applications in which the measurement of particle concentration is critically important, including biopharmaceutics development, protein aggregation studies, exosomes and microvesicles research [162-165].

### *Dynamic Light Scattering (DLS)*

DLS, also known as photon correlation spectroscopy (PCS) or quasi elastic light scattering (QELS), is a popular and routinely technique for measurement of size and differential size distribution of small particles in suspension used since 1960s [161,

166, 167]. In general, the technique is best used for submicron particles and applications include the determination of the size distribution of nanogolds, proteins, latex and silica beads, colloids, emulsion systems, liposomes and extracellular vesicles.

DLS is an ensemble measurement technique determining the average hydrodynamic diameter of particles dissolved or dispersed in a liquid by measuring the intensity fluctuations of scattered light produced by particles as they undergo Brownian motion [160, 168]. Analysis of these intensity fluctuations yields the rate of the random Brownian motion in liquid, modelled by the Stokes-Einstein equation reported below [166]. The Stokes-Einstein relation connects diffusion coefficient measured by dynamic light scattering to hydrodynamic diameter [169].

$$D_h = \frac{k_B T}{3\pi\eta D_t}$$

- $D_h$ : hydrodynamic diameter;
- $D_t$ : translational diffusion coefficient;
- $k_B$ : Boltzmann's constant;
- $T$ : thermodynamic temperature;
- $\eta$ : dynamic viscosity.

Sample temperature affects the particles rate and viscosity. The sample in a cell is illuminated with a laser beam: all particles crossing the beam will scatter light. The scattered light is collected with one of two detectors, either at a 90 degree (right angle) or 173 degree (back angle) scattering angle. The obtained optical signal shows random changes due to the randomly changing relative position of the particles in suspension under Brownian motion. The PSD is obtained by measuring these time-dependent intensity fluctuations of the scattered light, followed by applying a mathematical model derived from Brownian motion and light scattering theory.

Using this technique, an intensity-weighted mean hydrodynamic diameter (Z-average diameter) and a polydispersity index (PDI) are obtained. The term polydispersity is used to describe the amplitude of the distribution. PDI values smaller than 0.05 are rarely seen other than with highly monodisperse standards. Values greater than 0.7 indicate that the sample has a very broad size distribution and it is probably not suitable for the DLS technique. The values for different classes of dispersity are listed in Table 9.

**Table 9.** Approximate values for polydispersity parameters.

	Distribution type			
	monodisperse		polydisperse	
	<i>uniform</i>	<i>narrow</i>	<i>moderate</i>	<i>broad</i>
<b>PDI from DLS</b>	0.0	0.0-0.1	0.1-0.4	>0.4

A measurement is typically performed within 1 min and requires sample volumes as low as 20  $\mu\text{L}$ . Sample concentration range is not a critical factor for DLS and particles can be dispersed in a variety of liquids, only whose refractive index and viscosity need to be known for interpreting data.

The ease of use and the ability to analyse a large range of particulate sizes, materials and dispersion media has made DLS one of the most common and user-friendly measurement techniques able to yield relatively precise and consistent results that can be obtained in a rather short period of time.

### *Multi-Angle Light Scattering (MALS)*

MALS represents a static light scattering technique suitable for the measurement of the absolute molecular mass of polymers, as well as molecular size of particles expressed as the  $R_g$  value. Applications of MALS can be the determination of size of biopolymers such as polysaccharides, natural and synthetic polymers, large protein complexes such as virus-like particles, liposomes or exosomes, extracellular vesicles, and large protein aggregates [170].

A laser source is most often used and the technique is also referred to as multi-angle laser light scattering (MALLS) [171]. In the last few years, since all commercial light scattering instrumentations use laser sources instead of conventional light beams, mentioning the light source is not needed and the term MALS is more commonly used. MALS studies the angular dependence of the time-averaged scattering intensity to determine the mass-averaged root mean square radius (RMS), commonly known as radius of gyration  $R_g$ .

In MALS analysis, a laser beam is passed through the sample chamber and the suspended particles crossing the path of the beam scatter light in all directions. Laser light can be scattered from different parts of the particle reaching the detectors with different phases (anisotropic scattering). MALS involves the measurement of scattered light intensity caught by multiple detectors placed at fixed angles around the particle. The number of angles varies between 2 and 20 angles, which are able to detect the re-radiated light simultaneously. The intensity of the light scattered is directly related to its molecular mass, as described by the Rayleigh equation reported below.

$$\frac{KC}{R_\theta} = \left( \frac{1}{M} + 2A_2C \right) \frac{1}{P(\theta)}$$

- K: optical constant;
- $R_\theta$ : Rayleigh ratio;
- M: molecular mass;
- $A_2$ : 2<sup>nd</sup> virial coefficient;
- C: sample concentration;
- $P(\theta)$ : shape (or form) factor.

$P(\theta)$  takes into account the shape of the particle and allows obtaining size information from the angular dependence of the intensity of the scattered light. The total amount of light scattered at each angle is given by the contribution of each of the



scattering centers present in the volume of a large macromolecule, obtaining  $R_g$  value. MALS can examine sizes from 10 nm to several hundred nanometers, without calibration against standards or assumptions on shape. If the particle can be represented by a sphere, the  $R_g$  can be related to its geometrical dimensions (geometric radius,  $R_{geo}$ ) [172].

MALS detector can be coupled to a fractionation module such as size exclusion chromatography (SEC-MALS), representing the most common method for MALS characterization of size distribution of homogeneous or heterogeneous samples [173]. In this way, the sample is chromatographically separated by its hydrodynamic volume and molar mass (MM) and  $R_g$  can be assessed at each elution volume, achieving accurate size distributions limited in resolution only by the separation technique [163]. MALS coupled to a size exclusion chromatographic system provides accurate and reproducible gyrations size values, complementary to those obtained by other size-analysing techniques.

#### *Nanoparticle tracking Analysis (NTA)*

NTA is an alternative light-scattering technique useful for the evaluation of size and enumeration of individual particles in liquids, ranging between 10 and 2000 nm in size [174, 175]. NTA allows the analysis of a wide range of different particles in a wide range of solvent types, with no need for multi-angle measurements. NTA can be employed for studying emulsion systems, virus-like particles, extracellular vesicles, evaluating also aggregation dynamics and drug delivery [157, 164]. The hydrodynamic radius  $R_h$  of particles is determined by NTA in a similar fashion as DLS [176]. Like DLS, the particle diameter is calculated via the Stokes-Einstein equation by direct measuring the diffusion coefficient of particles moving under Brownian motion, relating the rate of particle motion to particle size [177].

More practically, in a NTA experiment, a finely focused laser beam hits a dilute suspension of particles contained in the sample analysis module through a glass prism [175]. The low angle refracted laser beam illuminates the particles through the sample. Illuminated particles are visualized using a conventional optical microscope,

fitted with a scientific digital camera which catches light scattered from the particles in the field of view. The particles are seen as small points of light moving rapidly under Brownian motion. NTA allows the direct, real-time visualization and analysis of particles in liquids, which provides a deeper understanding of the sample in analysis [176]. After the video collection, the NTA software tracks the center of each individual particle's Brownian movement in two dimensions on a frame-by-frame basis and simultaneously calculates their size and total number [178]. By following each particle as centres of the spots of scattered light for a number of steps (video frames), the average distance moved between frames is then calculated and from this the diffusion coefficient for each particle is determined. The rate of individual particle movement is used to calculate the sphere equivalent hydrodynamic diameter by applying the two-dimensional Stokes-Einstein equation [164]:

$$\langle x,y \rangle^2 = \frac{K_B T_t}{3\pi\eta d_h}$$

- $\langle x,y \rangle^2$ : mean square displacement (MSD);
- $K_B$ : Boltzmann's constant;
- $T_t$ : thermodynamic temperature;
- $\eta$ : dynamic viscosity;
- $d_h$ : hydrodynamic diameter.

The additional ability of NTA to see particles directly and individually allows particle concentration to be estimated. Particle concentration can be estimated from extrapolating the number of particles detected at any given instant per volume unit through knowing the scattering volume. This goes well beyond the simple measurement of particle size. Analysis times can be as low as 10 seconds for optimum concentrations of particles between  $2 \times 10^8$  and  $2 \times 10^9$  particles/mL [175]. This range of concentration amounts to a range of 10-100 particles within the field of view, optimal to achieve precise estimates of particle concentration analysis. Too many



particles can cause severe interference, while too few particles may not be representative of the sample, both of which can lead to misleading results.

In addition, with fluorescent labelling, NTA can be used to determine the phenotype of a subgroup of vesicles [179].

NTA is expected to become an important tool in research fields, including bacteriology, vaccinology, immunology, biomedical diagnostics, material science, where the optical characterization of nanoparticles is of critical importance.

## 3.2 Materials and methods

### 3.2.1 NTS parent strains for GMMA production

*S. Typhimurium* isolate SGSC1418 (LT-2 collection, University of Calgary), *S. Typhimurium* 2192 (SGSC2192, SARA collection), and *S. Enteritidis* SA618 (CEESA EASSA II collection of Quotient Bioresearch Limited) were chosen as parent strains on the basis of a screen performed previously [119]. The *Salmonella* mutant strains used and their abbreviations are listed in Table 10.

**Table 10.** Strains used in this study and their abbreviations.

Strain abbreviation name	Genotype
STm 1418 $\Delta tolR$	<i>S. Typhimurium</i> 1418 $\Delta tolR::aph$
STm 1418 $\Delta tolR \Delta wbaP$	<i>S. Typhimurium</i> 1418 $\Delta tolR::aph \Delta wbaP::cat$
STm 2192 $\Delta tolR \Delta pagP \Delta msbB$	<i>S. Typhimurium</i> 2192 $\Delta tolR::aph \Delta pagP::cat \Delta msbB::tetRA$
SEn 618 $\Delta tolR \Delta msbB \Delta pagP$	<i>S. Enteritidis</i> 618 $\Delta tolR::aph \Delta msbB::tetRA \Delta pagP::cat$

Mutants were described in the previous chapter [124]. In the case of STm 1418  $\Delta tolR \Delta wbaP$ , the chloramphenicol resistance gene *cat* was used to replace the *wbaP* gene. GMMA were produced and purified as described in the previous chapter [124]. After purification, all GMMA samples were suspended in PBS and then 0.22  $\mu\text{m}$  filtered.

### 3.2.2 GMMA protein quantification





GMMA quantities are expressed as total protein content estimated by micro BCA (Thermo Scientific). A 2 mg/mL solution of serum bovine albumin (BSA) was used to create a calibration curve in the 5 to 20  $\mu\text{g/mL}$  range. Samples were diluted with MilliQ water in order to obtain sample protein concentration in the range of the calibration curve. Samples and calibration curves were created in duplicates and to a final volume of 500  $\mu\text{L}$ . The Micro BCA Reagent was prepared according to manufacturer's instructions and 500  $\mu\text{L}$  were added to each samples. Samples were incubated for 1 h at 60 °C in a pre-heated thermostatic bath. Cooled-down samples were analysed using a spectrophotometer and absorbance was measured at 562 nm.

### 3.2.3 Dynamic Light Scattering (DLS)

DLS measurements were performed with a Malvern Zetasizer Nano ZS (Malvern, Herremberg, Germany) equipped with a 633 nm He-Ne laser and operating at an angle of 173°. Scattering light detected at 173° was automatically adjusted by laser attenuation filters. For data analysis the viscosity and refractive index (RI) of PBS buffer solution (at 25 °C) were used. The software used to collect and analyse the data was the Zetasizer software version 7.11. Temperature was set at 25 °C. 80  $\mu\text{L}$  of each sample at 50, 125, 200  $\mu\text{g/mL}$  protein content were measured in duplicates in single-use polystyrene micro cuvette (ZEN0040, Alfatest) with a path length of 10 mm. For GMMA STm 1418  $\Delta\text{tolR}$   $\Delta\text{wbaP}$ , 40  $\mu\text{L}$  at 50  $\mu\text{g/mL}$  protein content were measured once. The hydrodynamic diameter of GMMA was expressed by a Z-average value of three measurements for each replicate, providing also a PDI of the size values calculated.

### 3.2.4 Size Exclusion Chromatography coupled to Multi-Angle Light Scattering (SEC-MALS)

GMMA samples were analysed by HPLC-SEC with Tosoh TSKgel G6000PW (30 cm x 7.5 mm) + G4000PW (30 cm x 7.5 mm) columns in series equilibrated in PBS (PBS tablets, Medicago) and with in-line UV, fluorescence emission, dRI (Refraction



index detector) and MALS detectors. A fused silica cell and a 660 nm laser source were used. A volume of 80  $\mu\text{L}$  of samples with concentrations of 150 and 100  $\mu\text{g/mL}$  protein content were injected and eluted with a flow rate of 0.5 mL/min (run time 70 min). All dilutions were made in PBS (Dispersant RI 1.333). MALS data were collected and analysed using ASTRA 6 software (Wyatt Technology). The size of GMMA was expressed by the  $R_n$ ,  $R_w$  and  $R_z$  values determined by Astra Particle template assuming spherical shape ( $R_{\text{geo}}$ ). Size values were obtained from the MALS detector without the need of the solute concentration and the sample RI increment.

### 3.2.5 Nanoparticle Tracking Analysis (NTA)

NS300 Nanosight instrument (Nanosight Ltd, Salisbury, UK) equipped with a CMOS camera and a 488 nm monochromatic laser beam was used. Data acquisition and processing were performed using NTA software 3.2 build 3.2.16. Automatic settings for the minimum track length, the minimal expected particle size and blur setting were applied. Viscosity settings for water were applied and automatically corrected for the temperature used. Measurements were performed at room temperature ranging from 22 to 25  $^{\circ}\text{C}$ . Particle movement was analysed by NTA software with camera level at 16, slider shutter at 1300 and slider gain at 512). Different detection threshold values were tested, adjusted for the sample appearance after dilution. Five movies of 30 s at 25 frames per second were recorded, generating five replicate histograms that were averaged. Several dilutions of the samples were analysed and duplicates were recorded for every diluted sample. GMMA samples were PBS diluted in low binding eppendorf tubes (Costar, Corning) and dilutions were prepared just before analysis. Samples were slowly injected in the sample chamber using a 1 mL syringe in 5 to 10 seconds, after gently mixing. Samples were recorded under controlled flow, using the NanoSight syringe pump (speed 20). Each video was then analysed to determine the respective mean and mode (particle size that appears most often within a given preparation) GMMA size. In addition to these values, standard deviation (SD) and percentile undersize values (D10, D50, D90) were collected. SD, D10, D50, D90 were a measure of the spread of PSD within the



samples. Concentrations of samples are reported either as particles per mL and particles per frame.

### 3.2.6 HPLC-SEC

In order to obtain more homogenous GMMA samples, a volume of 100  $\mu$ L with a concentration of 1,000  $\mu$ g/mL protein content was fractionated by HPLC-SEC. Tosoh TSKgel G6000PW (30 cm x 7.5 mm) + G4000PW (30 cm x 7.5 mm) columns in series equilibrated in PBS (PBS tablets, Medicago) were used with in-line UV detector. Samples were eluted with PBS at a flow rate of 0.5 mL/min (run time 70 min). GMMA peaks were fractionated in 1.7 mL low binding eppendorf tubes monitoring the 280 nm elution profile and collecting fractions at the rate of one tube per minute.

## 3.3 Results

GMMA size distribution has been previously investigated by means of Atomic Force Microscope (AFM). AFM analysis was performed by Dr. Denis Scaini and Dr. Ilaria Rago at Elettra Sincrotrone Trieste (Area Science Park, Trieste, Italy). Unfortunately, no satisfactory results were achieved, proving the difficulty to yield positive results using this labour-intensive technique on GMMA samples.

### 3.3.1 Size distribution analysis by DLS

SEn 618  $\Delta tolR \Delta msbB \Delta pagP$ , STm 2192  $\Delta tolR \Delta pagP \Delta msbB$ , STm 1418  $\Delta tolR$  GMMA were analysed at 50, 125, 200  $\mu$ g/mL protein concentrations. STm 1418  $\Delta tolR \Delta wbaP$  GMMA were analysed at 50  $\mu$ g/mL protein content. Z-average diameter and PDI are summarized in Table 11.

**Table 11.** Z-average diameters and relative PDI values of SEn and STm GMMA analysed by DLS.

GMMA	Protein concentration μg/mL	Z-average diameter nm	PDI
SEn 618 $\Delta tolR$ $\Delta msbB$ $\Delta pagP$	50	111.07±0.93	0.15
	125	112.02±0.46	0.16
	200	112.32±0.89	0.15
	<b>Mean value</b>	<b>111.80</b>	
STm 2192 $\Delta tolR$ $\Delta pagP$ $\Delta msbB$	50	103.47±0.69	0.19
	125	102.92±0.76	0.18
	200	102.48±0.67	0.19
	<b>Mean value</b>	<b>102.96</b>	
STm 1418 $\Delta tolR$	50	91.53±0.46	0.18
	125	91.45±0.88	0.17
	200	91.23±0.38	0.17
	<b>Mean value</b>	<b>91.40</b>	
STm 1418 $\Delta tolR$ $\Delta wbaP$	50	<b>57.60</b>	0.26

No differences were found by analysing the samples at different protein concentrations. SEn 618  $\Delta tolR$   $\Delta msbB$   $\Delta pagP$  GMMA exhibited a Z-average diameter of 111.80 nm. STm 2192  $\Delta tolR$   $\Delta pagP$   $\Delta msbB$  and STm 1418  $\Delta tolR$  GMMA were characterized by a mean value of 102.96 and 91.40 nm, respectively.

These GMMA showed a different average diameter with respect to SEn GMMA of ~10 (7.9% less) and ~20 nm (18.2% less), respectively. STm 1418  $\Delta tolR$   $\Delta wbaP$  GMMA were characterized by a smaller size, 37.0 % less of the GMMA produced by the parent strain (STm 1418  $\Delta tolR$ ) (Fig. 20).

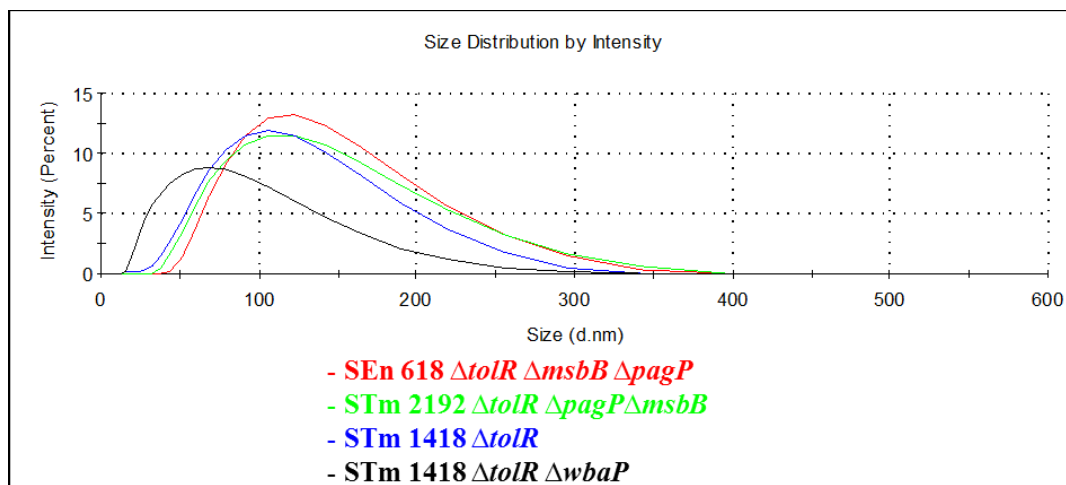


**Fig. 20.** DLS size distribution of SEn 618  $\Delta tolR \Delta msbB \Delta pagP$ , STm 2192  $\Delta tolR \Delta pagP \Delta msbB$ , STm 1418  $\Delta tolR$  and STm 1418  $\Delta tolR \Delta wbaP$  GMMA.

PDI values (Table 11) indicated a moderate polydispersity for all the GMMA samples analysed.

SEn 618  $\Delta tolR \Delta msbB \Delta pagP$  and STm 2192  $\Delta tolR \Delta pagP \Delta msbB$  GMMA were fractionated by HPLC-SEC. Three adjacent fractions (Fig. 21) were collected and further analysed by DLS.

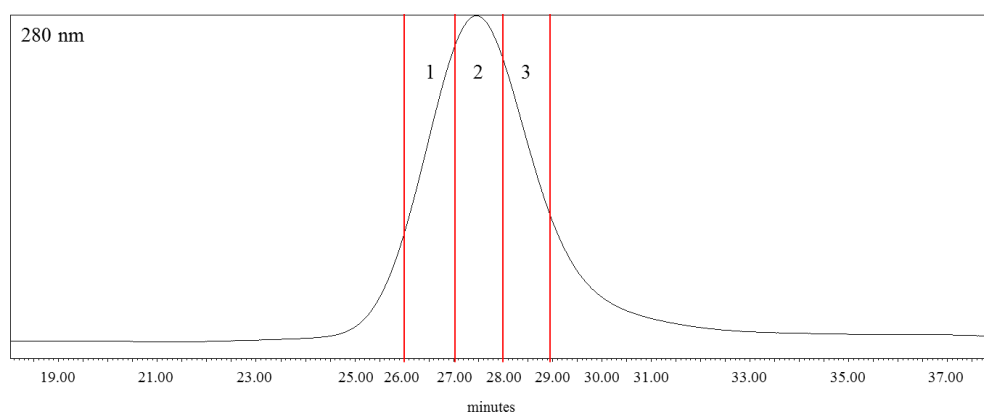


**Fig. 21.** Size exclusion chromatography of SEn 618  $\Delta tolR \Delta msbB \Delta pagP$  GMMA. UV detection at 280 nm. Three different fractions were collected for further DLS analysis.

The average diameter and the PDI values of the collected fractions are summarized in Table 12.

**Table 12.** Average diameters and relative PDI values of fractions of SEn 618  $\Delta tolR \Delta msbB \Delta pagP$  and STm 2192  $\Delta tolR \Delta pagP \Delta msbB$  GMMA analysed by DLS.

GMMA	Fraction	Protein concentration $\mu\text{g/mL}$	Z-average diameter nm	PDI
SEn 618 $\Delta tolR$ $\Delta msbB \Delta pagP$	1	40	116.30 $\pm$ 0.89	0.14
	2	50	91.28 $\pm$ 0.23	0.08
	3	40	84.10 $\pm$ 0.62	0.16
	Mean value			<b>97.20</b>
STm 2192 $\Delta tolR$ $\Delta pagP \Delta msbB$	1	21	100.27 $\pm$ 0.21	0.09
	2	50	81.69 $\pm$ 0.25	0.06
	3	35	77.46 $\pm$ 1.15	0.16
	Mean value			<b>86.47</b>

Fractions 2, corresponding to the central area of the GMMA samples, showed a lower PDI with respect to the corresponding PDI values of the unfractionated populations (Table 11). Fraction 1 of both SEn 618 and STm 2192 GMMA showed a particle size similar to that found for unfractionated GMMA, confirming that DLS over weights large particles. Fractions 2 and 3 for both GMMA samples showed mean hydrodynamic diameters strongly decreased respect to whole GMMA population (around 19% less for fractions 2 and 25% less for fractions 3). The mean size for the three fractions is smaller respect to the corresponding value of the unfractionated GMMA (13.1% less for SEn GMMA, 16.0% less for STm ones).

### 3.3.2 Size distribution analysis by SEC-MALS

HPLC-SEC fluorescence emission profile of GMMA samples from all the strains analysed revealed very low residual soluble protein contaminants (< 5%), indicating good purity of the samples. Considering this, almost all protein content resulted to be located in the GMMA thus providing an easy way to quantify GMMA content.

GMMA preparations from SEn 618  $\Delta tolR \Delta msbB \Delta pagP$ , STm 2192  $\Delta tolR \Delta pagP \Delta msbB$ , STm 1418  $\Delta tolR$  GMMA were analysed at 100 and 150  $\mu\text{g/mL}$  protein

content. STm 1418  $\Delta tolR \Delta wbaP$  GMMA were analysed at 100  $\mu\text{g/mL}$  protein content.  $2 \times R_n$ ,  $2 \times R_w$ , and  $2 \times R_z$ , results obtained are reported in Table 13.

**Table 13.** MALS diameter values and relative uncertainty values of SEn and STm GMMA analysed by SEC-MALS.

GMMA	Protein concentration $\mu\text{g/mL}$	$2 \times R_n$ nm	$2 \times R_w$ nm	$2 \times R_z$ nm
SEn 618 $\Delta tolR \Delta msbB \Delta pagP$	100	73.20 $\pm$ 0.88	74.60 $\pm$ 0.90	76.20 $\pm$ 0.91
	150	70.40 $\pm$ 0.70	71.80 $\pm$ 0.72	73.60 $\pm$ 0.74
	Mean value	<b>71.80</b>	<b>73.20</b>	<b>74.90</b>
STm 2192 $\Delta tolR \Delta pagP \Delta msbB$	100	68.2 $\pm$ 0.75	69.80 $\pm$ 0.77	72.20 $\pm$ 0.79
	150	67.40 $\pm$ 0.67	69.00 $\pm$ 0.69	71.40 $\pm$ 0.71
	Mean value	<b>67.80</b>	<b>69.40</b>	<b>71.80</b>
STm 1418 $\Delta tolR$	100	70.00 $\pm$ 0.91	71.40 $\pm$ 0.86	73.80 $\pm$ 0.89
	150	70.00 $\pm$ 0.91	71.60 $\pm$ 0.86	73.80 $\pm$ 0.89
	Mean value	<b>70.00</b>	<b>71.50</b>	<b>73.80</b>
STm 1418 $\Delta tolR \Delta wbaP$	100 (peak 1)	<b>98.20</b>	<b>100.00</b>	<b>101.80</b>
	100 (peak 2)	<b>51.00</b>	<b>52.60</b>	<b>55.40</b>

Size distribution of GMMA samples was independent from the protein concentration at which samples were analysed. SEn 618  $\Delta tolR \Delta msbB \Delta pagP$  (Fig. 22), STm 2192  $\Delta tolR \Delta pagP \Delta msbB$  and STm 1418  $\Delta tolR$  GMMA were characterized by a similar  $2 \times R_z$  value ( $\sim 70$  nm).  $2 \times R_z$  values obtained by SEC-MALS were smaller than  $Z$ -average diameters obtained by DLS. Differences of  $\sim 40$  nm (33.0%) for SEn 618  $\Delta tolR \Delta msbB \Delta pagP$ ,  $\sim 30$  nm (30.3%) for STm 2192  $\Delta tolR \Delta pagP \Delta msbB$  and  $\sim 20$  nm (19.1%) for STm 1418  $\Delta tolR$  GMMA were observed.

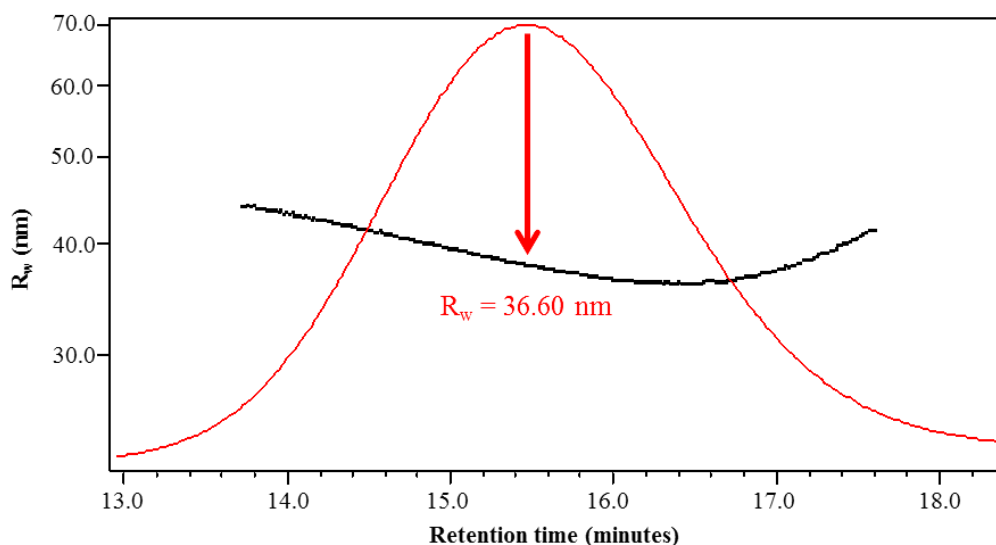


**Fig. 22.** SEC-MALS chromatogram of SEn 618  $\Delta tolR \Delta msbB \Delta pagP$  GMMA, with indication of the  $R_w$  value corresponding to the apex of light scattering detection.

Unlike DLS, showing one single population, SEC-MALS analysis of STm 1418  $\Delta tolR \Delta wbaP$  GMMA revealed two main peaks, with  $2 \times R_z$  of 101.80 and 55.40 nm, respectively (Fig. 23). In agreement with DLS analysis, size of STm 1418  $\Delta tolR \Delta wbaP$  GMMA was confirmed to be smaller with respect to the other GMMA analysed (26.3%), but the gap between Z-average and  $2 \times R_z$  (3.8%), for the smaller population was not large, differently from what observed for the other GMMA analysed.



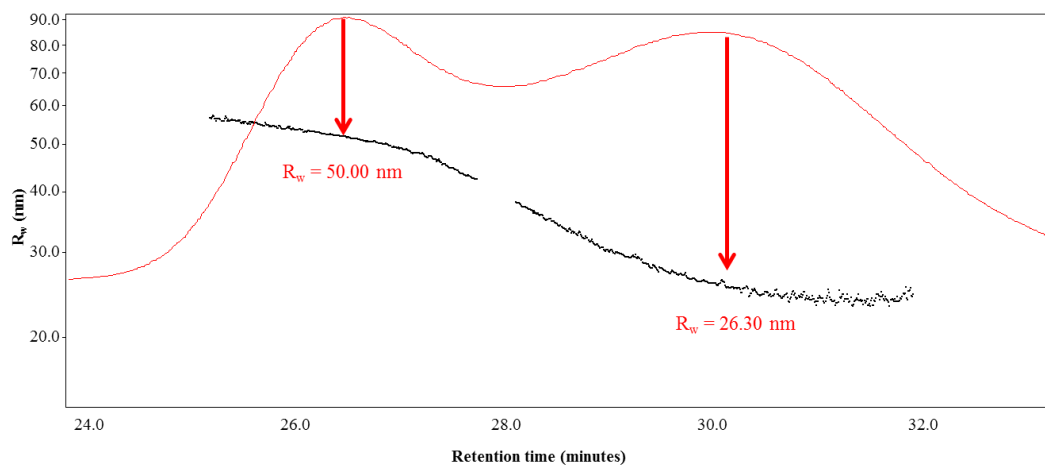


**Fig. 23.** SEC-MALS chromatogram of STm 1418  $\Delta tolR \Delta wbaP$  GMMA, which were characterized by a double peak.

Similarly to DLS analyses, samples deriving from HPLC-SEC fractionation (Fig. 21) of SEn 618  $\Delta tolR \Delta msbB \Delta pagP$  and STm 2192  $\Delta tolR \Delta pagP \Delta msbB$  GMMA were analysed by SEC-MALS. Results relative to the collected fractions are summarized in Table 14

**Table 14.** MALS diameter values and relative uncertainty values of fractions of SEn 618  $\Delta tolR \Delta msbB \Delta pagP$  and STm 2192  $\Delta tolR \Delta pagP \Delta msbB$  GMMA analysed by SEC-MALS.

GMMA	Fractions	Protein concentration $\mu\text{g/mL}$	$2 \times R_n$ nm	$2 \times R_w$ nm	$2 \times R_z$ nm
SEn 618 $\Delta tolR$ $\Delta msbB$ $\Delta pagP$	1	40	78.60 $\pm$ 4.09	79.40 $\pm$ 4.05	80.20 $\pm$ 4.01
	2	64	67.00 $\pm$ 1.01	68.40 $\pm$ 0.96	70.20 $\pm$ 0.98
	3	41	58.00 $\pm$ 1.51	59.20 $\pm$ 1.48	61.2 $\pm$ 1.53
		<b>Mean value</b>		<b>67.87</b>	<b>69.00</b>
STm 2192 $\Delta tolR$ $\Delta pagP$ $\Delta msbB$	1	21	80.00 $\pm$ 0.96	81.00 $\pm$ 0.97	82.20 $\pm$ 0.99
	2	50	67.60 $\pm$ 0.81	68.20 $\pm$ 0.82	70.00 $\pm$ 0.84
	3	35	58.60 $\pm$ 0.94	59.80 $\pm$ 0.96	61.40 $\pm$ 0.98
		<b>Mean value</b>		<b>68.73</b>	<b>69.67</b>

Fractions 2 showed  $2 \times R_z$  values similar to the values found for SEC-MALS analysis of the whole GMMA population. Fractions 1 and 3, instead were characterized by higher ( $\sim 10$  nm) and lower ( $\sim 10$  nm) size values, respectively.

### 3.3.3 Size distribution analysis by NTA

GMMA from SEn 618  $\Delta tolR \Delta msbB \Delta pagP$  (Fig. 24), STm 2192  $\Delta tolR \Delta pagP \Delta msbB$ , STm 1418  $\Delta tolR$  and STm 1418  $\Delta tolR \Delta wbaP$  GMMA were analysed by NTA. Screen gain and camera level (shutter speed and camera gain) were set at values 2 and 16, respectively, and they were selected based on the visually brightest detection of particles without the occurrence of abundant over-scattering events. Detection threshold (the scattering intensity threshold above which particles are tracked) was initially set at the value of 3.

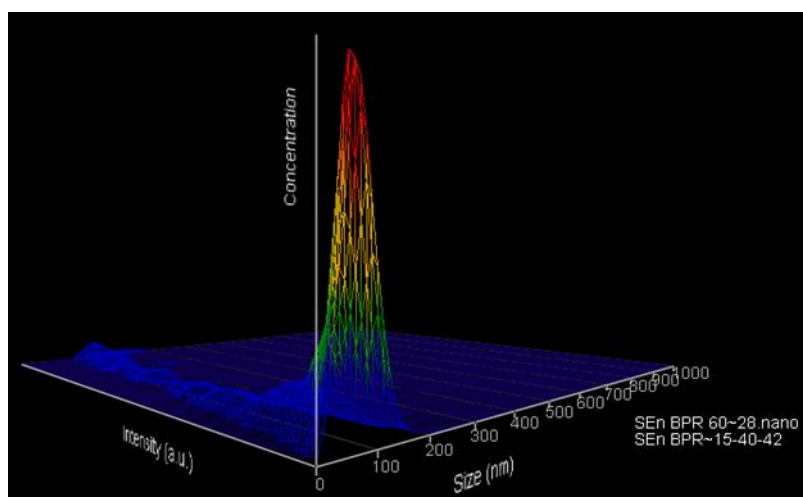


**Fig 24.** NTA graph of SEn 618  $\Delta tolR \Delta msbB \Delta pagP$  GMMA, in which particle size, particle concentration and relative intensity are plotted together.

Mean and mode hydrodynamic diameters for SEn 618  $\Delta tolR \Delta msbB \Delta pagP$  GMMA analysed at different dilutions are reported in Table 15.

**Table 15.** Mean and mode hydrodynamic diameter of SEn 618  $\Delta tolR \Delta msbB \Delta pagP$  GMMA analysed by NTA.

Sample dilution	Protein concentration $\mu\text{g/mL}$	Mean nm	Mode nm	SD nm	D10 nm	D50 nm	D90 nm
10000x (1)	$1.39 \times 10^{-1}$	106.2 $\pm$ 1.3	88.6 $\pm$ 2.9	37.4 $\pm$ 1.0	54.5 $\pm$ 2.1	88.8 $\pm$ 1.7	152.0 $\pm$ 2.5
10000x (2)	$1.39 \times 10^{-1}$	106.5 $\pm$ 0.8	90.2 $\pm$ 3.7	38.4 $\pm$ 1.2	56.6 $\pm$ 2.0	88.2 $\pm$ 1.7	148.5 $\pm$ 2.0
25000x (1)	$5.82 \times 10^{-2}$	99.3 $\pm$ 1.3	80.5 $\pm$ 2.2	35.7 $\pm$ 1.1	51.3 $\pm$ 2.3	81.7 $\pm$ 1.8	134.4 $\pm$ 2.7
25000x (2)	$5.82 \times 10^{-2}$	105.3 $\pm$ 2.1	84.0 $\pm$ 2.9	35.6 $\pm$ 0.6	59.0 $\pm$ 1.9	87.2 $\pm$ 1.9	143.9 $\pm$ 4.2
50000x (1)	$2.90 \times 10^{-2}$	90.3 $\pm$ 1.8	70.3 $\pm$ 6.1	36.2 $\pm$ 1.4	44.4 $\pm$ 1.8	73.2 $\pm$ 2.0	128.9 $\pm$ 4.1
50000x (2)	$2.90 \times 10^{-2}$	97.4 $\pm$ 2.7	87.8 $\pm$ 6.1	35.6 $\pm$ 1.1	51.1 $\pm$ 2.1	81.4 $\pm$ 2.7	131.5 $\pm$ 4.5
75000x (1)	$1.93 \times 10^{-2}$	92.0 $\pm$ 1.4	76.1 $\pm$ 4.2	39.1 $\pm$ 3.2	45.3 $\pm$ 1.9	72.7 $\pm$ 1.6	128.9 $\pm$ 4.3
75000x (2)	$1.93 \times 10^{-2}$	94.5 $\pm$ 3.2	82.5 $\pm$ 3.8	32.6 $\pm$ 1.5	52.2 $\pm$ 4.9	77.2 $\pm$ 2.7	131.3 $\pm$ 5.6
100000x (1)	$1.45 \times 10^{-2}$	83.9 $\pm$ 2.2	61.6 $\pm$ 7.3	33.6 $\pm$ 1.4	37.6 $\pm$ 1.8	69.5 $\pm$ 3.7	124.1 $\pm$ 7.7
100000x (2)	$1.45 \times 10^{-2}$	92.0 $\pm$ 2.4	74.3 $\pm$ 8.9	35.0 $\pm$ 0.9	42.8 $\pm$ 1.3	76.2 $\pm$ 3.1	136.5 $\pm$ 3.1
125000x (1)	$1.16 \times 10^{-2}$	78.7 $\pm$ 1.9	59.8 $\pm$ 1.7	36.7 $\pm$ 2.5	36.3 $\pm$ 1.5	57.5 $\pm$ 2.4	109.3 $\pm$ 1.6
125000x (2)	$1.16 \times 10^{-2}$	83.5 $\pm$ 1.7	71.1 $\pm$ 4.2	35.0 $\pm$ 1.3	36.4 $\pm$ 3.1	66.5 $\pm$ 1.1	119.2 $\pm$ 2.6
<b>Average</b>		<b>93.4</b>	<b>77.1</b>	<b>36.1</b>	<b>46.1</b>	<b>76.0</b>	<b>131.8</b>

SEn 618  $\Delta tolR \Delta msbB \Delta pagP$  GMMA were characterized by averaged mean and mode values of 93.4 nm and 77.1 nm, respectively. NTA analyses did not show an acceptable reproducibility among experiments. Standard deviation SD, D10, D50 and D90 percentile values showed that GMMA sample was quite polydisperse.

NTA technique was also investigated to calculate particles concentration. Effective protein concentrations ( $\mu\text{g/mL}$ ) relative to each diluted sample were related to the measured concentrations provided by NTA (particles/mL) by calculation of particles/ $\mu\text{g}$  ratios. Linearity in the ratio among dilutions was expected. Results are summarized in Table 16.



**Table 16.** Particles concentration values of SEn 618  $\Delta tolR \Delta msbB \Delta pagP$  GMMA analysed by NTA.

Sample dilution	Protein concentration $\mu\text{g/mL}$	Particles/mL	Particles/frame	Particles/ $\mu\text{g}$
10000x (1)	$1.39 \times 10^{-1}$	$2.59 \times 10^9$	131.2	$1.86 \times 10^{10}$
10000x (2)	$1.39 \times 10^{-1}$	$2.50 \times 10^9$	127.0	$1.80 \times 10^{10}$
25000x (1)	$5.82 \times 10^{-2}$	$1.57 \times 10^9$	79.8	$2.70 \times 10^{10}$
25000x (2)	$5.82 \times 10^{-2}$	$1.34 \times 10^9$	68.2	$2.30 \times 10^{10}$
50000x (1)	$2.90 \times 10^{-2}$	$1.10 \times 10^9$	55.7	<b><math>3.79 \times 10^{10}</math></b>
50000x (2)	$2.90 \times 10^{-2}$	$9.49 \times 10^8$	48.2	$3.27 \times 10^{10}$
75000x (1)	$1.93 \times 10^{-2}$	$7.24 \times 10^8$	36.7	<b><math>3.75 \times 10^{10}</math></b>
75000x (2)	$1.93 \times 10^{-2}$	$6.40 \times 10^8$	32.5	$3.32 \times 10^{10}$
100000x (1)	$1.45 \times 10^{-2}$	$7.39 \times 10^8$	37.5	$5.11 \times 10^{10}$
100000x (2)	$1.45 \times 10^{-2}$	$5.76 \times 10^8$	29.2	<b><math>3.99 \times 10^{10}</math></b>
125000x (1)	$1.16 \times 10^{-2}$	$8.29 \times 10^8$	42.1	$7.12 \times 10^{10}$
125000x (2)	$1.16 \times 10^{-2}$	$7.74 \times 10^8$	39.3	$6.65 \times 10^{10}$

At the different dilutions, there was no clear correlation between protein content and particles concentration. Linearity in particles/ $\mu\text{g}$  ratios was obtained only for three dilution factors (50000x, 75000x and 100000x).

Different detection threshold values were applied in order to investigate the effect of this variable on the analysis (Table 17).

**Table 17.** Influence of detection threshold on NTA size and concentration estimations of SEN 618  $\Delta tolR$   $\Delta msbB$   $\Delta pagP$  GMMA.

Sample dilutions	Detection threshold	Protein concentration $\mu\text{g/mL}$	Mean nm	Mode nm	Particles/mL	Particles/frame	Particles/ $\mu\text{g}$
<b>50000x</b>	3	$2.90 \times 10^{-2}$	92.90	81.70	$1.02 \times 10^9$	51.95	$3.53 \times 10^{10}$
	5	$2.90 \times 10^{-2}$	98.45	90.40	$8.06 \times 10^8$	40.90	$2.78 \times 10^{10}$
	7	$2.90 \times 10^{-2}$	100.80	94.55	$7.10 \times 10^8$	36.05	$2.45 \times 10^{10}$
	9	$2.90 \times 10^{-2}$	102.70	91.00	$6.26 \times 10^8$	31.80	$2.16 \times 10^{10}$
	11	$2.90 \times 10^{-2}$	105.15	97.65	$5.54 \times 10^8$	28.10	$1.91 \times 10^{10}$
	14	$2.90 \times 10^{-2}$	107.50	102.35	$4.75 \times 10^8$	24.10	$1.64 \times 10^{10}$
	17	$2.90 \times 10^{-2}$	109.80	101.80	$4.22 \times 10^8$	23.9	$1.45 \times 10^{10}$
<b>Average</b>			<b>102.38</b>	<b>94.21</b>			
<b>75000x</b>	3	$1.93 \times 10^{-2}$	92.20	77.25	$6.82 \times 10^8$	34.6	$3.25 \times 10^{10}$
	5	$1.93 \times 10^{-2}$	99.15	89.00	$5.20 \times 10^8$	26.40	$2.69 \times 10^{10}$
	7	$1.93 \times 10^{-2}$	101.50	87.75	$4.57 \times 10^8$	23.15	$2.37 \times 10^{10}$
	9	$1.93 \times 10^{-2}$	104.45	93.40	$4.02 \times 10^8$	20.35	$2.08 \times 10^{10}$
	11	$1.93 \times 10^{-2}$	106.65	85.90	$3.57 \times 10^8$	18.15	$1.85 \times 10^{10}$
	14	$1.93 \times 10^{-2}$	110.00	90.45	$3.06 \times 10^8$	15.50	$1.58 \times 10^{10}$
	17	$1.93 \times 10^{-2}$	112.65	101.95	$2.72 \times 10^8$	13.80	$1.41 \times 10^{10}$
<b>Average</b>			<b>103.80</b>	<b>89.24</b>			

Increasing the detection threshold, large GMMA particles were detected and tracked, resulting in increased size values (both mean and mode), whereas the GMMA concentration decreased, due to the reduction of the number of detectable GMMA. Small or low scattering particles were not considered by NTA software in the calculation of the resulting size and concentration. Detection threshold needs to be selected by the operator according to the sample and to its dilution to have consistent results. Table 18 summarizes analysis performed on different diluted samples, by adjusting the detection threshold and obtaining consistent results both in terms of size and concentration (Fig. 25).

**Table 18.** Detection threshold values adjusted for scalar dilutions of SEn  $\Delta tolR \Delta msbB \Delta pagP$  GMMA.

Sample dilution	Detection threshold	Protein concentration $\mu\text{g/mL}$	Mean nm	Mode nm	Particles/mL	Particles/frame	Particles/ $\mu\text{g}$
10000x	3	$1.39 \times 10^{-1}$	<b>106.05</b>	<b>86.65</b>	$2.55 \times 10^9$	129.1	<b><math>1.83 \times 10^{10}</math></b>
25000x	7	$5.82 \times 10^{-2}$	<b>108.40</b>	<b>90.85</b>	$1.10 \times 10^9$	6158.35	<b><math>1.90 \times 10^{10}</math></b>
50000x	11	$2.90 \times 10^{-2}$	<b>105.15</b>	<b>97.65</b>	$5.54 \times 10^8$	28.10	<b><math>1.91 \times 10^{10}</math></b>
75000x	11	$1.93 \times 10^{-2}$	<b>106.65</b>	<b>85.90</b>	$3.57 \times 10^8$	18.15	<b><math>1.85 \times 10^{10}</math></b>
100000x	14	$1.45 \times 10^{-2}$	<b>103.90</b>	<b>98.40</b>	$2.82 \times 10^8$	14.30	<b><math>1.95 \times 10^{10}</math></b>
Average			<b>106.03</b>	<b>91.89</b>			<b><math>1.89 \times 10^{10}</math></b>

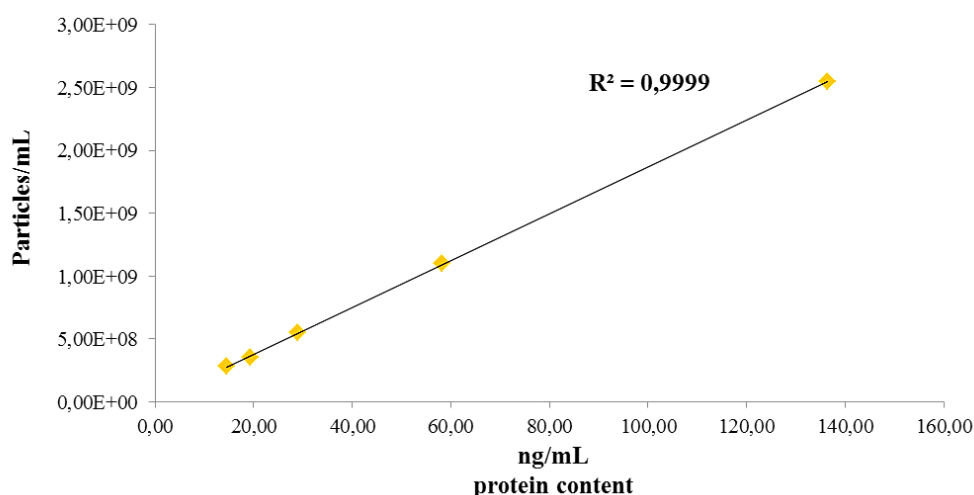


**Fig. 25.** Linear correlation between particles/mL concentration measured by NTA at specific detection threshold values and effective protein concentration ( $\mu\text{g/mL}$ ) of SEn 618  $\Delta tolR \Delta msbB \Delta pagP$  GMMA.

Mean value found by this way was in agreement with Z-average by DLS (106.03 vs 111.80 nm). To be noted that mode values similar to the DLS hydrodynamic diameter of fraction 2 obtained after fractionation of the GMMA sample (91.89 vs 91.28 nm) were achieved.

The analysis of a more homogenous sample was performed by analysing fraction 2 from SEC fractionation of SEn 618  $\Delta tolR \Delta msbB \Delta pagP$  (Fig. 21). The fraction was analysed at two different dilutions (1000x and 2000x) (Table 19). Video and analysis



settings were selected before analysis in accordance to sample visualization (screen gain 2, camera level 16, and detection threshold 7).

**Table 19.** Size and concentration estimations of fraction 2 analysed by NTA after HPLC-SEC fractionation of SEN 618  $\Delta tolR \Delta msbB \Delta pagP$  GMMA.

Sample dilution	$\mu\text{g}/\text{mL}$	Mean nm	Mode nm	SD nm	D10 nm	D50 nm	D90 nm	Particles/mL	Particles/frame	Particles/ $\mu\text{g}$
<b>1000x</b>	$6.39 \times 10^{-2}$	92.6	79.2	21.6	60.8	77.7	112.9	$1.53 \times 10^9$	77.6	$2.39 \times 10^{10}$
<b>2000x</b>	$3.20 \times 10^{-2}$	93.2	83.6	24.8	60.5	78.4	110.8	$6.69 \times 10^8$	33.95	$2.09 \times 10^{10}$
<b>Average</b>		<b>92.9</b>	<b>81.4</b>	<b>23.2</b>	<b>60.6</b>	<b>78.1</b>	<b>111.8</b>			<b><math>2.24 \times 10^{10}</math></b>

More similarity between mean and mode hydrodynamic diameter was observed, differently from what found for the unfractionated GMMA. Lower SD and D90 and higher D10 values clearly showed that a more homogenous sample was obtained. The average value of the mean diameters for the two dilutions calculated at the same detection threshold is very similar to the DLS hydrodynamic diameter measured for the same fraction (92.9 vs 91.3 nm). Linearity of concentration at the two dilutions tested was observed.

STm 2192  $\Delta tolR \Delta pagP \Delta msbB$ , STm 1418  $\Delta tolR$  and STm 1418  $\Delta tolR \Delta wbaP$  GMMA were also analysed by NTA. Several analysis were done per each sample at different dilutions, by selecting the more appropriate video and analysis values, being sure to obtain consistent results both in terms of size and concentration. Table 20 summarizes results obtained.

**Table 20.** NTA results of SEn 618  $\Delta tolR \Delta msbB \Delta pagP$ , STm 2192  $\Delta tolR \Delta pagP \Delta msbB$ , STm 1418  $\Delta tolR$  and STm 1418  $\Delta tolR \Delta wbaP$  GMMA.

GMMA sample		Mean nm	Mode nm	Particles/ $\mu$ g
SEn 618 $\Delta tolR$ $\Delta msbB \Delta pagP$	Whole population	106.0	91.9	$1.89 \times 10^{10}$
	Central fraction (2)	92.9	81.4	/
STm 2192 $\Delta tolR$ $\Delta msbB \Delta pagP$	Whole population	102.5	78.6	$1.09 \times 10^{10}$
	Central fraction (2)	83.6	77.4	/
STm 1418 $\Delta tolR$	Whole population	95.8	85.6	$1.47 \times 10^{10}$
	Central fraction (2)	84.9	74.5	/
STm 1418 $\Delta tolR$ $\Delta wbaP$	Whole population	77.0	52.30	$3.32 \times 10^9$

Unfractionated and SEC central fraction of STm 2192  $\Delta tolR \Delta msbB \Delta pagP$  and STm 1418  $\Delta tolR$  GMMA showed a similar behaviour as seen for SEn GMMA. The mode diameters of the unfractionated samples were similar to the mean values of the fraction corresponding to the central area of the GMMA samples. NTA analysis of STm  $\Delta tolR \Delta wbaP$  GMMA revealed a high difficulty in proper tracking and enumerating particles, probably due to their smaller dimensions and to their higher polydispersity (Fig. 23, 26).



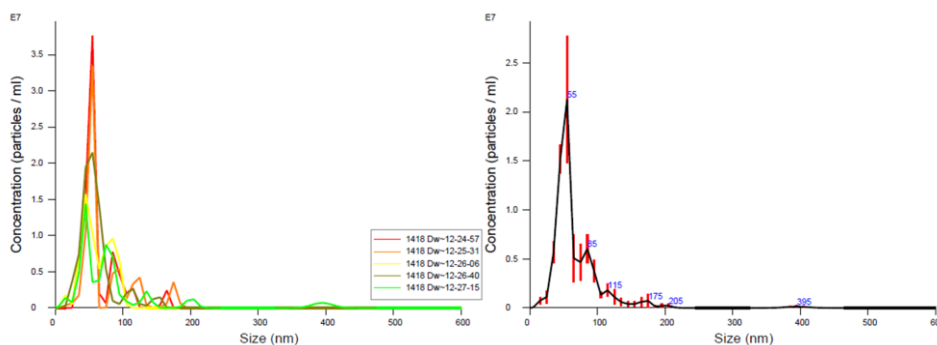


Fig. 26. NTA graphs of STm 1418  $\Delta tolR \Delta wbaP$  GMMA.

### 3.3.4 Comparison of DLS, MALS and NTA results

Dimensional analyses performed on SEn 618  $\Delta tolR \Delta msbB \Delta pagP$ , STm 2192  $\Delta tolR \Delta pagP \Delta msbB$ , STm 1418  $\Delta tolR$  and STm 1418  $\Delta tolR \Delta wbaP$  GMMA are summarized in Table 21.

**Table 21.** Summary of the analyses performed by DLS, SEC-MALS and NTA on SEn 618  $\Delta tolR \Delta msbB \Delta pagP$ , STm 2192  $\Delta tolR \Delta pagP \Delta msbB$ , STm 1418  $\Delta tolR$  and STm 1418  $\Delta tolR \Delta wbaP$  GMMA.

GMMA sample		DLS	SEC-MALS			NTA	
		Z-average diameter nm	2 x R <sub>n</sub> nm	2 x R <sub>w</sub> nm	2 x R <sub>z</sub> nm	Mean diameter nm	Mode diameter nm
SEn 618	Whole	111.8	71.8	73.2	74.9	106.0	91.9
	$\Delta tolR$ population						
	$\Delta msbB \Delta pagP$ Central fraction (2)						
STm 2192	Whole	103.0	67.8	69.4	71.8	102.8	78.6
	$\Delta tolR$ population						
	$\Delta msbB \Delta pagP$ Central fraction (2)						
STm 1418	Whole	91.4	70.0	71.5	73.8	95.8	85.6
	$\Delta tolR$ Central fraction (2)						
STm 1418	Whole	na	na	na	na	84.9	74.5
STm 1418	Whole	57.6	51.0	52.6	55.4	77.0	52.3
$\Delta tolR \Delta wbaP$ population							

na: not analysed.



Unfractionated GMMA shed by SEn 618  $\Delta tolR \Delta msbB \Delta pagP$ , STm 2192  $\Delta tolR \Delta pagP \Delta msbB$ , STm 1418  $\Delta tolR$  were characterized by different DLS hydrodynamic diameters, ranging from 111.8 to 91.4 nm. STm 1418  $\Delta tolR \Delta wbaP$ , instead, showed an average hydrodynamic size of 57.6 nm. For all OAg-positive (OAg<sup>+</sup>) GMMA, Z-average size by DLS was higher compared to the  $2 \times R_z$  values obtained by SEC-MALS. Not the same was found for OAg-negative (OAg<sup>-</sup>) GMMA, suggesting that the values by DLS were not only related to the overestimation of large particles by this method. The difference observed could be related to the presence of the OAg chains displayed on GMMA surface, which play an important role in determining the behaviour of GMMA in solution. OAg<sup>+</sup> GMMA were in fact characterized by a similar SEC-MALS diameter value of around 70 nm.

OAg chains specificities, including tridimensional conformation, number of repeating units, *O*-acetylation and glycosylation level, as well as the amount of lipid A, its structure and the percentage of OAg chains respect to total LPS molecules can determine the overall size of GMMA (Table 22). By looking at these characteristics, it was found a correlation between DLS diameters and number of OAg chains per GMMA particle (Fig. 27).

**Table 22.** Characterization of SEn 618  $\Delta tolR \Delta msbB \Delta pagP$ , STm 2192  $\Delta tolR \Delta pagP \Delta msbB$ , STm 1418  $\Delta tolR$  and STm 1418  $\Delta tolR \Delta wbaP$  GMMA trying to correlate GMMA size with their main features.

GMMA sample	OAg	Lipid A type	Z-average nm	2 x R <sub>z</sub> nm	μg protein/GMMA	OAg MM kDa	molar % OAg/Lipid A	OAg molecules/GMMA	Lipid A molecules/GMMA
<b>SEn 618</b>									
$\Delta tolR$ $\Delta msbB$ $\Delta pagP$	OAg <sup>+</sup>	penta	111.8	74.9	5.30 x 10 <sup>11</sup>	30.0	16.6	2812	16960
<b>STm 2192</b>									
$\Delta tolR$ $\Delta msbB$ $\Delta pagP$	OAg <sup>+</sup>	penta	103.0	71.8	9.19 x 10 <sup>11</sup>	34.6	10.2	2204	21527
<b>STm 1418</b>									
$\Delta tolR$	OAg <sup>+</sup>	hepta/hexa	91.4	73.8	6.78 x 10 <sup>11</sup>	32.9	7.0	768	11035
<b>STm 1418</b>									
$\Delta tolR$ $\Delta wbaP$	OAg <sup>-</sup>	hepta/hexa	57.6	55.4	3.01 x 10 <sup>10</sup>	/	/	/	49248

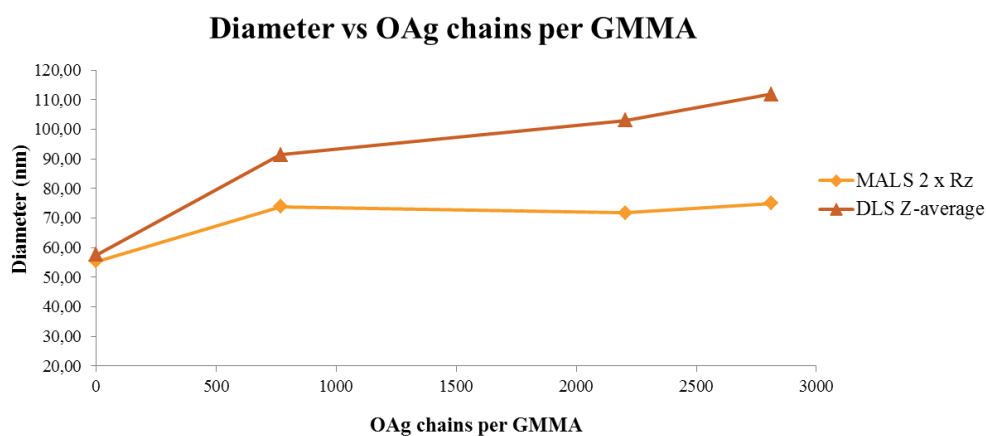


**Fig. 27.** Correlation between DLS Z-average diameter and MALS 2 x R<sub>z</sub> values and number of OAg chains per GMMA particle.

Average size of OAg chains was similar for all OAg<sup>+</sup> GMMA tested and no correlation was found between GMMA size and protein or lipid A content (Fig 28, 29).

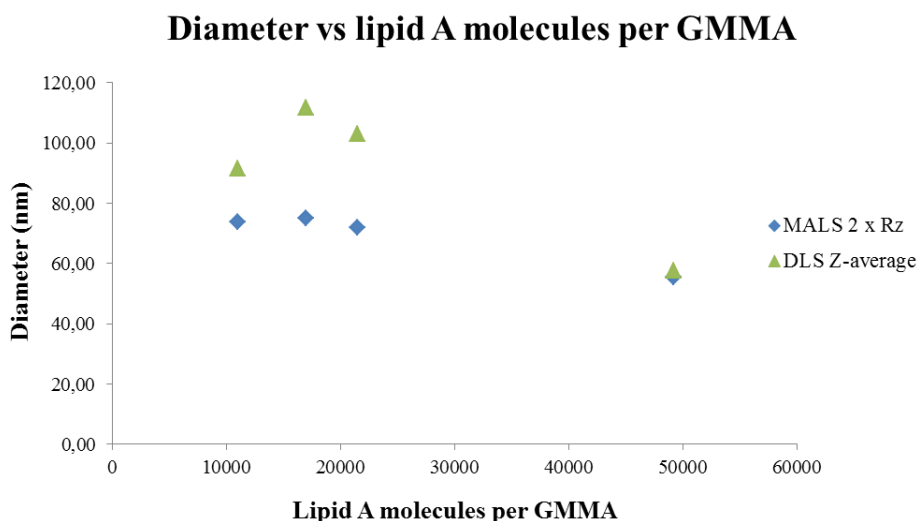


**Fig. 28.** Lack of correlation between DLS Z-average diameter and MALS 2 x R<sub>z</sub> values and number of lipid A molecules per GMMA particle.

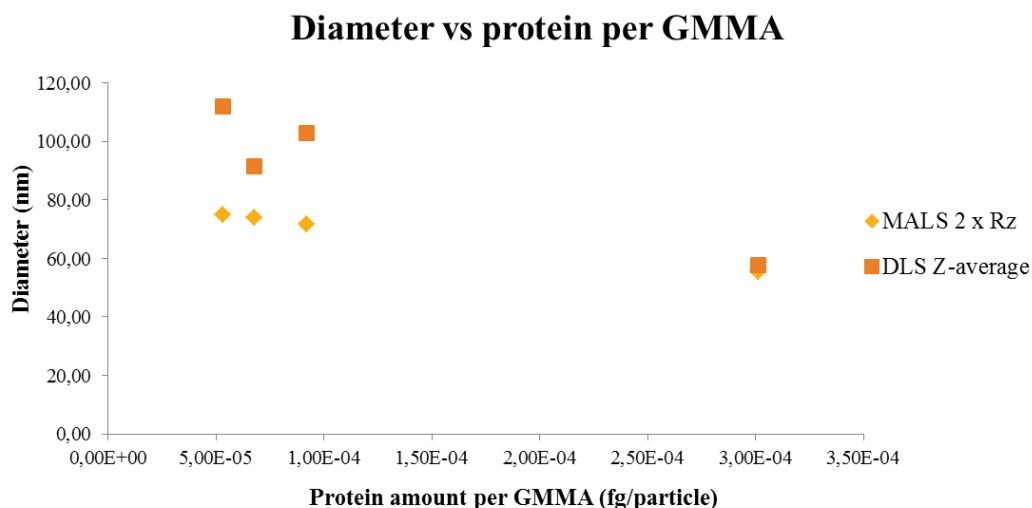


**Fig. 29.** Lack of correlation between DLS Z-average diameter and MALS 2 x R<sub>z</sub> values and µg protein per GMMA particle.



As expected, NTA hydrodynamic mean diameters of unfractionated OAg<sup>+</sup> GMMA were found to be similar to the Z-average values determined by DLS (Table 21). NTA presented the advantage to provide not only an average size value like DLS, but also a mode value, overcoming the problem of the DLS analysis. Analysing both unfractionated OAg<sup>+</sup> GMMA samples and the SEC fractions corresponding to the central area of the GMMA population allowed better understanding of this. In fact, the NTA mode values of the unfractionated samples were in agreement with the DLS Z-average diameters of the central fraction of the OAg<sup>+</sup> GMMA samples. Moreover, as expected, the mode values of the unfractionated and mean diameters of the central fractions both obtained by NTA were in good accordance. An appreciable aspect provided by NTA is represented by a deeper evaluation of GMMA samples. In particular, SD, D10, D50 and D90 percentile values add more information on particle sample characterization. For unfractionated GMMA, the difference between mean and mode values, as well as SD, D10, D50 and D90 values, clearly showed that GMMA samples were quite polydisperse. This moderate polydispersity made the analysis more difficult and the need to adjust the video and analysis settings during NTA sample visualization was indispensable. Fractionation of GMMA represented the way to achieve more homogeneity in size and scattering intensity shown by each particle visualized. Analysis of more homogeneous samples made manageable to obtain more consistent and reproducible results, requiring also a quite slight or no adjustment of NTA software settings. More homogeneity was also observed by the smaller gap between mean and mode sizes, as well as the low SD value and the small gap between D10 and D90 percentile values. In the case of the STm 1418  $\Delta tolR \Delta wbaP$  OAg<sup>-</sup> GMMA, NTA was able to confirm a smaller size respect to the other GMMA and similarity was observed with DLS and MALS size values (~50 nm), confirming that OAg<sup>-</sup>  $\Delta wbaP$  GMMA are much smaller respect to OAg<sup>+</sup> ones. Z average and  $2 \times R_z$  values resulted more in agreement, suggesting that the OAg shell around GMMA plays a role in determining the behaviour of GMMA in solution. It was above reported that NTA data interpretation was quite complex, both in size and concentration determination.



### 3.5 Discussion

Particle size distribution is an important parameter to check quality, consistency of production and stability of GMMA samples. Here, DLS, MALS and NTA were compared for the analysis of GMMA from different strains.

DLS allowed precise and reliable GMMA particle size analysis in few minutes, with rapid and simple sample preparation and instrument set up. A major drawback of DLS is that it is inherently sensitive to the presence of large particles in the sample in analysis [176] as verified by analysing unfractionated and fractionated GMMA samples. It is expected that the DSL Z-average size distribution of polydisperse samples is biased by even a small number of large particles, because such particles scatter light more efficiently than small ones [180, 181]. DLS measurements require careful data interpretation, especially when polydisperse or multimodal particle samples are investigated, including comparison with other size-analysing techniques, also based on different physical properties.

SEC-MALS is a rapid and robust method for GMMA size characterization, able to separate, characterize and quantify generally occurring contaminants, such as free soluble protein and DNA. Both DLS and MALS provide size measurements based on absolute analyses of samples in solution, independently of calibration standards. DLS and MALS technologies are complementary and independent, analysing different properties of the scattered light.

NTA is an alternative light scattering technology that simultaneously but individually tracks and analyses the trajectories of GMMA in suspension. Many of the problems associated with ensemble techniques as DLS are overcome. NTA can detect small, weakly-scattering particles among large, strong-scattering ones that would dominate the size distribution of a particle sample analysed by DLS. NTA is also able to resolve bimodal particle populations at resolutions that are significantly better than those achieved by DLS [176]. NTA not only allows size determination, but also counting particles number. However, for NTA analysis, a range of parameters need to be adjusted both for video capture (camera gain and shutter speed) and data elaborations (filter settings, background subtraction, removal of blurring, minimum



track length, minimum expected particle size and detection threshold). Standardization of the NTA techniques is difficult to be achieved due to the high number of options that the user can select before a NTA experiment [164], which is highly operator dependent [157, 162, 176, 178, 182]. Our study confirmed that detection threshold is one of the parameters that can strongly affect both size and concentration NTA estimations [162]. In particular, NTA analyses did not show an acceptable reproducibility among experiments performed using scalar-diluted samples at a fixed detection threshold value, both in GMMA size and concentration. Fixed video capture and video analysis parameters should not be used and a skilled operator is required in order to achieve reproducible size and concentration values.

In conclusion, all the three techniques provided complementary information allowing a more complete evaluation of GMMA size.

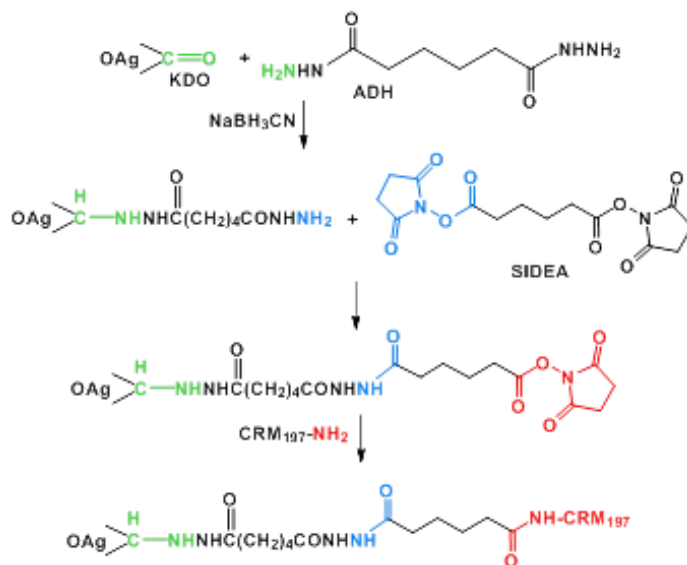


#### **4. KDO reactivity and selectivity in the synthesis of OAg-CRM<sub>197</sub> glycoconjugate vaccines**



## 4.1 Introduction

Covalent conjugation of the OAg component of LPS to an appropriate carrier protein represents one of the main strategies for the development of a bivalent vaccine against iNTS [72, 79, 80, 108]. In the strategy adopted by GVGH, *S. Typhimurium* and *S. Enteritidis* OAg chains are independently linked to CRM<sub>197</sub>, a non-toxic variant of diphtheria toxin [105] as carrier protein [77, 107]. The terminal unit of the LPS core oligosaccharide (OS), the 3-Deoxy-D-manno-oct-2-ulosonic acid (KDO) sugar, is expected to be involved in the selective linkage of OAg to the protein through the introduction of linker molecules, without impact on epitopes of OAg chain, which is the key target antigen for immunogenicity [106]. Reductive amination of KDO with adipic acid dihydrazide (ADH) and activation of free ADH hydrazide group with adipic acid bis-(N-hydroxysuccinimide) ester (SIDEA) are then followed by conjugation to the lysine residues of CRM<sub>197</sub> [106, 107] (Scheme 2).



**Scheme 2.** OAg conjugation steps for the synthesis of OAg-CRM<sub>197</sub> glycoconjugates [106].

OAg chains are extracted from bacteria, by performing direct acetic acid hydrolysis in the fermentation broth [118]. Hydrolysis cleaves the labile linkage between the core OS and the lipid A of LPS, releasing the OAg chains in the

supernatant and leaving the lipid A within the bacterial pellet (Fig. 30). The resulting OAg chains have KDO as the reducing terminus, available for conjugation [73, 183, 184].

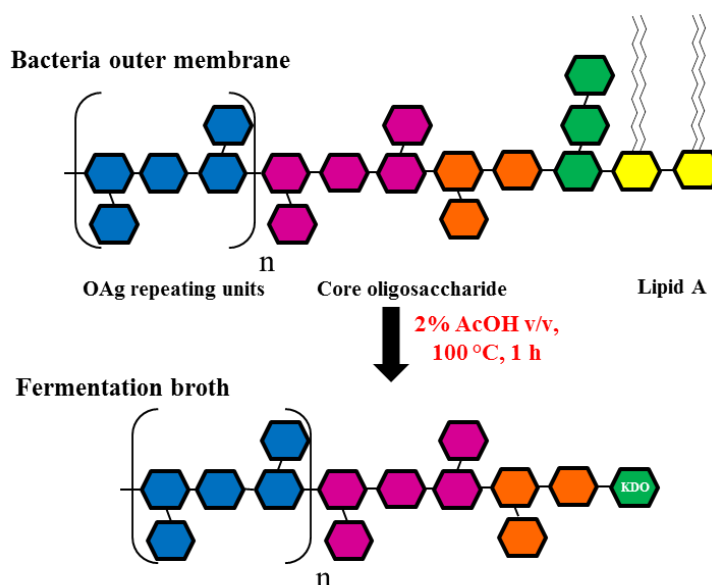


**Fig. 30.** *Salmonella* OAg chains extraction by acetic acid hydrolysis performed directly on bacteria. OAg chains are released in the fermentation broth removed of the toxic lipid A [118].

This process was successfully applied to various *Salmonella enterica* serovars, obtaining good yields of high-quality material. However, there is no evidence that, after this acid treatment on bacteria, the KDO is left at the reducing end with its native structure [185-187].

Previous attempts of identification of the terminal KDO were complicated by the presence of many OAg repeating units with respect to only one KDO sugar per chain. Furthermore structural rearrangements of KDO in unreactive forms to classical methods for KDO quantification can happen [187-193]. After mild acid hydrolysis of the LPS for lipid A removal, the terminal KDO may undergo lactonization, formation of anhydro derivatives, and other not well characterized artifacts which make identification and quantification of KDO much complex [194, 195] (Fig. 31).

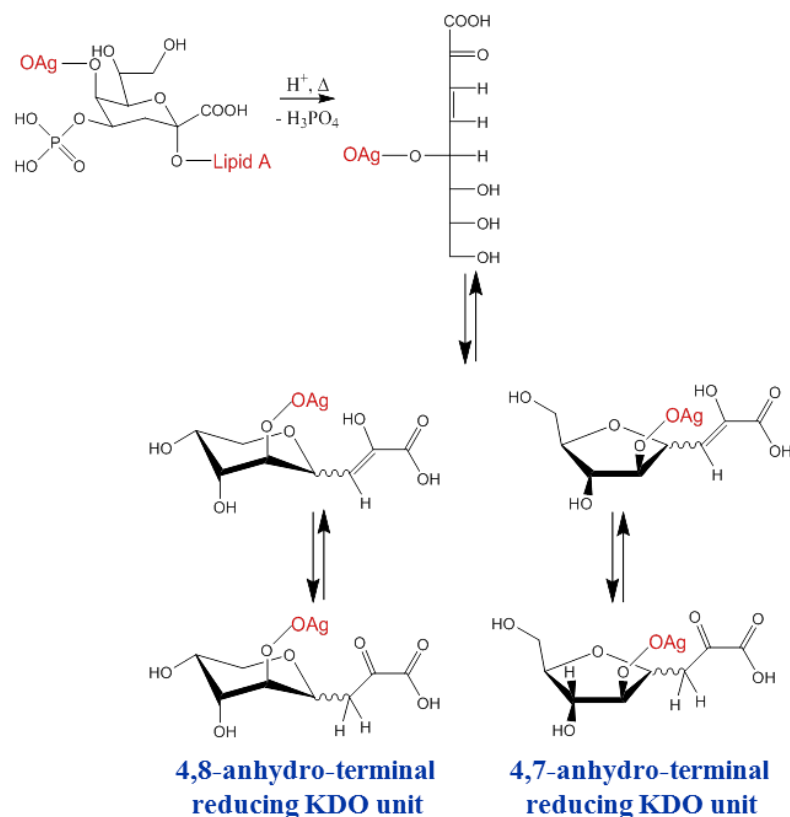


**Fig. 31.** 4-linked phosphate-KDO structural rearrangements observed during mild acid hydrolysis for lipid A removal (adapted from Sioud *et al*) [196].

The high reactivity of KDO in reductive amination reactions has been imputed to the formation of anhydro derivatives (Fig. 31), which have the ketone group not involved in an hemiketal linkage [194, 197].

In order to facilitate the investigation on KDO structure and reactivity, core OS from OAg<sup>-</sup> GMMA and oligosaccharides deriving from the exopolysaccharide produced by *B. cepacia* strain BTS13 containing KDO [198] were used as model molecules. Core OS was also used as model for the synthesis and the characterization of CRM<sub>197</sub> conjugates.

These studies have contributed to better characterize the *Salmonella* antigens and help to improve manufacturing processes for OAg-based glycoconjugate vaccines synthesis and characterization.



## 4.2 Materials and Methods

### 4.2.1 *B. cepacia* strain BTS13 for exopolysaccharide (EPS) production

*B. cepacia* strain BTS13 [199] was isolated from a cystic fibrosis patient attending the Cystic Fibrosis Regional Centre of Friuli-Venezia Giulia (Trieste, Italy). The EPS was obtained as already described [198].

### 4.2.2 *B. cepacia* BTS13 EPS hydrolysis and oligosaccharides purification

Mild acid hydrolysis (v/v 1% acetic acid at 100 °C for 3 h) was performed on a 2 mg/mL EPS solution. After evaporation of the acid under reduced pressure, the oligosaccharides were recovered by freeze-drying. Gel filtration chromatography on a Bio-Gel P-10 column (90 cm x 1.6 cm i.d., Bio-rad) with differential refractive index detection (dRI, WGE Dr. Bures Δn-1000, Labservice Analytica) was used to fractionate the oligosaccharides of different size. The mobile phase was NaNO<sub>3</sub> 0.05 M at the flow rate of 8 mL/h. Fractions were collected at 15 min intervals and were desalted by gel filtration chromatography on a Bio-Gel P-2 column (90 cm x 1.6 cm i.d., flow rate 8 mL/h, Bio-Rad).

### 4.2.3 STm 1418 Δ*tolR* Δ*wbaP* GMMA production and characterization

GMMA were produced and purified as described in the Chapter 3.

### 4.2.4 LPS core OS purification

For extraction of the LPS core OS from GMMA, a mild acid hydrolysis (v/v 2% acetic acid at 100 °C for 1 h) was performed directly on the GMMA suspension (protein concentration of 1 mg/mL). The core OS released into the supernatant was recovered following centrifugation (14000 rpm, 1 h, 4 °C). The acidic supernatant was evaporated under reduced pressure and washed 3 times with water, in order to



remove the residual acetic acid, and then freeze-dried. Gel filtration chromatography was performed as described above on the same Bio-Gel P-10 column. Fractions were desalted by gel filtration chromatography on a Bio-Gel P-2 column (90 cm x 1.6 cm i.d., flow rate 8 mL/h, Bio-Rad) or on a Sephadex G-10 column (14 cm x 1.6 cm i.d., flow rate 1.6 ml/min, GE Healthcare Life Sciences).

#### **4.2.5 De-phosphorylation of core OS**

LPS core OS was solubilized in 48% HF at a concentration of 40 mg/mL, and mixed at 4 °C for 48 h. Residual HF was neutralized by adding CaCO<sub>3</sub> powder. De-phosphorylated core OS was purified on PD-10 desalting column packed with Sephadex G-25 resin (GE Healthcare Life Sciences) and freeze-dried.

#### **4.2.6 Reduction of native and de-phosphorylated core OS**

Native and de-phosphorylated core OS were solubilized in water at a concentration of 8 mg/mL and NaBH<sub>4</sub> was added. The solutions were mixed at RT for 16 h. At the end, residual NaBH<sub>4</sub> was neutralized by adding 50% AcOH. Products were evaporated under reduced pressure three times with 10% AcOH in MeOH and three times with MeOH. Reduced oligosaccharides were purified on PD-10 desalting column packed with Sephadex G-25 resin (GE Healthcare Life Sciences) and freeze-dried.

#### **4.2.7 LPS core OS characterization**

Structural analysis of purified core OS and/or its derivatives was performed by HPAEC-PAD, HPLC-SEC after derivatization with semicarbazide, and <sup>1</sup>H NMR, as reported in Chapter 2. Heptose (Hep) was estimated by HPAEC-PAD after de-phosphorylation with HF and acid hydrolysis of the core OS to release the monosaccharides. Commercial monosaccharide was used for building the calibration curves in the range 0.5-10 µg/mL. Core OS samples, diluted to have Hep content in



the range 0.5-10  $\mu\text{g/mL}$ , were hydrolysed at 100 °C for 4 h in 1 M trifluoroacetic acid (TFA). After the hydrolysis, samples were chilled at 2-8 °C for about 30 min, dried by SpeedVac overnight, dissolved in water, and filtered using 0.45- $\mu\text{m}$  Acrodisc (PALL) filters before chromatographic analysis. HPAEC-PAD was performed with a Dionex ICS3000 equipped with a CarboPac PA10 column (4 x 250 mm) coupled with a PA10 guard column (4 x 50 mm). A flow rate of 1 mL/min was used, eluting with 18 mM NaOH for 20 min and then with 100 mM AcONa in 28 mM NaOH for 10 min. The effluent was monitored using an electrochemical detector in the pulse amperometric mode with a gold working electrode and an Ag/AgCl reference electrode. The Dionex standard quadruple-potential waveform for carbohydrates was used. The resulting chromatographic data were processed using Chromeleon software 6.8. The standards were hydrolysed and analysed in the same way as samples. 2,4,6-trinitrobenzene sulfonic acid (TNBS) colorimetric method was performed for amino groups quantification [200, 201].

#### **4.2.8 ESI-MS analysis**

Electrospray Ionization mass spectra were recorded on a Bruker Esquire 4000 ion trap mass spectrometer connected to a syringe pump for the injection of the samples. The instrument was calibrated using a tune mixture provided by Bruker. Oligosaccharides were dissolved in 50% aqueous methanol-11 mM  $\text{NH}_4\text{OAc}$ . Samples were injected at 180  $\mu\text{L/h}$ . Detection was performed both in the positive and negative ion modes.

#### **4.2.9 MALDI-TOF-MS analysis**

Matrix-Assisted Laser Desorption Ionization - Time of Flight mass spectra were recorded by UltraFlex III MALDI-TOF/TOF instrument (Bruker GmbH) in linear mode and with negative ion detection or by a Perceptive (Framingham, MA, USA) Voyager STR equipped with delayed extraction technology. Ions formed by a pulsed UV laser beam (nitrogen laser,  $\lambda = 337 \text{ nm}$ ) were accelerated by 24 kV. The mass



spectra were the result of 256 laser shots. The samples for analysis were prepared by mixing 2  $\mu\text{L}$  of product and 2  $\mu\text{L}$  of 2,5-dihydroxybenzoic acid (DHB) 50 mg/mL in 50% acetonitrile (ACN) v/v as matrix solution. 2  $\mu\text{L}$  of each mixture were deposited on samples plate, dried at room temperature for 10 min and subjected to the spectrometer analysis.

#### **4.2.10 Reaction of core OS with adipic acid dihydrazide (ADH)**

Core OS were solubilized in 100 mM AcONa pH 4.5 at a concentration of 40 mg/mL. ADH and  $\text{NaBH}_3\text{CN}$  were added as solids, both with a ratio 2.4:1 by weight with respect to the oligosaccharide (quantified based on Gal quantification by HPAEC-PAD). The solution was mixed at 30 °C for 2 h. The reaction mixture was diluted in 6 M NaCl and purified on a Biogel P-10 column (90 cm x 1.6 cm i.d., Bio-Rad). The mobile phase was  $\text{NaNO}_3$  0.05 M at the flow rate of 0.15 mL/min. Biogel P-10 fractions corresponding to the reaction product were desalted by gel filtration chromatography on a Sephadex G-10 column 28 mL (14 cm x 1.6 cm i.d., flow rate 1.6 ml/min, GE Healthcare Life Sciences).

#### **4.2.11 Characterization of core OS-ADH intermediate**

Derivatized core OS were characterized by HPAEC-PAD for neutral sugars quantification and by HPLC-SEC for verifying aggregation or degradation after modification. TNBS colorimetric method was used for total  $\text{NH}_2$  group quantification after introduction of ADH using ADH as standard and subtracting the number of  $\text{NH}_2$  groups already present on the un-derivatized oligosaccharide. Free ADH was detected by Reversed Phase - High Performance Liquid Chromatography (RP-HPLC) after derivatization with TNBS. A 600 nmol/mL solution of ADH was used to create a calibration curve in the 0.8 to 20 nmol/mL of amino groups range. Samples were diluted with MilliQ water in order to obtain sample amino groups concentration in the range of the calibration curve. Samples and calibration curves were created in duplicates and to a final volume of 250  $\mu\text{L}$ . A volume of 250  $\mu\text{L}$  of 70 mM Sodium



Phosphate pH 7.5 solution and a volume of 250  $\mu$ L of 0.1% solution of TNBS were added to standards and samples. Samples were incubated for 2 h at 40 °C in a pre-heated thermostatic bath. Cooled-down samples (10  $\mu$ L injected) were eluted on a Kinetex reversed-phase column (2.6  $\mu$ m, 50x4.6 mm, Phenomenex) on a Waters Acquity H Class UPLC system with in-line UV, fluorescence emission, dRI detectors. Samples were eluted with a flow rate of 1.0 mL/min and eluent mixture was generated by pump system. The eluent program (total run time 50 minutes) was: 90% water, 10% ACN in isocratic condition for 10 min; linear gradient to 10% water, 90% ACN in 10 minutes; 10% water, 90% ACN in isocratic condition for 10 minutes; 90% water, 10% ACN in isocratic condition for 20 minutes (column re-equilibration). Detection was done at 425 nm. The amount of free ADH was calculated using the calibration curve built with the peak areas of derivatized ADH standards at 425 nm. Activation on the terminus KDO with ADH was calculated as moles of linked ADH/moles of core OS % (taking into account Gal amount derived by HPAEC-PAD analysis).

#### **4.2.12 Reaction of core OS-ADH and core OS with adipic acid bis-(N-hydroxysuccinimide) ester (SIDEA)**

For verifying reactivity of PPEtN  $\text{NH}_2$  groups at two different pH, oligosaccharides were dissolved at 10 mg/mL in DMSO/ $\text{H}_2\text{O}$  9:1 with addition of triethanolamine (TEA) (molar ratio TEA/total  $\text{NH}_2$  groups = 5) or in DMSO/HCl 82.5 ppm 9:1 (v/v). When the oligosaccharides were completely solubilized, SIDEA was added as solid (molar ratio SIDEA/total  $\text{NH}_2$  groups = 3). The solution was mixed at RT for 3 h. In the case of core OS derivatization, unreacted free SIDEA was then precipitated by addition of water (90% volume in the resulting solution) and then washing the pellet with water (3 times with 1/2 of the volume added for the precipitation) and the supernatant lyophilized. For core OS-ADH, reaction product was precipitated by addition of 1,4-dioxane (90% volume in the resulting solution) and then the pellet was washed with the same organic solvent (3 times with 1/2 of the volume added for the precipitation) to remove residual free SIDEA and lyophilised.





Reaction conditions were adjusted for the synthesis of the intermediates to be conjugated to CRM<sub>197</sub>. Core OS and core OS-ADH were dissolved in DMSO/HCl 82.5 ppm 9:1 (v/v) at a concentration of 5 mg/mL (core OS-ADH) or 10 mg/mL (core OS). After their complete solubilisation, SIDEA was added as solid (molar ratio SIDEA/total NH<sub>2</sub> groups = 12). The solution was mixed at RT for 1 h. Purification was performed by precipitation of unreacted SIDEA by addition of HCl 82.5 ppm (1:1 v/v respect to reaction mixture) and precipitation of oligosaccharides by addition of ethanol (90% volume in the resulting solution). The pellet was then washed with the same organic solvent (twice with 1.5 times of the reaction volume), to remove residual free SIDEA, and lyophilised.

#### 4.2.13 Characterization of SIDEA-derivatized core OS intermediates

SIDEA-derivatized intermediates were characterized by HPAEC-PAD for neutral sugars quantification and by HPLC-SEC for verifying aggregation or degradation after modification on TSK gel G3000 PWXL column (30 cm x 7.8 mm; particle size 7 μm, Tosoh Bioscience) and with UV, fluorescence emission, dRI detectors. TNBS colorimetric method was used for the residual NH<sub>2</sub> groups quantification after introduction of SIDEA using 6-aminohexanoic acid (core OS) or ADH (core OS-ADH) as standard. Total active ester groups introduced with SIDEA were quantified by RP-HPLC as N-hydroxysuccinimide (NHS) groups. A 100 nmol/mL solution of NHS was used to create a calibration curve of NHS in the 3 to 50 nmol/mL range. Samples were diluted with MilliQ water in order to obtain samples NHS concentration in the range of the calibration curve. Samples and calibration curves were created in duplicates. A volume of 50 μL was injected and analysed on a Gemini-NX C18 reversed-phase column (5.0 μm, 110A, 250x4.6 mm, Phenomenex) on a Waters Acquity H Class UPLC system with in-line UV, fluorescence emission, dRI detectors. Samples were eluted with a flow rate of 1.0 mL/min and eluent mixture was generated by pump system. The eluent program (total run time 8 minutes) was: 80% 10 mM tert-butyl ammonium bromide (TBABr) in 0.17% ammonium hydroxide, 20% ACN in isocratic condition for 8 min. Detection was done at 260 nm. Percentage

of derivatization with SIDEA was calculated as molar ratio % of derivatized  $\text{NH}_2$  groups/total  $\text{NH}_2$  groups present prior the reaction by TNBS colorimetric assays. Percentage of active ester groups was calculated as molar % of total active NHS groups introduced/derivatized  $\text{NH}_2$  groups.

#### 4.2.14 Synthesis of core OS-CRM<sub>197</sub> conjugates

SIDEA-derivatized core OS intermediates were solubilized in 100 mM  $\text{NaH}_2\text{PO}_4$  buffer pH 7.2 and CRM<sub>197</sub> was added to give a protein concentration of 5 mg/mL and a molar ratio of active ester groups to CRM<sub>197</sub> of 30 to 1. The reactions were mixed at RT for 3 h. Conjugates were purified by 2 mL Vivaspin (cut off 30 kDa, Sartorius AG) against 5 mM  $\text{NaH}_2\text{PO}_4$  pH 7.2.

#### 4.2.15 Characterization of purified OS-CRM<sub>197</sub> conjugates

Neutral sugars content was quantified by HPAEC-PAD, protein content by micro BCA protein assay and the molar ratio of oligosaccharide content (relative to Gal amount by HPAEC-PAD) with respect to protein amount was calculated. HPLC-SEC analysis was used to characterize conjugates, in comparison with unconjugated oligosaccharide and free CRM<sub>197</sub>. Conjugates were eluted on a TSK gel 3000PW-XL with guard column in 0.1 M NaCl, 0.1 M  $\text{NaH}_2\text{PO}_4$ , 5%  $\text{CH}_3\text{CN}$ , pH 7.2, mobile phase at the flow rate of 0.5 mL/min. Core OS average loading on CRM<sub>197</sub> was determined by MALDI-TOF analysis. A volume of 2  $\mu\text{L}$  of conjugates was mixed with 2  $\mu\text{L}$  of a saturated solution of Super DHB in 50% acetonitrile solution containing 0.1% TFA. A volume of 2  $\mu\text{L}$  of the mix was spotted on a MTP 384 stainless steel target (Bruker Daltonics GmbH, Bremen, Germany) and allowed to air-dry. Measurements were recorded on an UltraFlex III (Bruker GmbH) MALDI-TOF/TOF MS in linear mode. External calibration was performed by spotting a volume of 2  $\mu\text{L}$  of protein calibration standard II (Bruker Daltonics) containing the following proteins: trypsinogen (23,982 Da), protein A (44,613 Da) and bovine serum albumin (66,431 Da). All mass spectra were recorded by summing up to 400 laser

shots. The Flex Analysis software packages provided by the manufacturer were used for data processing. Glycoconjugates were analysed by SDS-PAGE for verifying conjugate formation. 7% Tris-acetate gels (NuPAGE, Invitrogen) were used. The samples (5-20  $\mu\text{L}$  with a protein content of 5-10  $\mu\text{g}$ ) were mixed with NuPAGE LDS sample buffer (1/5 v/v). The gel, containing loaded samples, was electrophoresed at 45 mA in NuPAGE Tris-Acetate SDS running buffer (20x, Invitrogen) and stained with Simply Blue Safe Stain (Invitrogen).

#### **4.2.16 Synthesis and characterization of OAg-ADH-SIDEA-CRM<sub>197</sub> conjugate**

The conjugate was produced by Renzo Alfini and characterized as described by Stefanetti *et al* [107]. OAg purified from 2192 *S. Typhimurium* strain was used for conjugation. OAg-CRM<sub>197</sub> conjugate with an OAg/protein ratio of 2.29 and an average number of 5 sugar chains linked to CRM<sub>197</sub> was subjected to chemical de-glycosylation and trypsin digestion as the core OS-CRM<sub>197</sub> conjugates.

#### **4.2.17 Glycoconjugates de-glycosylation by trifluoromethanesulphonic acid (TFMS) [202].**

Such procedure was applied to core OS-CRM<sub>197</sub> and OAg-ADH-SIDEA-CRM<sub>197</sub> conjugates. An amount of 200  $\mu\text{g}$  of protein was diafiltered using 30 kDa Vivaspin 2 (Sartorius AG) against water for a complete removal of salt and lyophilized. The reactive mixture was prepared under  $\text{N}_2$ , mixing TFMS and anisole in a ratio 10:1 v/v. A volume of 50  $\mu\text{L}$  was added under  $\text{N}_2$  to the lyophilized samples and gently mixed. After a complete dissolution, the solution was mixed at 4 °C for 2 h. The reaction was stopped by adding 60% pyridine at -20 °C. The solution was dialysed at 4 °C against 50 mM  $\text{NH}_4\text{HCO}_3$  pH 8 in Slide-a-Lyzer membrane (cut off 10 kDa, Thermofisher) for pyridine and monosaccharides removal.

#### **4.2.18 Trypsin digestion of de-glycosylated conjugates**



An amount of 100  $\mu\text{g}$  of TFMS-de-glycosylated conjugates in 50 mM  $\text{NH}_4\text{HCO}_3$  pH 8 was subjected to trypsin enzymatic digestion. A 200  $\mu\text{g}/\text{mL}$  trypsin solution was added to give a w/w ratio of CRM<sub>197</sub> to trypsin of 20 to 1. The solution was mixed at 37 °C for 16 h and stored at -80° C.

#### **4.2.19 MALDI-MS analysis for peptide mapping**

Spectra were recorded by UltraFlex III MALDI-TOF/TOF instrument (Bruker GmbH) both in reflection and linear mode and with positive ion detection ( $m/z$  range between 500 and 5800) by Dr. Laura Salvini (Toscana Life Sciences, Siena, Italy). A volume of 2  $\mu\text{L}$  of de-glycosylated/digested conjugates was mixed with 2  $\mu\text{L}$  of a saturated solution of  $\alpha$ -cyano-4-hydroxycinnamic (HCAA) in 50% ACN solution containing 0.1% TFA. A volume of 2  $\mu\text{L}$  of the mix was spotted on a MTP 384 stainless steel target (Bruker Daltonics GmbH, Bremen, Germany) and allowed to air-dry. MS analysis data were elaborated using Biotools and Sequence editor softwares (Bruker, GmbH).

#### **4.2.20 LC-ESI-MS analysis for peptide mapping**

Conjugates peptide mapping analysis was performed by Dr. Stefano Gotta (GSK Analytical R&D Mass Spectrometry, Siena, Italy). De-glycosylated/digested conjugates were separated by liquid chromatography (LC) on an ACQUITY UPLC I-Class system (Waters) coupled to a Q Exactive Plus HRMS (Thermo Scientific). Peptides were loaded and separated on an Acquity UPLC CSH C18 130Å column (1 mm X 150 mm, 1.7  $\mu\text{m}$ , Waters) set at 50 °C using a flow rate of 0.05 mL/min in gradient mode. Mobile phase A consisted of 3% ACN 0.1% formic acid in water and mobile phase B of 0.1% formic acid in ACN. The following gradient was used: 0-28% B in 40 min, 28-85% B in 5 min, holding at 85% B for 5 min and re-equilibration at 0% B for 10 min. The injection volume was 10  $\mu\text{L}$ . For each sample the LC-MS/MS runs were performed in triplicate. The mass spectrometric method used was an automated Data-Dependent Acquisition (DDA) based on the top 5



precursors. The acquisition software was XCalibur, version 3.0.63 (Thermo Scientific) and the mass spectrometer was a Q Exactive Plus from Thermo Scientific. The ESI source was operated in positive mode with the following parameters: capillary temperature, 320 °C; spray voltage, 3.5 kV; sheath gas (nitrogen) flow rate, 35; and aux gas flow, 15. Data was acquired using full MS scan (resolution: 70.000; AGC target: 3e6; Maximum IT: 200 ms; scan range: m/z 300-1600) and collision induced dissociation (CID) based data dependent MS/MS (DDMS2) (Resolution: 17.500; AGC target: 1e5; Maximum IT: 150 ms; Loop count: 5; TopN = 5; Isolation window: m/z 3.0; Scan range: m/z 200-2000; NCE: 26; Underfill ratio: 3.8%; intensity threshold: 2.5e4; Apex trigger: 6-12 s; Dynamic exclusion: 12 s).

Peptide identifications, ion map alignment, and area quantification were carried out using the software Peak Studio 8.0 (BSI, Waterloo, ON) with the following parameters: 15 ppm parent mass error tolerance and 0.05 Da fragment mass tolerance, a maximum of 4 allowed missed cleavages, semi-tryptic specificity. Oxidation (M), de-amidation (NQ), pyro-Gln (Q), and the specific linker-carbohydrate adducts on lysine (K), were set as variable modifications. Database search was performed using a custom database made of the CRM<sub>197</sub> sequence and a consistent list of classical contaminants. False discovery rate (FDR) estimation was enabled by the use of a corresponding decoy database. A FDR <0.1% was applied as a confidence filter of peptide identifications.

## 4.3 Results

### 4.3.1 Characterization of core OS from STm 1418 $\Delta tolR \Delta wbaP$ GMMA

With the aim of facilitating the investigation on KDO structure and reactivity, GMMA shed by a mutant of *S. Typhimurium* 1418 strain with *tolR* and *wbaP* gene deletions (STm 1418  $\Delta tolR \Delta wbaP$ ) were produced. The deletion *wbaP* led to the synthesis of LPS lacking the OAg repeats [203]. Their absence with the achievement of a lipo-oligosaccharide (LOS) on GMMA surface, made easier to verify the KDO

presence, to evaluate its structure after mild acid hydrolysis and to study its reactivity in the conjugation process to CRM<sub>197</sub>.

Sugar composition of purified core OS (Table 23) is in agreement with *Salmonella* LPS structure reported in the literature [204] (Fig.32).

**Table 23.** Characterization of core OS extracted from STm 1418  $\Delta tolR \Delta wbaP$  GMMA. Neutral sugars were determined by HPAEC-PAD, HPLC-SEC/semicarbazide was used for KDO quantification, and TNBS colorimetric assay for pyrophosphorylethanolamine (PPEtN) quantification.

Core OS	Gal	Glc	GlcNAc	Hep*	KDO	PPEtN
<b>Molar ratios</b>	1.00	0.95	0.43	1.54	0.52	0.49

\*Hep quantification after core OS de-phosphorylation.

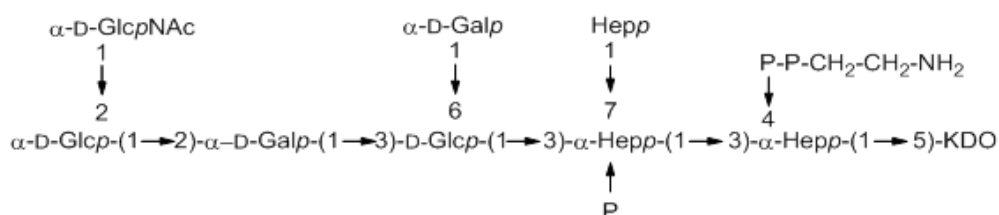


**Fig. 32.** *Salmonella* LPS core OS structure, as reported in literature for *Salmonella* strains [204].

Core OS resulted 100% substituted with PPEtN (as verified by TNBS), indicating also PPEtN stability in the extraction conditions.

The extracted oligosaccharide was analysed by ESI-MS (both positive and negative ion polarity (Fig. 33).

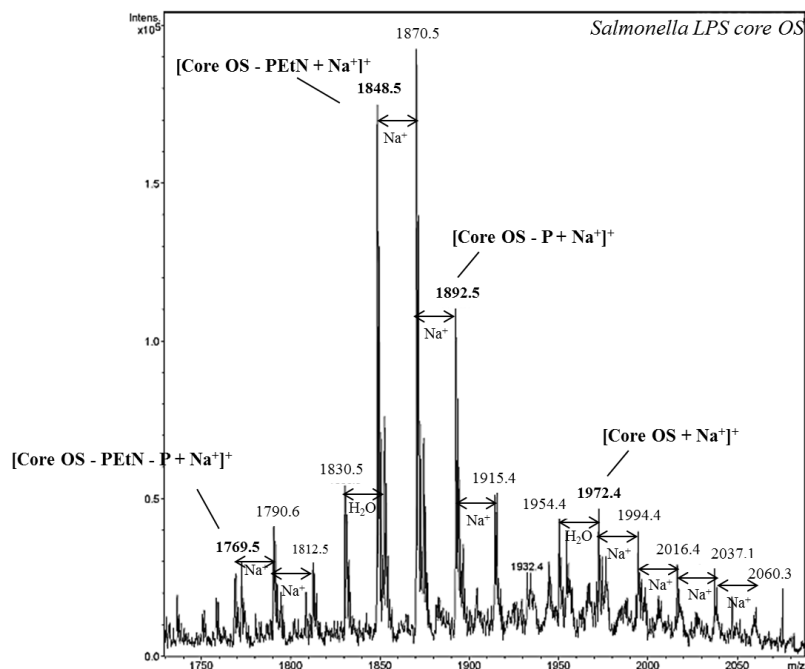


**Fig. 33.** ESI-MS spectrum of core OS (positive ion polarity). Ion having 1972.4 u corresponds to the sodium adduct of the core OS. Ion having 1892.5 u was attributed to core OS lacking a phosphate group (P), ion at 1848.5 u corresponds to the core OS lacking PEtN group. Ion having 1769.5 u was attributed to the core OS lacking P and PEtN (or PPEtN).

The presence of only one KDO unit per core OS chain after mild acid hydrolysis was confirmed. In the positive ion polarity mass spectrum, the ion having 1972.4 u corresponds to the sodium adduct of core OS reported in Fig. 32 [204], and ions lacking pyrophosphorylethanolamine (PPEtN), phosphorylethanolamine (PEtN) and phosphate (P) groups were detected. The ion at 1870.5 u was selected for performing tandem mass spectra (MS<sup>2</sup>), that resulted in the molecular fragmentations consistent with the *Salmonella* LPS core OS structure (data not shown). Differently from data reported in literature, the presence of terminal KDO in its native form was verified. The ions shifted of 18 u (elimination of a water molecule) from the pseudomolecular ions were also detected but these dehydrated forms are commonly observed in positive and negative ion polarity mass spectra of carbohydrates. Data were confirmed by MALDI-MS analysis.



$^1\text{H}$  NMR spectrum of core OS (Fig. 34) showed the typical signals of the terminal non-reducing KDO in its native form, in equilibrium between the  $\alpha$  and  $\beta$  forms.

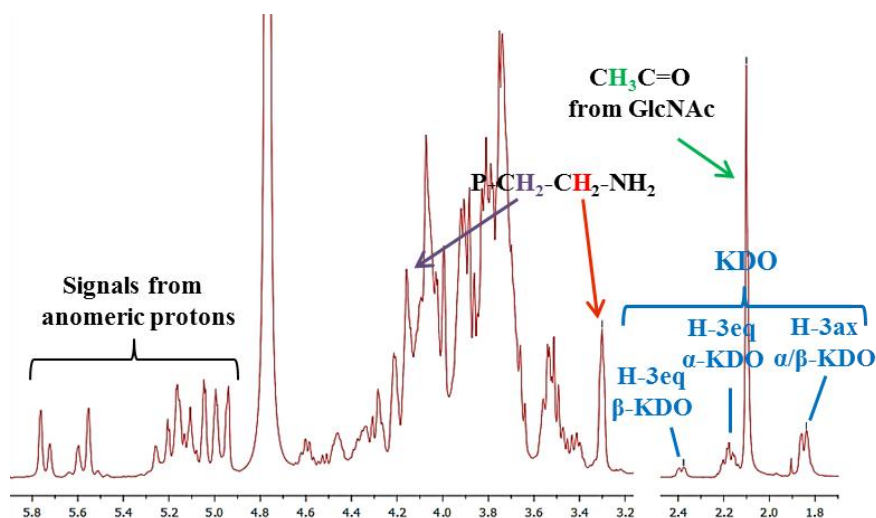
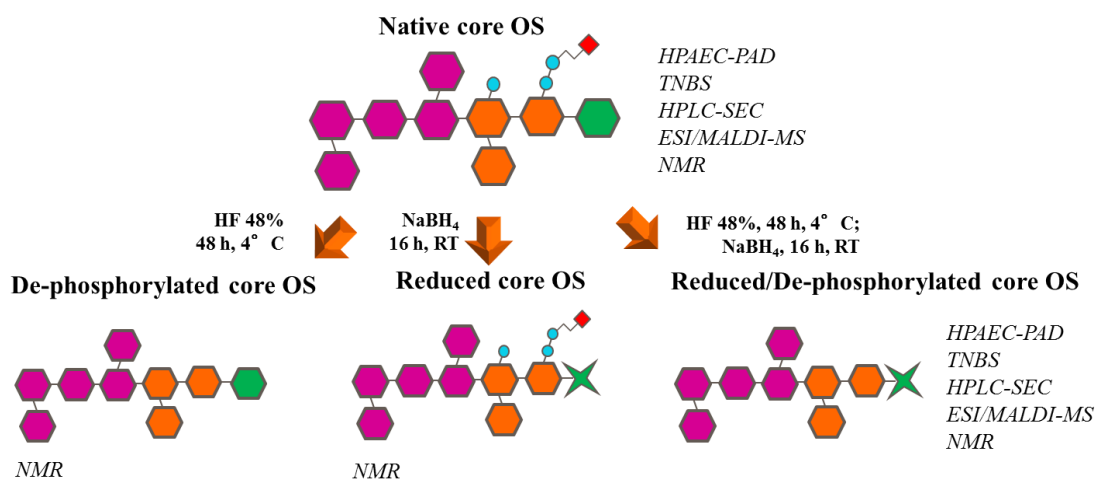


**Fig. 34.**  $^1\text{H}$  NMR spectrum of *Salmonella* LPS core OS. Three small signals between 2.4 and 1.8 ppm were attributed to the two H-3 of non-reducing KDO, involved in the equilibrium between the  $\alpha$  and  $\beta$  forms. The resonance at 2.1 ppm was attributed to the methyl group of the *N*-acetyl substituent of GlcNAc. Resonances at 3.1 and 4.2 ppm were attributed to the protons of PPEtN.

Assignments of the major peaks were done according to the literature [205, 206]. Bi-dimensional NMR spectra of the native core OS were rather complex due to the non-stoichiometric presence of phosphate groups and to the  $\alpha$  and  $\beta$  equilibrium of KDO. In order to simplify the NMR spectra, the core OS A was subjected to reduction and to de-phosphorylation, performed independently and sequentially (Scheme 3).





**Scheme 3.** Structural modifications performed on native core OS and indication of the analytical methods performed on each oligosaccharide sample.

The three different samples were compared with the native unmodified core OS by <sup>1</sup>H NMR, which confirmed the success of the reactions showing modifications of resonances of the anomeric protons the core OS sugars and KDO H-3 signals (Fig. 35).

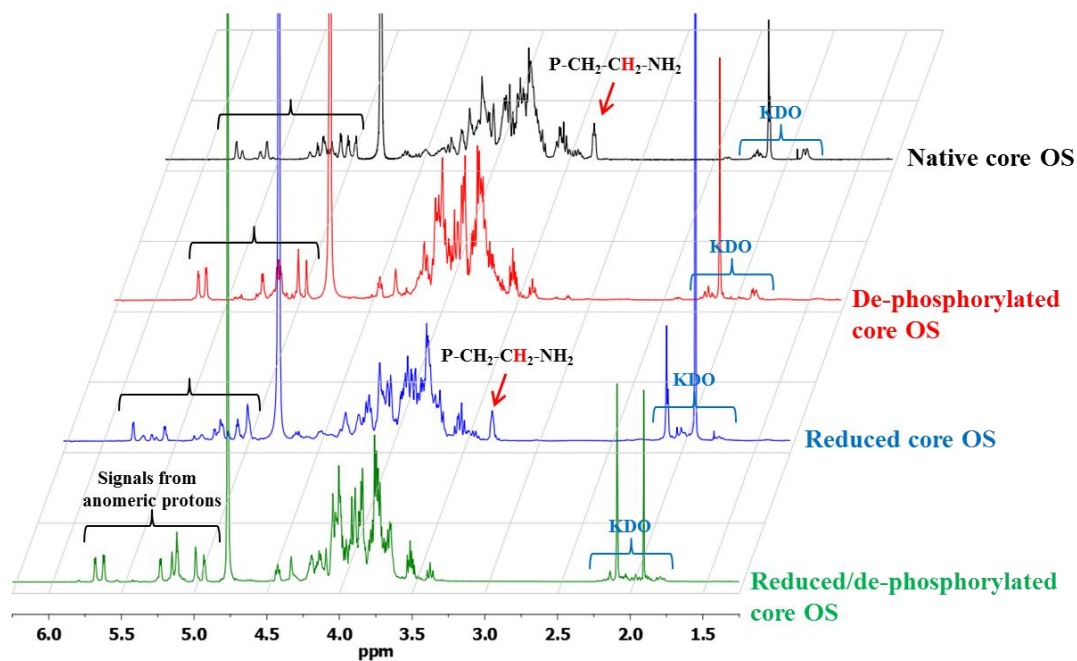


**Fig. 35.** <sup>1</sup>H NMR spectrum of modified core OS. Complete removal of phosphate substituents was obtained. Simplification of oligosaccharide anomeric protons resonances after de-phosphorylation and variation of the KDO H-3 signals after reduction were observed.

MALDI-MS analysis (both in positive and negative ion polarity) of the reduced/de-phosphorylated core OS gave the expected ions (Fig. 36) and again confirmed the presence of no anhydro KDO.

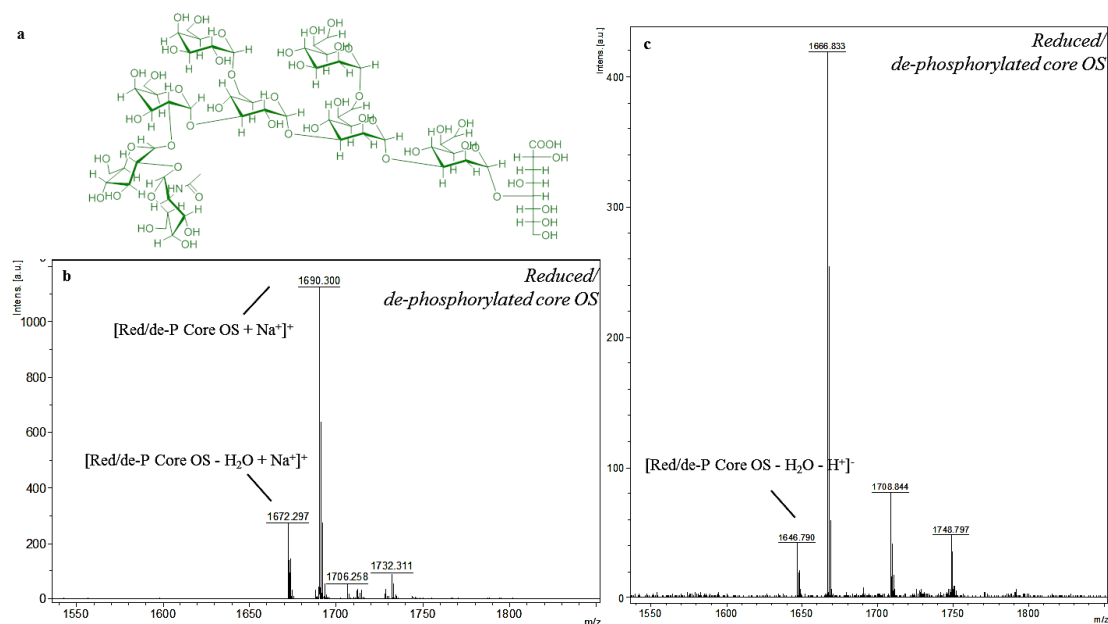


**Fig. 36.** MALDI-MS spectrum of reduced/de-phosphorylated core OS recorded in positive (b) and negative (c) ion polarity. In panel b, ion having 1690.3 u was attributed to the sodium adduct of the reduced/de-phosphorylated core OS structure (a). In panel c, ion having 1666.8 u was attributed to the reduced/de-phosphorylated core OS structure (a).

#### 4.3.2 Characterization of the oligosaccharides from *B. cepacia* BTS 13 EPS

The EPS produced by BTS13 strain of *B. cepacia* was also used for KDO structure evaluation, since the repeating unit of the BTS13 EPS contains one KDO residue, linked as the KDO in *Salmonella* LPS molecules [198] (Fig. 37).

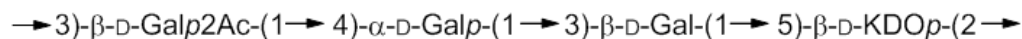


**Fig. 37.** Repeating unit of the EPS produced by *B. cepacia* BTS13 [198].

The EPS was subjected to mild acid hydrolysis to cleave the acid-labile ketosidic linkage between the position 2 of KDO and the position 3 of Gal. Oligosaccharides of 1, 2 and 3 repeating units having the KDO at the reducing end were obtained. The

tetrasaccharide (BTS13 tetra) was used for KDO structure investigation. ESI-MS analysis confirmed the presence of the terminal KDO unit in its native form, as already assessed by the analysis performed on the *Salmonella* LPS core OS (data not shown).

### 4.3.3 Investigation on KDO reactivity

The reaction of imine formation with semicarbazide [148] was used for evaluating KDO reactivity, comparing different terminal KDO-containing and KDO-related molecules. OAg from STm 2192 wild type strain and BTS13 tetra were compared with KDO ammonium salt and sodium pyruvate, an  $\alpha$ -keto acid structurally correlated to the KDO anhydro compounds [191, 193, 194] (Fig. 31), at the same KDO molar concentration, in the reaction with semicarbazide (Fig. 38).

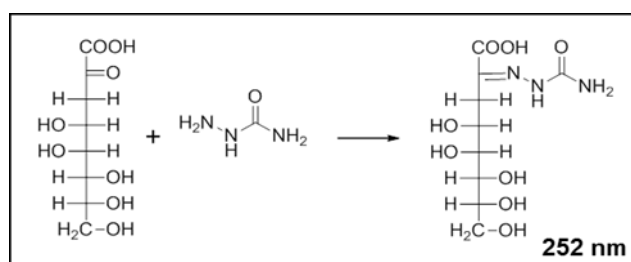


**Fig. 38.** Scheme of the reaction of derivatization of the C=O group of KDO with semicarbazide.

The kinetic of reaction performed at 30 °C was monitored by HPLC-SEC, analysing the absorbance (Abs) of the reaction products at 252 nm (Fig. 39). It has been previously verified in GVGH that the reaction with semicarbazide gave high absorbance values with  $\alpha$ -ketoacid compounds (like KDO and pyruvic acid), while absorptions 100 folds lower were obtained for sugars like Rha, Glc and fructose.

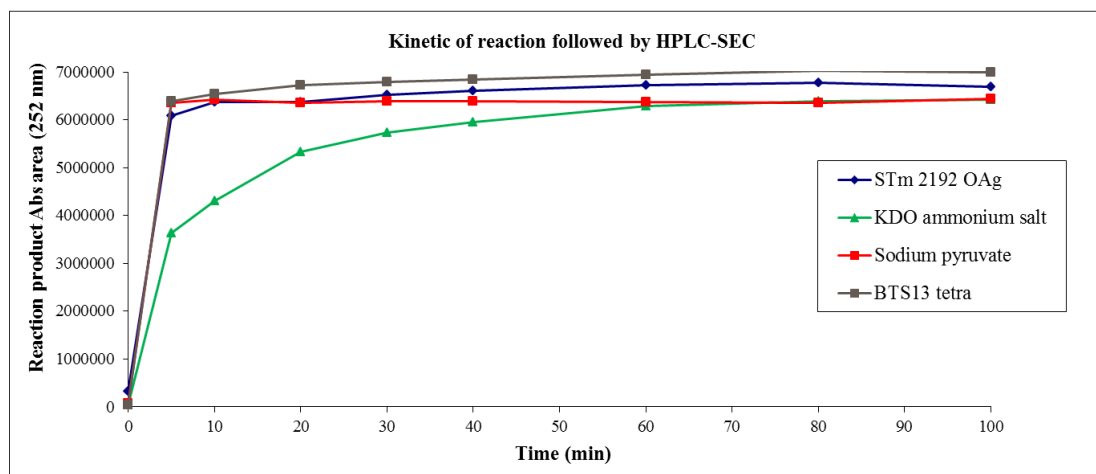
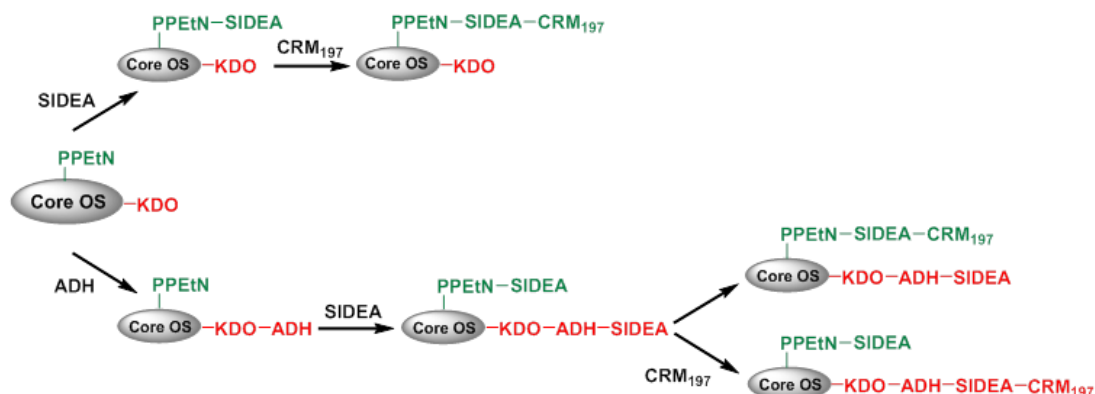


**Fig. 39.** Kinetic of reaction of KDO monosaccharide (ammonium salt), sodium pyruvate, STm 2192 OAg and BTS13 tetra with semicarbazide (Abs area of the reaction products peak detected at 252 nm over time). All samples were analysed at the same KDO molar concentration.

The reaction rate of the KDO monosaccharide was slower than the reaction of the KDO at the reducing end of OAg and BTS13 tetra samples, which was interestingly similar to that of pyruvate. Having established that KDO is in its native form at the end of OAg chains, its high reactivity in the imine formation might be due to its C-5 linkage to the sugar chain.

#### 4.3.4 Core OS conjugation to CRM<sub>197</sub>

ADH and SIDEA were introduced on core OS molecules according to Scheme 2. ADH was expected to react with the terminal KDO units, whereas the reaction step with SIDEA could involve amino groups of both ADH and PPEtN, for which a 100% substitution was found. SIDEA reaction was investigated with and without derivatization of KDO with ADH (Scheme 4).



**Scheme 4.** Reactions performed on core OS chains for the conjugation with CRM<sub>197</sub>.

#### *Core OS reductive amination with ADH*

Reaction of core OS with ADH was performed in order to investigate on the first step of conjugation (Scheme 2 and 4) and verify the effective involvement of KDO in the reaction. Synthesis and purification processes were optimized for reaction of short oligosaccharide chains and showed high yield of activation (100%) and recovery after purification (72%). A very low amount of free ADH (0.8% respect to total ADH) was also detected. MALDI-MS (negative ion polarity) of core-OS-ADH confirmed the expected product formation (ion at 2106.6 u). Sodium counterions, due to the presence of carboxyl and phosphate groups, as well core OS lacking phosphorylethanolamine (PEtN) were detected (Fig. 40). Presence of dimers (core OS-ADH-core OS) or unreacted core OS (or with reduced KDO) were not detected.

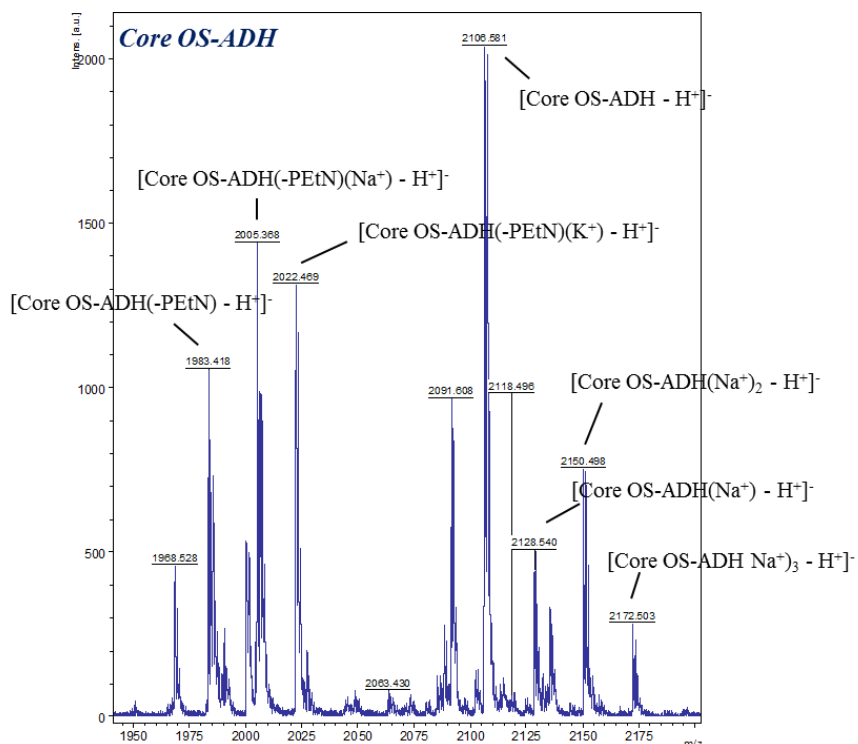


**Fig. 40.** MALDI-MS spectrum of core OS-ADH (negative ion polarity). The ion at 2106.6 u was attributed to the formation of the reaction product, whereas the ion at 1983.4 was attributed to the reaction product lacking phosphorylethanolamine PEtN.

HPLC-SEC analysis showed a single peak confirming no dimers formation. Analysis of core-ADH by semicarbazide showed no further KDO reactivity, suggesting that C=O group of the KDO was effectively the sugar involved in this reaction.

#### *Synthesis of core OS-SIDEA intermediate*

Core OS-SIDEA intermediate was synthesized without introduction of ADH on the terminal KDO to verify PPEtN reactivity. Reaction was performed in basic and acidic conditions (Table 24). Introduction of SIDEA on core OS chain was confirmed at both pH values by MALDI-MS analysis (Fig. 41), with 90% PPEtN groups derivatized in both cases, as estimated by TNBS assay. Moreover, stability of the products after 8 days at 37 °C was verified.

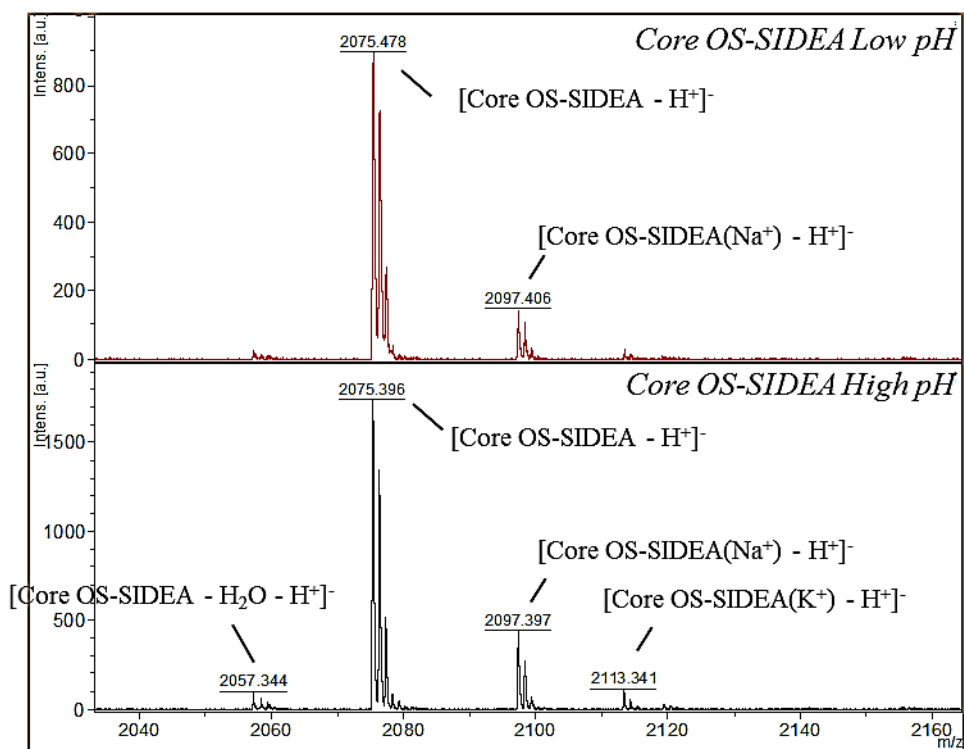


**Fig. 41.** MALDI-MS spectra of the core OS-SIDEA compounds synthesized at high and low pH. The ion at 2075.4 u was attributed to the formation of the reaction product, with activation of PPEtN amino groups with SIDEA.

Analysis of core OS-SIDEA compound by HPLC-SEC showed a peak (20% dRI area respect to the main peak) that could be attributed to dimers formation.

The reaction conditions for the synthesis of the core OS-SIDEA intermediate were adjusted in order to minimize the formation of dimers and SIDEA hemiester reactive group hydrolysis (Table 24).



**Table 24.** Characterization of core OS-SIDEA intermediates obtained by working in different conditions.

<b>Reaction conditions</b>	<b>% NH<sub>2</sub> derivatization (by TNBS)</b>	<b>% active ester groups (by RP-HPLC)*</b>
Core OS concentration 10 mg/mL, Core OS concentration 10 mg/mL, DMSO/H <sub>2</sub> O 9:1 + TEA (molar ratio TEA/total NH <sub>2</sub> groups = 5), SIDEA/total NH <sub>2</sub> groups molar ratio 3, RT, 3h	<b>90.2</b>	<b>nd</b>
Core OS concentration 10 mg/mL, DMSO/HCl 82.5 ppm 9:1, SIDEA/total NH <sub>2</sub> groups molar ratio 3, RT, 3h	<b>91.2</b>	<b>nd</b>
Core OS concentration 10 mg/mL, DMSO/HCl 82.5 ppm 9:1, SIDEA/total NH <sub>2</sub> groups molar ratio 12, RT, 1h	<b>64.4</b>	<b>75.6</b>

\*with respect to PPEtN NH<sub>2</sub> group reacted; nd = not determined.

An acceptable PPEtN amino group derivatization was obtained, together with a good retention of reactive SIDEA hemiester groups, available for conjugation.

Analysis by MALDI-MS confirmed the synthesis of the active intermediate (Fig. 42).

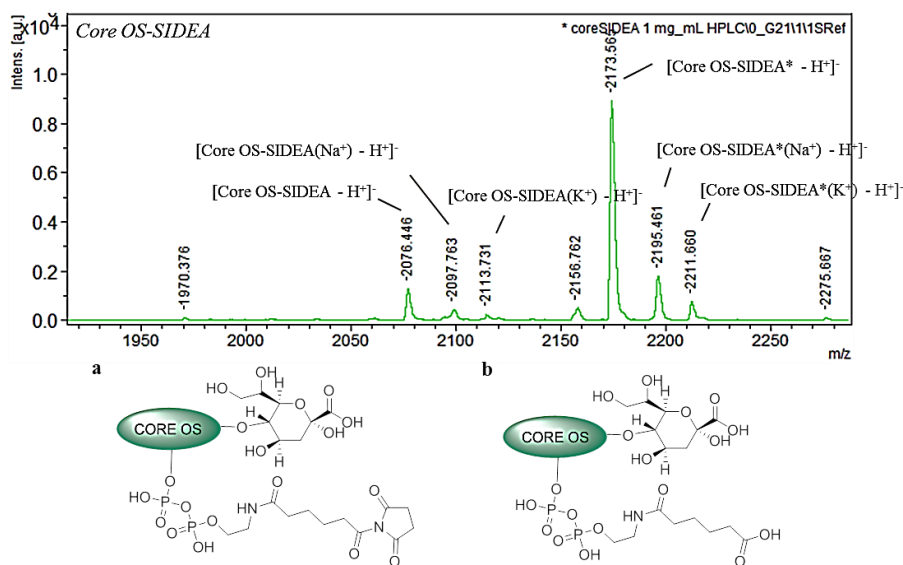


**Fig. 42.** MALDI-MS spectra of the core OS-SIDEA intermediate synthesized at low pH. The ion at 2173.6 u was attributed to the core OS derivatized with SIDEA on PPEtN amino group (a), the ion at 2076.4 u was attributed to the same product after hydrolysis of the NHS ester (b).

Core OS-SIDEA product was analysed by HPLC-SEC which showed the absence of dimers (data not shown). The core OS-SIDEA intermediate was used for conjugation to CRM<sub>197</sub>.

#### *Synthesis of core OS-ADH-SIDEA intermediate*

After introduction of ADH, SIDEA could react both with ADH hydrazide amino group and PPEtN amino group (Scheme 4, Table 25).

**Table 25.** Characterization of core OS-ADH-SIDEA intermediates obtained by working in different conditions.

<b>Reaction conditions</b>	<b>% NH<sub>2</sub> derivatization (by TNBS)</b>	<b>% active ester groups (by RP-HPLC)*</b>	<b>% dimerization</b>
Core OS concentration 10 mg/mL, Core OS concentration 10 mg/mL, DMSO/H <sub>2</sub> O 9:1 + TEA (molar ratio TEA/total NH <sub>2</sub> groups = 5), SIDEA/total NH <sub>2</sub> groups molar ratio 3, RT, 3h	<b>91.6</b>	<b>20.8</b>	<b>50.0</b>
Core OS concentration 10 mg/mL, DMSO/HCl 82.5 ppm 9:1, SIDEA/total NH <sub>2</sub> groups molar ratio 3, RT, 3h	<b>93.8</b>	<b>32.1</b>	<b>29.0</b>
Core OS concentration 5 mg/mL, DMSO/HCl 82.5 ppm 9:1, SIDEA/total NH <sub>2</sub> groups molar ratio 12, RT, 1h	<b>93.4</b>	<b>47.2</b>	<b>22.0</b>

\*with respect to reacted NH<sub>2</sub> groups.

Reaction of PPEtN NH<sub>2</sub> with SIDEA was confirmed also in the presence of ADH linker, both at high and low pH. Derivatization occurred on ADH and PPEtN of the same molecule. The percentage of derivatized amino groups (including both ADH and PPEtN) was in fact of 92% at high pH and of 94% at low pH, respectively. Major part of the active groups resulted hydrolysed, especially at high pH.

MALDI-MS analysis of the products confirmed the simultaneous reaction of the two amino groups present on the oligosaccharide chains (Fig. 43) and the reaction product of core OS-ADH with SIDEA was designed as core OS-ADH-(SIDEA)<sub>2</sub>.

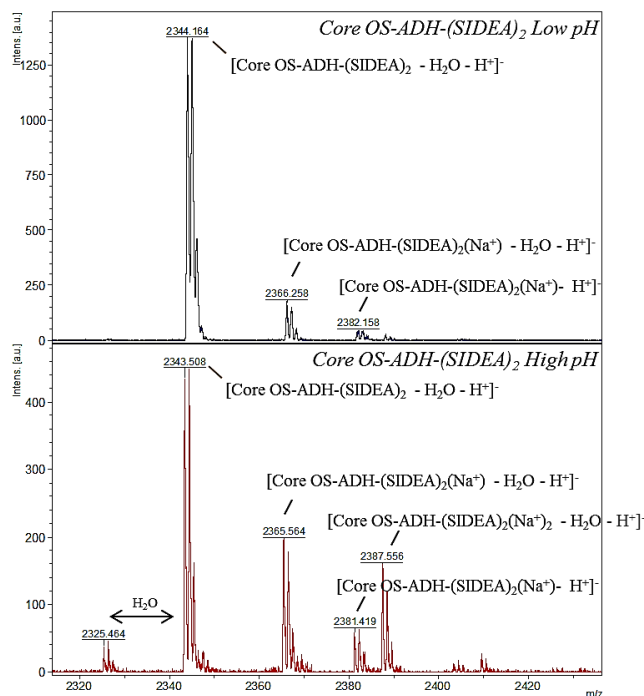


**Fig. 43.** MALDI-MS (negative ion polarity) spectra of core OS-ADH derivatized with ADH at high and low pH. The ion at 2343.5 u was attributed to the formation of the reaction product, with activation of both ADH and PPEtN amino groups with SIDEA.

HPLC-SEC analysis revealed that core OS-ADH-(SIDEA)<sub>2</sub> products were characterized by a double peak, due to possible dimerization of the product during the reaction, with dimer species constituting 50% and 29% of the total area for the product obtained at high and low pH, respectively.

The reaction with SIDEA was then performed at low pH, with a shorter reaction time and with a high excess of SIDEA with respect to amino groups content, in order to minimize hemiester groups hydrolysis and dimerization side products (Table 25). 93% NH<sub>2</sub> groups resulted derivatized with 47% active ester groups. MALDI-MS analysis of the product again confirmed the simultaneous reaction of the two amino groups present on the oligosaccharide chains with SIDEA. In this case dimers formation was not completely abolished as revealed by HPLC-SEC analysis (dimer was 22% of the total area by dRI). The intermediate obtained was conjugated to CRM<sub>197</sub>.

*Conjugation with CRM<sub>197</sub>*

Core OS-ADH-(SIDEA)<sub>2</sub> and core OS-SIDEA intermediates were conjugated to the lysine (Lys) residues of CRM<sub>197</sub>. Analysis by HPLC-SEC (fluorescence detection), SDS-PAGE and MALDI-MS confirmed conjugate formation [207] (Fig. 44).

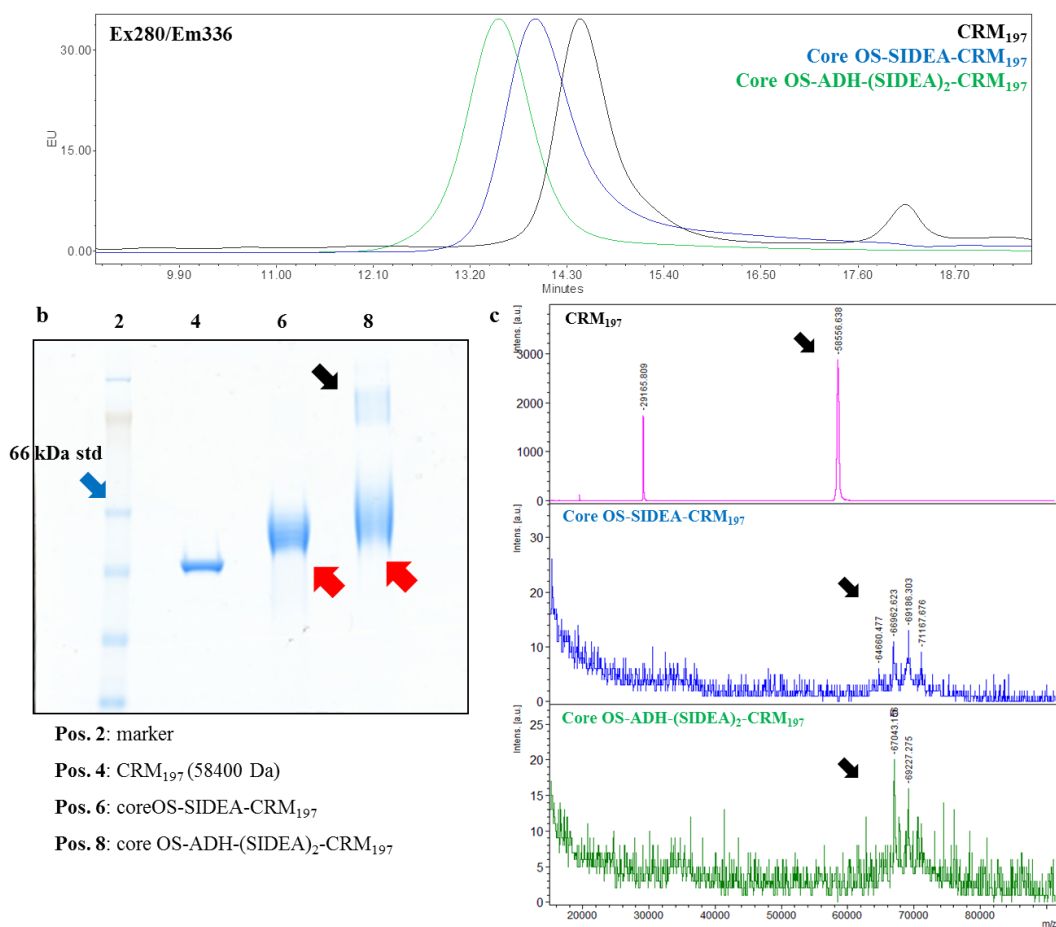


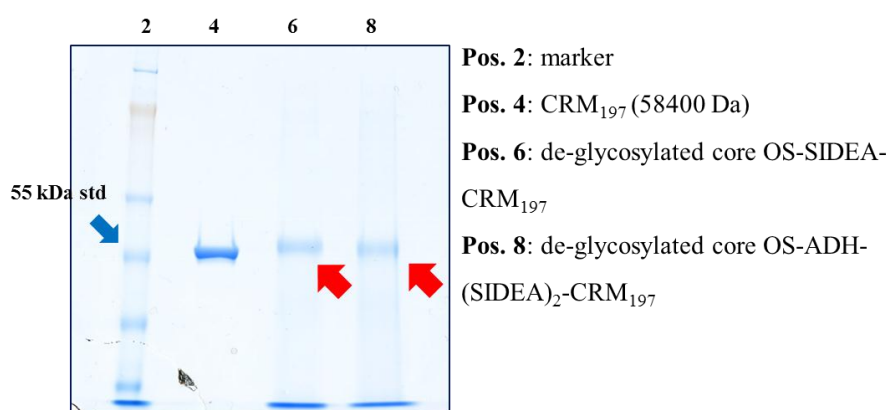
**Fig. 44.** HPLC-SEC (a), SDS-PAGE (b) and MALDI-MS (c) analysis of conjugates.

In the case of the core OS-ADH-(SIDEA)<sub>2</sub> conjugate a smear at molecular weight of around 100 kDa, in addition to that between 55 and 66 kDa, was detected in the gel, suggesting the formation of protein dimers (Fig. 44-b). For both conjugates, MALDI-

MS spectra showed an average number of 5 oligosaccharide chains linked per CRM<sub>197</sub> (Fig. 44-c).

#### 4.3.5 Glycosylation sites of core OS- and OAg-CRM<sub>197</sub> conjugates

OS-CRM<sub>197</sub> conjugates were subjected to de-glycosylation procedure with TFMS. SDS-PAGE of the resulting products showed that the reaction was successful without impact on CRM<sub>197</sub> integrity (Fig. 45). Same procedure was then applied to a *S. Typhimurium* 2192 OAg-ADH-SIDEA-CRM<sub>197</sub> conjugate, characterized by having an average number of 5 sugar chains conjugated to CRM<sub>197</sub>.

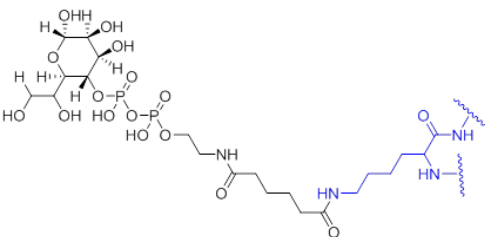
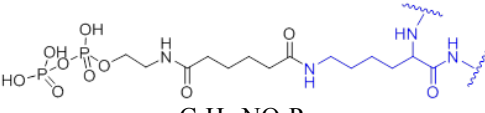
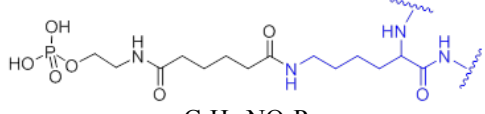
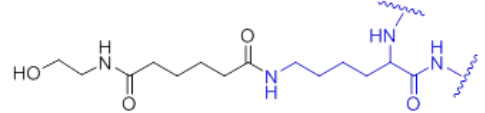
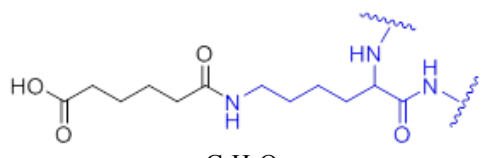


**Fig. 45.** SDS-PAGE analysis of TFMS-mediated de-glycosylated conjugates compared to CRM<sub>197</sub>.

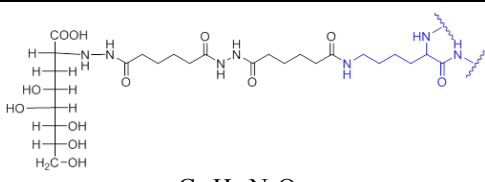
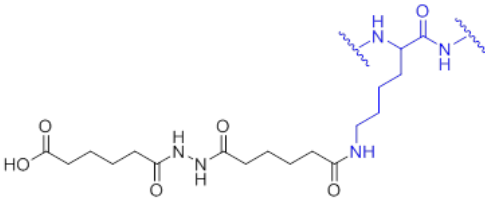
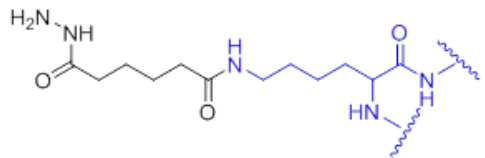
After de-glycosylation, the products were subjected to trypsin digestion and analysed by MALDI-MS [208]. In the case of the core OS-SIDEA-CRM<sub>197</sub> conjugate, the linkage between the oligosaccharide chain and CRM<sub>197</sub> can be formed only through the active ester group of SIDEA linked to PPEtN (Scheme 4). In the case of core OS-ADH-(SIDEA)<sub>2</sub>-CRM<sub>197</sub>, as for OAg-ADH-SIDEA-CRM<sub>197</sub>, the linkage to CRM<sub>197</sub> can be formed through both the SIDEA linked to PPEtN and the SIDEA linked to ADH, introduced through reductive amination of terminal KDO (Scheme 4). The sugar chain could be attached through one point to CRM<sub>197</sub>, or form a bridge on the protein. Also two molecules of CRM<sub>197</sub> can be linked to the same sugar chain.

TFMS has been reported to mediate the cleavage of the glycan bonds, leaving intact the innermost monosaccharide bound to the Lys residue [202, 209], but chemical structures due to solvolysis side reactions or to the lability of the phosphodiester linkage of PPEtN or of KDO-ADH-SIDEA linkages were also taken into account [210-212] (Table 26). Some of such chemical structures can clearly be specifically associated to the linkage of the sugar chain through the SIDEA linker on PPEtN or on ADH.

**Table 26.** Structural modifications of Lys residues searched after chemical de-glycosylation and enzymatic digestion of CRM<sub>197</sub> conjugates.

Name	Structure and chemical formula	Conjugation site on the sugar chain
Core OS-SIDEA	 $C_{15}H_{28}NO_{15}P_2$	PPEtN
Core OS-SIDEA-deHep	 $C_8H_{16}NO_9P_2$	PPEtN
Core OS-SIDEA-deP	 $C_8H_{15}NO_6P$	PPEtN
Core OS-SIDEA-dePP	 $C_8H_{14}NO_3$	PPEtN
Core OS-Adipoyl	 $C_6H_9O_3$	PPEtN/KDO

---

<b>Core OS-ADH<sub>2</sub>-KDO</b>		KDO
	$C_{20}H_{35}N_4O_{11}$	
<b>Core OS-ADH<sub>2</sub></b>		KDO
	$C_{12}H_{19}N_2O_5$	
<b>Core OS-ADH</b>		KDO
	$C_6H_{11}N_2O_2$	

---

The modification called “core OS-Adipoyl” (Table 26) does not allow discriminating between the two conjugation sites on the sugar chain (referred as “Undetermined” in MS analysis).

MALDI-MS analysis (Fig. 46) allowed identifying CRM<sub>197</sub> peptides having Lys residues with these modifications, without further information on the specific amino acids actually involved in the conjugation (Fig. 47). For unmodified CRM<sub>197</sub>, average sequence coverage of 55.3% was found. In the case of the conjugates, CRM<sub>197</sub> average coverage was of 64.7, 59.0 and 21.0% for core OS-SIDEA-CRM<sub>197</sub>, core OS-ADH-(SIDEA)<sub>2</sub>-CRM<sub>197</sub> and OAg-ADH-SIDEA-CRM<sub>197</sub>, respectively.



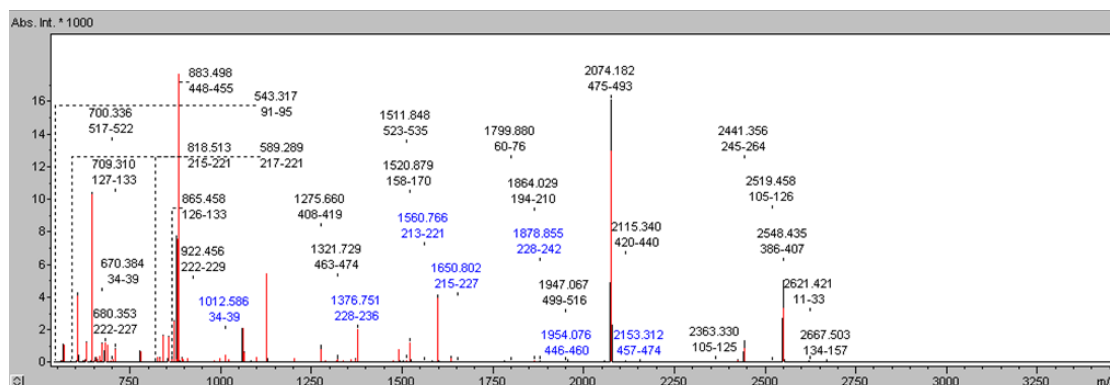


**Fig. 46.** MALDI-MS spectra of de-glycosylated and digested core-SIDEA-CRM<sub>197</sub> conjugate.

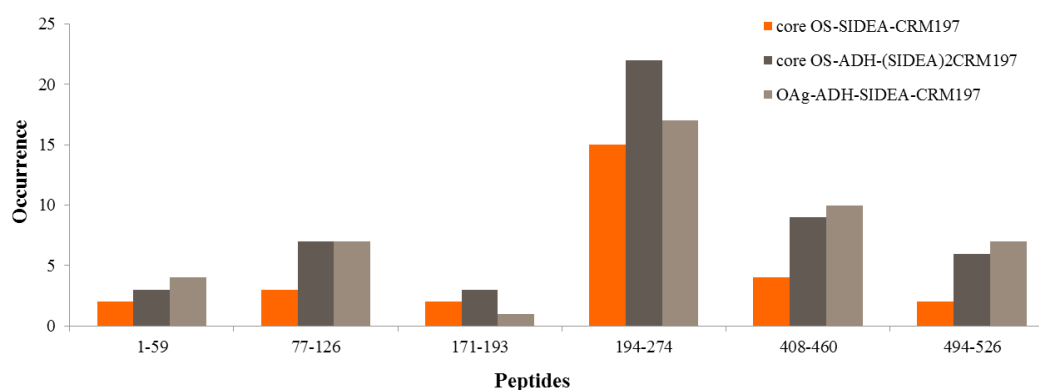


**Fig. 47.** Summary of the MALDI-MS analysis performed on core OS and OAg conjugates. CRM<sub>197</sub> peptides having Lys residues modified by the custom structural modifications due to glycoconjugation were grouped depending on occurrence of modifications in tryptic peptides.

A central area of CRM<sub>197</sub> (peptides 194-274) was found to be the most efficiently conjugated in all the conjugates. Different structural modifications on Lys residues (Table 26) were found, obtaining information on the regioselectivity of the conjugation process (Fig. 48).

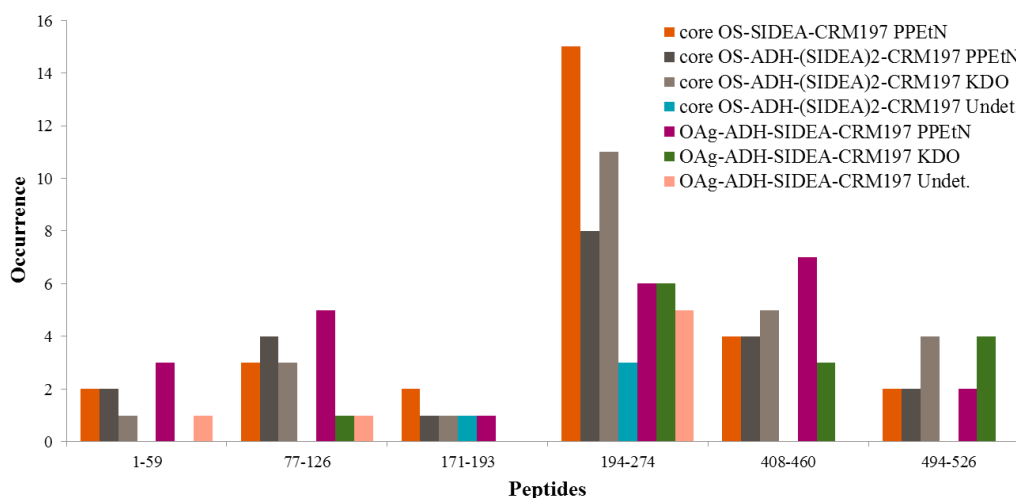


**Fig. 48.** Summary of the MALDI-MS analysis performed on core OS and OAg conjugates. CRM<sub>197</sub> peptides having Lys residues modified by the custom structural modifications due to conjugation were grouped depending on occurrence of modifications in tryptic peptides. Specific structural modifications were grouped depending on the regiochemistry of conjugation occurred.

For both core OS-ADH-(SIDEA)<sub>2</sub>-CRM<sub>197</sub> and OAg-ADH-SIDEA-CRM<sub>197</sub>, conjugation resulted involving both SIDEA linked to PPEtN and SIDEA linked to ADH.

Semiquantitative LC-ESI-MS analysis represented an improvement with respect to MALDI-MS and allowed to identify the specific Lys residues involved in conjugation. The three TFMS-de-glycosylated and trypsin digested conjugates were analysed and peptides with the expected mass value increment relative to the custom structural modifications were identified. Their corresponding fragmentation spectra were manually inspected for confirmation of the effective modification on Lys residues. List of Lys residues modified by conjugation for each conjugate is reported in Table 27.

Conjugation	Core OS- SIDEA- CRM197	Core OS- ADH(SIDEA) <sub>2</sub> - CRM197	OAg-ADH- SIDEA-CRM197
Site	Clustered Area	Clustered Area2	Clustered Area3
24	2,E+07	8,E+06	0,E+00
33	8,E+06	3,E+06	3,E+05
37	1,E+07	6,E+06	2,E+05
76	0,E+00	3,E+05	2,E+05
82	2,E+06	1,E+06	2,E+05
90	3,E+06	2,E+06	1,E+05
95	4,E+06	3,E+06	3,E+05
103	4,E+04	2,E+06	6,E+05
104	9,E+04	6,E+05	5,E+04
125	2,E+05	2,E+06	1,E+06
214	6,E+06	4,E+06	7,E+05
221	9,E+06	7,E+06	3,E+06
227	2,E+06	1,E+06	1,E+06
236	1,E+06	9,E+06	4,E+06
242	1,E+07	8,E+06	8,E+05
244	8,E+05	6,E+05	4,E+04
385	1,E+06	5,E+05	0,E+00
445	4,E+06	2,E+06	3,E+05
447	6,E+05	3,E+05	0,E+00
474	6,E+06	3,E+06	0,E+00
498	2,E+07	2,E+07	1,E+06
516	1,E+07	4,E+06	9,E+05
522	2,E+06	5,E+05	0,E+00
526	3,E+06	2,E+06	6,E+04

**Table 27.** Summary of the LC-ESI-MS analysis performed on core OS and OAg conjugates. Lys residues modified by the custom structural modifications due to conjugation were grouped depending on the clustered area of tryptic peptides having the expected mass value increments. Lys residues were ranked according to a colour scale: the widest clustered areas were represented in red, the smallest in green.

Peptide mapping by LC-ESI-MS confirmed that this conjugation chemistry is a highly random process involving a high number of Lys residues. In fact over thirty-nine CRM<sub>197</sub> Lys residues available for conjugation, twenty-four sites common to core OS conjugates were found modified. Some Lys residues were found unmodified in the case of the OAg conjugate. In particular, no conjugation was found for K24, K385, K447, K474 and K522.

In the case of core OS-ADH-(SIDEA)<sub>2</sub>-CRM<sub>197</sub> conjugate, the majority of conjugation involved the SIDEA linker present on the PPetN group of the core OS (Fig. 49).

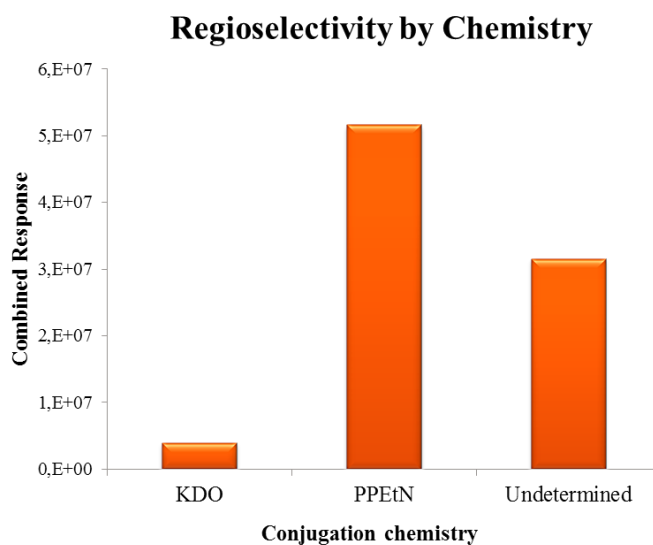


**Fig. 49.** Regioselectivity of core-ADH-(SIDEA)<sub>2</sub>-CRM<sub>197</sub> conjugate. Conjugation “via PPEtN” was preferred with respect to conjugation “via KDO”.

The same data were plotted to display the regioselectivity of conjugation of each identified site of linkage (Fig. 50).

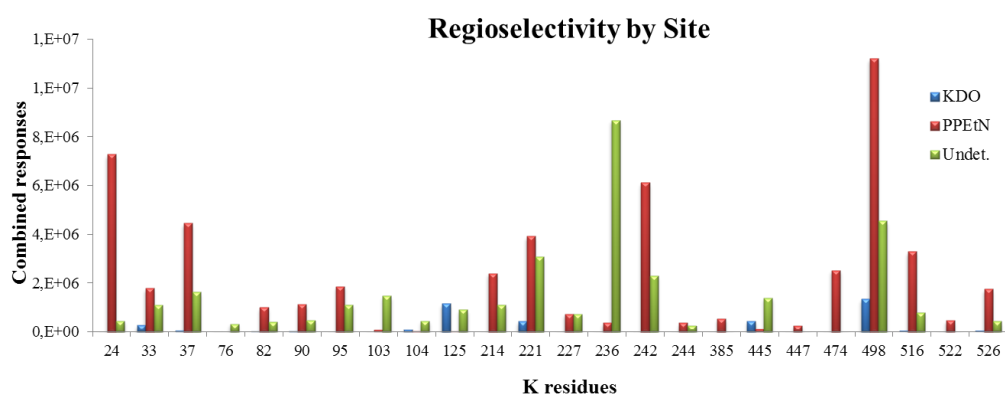


**Fig. 50.** Regioselectivity of conjugation of each identified site of linkage, relative to core OS-ADH-(SIDEA)<sub>2</sub>-CRM<sub>197</sub> conjugate.

Quite all the Lys residues were linked “via PPEtN”, except for K125 and K445 which preferred conjugation “via KDO”, although the effective contribute of the “undetermined” chemistry should be considered. In the case of OAg-ADH-SIDEA-



CRM<sub>197</sub> conjugate, the majority of the Lys residues structural modifications found was referred to the “undetermined” chemistry, with no major information about the effective conjugation chemistry involved.

In Fig. 51, the 3D structure of CRM<sub>197</sub> was displayed showing the exposition of the modified residues for the three conjugates tested. Colour coding had the following meaning:

- surface colour from red to blue, passing through white, represented the b-factor of residues, going from the more flexible areas in red to the more rigid areas in blue;
- all lysines in the CRM<sub>197</sub> sequence were highlighted in magenta. The ones which were found conjugated are highlighted in green, and the most conjugated ones (Table 27) are highlighted in yellow.

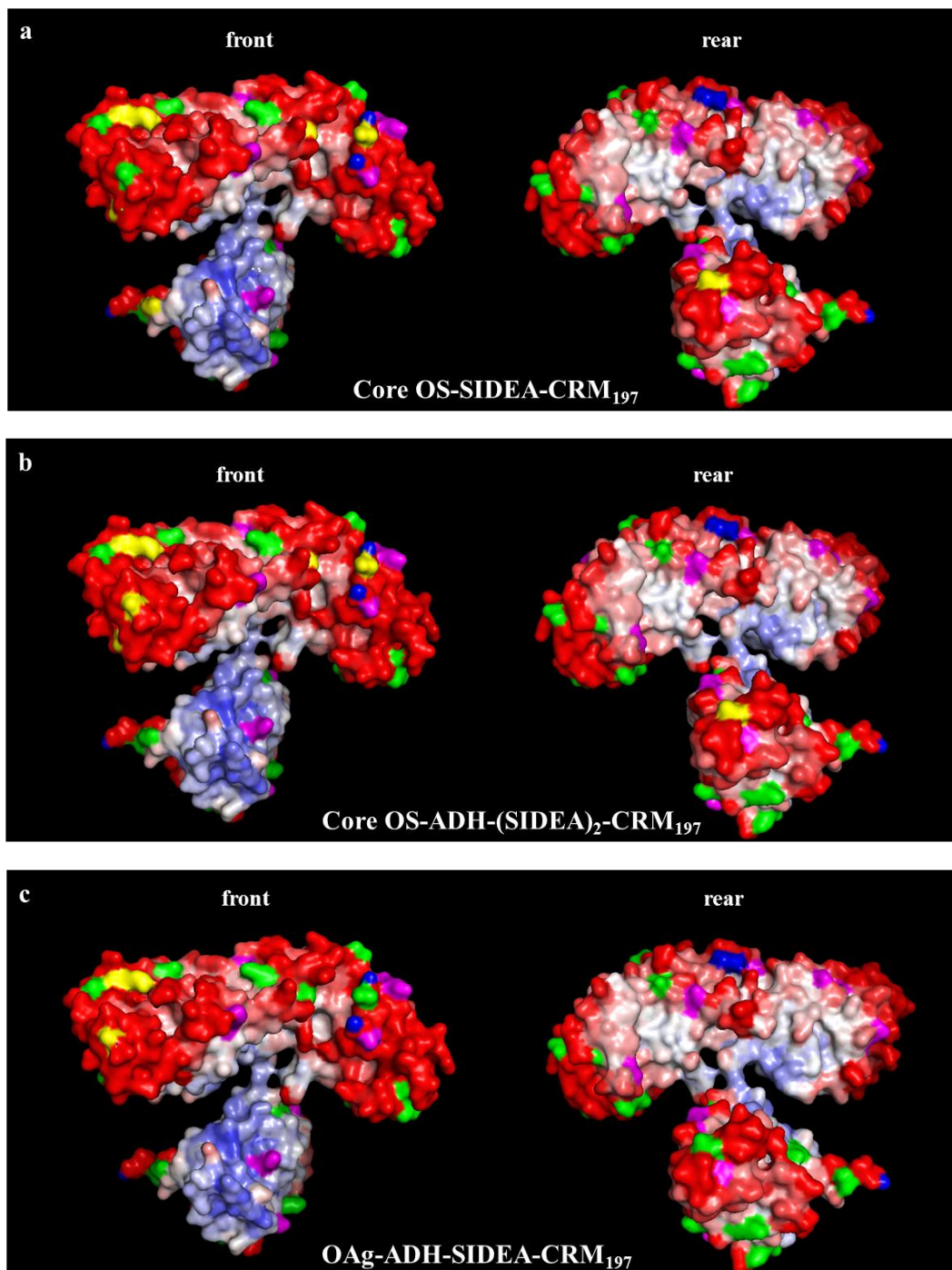


**Fig. 51.** 3D structure of CRM<sub>197</sub> with conjugated residues highlighted, relative to core-SIDEA-CRM<sub>197</sub> (a), core OS-ADH-(SIDEA)<sub>2</sub>-CRM<sub>197</sub> (b) and OAg-ADH-SIDEA-CRM<sub>197</sub> (c) conjugates.

Lys surface exposed were preferably conjugated. In particular, glycosylation sites were found to be in those regions of CRM<sub>197</sub> characterized by more flexibility [213].

#### 4.4 Discussion

GVGH conjugation approach for the synthesis of a vaccine against iNTS was based on the linkage of OAg chains to the carrier protein CRM<sub>197</sub>, after the introduction of ADH and SIDEA as linker molecules on the terminal KDO [106] (Scheme 2). However, presence and effective structure of KDO at the terminus of the OAg chains was never verified.

Here, for the first time, it was shown that the process of acid hydrolysis for OAg extraction directly from bacteria results in the presence of KDO at the reducing end of the sugar chains in its native structure, without formation of anhydro compounds or other artifacts, in contrast with scientific literature which has often reported about KDO structural alterations consequent to acid treatment. McNicholas *et al* reported that un-substituted KDO monosaccharide is rapidly converted in compounds following structural rearrangements, unreactive to the analytical methods for KDO quantification (periodic acid-thiobarbituric acid and semicarbazide assays) [191]. In my study, <sup>1</sup>H-NMR spectrum showed the characteristic signals for KDO at 2.4 and 1.8 ppm (equatorial H-3 and axial H-3 of KDO, respectively) and the absence of resonances due to olefinic or furoic KDO derivatives. At the same time, MS data clearly confirmed the presence of native KDO sugar after mild acid hydrolysis since the exact molecular mass of the native KDO-containing oligosaccharide were detected in ESI-MS and MALDI-MS spectra. Moreover, the absence of other KDO structural artifacts in MS spectra and the molecular fragmentation obtained by MS<sup>2</sup>, further confirmed this finding. Also McNicholas *et al* reported that no structure modifications occur in the case of 5-O-glycosyl-KDO [191]. The characterization of the oligosaccharides obtained after same mild acid hydrolysis applied to the EPS produced by *B. cepacia* strain BTS13 confirmed presence of KDO in its native form. The repeating unit of this PS contains the KDO sugar linked to the Gal unit in position 5 and results obtained are further confirmation that when the KDO is linked in 5, mild hydrolysis does not cause rearrangements. On the other hand, these structural rearrangements of KDO after acid hydrolysis have been reported when phosphate groups were linked to KDO at position 4 (Fig. 31) such as in *Bordetella*



[214], *Vibrio* [196] and *Aeromonas* [215] LPS. After mild acid hydrolysis, the phosphate group was easily released and eliminated ( $\beta$ -elimination mechanism), with following formation of a mixture of 4,7-anhydro- and 4,8-anhydro-3-Deoxy-oct-2-ulosonic acid units.

The KDO high reactivity in reaction of reductive amination was imputed to the formation of more reactive forms, characterized by having the ketone group not implicated in the sugar ring formation and more available for the reaction [194, 214]. Here, high reactivity of KDO in the reductive amination reaction was confirmed but could not be attributed to the formation of more reactive compounds [196]. The OAg and the BTS13 tetrasaccharide, at the same molar concentration of KDO, showed very similar kinetic of reaction with semicarbazide, corroborating the high reactivity of the KDO in its native structure and linked in position 5 to the sugar chain. In our case, KDO fast kinetic of reaction, comparable to sodium pyruvate and higher than KDO monosaccharide, could be attributed to its linkage to the sugar chain.

The step of reaction with SIDEA was deeply evaluated. OAg chains extracted from *Salmonella* bacteria were characterized by having a non-stoichiometric substitution with pyrophosphorylethanolamine (PPEtN) groups [106] and the use of ADH was preferred to the use of only SIDEA to guarantee a higher OAg chains conjugation efficiency [106]. In addition, lack of stability of the pyrophosphorylethanolamine linkage was also hypothesized. Here, it was verified that, even by performing the reaction with SIDEA at low pH and in the presence of ADH, conditions that could favour selectivity of ADH toward SIDEA, simultaneous reaction of PPEtN  $\text{NH}_2$  group and ADH occur with formation of an intermediate having two SIDEA linkers per sugar chain. This of course can have an impact on the formation of the following conjugate, opening possibility to protein dimers formation, as verified in the case of core OS-ADH-(SIDEA)<sub>2</sub>-CRM<sub>197</sub>. Preliminary data we obtained indicate stability of PPEtN groups. More work can be done in this context to verify the possibility to prefer direct conjugation on PPEtN  $\text{NH}_2$  group for OAg chains having a stoichiometric substitution so to allow formation of more defined conjugates.

Peptide mapping analysis of the conjugates confirmed that the conjugation chemistry used was highly random, involving a large number of Lys residues, with



preference for those surface exposed [216, 217]. K24, K37, K221, K242, K498, and K516 for core OS-SIDEA-CRM<sub>197</sub>, K24, K236, K242 and K498, for core OS-ADH-(SIDEA)<sub>2</sub>-CRM<sub>197</sub>, K125, K221 and K236 for OAg-ADH-SIDEA-CRM<sub>197</sub> were found more involved in glycosylation (Fig. 51, in yellow). There were some differences in conjugation site selectivity among the conjugates tested and respect to what reported by Moginger *et al* and Crotti *et al* in their studies of conjugation of just linker molecules or short oligosaccharides to CRM<sub>197</sub> [216, 218]. In comparison with OAg-CRM<sub>197</sub> conjugate, 5 additional Lys residues, K24, K385, K447, K474 and K522, were linked to core OS, suggesting that saccharide chain length can impact on conjugation site selectivity. Less accessible Lys can become available to shorter OS chains. Furthermore, the incorporation of one sugar chain could challenge the insertion of a second glycan moiety by steric hindrance or by causing conformational changes in the protein structure, masking some Lys in origin available, especially in the more flexible CRM<sub>197</sub> regions (Fig. 51, in red).

Peptide mapping analysis has not only allowed identification of the glycosylation sites on the protein, but also to understand the regioselectivity of the conjugation process. For both OS-ADH-(SIDEA)<sub>2</sub>-CRM<sub>197</sub> and OAg-ADH-SIDEA-CRM<sub>197</sub>, the linkage of sugar chains to CRM<sub>197</sub> seems to highly involve the SIDEA linker on PPEtN. This makes still more important to verify the stability of such linkage.

This work contributed to better understand the conjugation process used for the synthesis of *Salmonella* OAg-CRM<sub>197</sub> conjugates. The analytical methods developed can be applied to the characterization of other OAg-based glycoconjugate vaccines. The protocol developed for peptide mapping of the conjugates allows in depth characterization of the conjugates, and can be used to verify consistency of batch to batch production [219, 220]. It can also support investigation on the relationship between conjugate structure and immunogenicity [121, 221], improving rational vaccine design in the future.



## **5. Conclusions**



Development of analytical methods is of fundamental importance for vaccines release, to verify consistency of production, to assess their stability over time and assure a consistent immune response. Characterization of glycoconjugate vaccines is a complex procedure that involves tests on starting materials such as purified polysaccharides and carrier proteins, the derivatized intermediates prior to conjugation and the final purified glycoconjugate. Here a panel of analytical methods has been developed and used for full characterization of OAg-CRM<sub>197</sub> conjugate and its intermediates. In the case of GMMA only characterization of the final product is needed. However, GMMA are quite complex structures and careful characterization of key target antigens for immune response and of GMMA as particles is needed.

We have verified that mutations introduced in *S. Typhimurium* and *S. Enteritidis* wild type strains to increase GMMA release and reduce LPS toxicity can have an impact on OAg expression. The effective amount of OAg injected, rather than its density on GMMA, seems to determine the anti-OAg antibody response, a higher OAg to GMMA protein ratio should allow the use of a lower amount of GMMA per vaccine dose with potential benefits in relation to cost and safety of the vaccine. NTS GMMA having a penta-acylated lipid A, provoking the least stimulation of cytokine release from human PBMC compared to GMMA with wild type lipid A, and maintaining a good expression of OAg chains appear to be optimal components for a vaccine against iNTS.

*S. Typhimurium* and *S. Enteritidis* GMMA particle size distributions have been evaluated by means of different size-analysing techniques. All are fast methods that provide complementary information allowing a more complete evaluation of GMMA size. Number of OAg chains on the GMMA surface determines the behaviour of GMMA in solution, affecting hydrodynamic radius by DLS and NTA, but not gyration radius by MALS. MALS, coupled to a size exclusion chromatography module, allows checking of the purity of GMMA preparations. Like other methodologies based on scattered light, DLS batch measurements are inherently sensitive to the presence of large particles in polydisperse samples and is not able to distinguish subpopulations in multimodal samples. NTA allows single particles



visualization and their counting. This also allows determination of antigens density on GMMA surface.

Here for the first time, we have been able to identify KDO presence and structure at the terminus of OAg chains after their extraction by acetic acid hydrolysis of bacteria. Differently from what reported in literature, KDO maintained its native form, with no rearrangements in anhydro compounds. Anyway high reactivity of KDO in reaction of reductive amination was confirmed and related to its linkage to the OAg chain. All the steps for OAg conjugation to CRM<sub>197</sub> were in depth investigated, confirming that the conjugation chemistry used is highly random on the protein, but also not selective on the OAg chain. The linkage to the protein not only involves the terminal KDO sugar, but also the PPEtN group of the core region. This can result in protein dimers formation. Stability studies should be performed to verify that these two kinds of linkage involved in the process are equally stable. Alternative chemistries could be used to assure selective conjugation of the OAg chains, resulting in better defined and more consistent final products.

The methods developed and used here can be extended to the characterization of other OAg-based vaccines. In particular the method to study the glycosylation sites on the protein can support the investigation of the relation between conjugate structure and immune response, driving the rational design of improved conjugate vaccines.



## 6. References



- [1] Murray P, Rosenthal K, Kobayashi G, Pfaller M. Medical Microbiology. June 2005; 5th Edn. St. Louis, Mosby, Elsevier Science.
- [2] Nataro JP, Bopp CA, Fields PI, Kaper JB, Strockbine NA. *Escherichia*, *Shigella*, and *Salmonella*. Manual of Clinical Microbiology. 2011; 603-635 10th Edn. Versalovic J, Carroll KC, Funke G, Jorgensen JH, Landry ML, Warnock DW (Eds.) ASM, Washington, DC.
- [3] Jantsch J, Chikkaballi D, Hensel M. Cellular aspects of immunity to intracellular *Salmonella enterica* Immunological Reviews. 2011; 240:185-195.
- [4] Pegues DA, Miller SI. *Salmonella* Species, including *Salmonella* Typhi. Mandell, Douglas and Bennett's Principles and Practises of Infectious Diseases. 2010;7th Edn. Mandell GL, Bennett JE, Dolin R (Eds.) Elseviere, Philadelphia:2887-2903.
- [5] Weikel CS, Guerrant RL. Nosocomial salmonellosis Infection Control. 1985; 6:218-220.
- [6] Mermin J, Hutwagner L, Vugia D, Shallow S, Daily P, Bender J et al. Reptiles, amphibians, and human *Salmonella* infection: a population-based case-control study. Clin Infect Dis. 2004; 38(S3):S253-261.
- [7] Brenner FW, Villar RG, Angulo FJ, Tauxe R, Swaminathan B. Salmonella Nomenclature Journal of Clinical Microbiology. 2000; 38(7):2465-2467.
- [8] Kauffmann F, Edwards PR. Classification and Nomenclature of *Enterobacteriaceae*. J Bacteriol. 1944; 48:351-367.
- [9] Kauffmann F. The bacteriology of *Enterobacteriaceae*. Collected Studies of the Author and His Co-Workers, by F. Kauffmann. Copenaghen Munskgaard. 1966.
- [10] Grimont PAD, Weill FX. Antigenic Formulae of the *Salmonella* serovars. WHO Collaborating Centre for Reference and Research on Salmonella, 9th Edn. 2007.
- [11] Su LH, Chiu CH. *Salmonella*: Clinical Importance and Evolution of Nomenclature. Chang Gung Med J. 2007; 30(3):210-9.
- [12] Fookes M, Schroeder GN, Langridge GC, Blondel CJ, Mammina C, Connor TR et al. *Salmonella bongori* provedes insights into the evolution of the *Salmonellae*. PLoS Pathogens. 2011; 7(8):e1002191.
- [13] Langridge GC, Wain J, Nair S. Invasive Salmonellosis in Humans. EcoSal Plus. 2012; 5(1).
- [14] Feasey NA, Dougan G, Kingsley RA, Heyederman RS, Gordon MA. Invasive non-typhoidal *Salmonella* disease: an emerging and neglected tropical disease in Africa. Lancet. 2012; 378(9835):2489-2499.
- [15] Braden CR. *Salmonella enterica* serotype Enteritidis and eggs: a national epidemic in the United States. Clin Infect Dis. 2006; 43:512-5177.
- [16] Hohmann EL. Nontyphoidal Salmonellosis Clin Infect Dis. 2001; 32:263-269.
- [17] Gal-Mor O, Boyle EC, Grassl GA. Same species, different diseases: how and why typhoidal and non-typhoidal *Salmonella enterica* serovars differ. Frontiers in Microbiology. 2014; 5:1-19 (3919).
- [18] Velge P, Wiedermann A, Rosselin M, Abed N, Boumart Z, Chaussé AM, Grépinet O, Namdari F, Roche SM, Rossignol A, Virlogeux-Payant I. Multiplicity of *Salmonella* entry mechanisms, a new paradigm for *Salmonella* pathogenesis MicrobiologyOpen. 2012; 1(3):243-258.

- [19] Chen HM, Wang Y, Su LH, Chiu CH. Nontyphoid *Salmonella* infection: microbiology, clinical features, and antimicrobial therapy. *Pediatrics and Neonatology*. 2013; 54:147-152.
- [20] Crump JA, Heyderman RS. Invasive *Salmonella* infections in Africa. *Trans R Soc Trop Med Hyg*. 2014; 108(11):673-675.
- [21] Crump JA, Heyderman RS. A Perspective on Invasive *Salmonella* Disease in Africa. *Clin Infect Dis*. 2015; 61(S4):S235-240.
- [22] Crump JA, Sjolund-Karlsson M, Gordon MA, Parry CM. Epidemiology, Clinical Presentation, Laboratory Diagnosis, Antimicrobial Resistance, and Antimicrobial Management of Invasive *Salmonella* Infections. *Clinical Microbiology Reviews*. 2015; 28(4):901-937.
- [23] Watson KC. Isolation of *Salmonella* Typhi from the bloodstream. *J Lab Clin Med*. 1955; 46:128-134.
- [24] Crocker CG. Distribution of types of typhoid bacteria over Africa. *S Afr Med J*. 1957; 31:169-172.
- [25] MacLennan CA, Martin LB, Micoli F. Vaccines against invasive *Salmonella* Disease. Current status and future directions. *Human Vaccines & Immunotherapeutics*. 2014; 10(6):1478-1493.
- [26] MacLennan CA, Levine MM. Invasive nontyphoidal *Salmonella* disease in Africa: current status. *Expert Rev Anti Infect Ther*. 2013; 11(5):443-446.
- [27] Haeusler GM, Curtis N. Non-typhoidal *Salmonella* in Children: Microbiology, Epidemiology and Treatment. *Advances in Experimental Medicine and Biology*. 2013; 764:13-26.
- [28] Mastroeni P, Rossi O. Immunology, epidemiology and mathematical modelling towards a better understanding of invasive non-typhoidal *Salmonella* disease and rational vaccines approaches. *Expert Review of Vaccines*. 2016; 15(12):1545-1555.
- [29] Majowicz SE, Musto J, Scallan E, Angulo F, Kirk M, O'Brien SJ, Jones TF, Fazil A, Hoekstra RM. The Global Burden of Nontyphoidal *Salmonella* Gastroenteritis. *Clin Infect Dis*. 2010; 50:882-889.
- [30] Murray CJ, Vos T, Lozano R et al. Disability-adjusted life years (DALYs) for 291 diseases and injuries in 21 regions, 1990-2010: a systematic analysis for the Global Burden of Disease Study 2010. *Lancet*. 2012; 380:2197-2223.
- [31] Kirk MD, Pires SM, Black RE et al. Global and Regional Disease Burden of 22 Foodborne Bacterial, Protozoal, and Viral Diseases, 2010: A Data Synthesis. *PLoS Med*. 2015; 12(12):e1001921.
- [32] Tennant SM, MacLennan CA, Simon R, Martin LB, Khan MI. Nontyphoidal *Salmonella* Disease: Current status of vaccine research and development. *Vaccine*. 2016; 34(26):2907-2910.
- [33] Laupland KB, Schonhyder HC, Kennedy KJ, Lyytikainen O, Valiquette L, Galbraith J, Collignon P. *Salmonella enterica* bacteraemia: a multi-national population-based cohort study. *BMC Infect Dis*. 2010; 10(95):1-6.
- [34] Gordon MA, Graham SM, Walsh AL, Wilson L et al. Epidemics of Invasive *Salmonella enterica* serovar Enteritidis and *S. enterica* serovar Typhimurium Infection Associated with Multidrug Resistance among Adults and Children in Malawi. *Clin Infect Dis*. 2008; 46:963-969.





- [35] Okoro CK, Kingsley RA, Connor TR et al. Intracontinental spread of human invasive *Salmonella* Typhimurium pathovariants in sub-Saharan Africa. *Nature Genetics*. 2012; 44(11):1215-1223.
- [36] Ao TT, Feasey NA, Gordon MA, Keddy KH, Angulo FJ, Crump JA. Global Burden of Invasive Nontyphoidal *Salmonella* Disease, 2010. *Emerging Infectious Diseases*. 2015; 21(6):941-949.
- [37] Reddy EA, Shaw AV, Crump JA. Community-acquired bloodstream infections in Africa: a systematic review and meta-analysis. *Lancet Infect Dis*. 2010; 10(6):417-432.
- [38] Vieira A, Jensen AR, Pires SM, Karlsmose S, Wegener HC, Wong DLF. WHO Global Foodborne Infections Network Country Databank: a resource to link human and non-human sources of *Salmonella*. *Int Soc Vet Epidemiol Econ*. 2009; 643:512-517.
- [39] Tennant SM, Diallo S, Levy H et al. Identification by PCR of non-typhoidal *Salmonella enterica* serovars associated with invasive infections among febrile patients in Mali. *PLoS Negl Trop Dis*. 2010; 4(3):e621.
- [40] Gilchrist JJ, MacLennan CA, Hill AV. Genetic susceptibility to invasive *Salmonella* disease. *Nat Rev Immunol*. 2015; 15:452-463.
- [41] Mastroeni P, Ugrinovic S, Chandra A et al. Resistance and susceptibility to *Salmonella* infections: lessons from mice and patients with immunodeficiencies. *Rev Med Microbiol*. 2003; 14:53-62.
- [42] Eguale T, Gebreyes WA, Asrat D, Alemayehu H, Gunn JS, Engidawork E. Non-typhoidal *Salmonella* serotypes, antimicrobial resistance and co-infection with parasites among patients with diarrhea and other gastrointestinal complaints in Addis Ababa, Ethiopia. *BMC Infect Dis*. 2015; 15:497.
- [43] Uche IV, MacLennan CA, Saul A. A Systematic Review of the Incidence, Risk Factors and Case Fatality Rates of Invasive Nontyphoidal *Salmonella* (iNTS) Disease in Africa (1966 to 2014). *PLoS Negl Trop Dis*. 2017; 11(1):e0005118.
- [44] Gordon MA. *Salmonella* infections in immunocompromised adults. *J Infect*. 2008; 54:413-422.
- [45] Bronzan RN, Taylor TE, Mwenechanya J et al. Bacteraemia in Malawian children with severe malaria: prevalence, etiology, HIV co-infection, and outcome *J Infect Dis*. 2007; 195:895-999.
- [46] Calis JC, Phiri KS, Faragher EB et al. Severe anemia in Malawian children. *N Eng J* 2008; 358:888-899.
- [47] Feasey NA, Everett D, Faragher EB et al. Modelling the Contributions of Malaria, HIV, Malnutrition and Rainfall to the Decline in Paediatric Invasive Non-Typhoidal *Salmonella* Disease in Malawi. *PLoS Negl Trop Dis*. 2015(7);9:e0003979.
- [48] MacLennan CA, Gilchrist JJ, Gordon MA, Cunningham AF et al. Dysregulated humoral immunity to nontyphoidal *Salmonella* in HIV-infected African adults. *Science*. 2010;328:508-512.
- [49] Dougan G, John V, Palmer S, Mastroeni P. Immunology in salmonellosis. *Immunol Rev*. 2011; 240(1):196-210.
- [50] Abruzzi A, Fried B. Coinfection of *Schistosoma* (Trematoda) with bacteria, protozoa and helminths. *Adv Parasitol*. 2011;77:1-85.





- [51] Sigauque B, Roca A, Mandomando I, Morais L, Quinto L, Sacarlal J et al. Community-acquired bacteremia among children admitted to a rural hospital in Mozambique. *Pediatr Infect Dis J.* 2009; 28(2):108-113.
- [52] Gordon MA. Invasive Non-typhoidal *Salmonella* Disease - epidemiology, pathogenesis and diagnosis. *Curr Opin Infect Dis.* 2011; 24(5):484-489.
- [53] Vugia DJ, Samuel M, Farley MM, Marcus R, Shiferaw, Shallow S et al. Invasive *Salmonella* infections in the United States, FoodNet, 1996-1999: incidence, serotype distribution, and outcome. *Clin Infect Dis.* 2004; 38(S3):S149-516.
- [54] Gordon MA, Banda HT, Gondwe M, Gordon SB, Boeree MJ, Walsh AL et al. Non-typhoidal *Salmonella* bacteraemia among HIV-infected Malawian adults: high mortality and frequent recrudescence. *AIDS.* 2002; 16(12):1633-1641.
- [55] Crump JA, Ramadhani HO, Morrissey AB et al. Invasive bacterial and fungal infections among hospitalized HIV-infected and HIV-uninfected adults and adolescents in northern Tanzania. *Clin Infect Dis.* 2011; 52(3):341-348.
- [56] Graham SM, English M. Non-typhoidal *Salmonellae*: a management challenge for children with community-acquired invasive disease in tropical African countries. *Lancet* 2009; 373(9659):267-269.
- [57] Giglioli G. Paratyphoid C an Endemic Disease of British Guiana: a Clinical and Pathological Outline. B. Paratyphosum C as Pyogenic Organism: Case Reports. *Proc R Soc Med.* 1929; 23(2):165-177.
- [58] Mabey DCW, Brown A, Greenwood BM. Plasmodium falciparum malaria and *Salmonella* infections in Gambia children. *J Infect Dis.* 1987; 155(6):1319-1321.
- [59] Scott AJ, Berkley JA, Mwangi I, Ochola L, Uyoga S, Macharia A et al. Relation between falciparum malaria and bacteraemia in Kenyan children: population-based, case-control study and a longitudinal study. *Lancet.* 2011; 378(9799):1316-1323.
- [60] Clemens JD. Meeting on establishment of consortium to study invasive salmonellosis in Sub-Saharan Africa. *Emerg Infect Dis.* 2009; 15(7):e2.
- [61] Archibald LK, Reller LB. Clinical microbiology in developing countries. *Emerg Infect Dis.* 2001; 7(2):302-305.
- [62] Wadula J, von Gottberg A, Kilner D, de Jong G, Cohen C, Khoosal M, Keddy K, Crewe-Brown H. Nosocomial outbreak of extended-spectrum beta-lactamase-producing *Salmonella* isangi in pediatric wards. *Pediatr Infect Dis J.* 2009; 25(9):843-844.
- [63] Kruger T, Szabo D, Keddy KH, Deeley K, Marsh JW, Hujer AM, Bonomo RA, Paterson DL. Infections with nontyphoidal *Salmonella* species producing TEM-63 or a novel TEM enzyme, TEM-131, in South Africa. *Antimicrob Agents Chemoter.* 2004; 48(11):4263-4270.
- [64] MacLennan CA, Tennant SM. Comparing the Roles of Antibodies to Nontyphoidal *Salmonella enterica* in High- and low-Income Countries and Implications for Vaccine Development. *Clin Vaccine Immunol.* 2013; 20(1):1487-1490.
- [65] Varma JK, Molbak K, Barrett TJ, Beebe JL, Jones TF, Rabatsky-Ehr T et al. Antimicrobial-resistant nontyphoidal *Salmonella* is Associated with excess bloodstream infections and hospitalizations. *J Infect Dis.* 2005; 191(4):554-561.
- [66] Parry CM, Threlfall EJ. Antimicrobial resistance in typhoidal and nontyphoidal *salmonellae*. *Curr Opin Infect Dis.* 2008; 21(5):531-538.



- [67] Kingsley RA, Msefula CL, Thomson NR, Kariuki S, Holt SE, Gordon MA, Harris D et al. Epidemic multiple drug resistant *Salmonella* Typhimurium causing invasive disease in sub-Saharan Africa have a distinct genotype. *Genome Res.* 2009; 19(12):2279-2287.
- [68] Kariuki S, Gordon MA, Feasey N, Parry CM. Antimicrobial resistance and management of invasive *Salmonella* disease. *Vaccine.* 2015; 33(3):C21-29.
- [69] MacLennan CA, Levine MM. Vaccines for low-income countries. *Seminars in Immunology.* 2013; 25(2):114-123.
- [70] MacLennan CA, Saul A. Vaccines against poverty. *Proc Natl Acad Sci USA.* 2014; 111(34):12307-12312.
- [71] Principi N, Esposito S. Preventing invasive salmonellosis in children through vaccination. *Expert Rev Vaccines.* 2016; 15(7):897-905.
- [72] Simon R, Levine MM. Glycoconjugate vaccine strategies for protection against invasive *Salmonella* infections. *Human Vaccines & Immunotherapeutics.* 2012; 8(4):494-498.
- [73] Holst O. Structure of the Lipopolysaccharide Core Region. *Bacterial Lipopolysaccharides* YA Knirel And MA Valvano (Eds) - Springer-Verlag Wien. 2011.
- [74] Miller SI, Ernst RK, Bader MW. LPS, TLR4 and infectious disease diversity. *Nat Rev Microbiol.* 2005; 3(1):36-46.
- [75] Caroff M, Karibian JM, Haeffner-Cavaillon N. Structural and functional analyses of bacterial lipopolysaccharides. *Microbes Infect.* 2002; 4(9):915-926.
- [76] Rondini S, Lanzilao L, Necchi F, O'Shaughnessy C, Micoli F, Saul AJ, MacLennan CA. Invasive African *Salmonella* Typhimurium induces bacterial antibodies against O-antigens. *Microb Pathog.* 2013; 63:19-23.
- [77] Rondini S, Micoli F, Lanzilao L, Gavini M, Alfini A, Bradt C, Clare S, Mastroeni P, Saul A, MacLennan CA. Design of glycoconjugates vaccines against African *Salmonella enterica* serovar Typhimurium. *Infect Imm.* 2015; 83(3):996-1007.
- [78] Goh YS, Clare S, Micoli F, Saul A, Mastroeni P, MacLennan CA. Monoclonal Antibodies of a Diverse Isotype Induced by an O-antigen Glycoconjugate Vaccine Mediate in Vitro and In Vivo Killing of African Invasive Nontyphoidal *Salmonella*. *Infect Imm.* 2015; 83(9):3722-3731.
- [79] Simon R, Tennant SM, Wang JY, Schmidlein PJ, Lees A, Ernst RK, Pasetti MF, Galen JE, Levine MM. *Salmonella enterica* serovar enteritidis core O polysaccharide conjugated to H:g,m flagellin as a candidate vaccine for protection against invasive infection with *S. enteritidis*. *Infect Imm.* 2011; 79(10):4240-4249.
- [80] Watson DC, Robbins JB, Szu SC. Protection of Mice against *Salmonella* typhimurium with an O-specific polysaccharide-protein conjugate vaccine. *Infect Imm.* 1992; 60(11):4679-4686.
- [81] Carlin NI, Svenson SB, Lindberg AA. Role of monoclonal O-antigen antibody epitope specificity and isotype in protection against experimental mouse typhoid. *Microb Pathog.* 1987; 2(3):171-183.
- [82] Singh SP, Williams YU, Benjamin WH, Klebba PE, Boyd D. Immunoprotection by monoclonal antibodies to the porins and lipopolysaccharide of *Salmonella* typhimurium. *Microb Pathog.* 1996; 21(4):249-263.

- [83] Aizawa SI. Flagellar assembly in *Salmonella* Typhimurium. *Mol Microbiol.* 1996; 19(1):1-5.
- [84] Joys TM. The covalent structure of the phase-1 flagellar filament protein of *Salmonella* Typhimurium and its comparison with other flagellins. *J Biol Chem.* 1985; 260(29):15758-15761.
- [85] Eom JS, Seok Kim J, Im Jang J, Kim BH, Young Yoo S, Hyeon Choi J, Bang IS, Lee IS, Keun Park Y. Enhancement of host immune responses by oral vaccination to *Salmonella enterica* serovar Typhimurium harboring both FliC and FliB flagella. *PLoS One.* 2013; 8(9):e74850.
- [86] Bobat S, Flores-Langarica A, Hitchcock J, Marshall JL, Kingsley RA et al. Soluble flagellin, FliC, induces an Ag-specific Th2 response, yet promotes T-bet-regulated Th1 clearance of *Salmonella* typhimurium infection. *Eur J Immunol.* 2011; 41(6):1606-1618.
- [87] Simon R, Wang JY, Boyd MA, Tulapurkar ME, Ramachandran G, Tennant SM, Pasetti M, Galen JE, Levine MM. Sustained protection in mice immunized with fractional doses of *Salmonella* Enteritidis core and O polysaccharide-flagellin glycoconjugates. *PLoS One.* 2013; 8(5):e64680.
- [88] Cunningham AF, Khan M, Ball J, Toellner KM, Serre K, Mohr E, MacLennan IC. Responses to the soluble flagellar protein FliC are Th2, while those to FliC on *Salmonella* are Th1. *Eur J Immunol.* 2004; 34(11):2986-2995.
- [89] Flores-Langarica A, Marshall JL, Hitchcock J, Cook C, Jobanputra J, Bobat S et al. Systemic flagellin immunization stimulates mucosal CD103+ dendritic cells and drives Foxp3+ regulatory T cell and IgA responses in the mesenteric lymph node. *J Immunol.* 2012; 189:5745-5754.
- [90] Galdiero S, Falanga A, Cantisani M, Tarallo R, Della Pepa ME, D'Oriano V, Galdiero M. Microbe-host interactions: structure and role of Gram-negative bacterial porins. *Curr Protein Pept Sci.* 2012; 13(8):843-854.
- [91] Gehring KB, Nikaido H. Existence and purification of porin heterotrimers of *Escherichia coli* K12 OmpC, OmpF, and PhoE proteins. *J Biol Chem.* 1989; 264(5):2810-2815.
- [92] Nikaido H. Molecular basis of bacterial outer membrane permeability revisited. *Microbiol Mol Biol Rev.* 2003; 67(4):593-656.
- [93] Tennant SM, Levine MM. Live attenuated vaccines for invasive *Salmonella* infections. *Vaccine.* 2015; 33(3):C36-41.
- [94] Mastroeni P, Chabalgoity JA, Dunstan SJ, Maskell DJ, Dougan G. *Salmonella*: immune response and vaccines. *Vet J.* 2001; 161(2):132-164.
- [95] Tennant SM, Wang JY, Galen JE, Simon R, Pasetti MF, Gat O, Levine MM. Engineering and preclinical evaluation of attenuated nontyphoidal *Salmonella* strains serving as live oral vaccines and as reagent strains *Infect Immun.* 2011; 79(10):4175-4185.
- [96] Tennant SM, Schmidlein P, Simon R, Pasetti MF, Galen JE, Levine MM. Refined Live Attenuated *Salmonella enterica* Serovar Typhimurium and Enteritidis Vaccines Mediate Homologous and Heterologous Serogroup Protection in Mice. *Infect Immun* 2015; 83(12):4504-4512.
- [97] Hindle Z, Chatfield SN, Phillimore J, Bentley M, Johnson J et al. Characterization of *Salmonella enterica* derivatives harboring defined *aroC* and

*Salmonella* pathogenicity island 2 type III secretion system (ssaV) mutations by immunization of healthy volunteers. *Infect Immun*. 2002; 70(7):3457-3467.

[98] Costantino P, Rappuoli R, Berti F. The design of semi-synthetic and synthetic glycoconjugate vaccines. *Expert Rev Drug Discov*. 2011; 6(10):1045-1066.

[99] Pichichero ME. Protein carriers of conjugate vaccines: characteristics, development, and clinical trials. *Hum Vaccin Immunother*. 2013; 9(12):2505-2523.

[100] Tontini M, Berti F, Romano MR, Proietti D, Zambonelli C, Bottomley MJ, De Gregorio E, Del Giudice G, Rappuoli R, Costantino P, Brogioni G, Balocchi C, Biancucci M, Malito E. Comparison of CRM<sub>197</sub>, diphtheria toxoid and tetanus toxoid as protein carriers for meningococcal glycoconjugate vaccines. *Vaccine*. 2013; 31(42):4827-4833.

[101] Tontini M, Romano MR, Proietti D, Balducci E, Micoli F, Balocchi C, Santini L, Masignani V, Berti F, Costantino P. Preclinical studies on new proteins as carrier for glycoconjugate vaccines. *Vaccine*. 2016; 34(42):4235-4242.

[102] Konadu E, Shiloach J, Bryla DA, Robbins JB, Szu SC. Synthesis, characterization, and immunological properties in mice of conjugates composed of detoxified lipopolysaccharide of *Salmonella* paratyphi A bound to tetanus toxoid with emphasis on the role of O acetyls. *Infect Immun*. 1996; 64(7):2709-2715.

[103] Konadu EY, Lin FY, Ho VA, Van Bay P, Thanh TC, Khiem HB, Trach DD, Karpad AB, Li J et al. Phase 1 and phase 2 studies of *Salmonella enterica* serovar paratyphi A O-specific polysaccharide-tetanus toxoid conjugates in adults, teenagers, and 2- to 4-year-old children in Vietnam. *Infect Immun*. 2000; 68(3):1529-1534.

[104] Amini V, Kazemian H, Yamchi JK, Feysa SG, Aslani S, Shavalipour A, Hourii H, Hoorijani M, Halaji M, Heidari H. Evaluation of the Immunogenicity of Diphtheria Toxoid Conjugated to *Salmonella* Typhimurium-Derived OPS in a Mouse Model: A Potential Vaccine Candidate Against Salmonellosis. *Iran Red Crescent Med J*. 2016; 18(7):e34135.

[105] Broker M, Costantino P, DeTora L, McIntosh ED, Rappuoli R. Biochemical and biological characteristics of cross-reacting material 197 CRM<sub>197</sub>, a non-toxic mutant of diphtheria toxin: use as a conjugation protein in vaccines and other potential clinical applications. *Biologicals*. 2011 ;39(4):195-204.

[106] Micoli F, Rondini S, Gavini M, Lanzilao L, Medagliani D, Saul A, Martin LB. O:2-CRM<sub>197</sub> conjugates against *Salmonella* Paratyphi A. *PloS One*. 2012; 7(11):e47039.

[107] Stefanetti G, Rondini S, Lanzilao L, Saul A, MacLennan CA, Micoli F. Impact of conjugation chemistry on the immunogenicity of *S. Typhimurium* conjugate vaccines. *Vaccine*. 2014; 32(46):6122-6129.

[108] Svenson SB, Lindberg AA. Artificial *Salmonella* vaccines: *Salmonella* typhimurium O-antigen-specific oligosaccharide-protein conjugates elicit protective antibodies in rabbits and mice. *Infect Immun*. 1981; 32(2):490-496.

[109] Gil-Cruz C, Bobat S, Marshall JL, Kingsley RA, Ross EA, Henderson IR, Leyton DLS, Coughlan RE et al. The porin OmpD from nontyphoidal *Salmonella* is a key target for a protective B1b cell antibody response. *Proc Natl Acad Sci USA*. 2009; 106(24):9803-9808.

[110] Goh YS, Grants AJ, Restif O, McKinley TJ, Armour KL, Clark MR, Mastroeni P. Human IgG isotypes and activating Fcγ receptors in the interaction of *Salmonella*





- enterica* serovar Typhimurium with phagocytic cells. *Immunology*. 2011; 133(1):74-83.
- [111] Secundino I, Lopez-Macias C, Cervantes-Barragan L, Gil-Cruz C, Rios-Sarabia N et al. *Salmonella* porins induce a sustained, lifelong specific bactericidal antibody memory response. *Immunology*. 2006; 117(1):59-70.
- [112] Salazar-Gonzalez RM, Maldonado-Bernal C, Ramirez-Cruz NE, Rios-Sarabia N, Beltran-Nava J et al. Induction of cellular immune response and anti-*Salmonella enterica* serovar typhi bactericidal antibodies in healthy volunteers by immunization with a vaccine candidate against typhoid fever. *Immunol Lett*. 2004; 93(2-3):115-122.
- [113] Toobak H, Rasooli I, Talei D, Jahangiri A, Owlia P, Darvish Alipour Astaneh S. Immune response variations to *Salmonella enterica* serovar Typhi recombinant porin proteins in mice. *Biologicals*. 2013; 41(4):224-230.
- [114] Berlanda Scorza F, Colucci AM, Maggiore L, Sanzone S, Rossi O, Ferlenghi I et al. High yield production process for *Shigella* outer membrane particles. *PLoS One*. 2012; 7(6):e35616.
- [115] Gerke C, Colucci AM, Giannelli C, Sanzone S, Vitali CG, Sollai L et al. Production of a *Shigella sonnei* Vaccine Based on Generalized Modules for Membrane Antigens (GMMA), 1790GAHB. *PLoS One*. 2015; 10(8):e0134478.
- [116] Maggiore L, Lu Y, Omasits U, Rossi O, Dougan G et al. Quantitative proteomic analysis of *Shigella flexneri* and *Shigella sonnei* Generalized Modules for Membrane Antigens (GMMA) reveals highly pure preparations. *Int J Med Microbiol* 2016; 306(2):99-108.
- [117] Podda A. Aims and role of Novartis Vaccines Institute for Global Health (NVGH). *Procedia in Vaccinology*. 2010; 2(2):124-127.
- [118] Micoli F, Rondini S, Gavini M, Pisoni I, Lanzilao L, Colucci AM, Giannelli C, Pippi F et al. A scalable method for O-antigen purification applied to various *Salmonella* serovars. *Anal Biochem*. 2013; 434(1):136-145.
- [119] Lanzilao L, Stefanetti G, Saul A, MacLennan CA, Micoli F, Rondini S. Strain Selection for Generation of O-Antigen-Based Glycoconjugate Vaccines against Invasive Nontyphoidal *Salmonella* Disease. *PLoS One*. 2015;10:e139847.
- [120] Stefanetti G, Saul A, MacLennan CA, Micoli F. Click Chemistry Applied to the Synthesis of *Salmonella* Typhimurium O-Antigen Glycoconjugate Vaccine on Solid Phase with Sugar Recycling. *Bioconjugate Chem*. 2015; 26(12):2507-2513.
- [121] Stefanetti G, Hu QY, Aimee U, Robinson Z, Allan M, Singh A et al. Sugar-Protein Connectivity Impacts on the Immunogenicity of Site-Selective *Salmonella* O-Antigen Glycoconjugate Vaccines. *Angewandte Chemie*. 2015; 127(45):13396-401.
- [122] Meloni E, CA, Micoli F, Sollai L, Gavini M, Saul A, Di Cioccio V, MacLennan Colucci AM. Simplified low-cost production of O-antigen from *Salmonella* Typhimurium Generalized Modules for Membrane Antigens (GMMA). *J Biotechnol*. 2015; 198:46-52.
- [123] Rossi O, Pesce I, Giannelli C, Aprea S, Caboni M, Citiulo F et al. Modulation of endotoxicity of *Shigella* generalized modules for membrane antigens (GMMA) by genetic lipid A modifications: relative activation of TLR4 and TLR2 pathways in different mutants. *J Biol Chem*. 2014; 289(36):24922-24935.
- [124] Rossi O, Caboni M, Negrea A, Necchi F, Alfini F, Micoli F, Saul A et al. Toll-Like Receptor Activation by Generalized Modules for Membrane Antigens from



Lipid A Mutants of *Salmonella enterica* Serovars Typhimurium and Enteritidis. Clin Vaccine Immunol. 2016; 23(4):304-314.

[125] MacLennan CA, Gondwe EN, Msefula CL, Kingsley RA, Thomson NR, White, NR et al. The neglected role of antibody in protection against bacteremia caused by nontyphoidal strains of *Salmonella* in African children. J Clin Invest. 2008; 118(4):1553-1562.

[126] McSorley SJ, Jenkins MK. Antibody is required for protection against virulent but not attenuated *Salmonella enterica* serovar typhimurium. Infect Immun. 2000; 68(6):3344-3348.

[127] Lindberg AA, LeMinor L. Methods Microbiol. 1984;15:1-142.

[128] Hellerqvist CG, Lindberg B, Svensson S. Structural studies on the O-specific side-chains of the cell-wall lipopolysaccharide from *Salmonella* Typhimurium 395 ms. Carb Res. 1968; 8:43-55.

[129] Hellerqvist CG, Lindberg B, Svensson S. Structural Studies on the O-Specific Side Chains of the Cell Wall Lipopolysaccharides from *Salmonella* typhi and *S. Enteritidis*. Acta Chemica Scandinavica 1969; 23:1588-1596.

[130] Micoli F, Ravenscroft N, Cescutti P, Stefanetti G, Londero S, Rondini S, MacLennan CA. Structural analysis of O-polysaccharide chains extracted from different *Salmonella* Typhimurium strains. Carb Res. 2014; 385:1-8.

[131] Onsare R, Micoli F, Lanzilao L, Alfini R, Okoro CK, Miugai AW, Revathi G, Saul A, Kariuki S, MacLennan CA, Rondini S. Relationship between antibody susceptibility and lipopolysaccharide O-antigen characteristics of invasive and gastrointestinal nontyphoidal *Salmonellae* isolates from Kenya. PLoS Negl Trop Dis. 2015; 9(3):e0003573.

[132] Parker CT, Liebana E, Henzler DJ, Guard-Petter J. Lipopolysaccharide O-chain microheterogeneity of *Salmonella* serotypes Enteritidis and Typhimurium. Environ Microbiol. 2001; 3(5):332-342.

[133] Slauch JM, Mahan MJ, Michetti P, Neutra MR, Mekalanos JJ. Acetylation (O-Factor 5) Affects the Structural and Immunological Properties of *Salmonella* typhimurium Lipopolysaccharide O Antigen. Infection and Immunity. 1995 ;63(2):427-441.

[134] Wollin R, Stocker BAD, Lindberg AA. Lysogenic Conversion of *Salmonella* typhimurium Bacteriophages A3 and A4 Consists of O-Acetylation of Rhamnose of the Repeating Unit of the O-Antigenic Polysaccharide Chain. J Bacteriol. 1987; 169(3):1003-1009.

[135] Helander IM, Moran A, Makela PH. Separation of two lipopolysaccharide populations with different contents of O-antigen factor 122 in *Salmonella enterica* serovar typhimurium. Mol Microbiol. 1992; 6(19):2859-2862.

[136] Ellis TN, Kuehn M. Virulence and immunomodulatory roles of bacterial outer membrane vesicles. Microbiol Mol Biol Rev. 2010; 74(19):81-94.

[137] Alaniz RC, Deatherage BL, Lara JC, Cookson BT. Membrane vesicles are immunogenic facsimiles of *Salmonella* typhimurium that potently activate dendritic cells, prime B and T cell responses, and stimulate protective immunity in vivo. J Immunol. 2007; 179(11):7692-7701.

[138] Raetz CR, Reynolds CM, Trent MS, Bishop RE. Lipid A modification systems in gram-negative bacteria. Annu Rev Biochem. 2007; 76:295-329.



- [139] Guo L, Lim KB, Poduje CM, Daniel M, Gunn JS, Hackett M, Miller SI. Lipid A acylation and bacterial resistance against vertebrate antimicrobial peptides. *Cell*. 1998; 95(2):189-198.
- [140] Kong Q, Six DA, Lui Q, Gu L, Roland KL, Raetz CRH, Curtiss R. Palmitoylation state impacts induction of innate and acquired immunity by the *Salmonella enterica* serovar typhimurium *msbB* mutant. *Infect Imm*. 2012;80:1302.
- [141] Khan SA, Everest P, Servos S, Foxwell N, Zahringer U, Brade H et al. A lethal role for lipid A in *Salmonella* infections. *Mol Microbiol*. 1998; 29(2):571-579.
- [142] Sunshine MG, Gibson BW, Engstrom JJ, Nichols WA, Jones BD, Apicella MA. Mutation of the *htrB* Gene in a Virulent *Salmonella* typhimurium Strain by Intergeneric Transduction: Strain Construction and Phenotypic Characterization. *J Bacteriol*. 1997; 179(17):5521-5533.
- [143] de Jong A, Thomas V, Simjee S, Godinho K, Schiessl B, Klein U et al. Pan-European monitoring of susceptibility to human-use antimicrobial agents in enteric bacteria isolated from healthy food-producing animals. *J Antimicrob Chemother*. 2012; 67(3):638-651.
- [144] Lilleengen K. Typing of *Salmonella* dublin and *Salmonella* enteritidis by means of bacteriophage. *Acta Pathol Microbiol Scand*. 1950; 27(4):625-640.
- [145] Datsenko KA, Wanner BL. One-step inactivation of chromosomal genes in *Escherichia coli* K-12 using PCR products. *Proc Natl Acad Sci USA*. 2000; 97(12):6640-6645.
- [146] Total protein monograph 2.5.33. European Pharmacopoeia 8.
- [147] Rossi O, Maggiore L, Necchi F, Koeberling O, MacLennan CA Saul A, Gerke C. Comparison of colorimetric assays with quantitative amino acid analysis for protein quantification of Generalized Modules for Membrane Antigens (GMMA). *Mol Biotechnol*. 2015; 57(1):84-93.
- [148] MacGee J, Doudoroff M. A new phosphorylated intermediate in glucose oxidation. *J Biol Chem*. 1954; 210(2):617-626.
- [149] Albersheim P, Nevins DJ, English PD, Karr A. A method for the analysis of sugars in plant cell-wall polysaccharides by gas-liquid chromatography. *Carb Res*. 1967; 5(3):340-345.
- [150] Harris PJ, Henry RJ, Blakeney AB, Stone BA. An improved procedure for the methylation analysis of oligosaccharides and polysaccharides. *Carb Res*. 1984; 127(1):59-73.
- [151] Sweet DP, Shapiro RH, Albersheim P. Quantitative Analysis by Various g.l.c. Response-Factor Theories for Partially Methylated and Partially Ethylated Alditol Acetates. *Carb Res*. 1975; 40:217-225.
- [152] Gerwig GJ, KamerlingGJ, Vliegenthart JFG. Determination of the D and L configuration of neutral monosaccharides by high-resolution capillary g.l.c. *Carb Res*. 1978; 62(2):349-357.
- [153] Prehm P. Methylation of carbohydrates by methyl trifluoromethanesulfonate in trimethylphosphate. *Carb Res*. 1980; 78:372-374.
- [154] Li-Hsin Z, Rothman DL, Shulman RG. <sup>1</sup>H NMR visibility of mammalian glycogen in solution. *Proc Natl Acad Sci USA*. 1990; 87:1678-1680.
- [155] McMeechan A, Lovell MA, Cogan TA, Marston KL, Humphrey TJ, Barrow PA. Glycogen production by different *Salmonella enterica* serotypes: contribution of



functional glgC to virulence, intestinal colonization and environmental survival. *Microbiology* 2005; 151:3969-3977.

[156] Bonafonte MA, Solano C, Sesma B, Alvarez M, Mortuenga L, Garcia-Ros D, Gamazo C. The relationship between glycogen synthesis, biofilm formation and virulence in *salmonella* enteritidis. *FEMS Microbiol Lett.* 2000; 191(1):31-36.

[157] Gardiner C, Ferreira YA, Dragonic RA, Redman CW, Sargent IL. Extracellular vesicle sizing and enumeration by nanoparticle tracking analysis. *J Extracell Vesicles* 2013; 2:19671.

[158] Gardiner C, Shaw M, Hole P, Smith J, Tannetta D, Redman CW, Sargent IL. Measurement of refractive index by nanoparticle tracking analysis reveals heterogeneity in extracellular vesicles. *J Extracell Vesicles.* 2014; 3:25361.

[159] Roier S, Blume T, Klug L, Wagner GE, Elhenawy W, Zangger K, Prassl R, Reidl J, Daum G, Feldman MF, Schild S. A basis for vaccine development: Comparative characterization of *Haemophilus influenzae* outer membrane vesicles. *Int J Med Microbiol.* 2015; 305(3):298-309.

[160] Anderson W, Kozak D, Coleman VA, Jamting AK, Trau M. A comparative study of submicron particle sizing platforms: accuracy, precision and resolution analysis of polydisperse particle size distributions. *J Colloid Interface Sci.* 2013; 405:322-330.

[161] van der Pol A, Coumans F, Varga Z, Krumrey M, Nieuwland R. Innovation in detection of microparticles and exosomes. *J Thromb Haemost.* 2013; 11(S1):36-45.

[162] Maas SL, de Vrij J, van der Vlist EJ, Geragousian B, van Bloois L et al. Possibilities and limitations of current technologies for quantification of biological extracellular vesicles and synthetic mimics. *J Control Release.* 2015; 200:87-96.

[163] Sitar S, Kejzar A, Pahovnik D, Kogej K, Tusek-Znidaric M, Lenassi M, Zagar E. Size Characterization and Quantification of Exosomes by Asymmetrical-Flow Field-Flow Fractionation. *Anal Chem.* 2016; 87(18) :9225-9233.

[164] Dragovic RA, Gardiner C, Brooks AS, Tannetta DS, Ferguson DJ, Hole P et al. Sizing and phenotyping of cellular vesicles using Nanoparticle Tracking Analysis. *Nanomedicine.* 2011; 7(6):780-788.

[165] Wieser A, Storz E, Liegl G, Peter A et al. Efficient quantification and characterization of bacterial outer membrane derived nano-particles with flow cytometric analysis. *Int J Med Microbiol.* 2014; 304:1032-1037.

[166] Pecora R. Dynamic light scattering measurement of nanometer particles in liquids. *Journal of Nanoparticle Research.* 2000; 2:123-131.

[167] Berne BJ, Pecora R. *Dynamic Light Scattering with Applications to Chemistry, Biology and Physics* Dover Publications, Inc Mineola New York. 2000.

[168] Clark NA, Lunacek JH, Benedek GB. A study of Brownian motion using light scattering *Am J Phys.* 1970; 38(5):575-585.

[169] Frisken BJ. Revisiting the method of cumulants for the analysis of dynamic light-scattering data. *Appl Opt.* 2001; 40(24):4087-4091.

[170] Vezocnik V, Rebolj K, Sitar S, Ota K, Tusek-Znidaric M et al. Size fractionation and size characterization of nanoemulsions of lipid droplets and large unilamellar lipid vesicles by asymmetric-flow field-flow fractionation/multi-angle light scattering and dynamic light scattering. *Journal of Chromatography A.* 2015; 1418:185-191.





- [171] Bryant G, Abeynayake C, Thomas JC. Improved Particle Size Distribution Measurements Using Multiangle Dynamic Light Scattering. 2. Refinements and Applications. *Langmuir*. 1996; 12(26):6224-6228.
- [172] Arraud N, Linares R, Tan S, Gounou C, Pasquet JM, Mornet S, Brisson AR. Extracellular vesicles from blood plasma: determination of their morphology, size, phenotype and concentration. *J Thromb Haemost*. 2014; 12(5):614-627.
- [173] Wyatt PJ. Submicrometer Particle Sizing by Multiangle Light Scattering following Fractionation. *Journal of Colloid and Interface Science*. 1998; 197(1):9-20.
- [174] Wright M. Nanoparticle tracking analysis for the multiparameter characterization and counting of nanoparticle suspensions. *Methods Mol Biol*. 2012; 906:511-524.
- [175] Carr B, Hole P, Malloy A, Smith J, Weld A, Warren J. The real-time, simultaneous analysis of nanoparticle size, zeta potential, count, asymmetry and fluorescence. *NSTI Nanotech Technical Proc*. 2008; 1:866-870.
- [176] Filipe V, Hawe A, Jiskoot W. Critical evaluation of Nanoparticle Tracking Analysis (NTA) by NanoSight for the measurement of nanoparticles and protein aggregates. *Pharm Res*. 2010; 27(5):796-810.
- [177] Gallego-Urrea JA, Tuoriniemi J, Hasselov M. Applications of particle-tracking analysis to the determination of size distributions and concentrations of nanoparticles in environmental, biological and food samples. *TrAC Trends in Analytical Chemistry*. 2011; 30(3):473-483.
- [178] Van Der Meeren P, Kasinos M, Saveyn H. Relevance of two-dimensional Brownian motion dynamics in applying nanoparticle tracking analysis. *Methods Mol Biol*. 2010; 906:525-534.
- [179] Braeckmans K, Buyens K, Bouquet W et al. Sizing Nanomatter in Biological Fluids by Fluorescence Single Particle Tracking. *Nano Lett*. 2010; 10(11):4435-4442.
- [180] Jamting AK, Cullen J, Coleman VA, Lawn M, Herrmann J, Miles J, Ford J. Systematic Study Of Bimodal Suspensions Of Latex Nanoparticles Using Dynamic Light Scattering. *Adv Powder Technol*. 2011; 22(2):290-293.
- [181] Hoo CM, Starostin N, West P, Mecartney ML. A comparison of atomic force microscopy (AFM) and dynamic light scattering (DLS) methods to characterize nanoparticle size distributions. *J Nanopart Res*. 2008; 10:89-96.
- [182] Hole P, Sillence K, Hannell C, Maguire CM, Roesslein M, Suarez G, Capracotta S et al. Interlaboratory comparison of size measurements on nanoparticles using nanoparticle tracking analysis (NTA). *J Nanopart Res*. 2013; 15:2101.
- [183] Holst O, Rohrscheidt-Andrzejewski E, Brade H. Isolation and characterisation of 3-deoxy-D-manno-2-octulopyranosonate 7-(2-aminoethyl phosphate) from the inner core region of *Escherichia coli* K-12 and *Salmonella* minnesota lipopolysaccharides. *Carb Res*. 1990; 204:93-102.
- [184] Holst O. The structures of core regions form enterobacterial lipopolysaccharides - an update. *FEMS Microbiol Lett*. 2007; 271(1):3-11.
- [185] Osborn MJ. Studies on the gram-negative cell wall, I. Evidence for the role of 2-keto-3-deoxyoctonate in the lipopolysaccharide of *Salmonella* Typhimurium. *Proc Natl Acad Sci USA*. 1963; 50(3):499-506.



- [186] Heath EC, Ghalambor MA. 2-Keto-3-deoxy-octonate, a constituent of cell wall lipopolysaccharide preparations obtained from *Escherichia coli*. *Biochem Biophys Res Commun.* 1959; 10(4):340-345.
- [187] Droge W, Lehmann V, Luderitz O, Westphal O. Structural investigations on the 2-keto-3-deoxyoctonate region of lipopolysaccharides. *Eur J Biochem.* 1970; 14(1):175-184.
- [188] Caroff M, Lebbar S, Szabo L. Do endotoxins devoid of 3-deoxy-D-manno-2-octulosonic acid exist? *Biochem Biophys Res Commun.* 1987; 143(3) :845-847.
- [189] Caroff M, Lebbar S, Szabo L. Detection of 3-deoxy-2-octulosonic acid in thiobarbiturate-negative endotoxins. *Carb Res.* 1987; 161(1):c4-7.
- [190] Danan A, Mondange M, Sarfati SR, Szabo P. Synthesis and Behaviour under Acidic Conditions of 2-Deoxy-D-arabinoheptopyranose and 3-Deoxy-2-ketoaldonic Acids Bearing O-Phosphono or O-Glucosyl Substituents at Position  $\beta$  to the Carbonyl Function. *J Chem Soc Perkin Trans.* 1982; 1:1275-1282.
- [191] McNicholas PA, Batley M, Redmond JW. The reactions of 3-deoxy-d-manno-oct-2-ulosonic acid (KDO) in dilute acid. *Carb Res* 1987; 165:17-22.
- [192] Auzanneau FI, Charon D, Szabo L. Formation of methyl (2,7-anhydro-3-deoxy- $\alpha$ -D-manno-2-octulofuranos)onate upon methanolysis of 2,4,7,8-tetra-O-acetyl-3-deoxy- $\alpha$ -D-manno-2-octulopyranosono-1,5-lactone. *Carb Res.* 1991; 201(1):337-341.
- [193] Auzanneau FI, Charon D, Szabo L. Phosphorylated Sugars. Part 27. Synthesis and Reactions, in Acid Medium, of 5-O-Substituted Methyl 3-Deoxy- $\alpha$ -D-manno-oct-2-ulopyranosidonic Acid 4- Phosphates. *J Chem Soc Perkin Trans.* 1991; 1:509-517.
- [194] Volk WA, Salomonsky NL, Hunt D. Isolation of 4,7-anhydro- and 4,8-anhydro-3-deoxy-octulosonic acid following acid hydrolysis of *Xanthomonas Sinensis* lipopolysaccharide. *J Biol Chem.* 1972; 247(12):3881-3887.
- [195] Olsthoorn MMA, Haverkamp J, Thomas-Oates JE. Mass Spectrometric Analysis of *Klebsiella pneumoniae* ssp. pneumoniae Rough Strain R20 (O1- :K20-) Lipopolysaccharide Preparations: Identification of Novel Core Oligosaccharide Components and Three 3-Deoxy-D-manno-oct-2-ulopyranosonic Artifacts. *J Mass Spectrometry.* 1999; 34:622-636.
- [196] Sioud S, Jahouh F, Nashed M, Joly N, Banoub JH. Determination of distinctive carbohydrate signatures obtained from the *Aeromonas hydrophila* (chemotype II) core oligosaccharide pinpointing the presence of the 4-O-phosphorylated 5-O-linked Kdo reducing end group using electrospray ionization quadrupole orthogonal time-of-flight mass spectrometry and tandem mass spectrometry. *Rapid Comm Mass Spectrometry.* 2010; 24:2475-2490.
- [197] Grimmecke HD, Brade H. Studies on the reductive amination of 3-deoxy-D-manno-octulosonic acid (Kdo). *Glycoconj J.* 1998; 15(6):555-562.
- [198] Cescutti P, Impallomeni G, Garozzo D, Sturiale L, Herasimenka Y, Lagatolla C, Rizzo R. Exopolysaccharides produced by a clinical strain of *Burkholderia cepacia* isolated from a cystic fibrosis patient. *Carb Res.* 2003; 338(23):2687-2695.
- [199] Lagatolla C, Skerlavay S, Dolzani L, Tonin EA, Monti Bragadin C, Bosco M, Rizzo R, Giglio L, Cescutti P. Microbiological characterisation of *Burkholderia cepacia* isolates from cystic fibrosis patients: investigation of the exopolysaccharides produced. *FEMS Microbiol Lett.* 2002; 209(1):99-106.



- [200] Palmer DW, Peters T. Automated determination of free amino groups in serum and plasma using 2,4,6-trinitrobenzene sulfonate. *Clin Chem.* 1969; 15(9):891-901.
- [201] Satake K, Okuyama T, Ohashi M, Shinoda T. The Spectrophotometric determination of amine, amino acid and peptide with 2,4,6-trinitrobenzene-1-sulfonic acid. *J Biochem.* 1960; 47:654.
- [202] Edge ASB. Deglycosylation of glycoproteins with trifluoromethanesulphonic acid: elucidation of molecular structure and function. *Biochem J.* 2003; 376:339-350.
- [203] Saldias SM, Patel K, Marolda CL, Bittner M, Contreras I, Valvano MA. Distinct functional domains of the *Salmonella enterica WbaP* transferase that is involved in the initiation reaction for synthesis of the O antigen subunit. *Microbiology.* 2008; 154:440-453.
- [204] Jansson PE, Lindberg AA, Lindberg B, Wollin R. Structural Studies on the Hexose Region of the Core in Lipopolysaccharides from *Enterobacteriaceae*. *Eur J Biochem* 1981;115.
- [205] Olsthoorn MMA, Petersen BO, Schlecht S, Haverkamp J, Bock K, Thomas-Oates JE, Holst O. Identification of a novel core type in *Salmonella* lipopolysaccharide. Complete structural analysis of the core region of the lipopolysaccharide from *Salmonella enterica* sv. *Arizonae* O62. *J Biol Chem.* 1998; 273(7):3817-3829.
- [206] Olsthoorn MMA, Peterson BO, Duus J, Haverkamp J, Thomas-Oates JE, Bock K, Holst O. The structure of the linkage between the O-specific polysaccharide and the core region of the lipopolysaccharide from *Salmonella enterica* serovar Typhimurium revisited. *Eur J Biochem.* 2000; 267(7):2014-2027.
- [207] Monteiro MA, Baqar S, Hall ER, Chen YH, Porter CK, Bentzel DE, Applebee L, Guerry P. Capsule Polysaccharide Conjugate Vaccine against Diarrheal Disease Caused by *Campylobacter jejuni*. *Infect Imm.* 2009; 77(3):1128-1136.
- [208] Allen G. Chapter 3. Specific cleavage of the protein. *Laboratory Techniques in Biochemistry and Molecular Biology* (Eds Allen G). 1981; 9:43-71.
- [209] Edge AS, Faltynek CR, Hof L, Reichert LE Jr, Weber P. Deglycosylation of glycoproteins by trifluoromethanesulfonic acid. *Anal Biochem.* 1981; 118(1):131-137.
- [210] Lebl M, Pires J, Poncar P, Pokorny V. Evaluation of gaseous hydrogen fluoride as a convenient reagent for parallel cleavage from the solid support. *J Comb Chem.* 1999; 1(6):474-479.
- [211] Torok B, Busci I, Surya Prakash GK, Olah GA. Deprotection and cleavage of peptides bound to Merrifield resin by stable dimethyl ether-poly(hydrogen fluoride) (DMEPHF) complex. a new and convenient reagent for peptide chemistry. *Chem Commun.* 2002; 23:2882-2883.
- [212] Horvath E, Edwards AM, Bell JC, Braun PE. Chemical deglycosylation on a micro-scale of membrane glycoproteins with retention of phosphoryl-protein linkages. *J Neurosci Res.* 1989; 24(3):398-401.
- [213] Malito E, Bursulaya B, Chen C, Lo Surdo P, Picchianti M, Balducci E et al. Structural basis for lack of toxicity of the diphtheria toxin mutant CRM<sub>197</sub>. *Proc Natl Acad Sci USA.* 2012; 109(14):5229-5334.



- [214] Kubler-Kielb J, Vinogradov E, Lagergard T, Ginzberg A et al. Oligosaccharide conjugates of *Bordetella pertussis* and *bronchiseptica* induce bactericidal antibodies, an addition to pertussis vaccine. *Proc Natl Acad Sci USA*. 2011; 108(10):4087-4092.
- [215] Banoub J, El Aneed A, Cohen A, Martin P. Characterization of the O-4 phosphorylated and O-5 substituted Kdo reducing end group and sequencing of the core oligosaccharide of *Aeromonas salmonicida* ssp *salmonicida* lipopolysaccharide using tandem mass spectrometry. *Eur J Mass Spectrom*. 2004; 10(5):715-730.
- [216] Mogingen U, Resemann A, Martin CE, Parameswarappa S, Govindan S, Wamhoff EC, Broecker F, Suckau D, Pereira CL, Anish C, Seeberger PH, Kolarihc D. Cross Reactive Material 197 glycoconjugate vaccines contain privileged conjugation sites. *Sci Rep*. 2016; 6:20488.
- [217] Bardotti A, Averani G, Berti F, Berti S, Carinci V, D'Ascenzi S, Fabbri B, Giannini S et al. Physicochemical characterisation of glycoconjugate vaccines for prevention of meningococcal diseases. *Vaccine*. 2008; 26(18):2284-2296.
- [218] Crotti S, Zhai H, Zhou J, Allan M, Proietti D, Pansegrau W, Hu QY, Berti F, Adamo R. Defined conjugation of glycans to the lysines of CRM<sub>197</sub> guided by their reactivity mapping. *Chembiochem*. 2014; 15(6):836-843.
- [219] Jones C. Vaccines based on the cell surface carbohydrates of pathogenic bacteria. *An Acad Bras Cienc*. 2005; 77(2):293-324.
- [220] Ravenscroft N, Wheeler JX, Jones C. Bioanalysis of meningococcal vaccines. *Bioanalysis*. 2010; 2(2):343-361.
- [221] Avcy FY, Li X, Tsuji M, Kasper DL. A mechanism for glycoconjugate vaccine activation of the adaptive immune system and its implications for vaccine design. *Nature Medicine*. 2011; 17(12):1602-1609.
- [222] Preiss J. Bacterial glycogen synthesis and its regulation. *Ann Rev Microbiol*. 1984; 38:418-459.
- [223] Vines ED, Marolda CL, Balachandran A, Valvano MA. Defective O-Antigen Polymerization in *tolA* and *pal* Mutant of *Escherichia coli* in Response to Extracytoplasmic Stress. *J Bacteriol*. 2005; 187(10):3359-3368.



## Acknowledgements

It would not have been possible to work, reach the objectives and write this Ph.D. thesis without the guidance, support and help of a huge number of people.

The Ph.D. project was sponsored by GSK Vaccines Institute for Global Health S.r.l. (former Novartis Vaccine Institute for Global Health), part of the GSK group of companies.

First of all, a big thank to my Supervisor at the University of Trieste, Dr. Paola Cescutti and my co-supervisor at GVGH, Dr. Francesca Micoli, for their careful and passionate guidance and supervision during the Ph.D. and their several revisions and corrections to this thesis. Thanks for the time you have dedicated to me and for all the things you have taught me in these years. I enjoyed almost every moments spent with you, trying to assimilate as much as possible from you. I have been really impressed by your incredible skills, outstanding competences and knowledge. You have been a fundamental source of inspiration for the continuation of my education.

I thank Dr. Mariaelena Caboni and Dr. Aurel Negrea for strains generation (SEn 618  $\Delta toR/\Delta toR \Delta msbB/\Delta toR \Delta msbB \Delta pagP$  and STm 1418  $\Delta toR/\Delta toR \Delta msbB/\Delta toR \Delta htrB$ ) and bacteria growth for GMMA production. I thank Dr. Renzo Alfini for introducing me in the GVGH laboratories and for the purification of OAg from SEn 618 wild type and of GMMA produced by the mutants, for the preliminar studies on the structural characterization of the OAg component on GMMA and for the SDS-PAGE analysis of GMMA from mutated strains.

I thank the GSK Animal Care Facility for the mice immunizations and Dr. Luisa Lanzilao and Dr. Francesca Necchi (GVGH Immunoassay Unit) for the ELISA and the SBA analysis performed.

I thank Dr. Yunshan Goh for generation of the STm 1418  $\Delta toR \Delta wbaP$  mutant and Dr. Omar Rossi and Dr. Irene Beriotto for the bacteria growth for GMMA production.

I thank the GVGH Technical Development Unit for the strong support in their laboratories and for the fermentation, purification and analytical characterization of GMMA from SEn 618  $\Delta toR \Delta msbB \Delta pagP$  (BPR 6066, STm 2192  $\Delta toR \Delta pagP$





*ΔmsbB* (BPR 6063) and STm 1418 *ΔtolR* lot18Dec15 used for GMMA particle size distribution evaluation.

I thank Dr. Luisa Sturiale and Prof. Domenico Garozzo (Institute for Polymers, Composites and Biomaterials, CNR - National Research Council, Catania, Italy) for the MALDI-TOF MS analysis of the core OS.

I thank Dr. Laura Salvini and her team (Toscana Life Sciences, Head of Technology Facilities, Siena, Italy), Dr. Stefano Gotta and his team (GSK Analytical Research and Development Mass Spectrometry) for their help with MALDI-TOF MS and LC-ESI-MS analysis, respectively, and for their precious feedbacks and discussions about the MS results.

I thank Prof. Neil Ravenscroft and Dr. Aneesa Omar (University of Cape Town, South Africa) for the support in NMR spectra interpretation and NMR spectra recording, for the helpful feedbacks, wise suggestions and discussion during these years.

I thank Dr. Denis Scaini and Dr. Ilaria Rago (Elettra Sincrotrone Trieste, Area Science Park, Trieste, Italy) for the Atomic Force Microscope analysis of GMMA.

I am grateful to Prof. Roberto Rizzo (University of Trieste, Italy), Dr. Allan Saul (GVGH institute director), Prof. Calman MacLennan (Jenner Institute, University of Oxford, UK), Dr. Carlo Giannelli, Dr. Ivan Pisoni and Dr. Simona Rondini (GVGH) for the critical reading of the thesis and for their helpful advice, suggestions and support during my work at the University of Trieste and in GVGH.

I thank Dr. Francesco Berti (GSK Vaccines, Head of Antigen Design), Dr. Isabel Delany (GSK Vaccines, Head of Antigen Identification and Coordinator of GSK Ph.D. Students Academy) and Dr. Sylvie Carine Bertholet Girardin (former Coordinator of GSK Ph.D. Students Academy) for their help during the Student Management Committee Meetings organized during my permanence in GSK Vaccines.

I thank the Bacterial Polysaccharides team (Ambra Delneri, Aris Sveronis, Stefania Dolfi, Claudia Buriola, Marco Distefano, Barbara Bellich) of Department of Life Sciences in Trieste and the people working at the second floor of building C11.



I thank the GVGH Vaccine Chemistry team (Renzo Alfini, Giuseppe Stefanetti, Melissa Arcuri, Davide Oldrini, Roberta Di Benedetto) for their help during the laboratory activities. I thank Dr. Luigi Capriotti and Dr. Alessio Corrado for their help with TFMS de-glycosylation.

I thank the coordinators of the School of Molecular Biomedicine (Prof. Germana Meroni, Prof. Guidalberto Manfioletti and Prof. Licio Collavin) and the University of Trieste administrative members, especially Lorella Coceani.

I thank the GVGH administrative members for their useful help during my permanence in GVGH.

I thank Dr. Francesco Citiulo, Dr. Maria Grazia Aruta, Dr. Angela Daniele for their incredible support during my experience in Siena and for being sincere friends. I really enjoyed almost every seconds spent with you.

Above all, thanks to my parents for your continuative and unconditional support during these years and not only. Without you nothing would have been possible, and to you I dedicate this thesis.



## Annexes

### Communications

#### *Oral presentations:*

- “Characterization of the O-antigen component on candidate glycoconjugate and GMMA vaccines against nontyphoidal *Salmonella*” - XIV Convegno-Scuola sulla Chimica dei Carboidrati - Certosa di Pontignano, Siena (Italy) - 22-25<sup>th</sup> Jun. 2014.
- “Characterization of the OAg component on candidate glycoconjugate and GMMA vaccines against iNTS” - NVGH Work in Progress Meeting - GSK Vaccines campus, Siena (Italy) - 18<sup>th</sup> Aug. 2014.
- “Characterization of O-Antigen-based glycoconjugate and GMMA vaccines against iNTS” - Vaccine Design and Immune Responses (VADER) project review and management Meeting - GSK Vaccines, Siena (Italy) - 23<sup>th</sup> Oct 2014.
- “A basis for vaccine development: comparative characterization of *Haemophilus influenzae* outer membrane vesicles” - Sclavo-Behring Vaccines Institute for Global Health (SBVGH) Journal Club Meeting - GSK Vaccines campus, Siena (Italy) - 5<sup>th</sup> Mar. 2015.
- “Characterization of O-antigen based GMMA vaccines against iNTS” - SBVGH Work in Progress Meeting - GSK Vaccines campus, Siena (Italy) - 11<sup>th</sup> May 2015.
- “Characterization of polysaccharide-based vaccines” - Ph.D. Students Management Committee Meeting - GSK Vaccines campus, Siena (Italy) - 30<sup>th</sup> Jun. 2015.
- “Characterization of polysaccharide-based vaccines” - DSV Ph.D. School of Molecular Biomedicine Ph.D. Mid-Term presentations, University of Trieste, Trieste (Italy) - 2<sup>nd</sup> Oct. 2015.
- “23<sup>th</sup> International Symposium on Glycoconjugates trip report” - GSK Vaccines campus, Siena (Italy) - 31<sup>th</sup> Oct. 2015.





- “Characterization of polysaccharide-based vaccines” - VIII annual GSK Vaccines Ph.D. Students Workshop, GSK Vaccines campus, Siena (Italy) - 26-27<sup>th</sup> Nov. 2015.
- “KDO structure and reactivity in the synthesis of an O-antigen-based glycoconjugate vaccine against nontyphoidal *Salmonella*” - XV Convegno-Scuola sulla Chimica dei Carboidrati - Certosa di Pontignano, Siena (Italy) - 19-22<sup>th</sup> Jun. 2016.
- “Characterization of GMMA and glycoconjugate vaccines against nontyphoidal *Salmonella*” - GVGH Work in Progress Meeting - GSK Vaccines campus, Siena (Italy) - 21<sup>th</sup> Nov. 2016.
- “Characterization of GMMA and glycoconjugate vaccines against nontyphoidal *Salmonella*” - IX annual GSK Vaccines Ph.D. Students Workshop, GSK Vaccines campus, Siena (Italy) - 24-25<sup>th</sup> Nov. 2016.
- “Characterization of polysaccharide-based vaccines against invasive nontyphoidal *Salmonella* disease (iNTS)” - Ph.D. Students Management Committee Meeting - GSK Vaccines campus, Siena (Italy) - 13<sup>th</sup> Jan. 2017.

*Poster presentations:*

- G. De Benedetto, R. Alfini, R. Rizzo, A. Saul, S. Rondini, C. A. MacLennan, P. Cescutti, F. Micoli - “Characterization of the O-antigen component on candidate glycoconjugate and GMMA vaccines against nontyphoidal *Salmonella*” - XIV Convegno-Scuola sulla Chimica dei Carboidrati - Certosa di Pontignano, Siena (Italy) - 22-25<sup>th</sup> Jun. 2014.
- G. De Benedetto, R. Alfini, S. Rondini, A. Saul, C. A. MacLennan, P. Cescutti, F. Micoli - “Characterization of O-antigen-based GMMA vaccines against nontyphoidal *Salmonellae*” - VII Annual Novartis Vaccines Ph.D. Students Workshop, GSK Vaccines campus, Siena (Italy) - 25-26<sup>th</sup> Nov 2014.
- G. De Benedetto, R. Alfini, S. Rondini, A. Saul, C. A. MacLennan, P. Cescutti, F. Micoli - “Characterization of O-antigen-based GMMA vaccines against nontyphoidal *Salmonella*” - 23<sup>th</sup> International Symposium on Glycoconjugates, Split (Croatia) - 15-20<sup>th</sup> Sep. 2015.



- G. De Benedetto - “Characterization of polysaccharide vaccines against nontyphoidal *Salmonella*” - Summer Course Glycosciences - 14<sup>th</sup> European Training Course on Carbohydrates, Groningen (The Netherlands) - 12-16<sup>th</sup> Jun. 2016.
- R. Alfini, G. De Benedetto, R. Di Benedetto, P. Cescutti, M. Caboni, L. Lanzilao, F. Necchi, A. Saul, C. A. MacLennan, S. Rondini, F. Micoli - “Characterization of Generalized Modules for Membrane Antigens (GMMA) vaccine against nontyphoidal *Salmonella*” - Virus-like particle & Nano-particle vaccines (VLPNPV) 2016 - Leiden University Medical Centre, Leiden (The Netherlands) - 22-24<sup>th</sup> Jun. 2016.

*Ph.D. Project Publications:*

- **G. De Benedetto**, R. Alfini, P. Cescutti, M. Caboni, L. Lanzilao, F. Necchi, A. Saul, C. A. MacLennan, S. Rondini, F. Micoli - “Characterization of O-antigen delivered by Generalized Modules for Membrane Antigens (GMMA) vaccine candidates against nontyphoidal *Salmonella*” - 2017 - Vaccine, volume 35(3):419-426, DOI [10.1016/j.vaccine.2016.11.089](https://doi.org/10.1016/j.vaccine.2016.11.089)
- “Determination of nontyphoidal *Salmonella* GMMA particle size distribution” (Manuscript in preparation).
- “KDO reactivity and selectivity in the synthesis of OAg-CRM<sub>197</sub> glycoconjugate vaccines” (Manuscript in preparation).
- “Investigation on conjugation chemistry in the synthesis of OAg-CRM<sub>197</sub> glycoconjugate vaccines” (Manuscript in preparation).

*Other Publications:*

- P. Cescutti, **G. De Benedetto**, R. Rizzo - “Structural determination of the polysaccharide isolated from biofilms produced by a clinical strain of *Klebsiella pneumoniae*” - 2016 - Carbohydrate Research, volume 430:29-35, DOI [10.1016/j.carres.2016.05.001](https://doi.org/10.1016/j.carres.2016.05.001)
- M. Kowarik, M. Wetter, M. A. Hauptle, M. Braun, M. Steffen, S. Kemmler, P. Carranza, N. Ravenscroft, D. Sirena, P. Cescutti, **G. De Benedetto**, M. Wacker



- “Identification, biosynthesis and characterization of an *E. coli* O25b bioconjugate vaccine against a common cause of urinary tract infections” (Manuscript in preparation).

### Courses, Conferences and Workshops

#### *Courses:*

- Lezioni di biostatistica per scuole di specializzazione - Dott. L. Torelli - Cattinara Hospital, Trieste (Italy) - 10<sup>th</sup> Jan. 2014.
- Lettura critica di un articolo scientifico - Dott. F. Giudici - Cattinara Hospital, Trieste (Italy) - 16<sup>th</sup> Jan. 2014.
- Writing scientific manuscripts - Dr. K. Veitch - GSK Vaccines campus, Siena (Italy) - 27<sup>th</sup> Nov. 2014.
- Strategie avanzate di sviluppo metodo - troubleshooting avanzato - Phenomenex HPLC/UPLC course - Dott. A. Cannatà - GSK Vaccines campus, Siena (Italy) - 9-10<sup>th</sup> Apr. 2015.
- Tosoh Bioscience size exclusion chromatography in bioanalysis applications - GSK Vaccines campus, Siena (Italy) - 28<sup>th</sup> May 2015.
- From bench to bedside: principle of vaccine research and development - Dr. S. Ahmed - University of Siena, Siena (Italy) - 15-16<sup>th</sup> Jun. 2015.
- Grant writing skills and communication - GSK Vaccines campus, Siena (Italy) - 11-13<sup>th</sup> Apr. 2016.
- Evoluzione della cromatografia nel settore delle proteine - Troubleshooting: guida avanzata alla prevenzione e risoluzione dei problemi cromatografici e strumentali - Phenomenex HPLC/RP-HPLC course - Dott. A. Cannatà - GSK Vaccines campus, Siena (Italy) - 18-19<sup>th</sup> May 2016.
- Introduction to publishing your R&D non-clinical research - Dr. S. Meredith - GSK Vaccines campus, Siena (Italy) - 18-19<sup>th</sup> May 2016.
- GSK VxRD Science Academy Internal Seminars - GSK Vaccines campus, Siena (Italy)/Università degli Studi di Siena, Siena (Italy) - Jul. 2014/Dec. 2016.



- Master in Vaccinology and Pharmaceutical Clinical Development - GSK Sciences Academy - GSK Vaccines campus, Siena (Italy) - Jun. 2015/Jun. 2016.

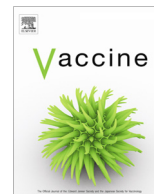
*Conferences and Workshops:*

- Short Winter School on Nano and Biotechnology - University of Trieste, Trieste (Italy) - 27-28<sup>th</sup> Jan. 2014.
- XIV Convegno-Scuola sulla Chimica dei Carboidrati - Certosa di Pontignano, Siena (Italy) - 22-25<sup>th</sup> Jun. 2014.
- Novartis Vaccines Institute for Global Health (NVGH) Scientific Advisory Board Meeting - GSK Vaccines campus, Siena (Italy) - 7-8<sup>th</sup> Jul. 2014.
- 2014 Novartis Vaccines Research Days Meeting - GSK Vaccines campus, Siena (Italy) - 14-18<sup>th</sup> Jul. 2014.
- Vaccine Design and Immune Responses (VADER) project review and management Meeting - GSK Vaccines, Siena (Italy) - 23<sup>th</sup> Oct 2014.
- VII Annual Novartis Vaccines Ph.D. Students Workshop, GSK Vaccines campus, Siena (Italy) - 25-26<sup>th</sup> Nov 2014.
- 2015 GSK Vaccines Research Days Meeting - GSK Vaccines campus, Siena (Italy) - 13-17<sup>th</sup> Jul. 2015.
- Global Health 2035: Mission Grand Conference - GSK Vaccines campus, Siena (Italy) - 18-19<sup>th</sup> Jul. 2015.
- 23<sup>th</sup> International Symposium on Glycoconjugates, Split (Croatia) - 15-20<sup>th</sup> Sep. 2015.
- DSV Ph.D. School of Molecular Biomedicine Ph.D. Mid Term presentations, University of Trieste, Trieste (Italy) - 2<sup>nd</sup> Oct. 2015.
- Genomics for diagnosis, treatment and preventions of infectious diseases (EUCLIDS workshop), GSK Vaccines campus, Siena (Italy) - 18<sup>th</sup> Nov. 2015.
- VIII annual GSK Vaccines Ph.D. Students Workshop, GSK Vaccines campus, Siena (Italy) - 26-27<sup>th</sup> Nov. 2015.
- GSK Vaccines Institute for Global Health (GVGH) project planning meeting, GSK Vaccines campus, Siena (Italy) - 27<sup>th</sup> Nov. 2015.



- GSK Vaccines Institute for Global Health (GVGH) meets IVI and Hilleman labs, GSK Vaccines campus, Siena (Italy) - 15<sup>th</sup> Feb. 2016.
- Summer Course Glycosciences - 14<sup>th</sup> European Training Course on Carbohydrates, Groningen (The Netherlands) - 12-16<sup>th</sup> Jun. 2016.
- XV Convegno-Scuola sulla Chimica dei Carboidrati - Certosa di Pontignano, Siena (Italy) - 19-22<sup>th</sup> Jun. 2016.
- 2016 GSK Vaccines Research and Development Days Meeting - GSK Vaccines campus, Siena (Italy) - 13-14<sup>th</sup> Jul. 2016.
- I Giovani e la Chimica in Friuli-Venezia Giulia, Società Chimica Italiana - University of Trieste, Trieste (Italy) - 29<sup>th</sup> Sep. 2016.
- IX annual GSK Vaccines Ph.D. Students Workshop, GSK Vaccines campus, Siena (Italy) - 24-25<sup>th</sup> Nov. 2016.





# Characterization of O-antigen delivered by Generalized Modules for Membrane Antigens (GMMA) vaccine candidates against nontyphoidal *Salmonella*



G. De Benedetto<sup>a,b</sup>, R. Alfani<sup>a</sup>, P. Cescutti<sup>b</sup>, M. Caboni<sup>c</sup>, L. Lanzilao<sup>a</sup>, F. Necchi<sup>a</sup>, A. Saul<sup>a</sup>, C.A. MacLennan<sup>d</sup>, S. Rondini<sup>a</sup>, F. Micoli<sup>a,\*</sup>

<sup>a</sup> GSK Vaccines Institute for Global Health (GVGH) S.r.l. (former Novartis Vaccines Institute for Global Health, NVGH), Via Fiorentina 1, 53100 Siena, Italy

<sup>b</sup> Dipartimento di Scienze della Vita, Ed. C11, Università degli Studi di Trieste, via L. Giorgieri 1, 34127 Trieste, Italy

<sup>c</sup> Antimicrobial Discovery Center, Department of Biology, 360 Huntington Ave., Boston, MA 02115, United States

<sup>d</sup> Jenner Institute, Nuffield Department of Medicine, University of Oxford, Old Road Campus Research Building, Roosevelt Drive, Oxford OX3 7DQ, UK

## ARTICLE INFO

### Article history:

Received 5 August 2016

Received in revised form 21 October 2016

Accepted 27 November 2016

Available online 18 December 2016

### Keywords:

*Salmonella* Typhimurium

*Salmonella* Enteritidis

Vaccine

O-antigen

GMMA

Outer membrane vesicles

## ABSTRACT

Invasive nontyphoidal *Salmonella* disease (iNTS) is a leading cause of death and morbidity in Africa. The most common pathogens are *Salmonella enterica* serovars Typhimurium and Enteritidis. The O-antigen portion of their lipopolysaccharide is a target of protective immunity and vaccines targeting O-antigen are currently in development. Here we investigate the use of Generalized Modules for Membrane Antigens (GMMA) as delivery system for *S. Typhimurium* and *S. Enteritidis* O-antigen. Gram-negative bacteria naturally shed outer membrane in a blebbing process. By deletion of the *tolR* gene, the level of shedding was greatly enhanced. Further genetic modifications were introduced into the GMMA-producing strains in order to reduce reactogenicity, by detoxifying the lipid A moiety of lipopolysaccharide. We found that genetic mutations can impact on expression of O-antigen chains. All *S. Enteritidis* GMMA characterized had an O-antigen to protein w/w ratio higher than 0.6, while the ratio was 0.7 for *S. Typhimurium*  $\Delta tolR$  GMMA, but decreased to less than 0.1 when further mutations for lipid A detoxification were introduced. Changes were also observed in O-antigen chain length and level and/or position of O-acetylation. When tested in mice, the GMMA induced high levels of anti-O-antigen-specific IgG functional antibodies, despite variation in density and O-antigen structural modifications.

In conclusion, simplicity of manufacturing process and low costs of production, coupled with encouraging immunogenicity data, make GMMA an attractive strategy to further investigate for the development of a vaccine against iNTS.

© 2016 Published by Elsevier Ltd.

## 1. Introduction

*Salmonella enterica* Typhimurium and Enteritidis are the most common serovars responsible for invasive nontyphoidal *Salmonella* disease (iNTS) in Africa [1–4], resulting in case-fatality rates of around 20% [5]. iNTS is closely associated with malaria and malnutrition among African infants and children, and with HIV infection in all age groups [6]. Antibiotics are not always available in rural African settings, and increasing levels of multidrug-resistance are limiting their effectiveness [7–9], making this disease a high priority for vaccine development. Currently, there are no licensed vac-

cines against iNTS and efforts are ongoing to identify protective antigens and best strategies for vaccine development [10,11].

Antibodies directed against the O-antigen (OAg) portion of *Salmonella* lipopolysaccharide (LPS) have been shown to be able to mediate killing [12–16] and protect against infection in animal models [14,15,17]. *S. Typhimurium* and *S. Enteritidis* OAg share a common backbone consisting of galactose (Gal), rhamnose (Rha), and mannose (Man), which serologically constitutes epitope O:12 [18]. A different 3,6-dideoxy-hexose residue is linked to Man in these two serovars: abequose (Abe), conferring O:4 specificity to *S. Typhimurium*, or tyvelose (Tyv), conferring O:9 specificity to *S. Enteritidis* (Fig. 1) [19,20]. *Salmonella* OAg can demonstrate high levels of heterogeneity in terms of chain length and variation in O-acetylation and glucosylation of the repeating units [14,21–24]. For *S. Typhimurium*, Abe may be O-acetylated at

\* Corresponding author.

E-mail address: [francesca.x.micoli@gsk.com](mailto:francesca.x.micoli@gsk.com) (F. Micoli).



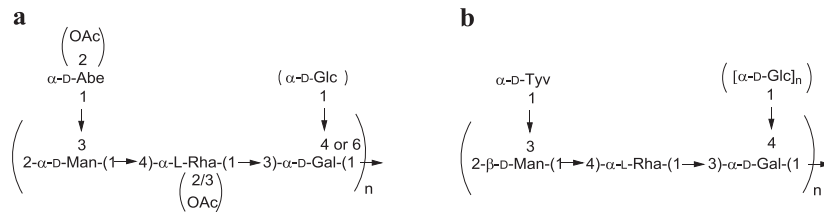


**Fig. 1.** OAg repeating unit structure of (a) *S. Typhimurium* (O:4,5) and (b) *S. Enteritidis* (O:9).

position C-2, which adds the O:5 specificity [25]. The additional presence of O-acetyl groups at C-2 and C-3 of Rha has also been reported [22,26]. OAg chains can also be variably glucosylated, with glucose (Glc) linked at C-4 (O:12<sub>2</sub> specificity) or C-6 (O:1 specificity) to Gal [21,27]. Studies in mice indicated that all these structural modifications can impact the immunogenicity of the corresponding glycoconjugate vaccines [14,23].

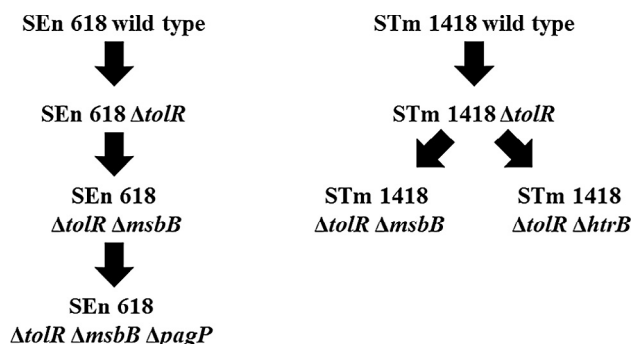
We are investigating a Generalized Modules for Membrane Antigens (GMMA) [28] approach to the development of a bivalent vaccine against *S. Typhimurium* and *S. Enteritidis* [29]. Gram-negative bacteria naturally shed outer membrane as blebs [30,31]. The release of blebs can be greatly increased by genetic manipulation of the bacteria resulting in GMMA. In *Salmonella*, deletion of the *tolR* gene affects the stability of the linkage between the inner and the outer membrane, and results in an enhanced shedding process [28,29,32,33]. GMMA derived from the surface of Gram-negative bacteria contain potent immunostimulatory components, such as lipoproteins and LPS, which can contribute to their immunogenicity, but also to reactogenicity [30,31]. In GMMA vaccine development, removal or modification of such components may alter the balance between reactogenicity and immunogenicity. One way to reduce the reactogenicity of LPS is to modify its acylation pathway, for example by deletion of *msbB*, *pagP* and *htrB* genes [29].

In this study, we report that mutations introduced to increase GMMA release and decrease reactogenicity are associated with changes in the structure of surface OAg. We investigate the impact of these changes on the antibody response to GMMA in mice and serum bactericidal activity of these antibodies *in vitro*.

## 2. Materials and methods

### 2.1. Strains

*Salmonella enterica* serovar Typhimurium isolate SGSC1418 (STm 1418) (LT-2 collection [34], University of Calgary) and Enteritidis SA618 (SEn 618) (CEESA EASSA II collection [35] of Quotient Bioresearch Limited), both isolated from animals, were chosen as



**Scheme 1.** GMMA of *S. Enteritidis* and *S. Typhimurium* mutated strains chosen for characterization [29].

parent strains [23]. Mutants were generated as previously described [29] (Scheme 1).

### 2.2. GMMA production and characterization

GMMA were produced and purified as described [29]. Total protein content was estimated by Lowry assay [36,37]. OAg sugar content was quantified by High-Performance Anion-Exchange Chromatography coupled to Pulsed Amperometric Detector (HPAEC-PAD) as previously described [21], after performing acid hydrolysis directly on GMMA. GMMA components did not interfere in the quantification of the OAg sugar monomers. The amount of core reducing end KDO (2-keto-3-deoxy-octonate) was assumed equal to the amount of lipid A and quantified by semicarbazide/High Performance Liquid Chromatography - Size Exclusion Chromatography (HPLC-SEC) method after sugar extraction [21]. The percentage of OAg chains was calculated as the molar ratio of their KDO divided by total KDO, including LPS molecules with just core. Lipid A structures were investigated by Matrix-Assisted Laser Desorption/Ionization-Mass Spectrometry (MALDI-MS) [29]. Protein pattern profile was analyzed by SDS-PAGE analysis (SI).

### 2.3. OAg purification and characterization

OAg extraction and purification from wild type bacteria was performed as previously described [38]. For extraction of the OAg from GMMA, a similar procedure was used as detailed in SI. Gel filtration chromatography with differential refractive index (dRI) detection was used to fractionate the OAg chains obtained after extraction from GMMA. Samples were run on Sephacryl S300 column (90 cm × 1.6 cm i.d.). The mobile phase was NaNO<sub>3</sub> 0.05 M at the flow rate of 8 mL/h. Fractions from Sephacryl S300 were desalted by gel filtration chromatography on Biogel P2 column (90 cm × 1.6 cm i.d., flow rate 8 mL/h) or on a Bioline preparative chromatographic system equipped with Superdex G30 column (90 cm × 1.0 cm i.d., flow rate 1.5 mL/min). OAg structural analysis was performed as previously reported [21]. OAg peak molecular weight (MP) was calculated by HPLC-SEC analysis by using dextrans as standards on TSK gel G3000 PWXL column (30 cm × 7.8 mm; particle size 7 μm; Cat. N. 808021) with TSK gel PWXL guard column (4.0 cm × 6.0 mm; particle size 12 μm; Cat. N. 808033) (Tosoh Bioscience) and with in-line dRI detector. 80 μL of samples 100 μg/mL polysaccharide content were injected and eluted at the flow rate of 0.5 mL/min with 0.1 NaCl, 0.1 NaH<sub>2</sub>PO<sub>4</sub>, 5% CH<sub>3</sub>CN, pH 7.2 as mobile phase.

### 2.4. High-Performance Liquid Chromatography - Size Exclusion Chromatography/Multi-Angle Light Scattering (HPLC-SEC/MALS)

GMMA samples were analyzed by HPLC-SEC with Sepax SRT-C 2000-1000 columns in series (Cat. N. 235980-7830; 235950-7830) equilibrated in PBS and with in-line UV, fluorescence emission, dRI and MALS detectors. 80 μL of samples 100 μg/mL protein content were injected and eluted with a flow rate of 0.5 mL/min.



MALS data were collected and analyzed using ASTRA 6 software (Wyatt Technology).

### 2.5. Immunogenicity of candidate *Salmonella* GMMA vaccines in mice and serological analysis

Five groups of eight 5-weeks old female CD1 mice were purchased from Charles River Laboratory and maintained at Novartis Vaccines Animal Care. Mice received two subcutaneous immunizations at 28 days interval with 200  $\mu$ L/dose of 1  $\mu$ g of OAg formulated with Alhydrogel (final concentration 0.7 mg/mL Al<sup>3+</sup>). Mice were bled before the first immunization (sera pooled for each group at day 0) and at days 14, 28 and 42 after the first immunization (collected as single sera). All animal protocols were approved by the local animal ethical committee (approval N. AEC201309) and by the Italian Minister of Health in accordance with Italian law. Individual mouse sera, collected at each time point, were tested for anti-OAg IgG antibody titers by ELISA, as previously described [23]. For each group, equal volumes of sera collected at day 42 from each mouse were pooled, and tested for serum bactericidal activity (SBA) against *S. Typhimurium* D23580, an endemic clinical isolate from Malawi [8,39], obtained from the Malawi-Liverpool-Wellcome Trust Clinical Research Programme, Blantyre, Malawi, or against the laboratory strain *S. Enteritidis* CMCC4314, (corresponding to ATCC4931) obtained from the Novartis Master Culture Collection (NMCC), as previously described [23]. Bactericidal activity was determined as serum dilutions necessary to obtain 50% colony forming units (CFU) reduction after 3 h incubation at 37 °C compared with CFU counted at time 0. To evaluate possible nonspecific inhibitory effects of baby rabbit complement (BRC) or mouse serum, bacteria were also incubated with SBA buffer and active BRC as negative control, and with pooled sera from a control placebo group diluted at the same dilutions of test sera (starting from 1:100) with active BRC. For all negative controls we did not observe any killing effect up to the highest serum concentration tested of 1:100 (assay's baseline).

Statistical and graphical analysis was performed using GraphPad Prism 6 software. The non-parametric Mann-Whitney test (two-tailed) and Kruskal-Wallis analysis with Dunn's test for post hoc analysis were used, respectively, to compare two or multiple groups. Response at day 14 and 42 for each group was compared by Wilcoxon matched-pairs signed rank test (two-tailed).

## 3. Results

As part of our previous work, several different *S. Typhimurium* and *S. Enteritidis* isolates were screened as sources of OAg for use in a bivalent glycoconjugate vaccine against iNTS [23]. Based on the results obtained, SEn 618 and STm 1418 strains were also selected for use as GMMA-producing strains. They were genetically modified through deletion of *tolR* gene for GMMA overproduction and of further genes ( $\Delta$ *msbB*,  $\Delta$ *htrB* and  $\Delta$ *pagP*) to reduce reactivity [29]. IL-6 release was used as an indicator for proinflam-

matory responses to toll like receptors (TLR) stimulation. The combination of  $\Delta$ *msbB* and  $\Delta$ *pagP* mutations provoked the least stimulation of cytokine release from human PBMC compared to GMMA with wild type lipid A. We also found that the residual activity was largely due to TLR2 activation, although GMMA significantly signaled through TLR4 [29]. Some of the resulting GMMA (Scheme 1) were here fully characterized and tested in mice.

### 3.1. OAg characterization of SEn 618 GMMA

OAg from SEn 618 wild type bacteria was fully characterized, as detailed in SI (Tables S1, S2; Fig. S1), and used as a comparison with OAg present on GMMA obtained from genetically modified GMMA-producing strains, in order to examine how mutations impacted on structural features.

HPLC-SEC fluorescence emission profile of GMMA samples from all mutated strains revealed very low residual soluble proteins (<5%), indicating good sample purity (Fig. S2). The particle size of GMMA from all mutated strains was similar, as estimated by HPLC-SEC analysis coupled with MALS detector (Table 1). The w/w ratio of OAg chains per mg of total protein was high for all SEn 618 GMMA. OAg chains constituted a low percentage of total LPS molecules containing core oligosaccharide, indicating that, for all mutants, a large proportion of LPS molecules contain very few or no OAg repeating units (Table 1). Analysis by SDS-PAGE performed on SEn 618  $\Delta$ *tolR*  $\Delta$ *msbB*  $\Delta$ *pagP* GMMA (Fig. S3) showed no major changes in the protein pattern compared to GMMA with no lipid A modification ( $\Delta$ *tolR*).

Following sugar extraction by acetic acid hydrolysis of GMMA suspensions, OAg populations were isolated by size exclusion chromatography and compared to the OAg population purified from the wild type strain (Fig. 2). OAg populations from all GMMA and wild type strain showed a similar average number of repeating units close to 25. GMMA produced from  $\Delta$ *tolR* single-mutant SEn 618 expressed an additional OAg population of relatively higher molecular weight (MW), with an average of 70 repeating units. This population also appeared to be present as a shoulder in the HPLC-SEC profile of the OAg from the wild type strain. The two OAg populations at different MW from  $\Delta$ *tolR* GMMA were quantified by the phenol-sulfuric acid assay. The higher MW (HMW) and lower MW (LMW) fractions represented 22% and 44% respectively of the total amount of sugar extracted. For GMMA derived from the other two 618 mutant strains, OAg chains accounted for 75% ( $\Delta$ *tolR*  $\Delta$ *msbB*) and 68% ( $\Delta$ *tolR*  $\Delta$ *msbB*  $\Delta$ *pagP*) of total sugar extracted. These percentages are in agreement with the molar ratios of OAg chains to total LPS molecules found (Table 1).

All OAg populations derived from all mutated as well as wild type SEn 618 strains revealed similar sugar composition by HPAEC-PAD and NMR (Table 2), in agreement with that expected for *S. Enteritidis* OAg [19]. All samples were characterized by low glucosylation levels of 8–11%, compared to 19% for the wild type OAg (Table 2).

O-acetylation levels were low for all *S. Enteritidis* OAg samples and decreased with the addition of mutations into the

**Table 1**  
Characterization of GMMA from SEn 618 and STm 1418 mutated strains.

GMMA	w/w OAg/GMMA protein ratio	molar % OAg chains/total LPS	nmol lipid A/mg GMMA protein	nm radius (MALS)
SEn 618 $\Delta$ <i>tolR</i>	0.6	14	156.6	22
SEn 618 $\Delta$ <i>tolR</i> $\Delta$ <i>msbB</i>	1.7	22	240.1	23
SEn618 $\Delta$ <i>tolR</i> $\Delta$ <i>msbB</i> $\Delta$ <i>pagP</i>	1.5	12	528.0	20
STm 1418 $\Delta$ <i>tolR</i>	0.66	10	172.8	22
STm 1418 $\Delta$ <i>tolR</i> $\Delta$ <i>msbB</i>	0.03	<1	108.2	15
STm 1418 $\Delta$ <i>tolR</i> $\Delta$ <i>htrB</i>	0.02	0.45	154.8	11

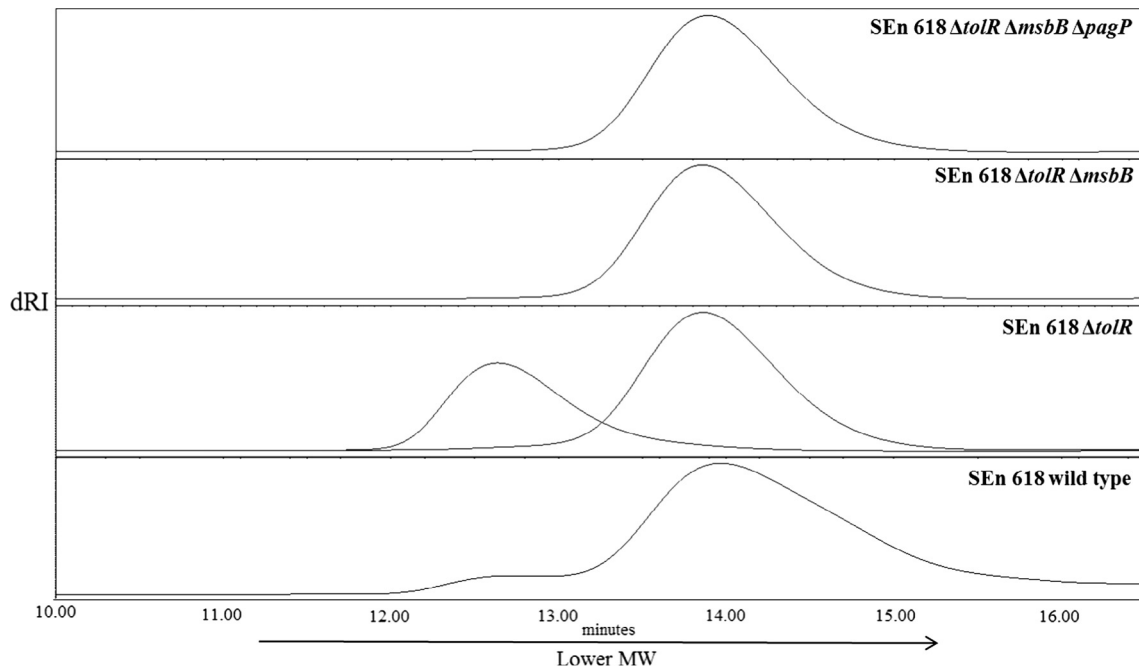


**Fig. 2.** HPLC-SEC chromatograms of OAg populations extracted from GMMA produced by mutated strains of SEN 618 and compared to OAg purified from the wild type SEN 618 isolate (dRI profiles; TSK gel 3000 PWXL column; NaPi 100 mM NaCl 100 mM 5% CH<sub>3</sub>CN pH 7.2; 0.5 mL/min; V<sub>0</sub> 11.20 min; V<sub>tot</sub> 23.29 min).

**Table 2**

Characterization of OAg populations extracted from GMMA produced by SEN 618 and STm 1418 mutated strains and comparison to the OAg from corresponding wild type strains. Sugar composition (molar ratio to Rha) and average number of repeating units (RU) calculated by HPAEC-PAD and HPLC-SEC/semicarbazide (assay for KDO quantification). O-acetylation (O-Ac) level calculated by <sup>1</sup>H NMR.

OAg	Tyv/Abe <sup>a</sup>	Rha	Man	Gal	Glc	Number RU (MP <sup>b</sup> )	O-Ac %
SEn 618 wild type	1.00	1.00	1.00	1.08	0.19	28 (27.3)	16
SEn 618 $\Delta tolR$ (HMW OAg)	0.99	1.00	1.04	1.05	0.12	70 (90.3)	8
SEn 618 $\Delta tolR$ (LMW OAg)	0.93	1.00	0.99	1.07	0.11	23 (30.3)	4
SEn 618 $\Delta tolR \Delta msbB$	0.97	1.00	1.00	1.05	0.09	26 (30.4)	3
SEn 618 $\Delta tolR \Delta msbB \Delta pagP$	0.97	1.00	0.99	1.06	0.08	27 (29.5)	2
STm 1418 wild type	1.00 <sup>a</sup>	1.00	1.00	1.00	0.80	na	73
STm 1418 $\Delta tolR$ (HMW OAg)	0.91 <sup>a</sup>	1.00	0.97	0.98	1.00	75 (104.7)	54
STm 1418 $\Delta tolR$ (LMW OAg)	0.93 <sup>a</sup>	1.00	0.98	1.04	0.96	25 (32.9)	79

<sup>a</sup> Calculated by <sup>1</sup>H NMR; na: not applicable.

<sup>b</sup> MP: peak molecular weight in kDa calculated by HPLC-SEC analysis by using dextrans as standards.

GMMA-producing strain, from 16% found in the wild type (non-GMMA) OAg to 2% for the OAg purified from the 'triple-mutant' GMMA (Table 2 and Fig. S4).

### 3.2. OAg characterization of STm 1418 GMMA

OAg from STm 1418 wild type strain has been fully characterized previously [21] (Table 2, Figs. 3 and S5–S6). Table 1 details the main characteristics of *S. Typhimurium* GMMA from corresponding mutant GMMA-producing strains. As for SEN 618 GMMA, all preparations had low residual soluble proteins, as indicated by HPLC-SEC analysis (data not shown). After the introduction of the  $\Delta tolR$  mutation, the w/w ratio of OAg chains per total protein amount was high (0.66), indicating maintenance of good levels of OAg expression. However, after the introduction of  $\Delta htrB$  or  $\Delta msbB$  mutations in the  $\Delta tolR$  strain, OAg to GMMA protein ratio was greatly reduced, consistent with inhibition of OAg production (Table 1). At the same time, MALS analysis showed that GMMA producing lower amounts of OAg chains were characterized by reduced size with respect to  $\Delta tolR$  GMMA (Table 1). As for SEN 618 GMMA, analysis of GMMA by SDS-PAGE analysis (Fig. S3)

showed similar proteins profile after introduction of mutations to reduce reactogenicity compared to GMMA with no lipid A modification ( $\Delta tolR$ ).

For  $\Delta tolR \Delta htrB$  GMMA, the presence of an extra polysaccharide was revealed, identified as glycogen by <sup>1</sup>H NMR [40] (Fig. S5A). In  $\Delta tolR \Delta msbB$  GMMA, very high levels of Glc were quantified by HPAEC-PAD analysis and HPLC-SEC (dRI) chromatography revealed the presence of an additional peak, thus strongly suggesting glycocon production by this mutant as well (Fig. S5B).

OAg from  $\Delta tolR$  GMMA showed two main populations with different average MW, consisting of 75 and 25 repeating units respectively, similar to those OAg populations from the corresponding wild type strain, but with different relative proportions (Table 2, Fig. 3). The two populations had the same sugar composition, in agreement with OAg from 1418 wild type strain, with glycosylation levels >80% (Table 2). Glycosidic linkage analysis confirmed that the main linkage for Glc was in position C-6 on the Gal residue (Table S4).

O-acetyl groups quantification by Gas Liquid Chromatography (GLC) and Gas Liquid Chromatography Coupled to Mass Spectrometry (GLC-MS) [21] performed on these populations detected the

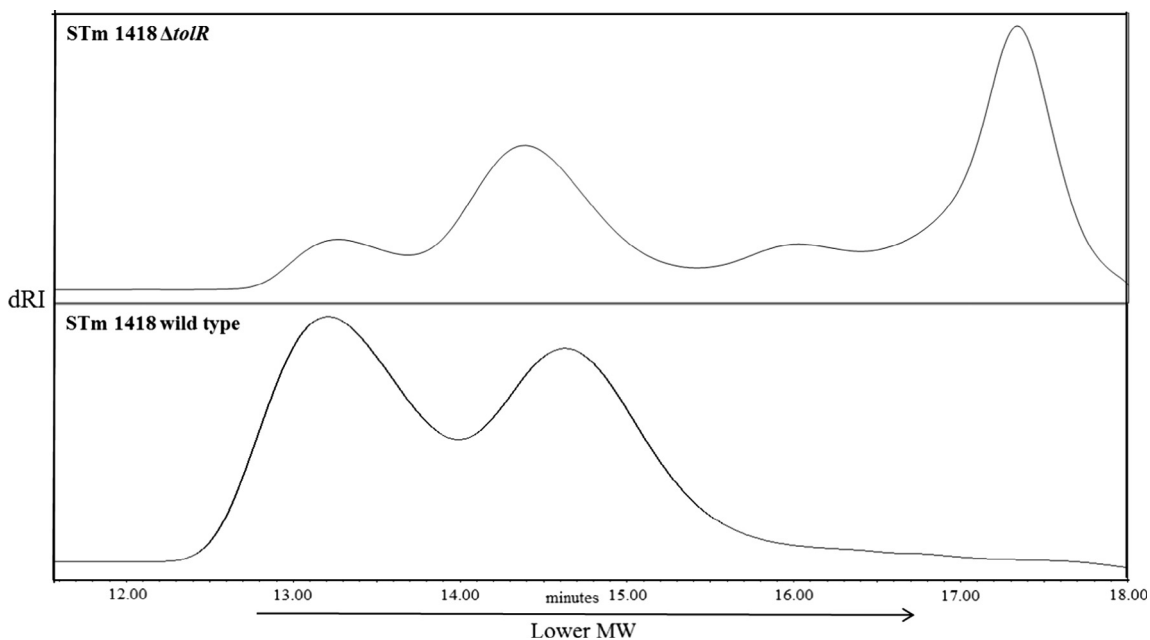


**Fig. 3.** HPLC-SEC chromatograms of the OAg populations extracted from STm GMMA of the  $\Delta tolR$  mutant and compared to the OAg purified from the wild type strain (TSK gel 3000 PWXL column; NaPi 100 mM NaCl 100 mM 5% CH<sub>3</sub>CN pH 7.2; 0.5 mL/min; V<sub>0</sub> 11.20 min; V<sub>tot</sub> 23.29 min). The component eluting at 17.30 min in the  $\Delta tolR$  OAg refers to the core of the LPS. Core fractions for wild type OAg were lost in the purification process.

presence of O-acetyl groups only on C-2 of Abe, with O-acetylation levels of 39% for the OAg population at HMW and 32% for that at LMW, compared to 52% for the wild type OAg (Table S5). <sup>1</sup>H NMR spectroscopy analysis [21] confirmed the presence of O-acetyl groups on C-2 of Abe (O-acetyl signal at 2.10 ppm, H-2 of Abe2OAc at 5.10 ppm) in both samples (43% for HMW, 69% for LMW OAg populations), as well as in the OAg produced by the wild type strain (73%). An additional peak at 2.17 ppm (12% for HMW, 10% for LMW OAg populations) (Fig. S6) was tentatively attributed to the O-acetyl group on C-2 of Rha, by comparison with the O-acetylation pattern assigned to the OAg from *S. Typhimurium* D23580 strain [21].

The low amount of OAg chains on the double mutant GMMA impeded their detailed structural characterization.

### 3.3. Immunogenicity in mice

Groups of mice were immunized with SEN 618  $\Delta tolR$  and  $\Delta tolR \Delta msbB \Delta pagP$  GMMA, and STm 1418  $\Delta tolR$ ,  $\Delta tolR \Delta msbB$  and  $\Delta tolR \Delta htrB$  GMMA. All the GMMA candidate vaccines were compared at the same OAg dose of 1  $\mu$ g. The main objective was to verify the ability of GMMA to induce an immune response and whether the observed OAg modifications, following the genetic manipulations required to generate GMMA-producing strains, affected immunogenicity in terms of anti-OAg responses. Fourteen days after the second injection, all GMMA were able to induce a serovar-specific anti-OAg IgG response, with no significant differences among GMMA of the same serovar (Mann-Whitney test for SEN 618 GMMA and Kruskal-Wallis for STm 1418 GMMA) (Fig. 4). However, more variability was observed in the anti-OAg IgG response induced in mice injected with SEN 618  $\Delta tolR \Delta msbB \Delta pagP$  GMMA (3 non-responders) compared to 618  $\Delta tolR$  GMMA, and with STm 1418  $\Delta tolR \Delta htrB$  GMMA compared to 1418  $\Delta tolR$  GMMA. All GMMA were able to boost the anti-OAg IgG response (same p value of 0.0078 comparing day 14 and day 42 response for each group). Immune sera were also bactericidal *in vitro* against *S. Typhimurium* D23580 or *S. Enteritidis* CMCC4314 (Fig. 4).

## 4. Discussion

GMMA are nano-sized particles, displaying high-densities of antigens and containing bacterial pathogen associated molecular patterns (PAMPs), with the potential to trigger strong immune responses [30,31]. Furthermore, GMMA can be produced efficiently, economically and rapidly [28,32,33], making them an attractive vaccine candidate, particularly for low and middle income countries.

A comprehensive panel of analytical methods has been assembled for GMMA characterization with particular attention to their surface OAg, which is a key target of protective antibody responses. Such methods allowed verification of whether mutations introduced into GMMA-producing strains impact on OAg expression and structure, enabling the identification of optimal potential GMMA candidate for inclusion in a vaccine against iNTS. Furthermore, such methods are of fundamental importance in the process of vaccine development, to ensure consistency of production, vaccine efficacy and to monitor stability of GMMA vaccines.

The  $\Delta tolR$  mutation introduced to increase GMMA production (approximately 300 mg OAg, obtained per liter of fermentation broth of SEN 618  $\Delta tolR$  and STm 1418  $\Delta tolR$  GMMA) was accompanied by changes in the OAg chain length distribution in both SEN 618 and STm 1418 strains. In contrast to what was observed for SEN 618  $\Delta tolR$  GMMA, the  $\Delta tolR$  mutation in the STm 1418 strain selected caused a reduction of the OAg population at HMW compared to the wild type strain. In addition, mutations to modify lipid A and reduce toxicity need to be carefully monitored as they may inhibit OAg production, as observed in this study with STm 1418 clones.

With STm 1418, a reduction in the amount of OAg was associated with the production of glycogen as additional polysaccharide on GMMA. Production of such polysaccharide was not observed in the panel of nontyphoidal *Salmonella* wild type strains we previously characterized [22,23]. We have also observed this phenomenon in other mutants, derived both from *S. Enteritidis* and *S. Typhimurium* GMMA-producing strains, when genetic

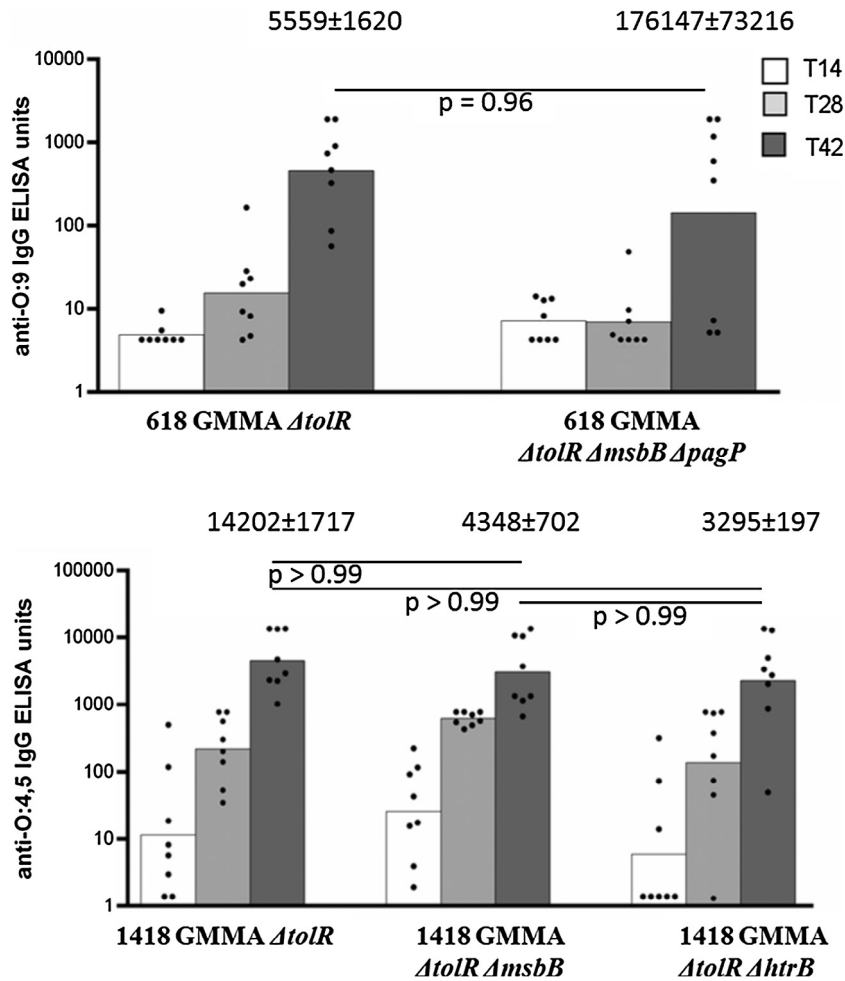


**Fig. 4.** Summary graphs of anti-OAg IgG geometric means (bars) and individual antibody levels (dots) induced in CD1 mice by GMMA vaccines injected at days 0 and 28 at 1  $\mu$ g OAg dose. Mice were bled before the first immunization (pooled sera from each group at day 0) and at days 14, 28 and 42 after the first immunization. ELISA limit of detection was calculated as 2.9 and as 2.2 ELISA units/mL for anti-O:9 and anti-O:4.5 IgG, respectively. Numbers above day 42 bars represent SBA results of pooled sera collected at day 42 from each group against *S. Enteritidis* CMCC4314 or *S. Typhimurium* D23580. SBA titers were calculated as the serum dilution necessary to obtain 50% bacterial killing after 3 h incubation at 37 °C compared with bacteria counted at time 0. Each serum pool was tested in triplicate in three independent experiments, except for SEn 618  $\Delta$ *tolR* serum, which was tested in duplicate. Initial serum dilution was 1:100.

mutations have resulted in low OAg expression (data not shown). The reasons for this are not clear and it would be interesting to verify whether there is a correlation between lack of OAg production and glycogen formation and what functional implications this may have. Glycogen has been described to be produced in enteric bacteria for energy storage and to accumulate in cytoplasmic granules [41]. Most specifically, glycogen production in *S. Enteritidis* has previously been shown to be related to virulence, colonization and resistance mechanisms; it is usually produced under limiting growth conditions or environmental stresses [42].

OAg chain length and O-acetylation level are parameters that are known to affect the immunogenicity of OAg-based vaccines [14,17,23,25]. Mutations introduced into the wild type strains also affected the OAg O-acetylation pattern. When tested in mice at the same OAg dose, all GMMA were able to induce anti-OAg IgG specific antibodies, with functional activity, independent of the OAg density on GMMA and with no major impact of any OAg structural modification. The effective amount of OAg injected, rather than its density on GMMA, may determine the anti-OAg antibody response. The implication of this observation is that a higher OAg to GMMA ratio should permit the use of a lower amount of GMMA per vaccine dose for the same anti-OAg antibody response. This will have potential benefits in relation to cost and safety of the vaccine.

In parallel work, same GMMA characterized here were assessed for their reactogenicity. We showed that the combination of  $\Delta$ *msbB* and  $\Delta$ *pagP* mutations is the optimal approach to minimize reactogenicity of *S. Enteritidis* and *S. Typhimurium* GMMA, resulting in uniformly penta-acylated lipid A [29]. GMMA from this triple mutant strain provoked the least stimulation of cytokine release from human PBMC, compared to GMMA with wild type lipid A, and stimulatory potential similar to that of a *Shigella sonnei* GMMA vaccine tested in Phase I clinical trials [29,32]. *S. Enteritidis* and *S. Typhimurium* GMMA with reduced toxicity, without a major impact on OAg expression level, seem to be good components for a vaccine against iNTS. We have verified that mutations introduced to reduce GMMA reactogenicity do not have a major impact on the protein pattern profile. A more accurate analysis will be done on final selected strains in order to identify nature and amount of the most abundant proteins, considering that they may be additional key mediators of functional antibody. It will be important to verify batch to batch consistency, and to investigate the contribution that anti-protein antibodies can have on the overall immune response induced by GMMA vaccines.

Simplicity of manufacturing process and low costs of production, coupled with encouraging immunogenicity data, make the GMMA vaccine approach particularly attractive. The comparison



of OAg-GMMA with other candidate vaccines under development against iNTS, such as live-attenuated and glycoconjugate vaccines, will be of great interest for the development of a successful and efficacious intervention against iNTS.

### Declaration of interests

RA, MC, LL, FN, AS, CAM, SR and FM were permanent employees of Novartis Vaccines Institute for Global Health (NVGH) at the time of the study. Following the acquisition of NVGH by the GSK group of companies in March 2015, RA, LL, FN, AS, SR and FM are now permanent employees of GSK Vaccines Institute for Global Health (GVGH), part of the GSK group of companies.

### Contributorship

GDB, RA, PC, MC, AS, CAM, SR, FM were involved in the conception and design of the study. GDB, RA, MC, LL, FN, SR, FM acquired the data. GDB, RA, PC, MC, LL, FN, AS, CAM, SR, FM analyzed and interpreted the results. All authors were involved in drafting the manuscript or revising it critically for important intellectual content. All authors had full access to the data and approved the manuscript before it was submitted by the corresponding author.

### Acknowledgments

This study was sponsored by Novartis Vaccines Institute for Global Health. The Institute has now become GSK Vaccines Institute for Global Health, part of the GSK group of companies. We also wish to thank Aurel Negrea for strains generation and Omar Rossi for SDS-PAGE analysis of GMMA from mutated strains. P. Cescutti and G. De Benedetto (Dipartimento di Scienze della Vita, Università di Trieste) thank the “Beneficentia Stiftung” (Vaduz, Lichtenstein) for funding the acquisition of the Bioline preparative chromatographic system.

### Appendix A. Supplementary material

Supplementary data associated with this article can be found, in the online version, at <http://dx.doi.org/10.1016/j.vaccine.2016.11.089>.

### References

- [1] MacLennan CA, Levine MM. Invasive nontyphoidal *Salmonella* disease in Africa: current status. *Expert Rev Anti Infect Ther* 2013;11:443–6.
- [2] Crump JA, Heyderman RS. A perspective on invasive *Salmonella* disease in Africa. *Clin Infect Dis* 2015;61(Suppl. 4):S235–40.
- [3] Crump JA, Sjolund-Karlsson M, Gordon MA, Parry CM. Epidemiology, clinical presentation, laboratory diagnosis, antimicrobial resistance, and antimicrobial management of invasive *Salmonella* infections. *Clin Microbiol Rev* 2015;28:901–37.
- [4] Kirk MD, Pires SM, Black RE, Caipo M, Crump JA, Devleeschauwer B, et al. World Health Organization estimates of the global and regional disease burden of 22 foodborne bacterial, protozoal, and viral diseases, 2010: a data synthesis. *PLoS Med* 2015;12:e1001921.
- [5] Ao TT, Feasey NA, Gordon MA, Keddy KH, Angulo FJ, Crump JA. Global burden of invasive nontyphoidal *Salmonella* disease, 2010(1). *Emerg Infect Dis* 2015;21:941–9.
- [6] Feasey NA, Dougan G, Kingsley RA, Heyderman RS, Gordon MA. Invasive nontyphoidal *Salmonella* disease: an emerging and neglected tropical disease in Africa. *Lancet* 2012;379:2489–99.
- [7] Gordon MA, Graham SM, Walsh AL, Wilson L, Phiri A, Molyneux E, et al. Epidemics of invasive *Salmonella enterica* serovar Enteritidis and *S. enterica* serovar Typhimurium infection associated with multidrug resistance among adults and children in Malawi. *Clin Infect Dis* 2008;46:963–9.
- [8] Kingsley RA, Msefula CL, Thomson NR, Kariuki S, Holt KE, Gordon MA, et al. Epidemic multiple drug resistant *Salmonella* Typhimurium causing invasive disease in sub-Saharan Africa have a distinct genotype. *Genome Res* 2009;19:2279–87.
- [9] Kariuki S, Gordon MA, Feasey N, Parry CM. Antimicrobial resistance and management of invasive *Salmonella* disease. *Vaccine* 2015;33(Suppl. 3):C21–9.
- [10] MacLennan CA, Martin LB, Micoli F. Vaccines against invasive *Salmonella* disease: current status and future directions. *Hum Vaccin Immunother* 2014;10:1478–93.
- [11] Simon R, Levine MM. Glycoconjugate vaccine strategies for protection against invasive *Salmonella* infections. *Hum Vaccin Immunother* 2012;8:494–8.
- [12] MacLennan CA. Vaccines for low-income countries. *Semin Immunol* 2013;25:114–23.
- [13] Rondini S, Lanzilao L, Necchi F, O’Shaughnessy C, Saul AJ, MacLennan CA. Invasive African *Salmonella* Typhimurium induces bactericidal antibodies against O-antigens. *Microb Pathog* 2013;63:19–23.
- [14] Rondini S, Micoli F, Lanzilao L, Gavini M, Alfini R, Brandt C, et al. Design of glycoconjugate vaccines against invasive African *Salmonella enterica* serovar Typhimurium. *Infect Immun* 2015;83:996–1007.
- [15] Goh YS, Clare S, Micoli F, Saul A, Mastroeni P, MacLennan CA. Monoclonal antibodies of a diverse isotype induced by an O-antigen glycoconjugate vaccine mediate in vitro and in vivo killing of African invasive nontyphoidal *Salmonella*. *Infect Immun* 2015;83:3722–31.
- [16] McSorley SJ, Jenkins MK. Antibody is required for protection against virulent but not attenuated *Salmonella enterica* serovar Typhimurium. *Infect Immun* 2000;68:3344–8.
- [17] Watson DC, Robbings JB, Szu SC. Protection of mice against *Salmonella* Typhimurium with an O-specific polysaccharide-protein conjugate vaccine. *Infect Immun* 1992;60:4679–86.
- [18] Lindberg AA, LeMinor L. *Methods Microbiol* 1984;15:1–142.
- [19] Hellerqvist CG, Lindberg B, Svensson S. Structural studies on the O-specific side chains of the cellwall lipopolysaccharides from *Salmonella* Typhi and *S. Enteritidis*. *Acta Chem Scandinavica* 1969;23:1588–96.
- [20] Hellerqvist C, Lindberg B, Svensson S. Structural studies on the O-specific side-chains of the cell-wall lipopolysaccharide from *Salmonella* Typhimurium 395 MS. *Carbohydr Res* 1968;8:43–55.
- [21] Micoli F, Ravenscroft N, Cescutti P, Stefanetti G, Londero S, Rondini S, et al. Structural analysis of O-polysaccharide chains extracted from different *Salmonella* Typhimurium strains. *Carbohydr Res* 2014;385:1–8.
- [22] Onsare RS, Micoli F, Lanzilao L, Alfini R, Okoro CK, Muigai AW, et al. Relationship between antibody susceptibility and lipopolysaccharide O-antigen characteristics of invasive and gastrointestinal nontyphoidal *Salmonellae* isolates from Kenya. *PLoS Negl Trop Dis* 2015;9:e0003573.
- [23] Lanzilao L, Stefanetti G, Saul A, MacLennan CA, Micoli F, Rondini S. Strain selection for generation of O-antigen-based glycoconjugate vaccines against invasive nontyphoidal *Salmonella* disease. *PLoS ONE* 2015;10:e0139847.
- [24] Parker CT, Liebana E, Henzler DJ, Guard-Petter J. Lipopolysaccharide O-chain microheterogeneity of *Salmonella* serotypes Enteritidis and Typhimurium. *Environ Microbiol* 2001;3:332–42.
- [25] Slauch JM, Mahan MJ, Micchetti P, Neutra MR, Mekalanos JJ. Acetylation (O-Factor 5) affects the structural and immunological properties of *Salmonella* Typhimurium lipopolysaccharide O-antigen. *Infect Immun* 1995;63:437–41.
- [26] Wollin R, Stocker BAD, Lindberg AA. Lysogenic conversion of *Salmonella* Typhimurium bacteriophages A3 and A4 consists of O-acetylation of rhamnose of the repeating units of the O-antigen polysaccharide chain. *J Bacteriol* 1987;169:1003–9.
- [27] Helander IM, Moran A, Makela PH. Separation of two lipopolysaccharide populations with different contents of O-antigen factor 122 in *Salmonella enterica* serovar Typhimurium. *Mol Microbiol* 1992;6:2857–62.
- [28] Berlanda Scorza F, Colucci AM, Maggiore L, Sanzone S, Rossi O, Ferlenghi I, et al. High yield production process for *Shigella* outer membrane particles. *PLoS ONE* 2012;7:e35616.
- [29] Rossi O, Caboni M, Negrea A, Necchi F, Alfini R, Micoli F, et al. TLR activation by Generalized Modules for Membrane Antigens (GMMA) from lipid A mutants of *Salmonella enterica* serovars Typhimurium and Enteritidis. *Clin Vaccine Immunol* 2016;23:304–14.
- [30] Ellis TN, Kuehn MJ. Virulence and immunomodulatory roles of bacterial outer membrane vesicles. *Microbiol Mol Biol Rev* 2010;74:81–94.
- [31] Alaniz RC, Deatherage BL, Lara JC, Cookson BT. Membrane vesicles are immunogenic facsimiles of *Salmonella* Typhimurium that potently activate dendritic cells, prime B and T cell responses, and stimulate protective immunity in vivo. *J Immunol* 2007;179:7692–701.
- [32] Gerke C, Colucci AM, Giannelli C, Sanzone S, Vitali CG, Sollai L, et al. Production of a *Shigella sonnei* vaccine based on Generalized Modules for Membrane Antigens (GMMA), 1790GAHB. *PLoS ONE* 2015;10:e0134478.
- [33] Meloni E, Colucci AM, Micoli F, Sollai L, Gavini M, Saul A, et al. Simplified low-cost production of O-antigen from *Salmonella* Typhimurium Generalized Modules for Membrane Antigens (GMMA). *J Biotechnol* 2015;198:46–52.
- [34] Lilleengen K. Typing of *Salmonella* Dublin and *Salmonella* Enteritidis by means of bacteriophage. *Acta Pathol Microbiol Scandinavica* 1950;27:625–40.
- [35] de Jong A, Thomas V, Simjee S, Godinho K, Schiessl B, Klein U, et al. Pan-European monitoring of susceptibility to human-use antimicrobial agents in enteric bacteria isolated from healthy food-producing animals. *J Antimicrob Chemother* 2012;67:638–51.
- [36] Total protein monograph 2.5.33. *European Pharmacopoeia* 8.
- [37] Rossi O, Maggiore L, Necchi F, Koeberling O, MacLennan CA, Saul A, et al. Comparison of colorimetric assays with quantitative amino acid analysis for protein quantification of Generalized Modules for Membrane Antigens (GMMA). *Mol Biotechnol* 2015;57:84–93.

- [38] Micoli F, Rondini S, Gavini M, Pisoni I, Lanzilao L, Colucci AM, et al. A scalable method for O-antigen purification applied to various *Salmonella* serovars. *Anal Biochem* 2013;434:136–45.
- [39] MacLennan CA, Gondwe EN, Msefula CL, Kingsley RA, Thomson NR, White SA, et al. The neglected role of antibody in protection against bacteremia caused by nontyphoidal strains of *Salmonella* in African children. *J Clin Invest* 2008;118:1553–62.
- [40] Li-Hsin Z, Rothman DL, Shulman RG.  $^1\text{H}$  NMR visibility of mammalian glycogen in solution. *Proc Natl Acad Sci USA* 1990;87:1678–80.
- [41] McMeechan A, Lovell MA, Cogan TA, Marston KL, Humphrey TJ, Barrow PA. Glycogen production by different *Salmonella enterica* serotypes: contribution of functional glgC to virulence, intestinal colonization and environmental survival. *Microbiology* 2005;151:3969–77.
- [42] Bonafonte MA, Solano C, Sesma B, Alvarez M, Montuenga L, Garcia-Ros D, et al. The relationship between glycogen synthesis, biofilm formation and virulence in *Salmonella* Enteritidis. *FEMS Microbiol Lett* 2000;191:31–6.